Modelling Spray Fluidised Bed Granulation

The University Of Sheffield.

Sheikh Nabhan Ahmed
Chemical and Biological Engineering
University of Sheffield

A thesis submitted for the degree of
Doctor of Philosophy

"All models are wrong,
but some are useful"
- George Box, 1976.

Acknowledgements

First and foremost I would like to give a huge thanks to Prof. Jim Litster for always providing me sincere kindness throughout this journey. You've really helped shape me to be the best person that I could be.

I would also like to thank my industrial collaborators at Syngenta for financing the research. The opportunities and positivity the company has shown me have all been beyond my expectations. Special thanks go to Dr. Christophe Grosjean, Dr. Elizabeth Rondeau and especially John Silverthorne who has mentored me throughout this journey. A big thanks to Michael Brozio and Joss Patel who both contributed greatly to this work through their long and arduous efforts at the Münchwilen pilot plant and Jealotts Hill.

External collaborators who influenced this work includes: Dr. Jianfeng Li (PSE), Dr. Stefan Bellinghausen (PSE), Dr. Li Ge Wang (PSE), Dr. Omid Arjmanji Tash (Certara).

The following group members at Sheffield who influenced this work: Dr. Rachel Smith, Dr. Kate Pitt and Dr. Bilal Ahmed.

Lastly, I would like to thank my close friends, Ryan, Charlie, Alex, Zak and Shelvin, all who helped me through many difficult periods. Friends who took every step with me along this journey, providing me with inspiration, courage and support when I needed it the most.

Abstract

Modelling Spray Fluidised Bed Granulation

By Sheikh Nabhan Ahmed

Research Supervisor: Professor James Litster

Industrial operation of particulate processes have historically been reliant on accumulated corporate knowledge that is assimilated by trial-and-error through decades of process operation. However, this accumulated knowledge is often poor at dealing with new issues which may arise due to new product formulations or new process conditions as the underlying science is not well established or misunderstood. Issues such as overfilling of packaging due to poor control of the bulk density and product which does not meet specification are recurring issues which the process engineer has to regularly tackle. As a response, food, pharmaceutical, detergent and, relevant to this thesis, the agrochemical industries have emphasised increased investments into developing understanding of the core scientific fundamentals of their processes. A convenient way to capture the fundamentals is to deploy a model-based approach.

Through this thesis, a coupled one-dimensional population balance model is proposed and implemented. The model framework considers the granule in four parts, the solid composition, the solvent content, gas content and solid within the solvent phase. With these internal co-ordinates, a novel wetting model is developed and validated which builds upon the work of Kariuki et al. [2013] and integrates the particle coating number into the continuous form of the population balance framework. Further to this, a novel agglomeration model is implemented which builds upon the

wetting model. The model considers agglomeration-likelihood as a function of the surface wetting in addition to the collision behaviour via the Stokes criterion. The model demonstrates that the collision and wetting behaviour both play a key role to growth and integrates them within a single framework for the first time.

The model is extended into a two-compartment framework. One compartment considers spray drying and the other compartment considers the bulk particle bed. The bulk bed compartment integrates the population balance framework, where the spray drying compartment is linked by a mass flow which feeds the population balance model with nuclei generated by spray drying. A sensitivity study is performed to characterise model behaviour and the role of drying in the overall granulation mechanisms.

This model framework is finally validated against experimental data performed on a pilot-scale continuous fluidised bed granulator. The process parameters which were varied are the spray rate, inlet air temperature, inlet fluidisation air flow rate and a combination of these. Lab-scale experiments were performed to feed the model with key formulation properties; the single particle drying curve and the sorption isotherm. Key model parameters such as the agglomeration rate constant, spray bypass ratio, spray droplet diameter and standard deviation were estimated using a single model experiment. The model then predicted successfully changes in all process parameters, which is a powerful validation of the model. This highlights that we can capture granulation phenomena such as the dependence on wetting and drying within particle growth, while not being reliant on computationally intensive methods such as computational fluid dynamics and discrete element modelling. This work provides a framework which may be attractive for industrial integration due to the low computational intensity whilst still capturing the complex physics of granulation.

Contents

1 Introduction **1**

1.1 The Industrial Problem 1

1.2 The Mechanisms of Wet Granulation 2

1.3 Population Balance Modelling 4

1.4 Thesis Objectives 5

2 Literature Review **6**

2.1 Granulation Mechanisms of a Top-spray Fluidised Bed Granulator . . 6

2.1.1 Process parameters and Rate Processes of Fluid Bed Granulation 7

2.1.2 Impact of the Spray and Process Geometry on Granulation Rate Mechanisms 11

2.1.3 Generalising the Rate Processes for Fluid Bed Granulation . . 14

2.2 Modelling Granulation Rate Mechanisms 17

2.2.1 Nucleation & Wetting 17

2.2.2 Layering & Agglomeration 24

2.2.3 Breakage & Attrition 33

2.2.4 Co-dynamics of Rate Mechanisms 34

2.3 Multi-dimensional Population Balance Models 36

2.3.1 Framework of a Multi-dimensional Population Model 36

2.3.2 Model Reduction of Multi-dimensional Models 38

2.3.3 Compartmentalised Frameworks 39

2.4 Conclusion 42

3 Development of a Mechanistic Growth Model for Liquid Layering in Fluid Bed Granulation **43**

3.1 Introduction 43

3.2 Multi-dimensional Population Balance Model For Layering 44

3.3 Model Development and Implementation 45

3.3.1 Development of a Kinetic Model for Liquid Layered Growth . 46
3.3.2 Discretisation Strategy 49
3.3.3 Model Initialisation 49
3.3.4 Experimental Method 49
3.4 Batch Fluid Bed Granulation 52
3.4.1 Effect of Spray Rate 53
3.4.2 Effect of Droplet Size 56
3.4.3 Effect of Contact Angle 57
3.4.4 Experimental and Model Comparisons 60
3.5 Conclusion 60

4 Development of a Mechanistic Agglomeration Model for Fluid Bed Granulation Processes 64
4.1 Introduction 64
4.2 Model Development and Implementation 65
4.2.1 Development of the Agglomeration Model 66
4.2.2 Model Parameters and Initialisation 70
4.3 Numerical Study 71
4.3.1 Model Analysis 71
4.3.2 Determining dominant growth mechanisms 81
4.4 Conclusion 83

5 Integrated Models for Fluid Bed Granulation 84
5.1 Introduction 84
5.2 Framework for Fluid Bed Granulation 85
5.3 Model Development for the Integrated Fluidised Bed Granulation Model 86
5.3.1 Mass and Energy Balances 86
5.3.2 Population Balance 92
5.3.3 Wetting 93
5.3.4 Agglomeration 94
5.3.5 Drying 95
5.3.6 Bed Hydrodynamics 97
5.3.7 Nucleation (one compartment only) 98
5.3.8 Spray Drying (two compartment only) 99
5.4 Model Implementation 101
5.5 Numerical Study 103
5.5.1 Effect of Initial Bed Mass 103

5.5.2 Effect of Mass Spray Rate . . . 105
5.5.3 Effect of Droplet/Nuclei Diameter . . . 109
5.5.4 Effect of Inlet Fluidisation Flow Rate . . . 112
5.5.5 Effect of Inlet Fluidisation Temperature . . . 114
5.6 Conclusion . . . 115

6 Experimental Studies of a Pilot-scale Top-spray Fluidised Bed 118
6.1 Introduction . . . 118
6.2 The Pilot-scale Fluidised Bed Granulator . . . 118
6.3 Materials and Methods . . . 120
6.3.1 Size Characteristics . . . 120
6.3.2 Bulk Density . . . 121
6.3.3 Specific Heat Capcity . . . 121
6.3.4 Granule Moisture Content . . . 121
6.3.5 Desorption Isotherms and Drying Curves . . . 122
6.4 Experimental Method and Design . . . 122
6.4.1 Calibrating the Moisture Sensor . . . 127
6.4.2 Quantification of the Statistical Impact on the Particle Size Distributions . . . 128
6.4.3 Fraction of Solvent Evaporated . . . 128
6.4.4 Relative Distance From Linear Growth . . . 129
6.5 Results and Discussion . . . 130
6.5.1 Influence of Spray Rate . . . 130
6.5.2 Influence of Inlet Air Temperature . . . 131
6.5.3 Influence of Inlet Air Flow Rate . . . 134
6.5.4 Influence of Combined Process Parameters . . . 136
6.5.5 Product Flow Rate Control . . . 139
6.5.6 Granule Moisture Content . . . 141
6.5.7 Relative Distance Against Linear Growth . . . 142
6.6 Conclusion . . . 143

7 Validation of a two-compartment integrated population balance model using pilot plant data 145
7.1 Introduction . . . 145
7.2 Model Formulation and Validation Strategy . . . 145
7.3 Results & Discussion . . . 148
7.4 Conclusion . . . 162

8 Conclusion & Future Work **165**
8.1 Major Conclusions 165
8.2 Future Work 166

A Simplified Analytical Model for Batch Growth and Drying **167**
A.1 Introduction 167
A.2 Particle Growth Model 167
A.3 Drying Model 169
A.4 Specific Mass Flowrate of Solvent 171
A.5 Model Parameters 172
A.6 Parametric Study 172
A.7 Conclusions 176

B Calculating the Bubble Phase Properties of a Fluidised Bed **178**

C Analytical Solution to the Agglomeration Number in Fluidised Beds **180**

D Pilot Plant Raw Data **184**

Bibliography **185**

List of Figures

1.1 Schematic of granulation mechanisms 2

2.1 Granulation rate process map for fluid bed melt granulation 10
2.2 Diagram of a typical setup for top-spray fluidised beds 12
2.3 Diagram of a typical setup for bottom spray fluidised bed 13
2.4 A unified rate process map for fluidised bed granulation 15
2.5 Distribution and Immersion Nucleation Mechanisms 18
2.6 Nucleation Regime Map 19
2.7 Probability of collision versus probability of successful wet collisions after Rieck et al. [2020] 35
2.8 Compartmentalisation 40
2.9 Three compartmental framework for Fluidised Bed Granulation . . . 41

3.1 Control volume for liquid layered growth 47
3.2 Equipment diagram 51
3.3 Key mass balance properties of the wetting only population balance model 53
3.4 Average particle size vs time 54
3.5 Average coating vs time 55
3.6 Average particle size vs time for varying droplet diameters 56
3.7 Average fraction coated vs time droplet diameter 57
3.8 Surface plots of average coating vs droplet diameter 58
3.9 Average particle size vs time for varying contact angles 59
3.10 Average fraction coated vs time droplet diameter 59
3.11 Experimental data vs Model 61
3.12 Comparisons of the size cut vs experiment 62

4.1 Types of coalescence interactions 69
4.2 Effect of spray rate on agglomeration model 72

4.3 The evolution of the normalised particle size distributions for the spray scenarios . . . 73
4.4 The agglomeration probability, η_{eff}, for a spray scenario of 0.1 (kg/kg.hr) 74
4.5 The agglomeration probability, η_{eff}, for a spray scenario of 0.3 (kg/kg.hr) 75
4.6 The Stokes criterion for a spray scenario of 0.1 (kg/kg.hr) . . . 77
4.7 The Stokes criterion for a spray scenario of 0.3 (kg/kg.hr) . . . 78
4.8 Effect of air flow rate on agglomeration model . . . 79
4.9 The evolution of the normalised particle size distributions for changing fluidisation ratios . . . 80
4.10 Comparison of the superficial velocity against the minimum . . . 81
4.11 The agglomeration number with time . . . 82

5.1 Simplified rate process diagram for fluid bed granulation . . . 85
5.2 Model framework for fluidised bed granulation . . . 87
5.3 Control volume of the one-compartment fluidised bed granulator . . . 89
5.4 Control volume of the two-compartment fluidised bed granulator . . . 90
5.5 Effect of initial bed mass on the holdup within the granulator . . . 103
5.6 Effect of initial bed mass on the outlet mass flow rate from the granulator 104
5.7 Effect of initial bed mass on the outlet streams from the screen . . . 105
5.8 Evolution of the average particle size from the fluidised bed outlet . . 106
5.9 Evolution of the average particle size in the product stream . . . 106
5.10 The normalised mass density distribution at $t = 3hours$ . . . 107
5.11 The average particle size for varying mass spray rates . . . 107
5.12 The outlet humidity for all model formulations . . . 108
5.13 The mass average particle size for changing droplet/nuclei diameter for all four model formulations. . . . 110
5.14 The mass density distribution for changing droplet/nuclei diameter for all four model formulations at $t = 3hours$ . . . 110
5.15 The droplet size distribution of the atomised droplets in the spray drying compartment for the two compartment models. . . . 111
5.16 The relative humidity and temperature for the spray drying compartment in the two compartment model . . . 111
5.17 The mass average particle size for changing fluidisation air flow rate for all four model formulations. . . . 112
5.18 The granule moisture content within the granule bed for all four model formulations. . . . 113

5.19 The mass holdup and discharge rate from the particle bed 114
5.20 The mass average particle size for changing inlet fluidisation air temperature for all four model formulations. 115
5.21 The temperatures of the solid, vapour and when applicable the spray drying compartment for varying temperatures. 116
5.22 The moisture content of the granule phase and the spray drying compartment for varying temperatures 116

6.1 Diagram of the experimental pilot scale unit 119
6.2 The initial size distribution of Placebo A7946T 121
6.3 Experimental desorption isotherm data 123
6.4 Experimental drying curves 123
6.5 Pilot plant experimental matrix 126
6.6 Calibration curve for the moisture sensor M21 129
6.7 Size characteristics of varying spray rates within a pilot scale fluidised bed granulator 132
6.8 Drying characteristics of varying spray rates within a pilot scale fluidised bed granulator 133
6.9 Size characteristics of varying inlet air temperatures within a pilot scale fluidised bed granulator 134
6.10 Drying characteristics of varying inlet air temperatures within a pilot scale fluidised bed granulator 135
6.11 Size characteristics of varying inlet air flow rates within a pilot scale fluidised bed granulator 136
6.12 Drying characteristics of varying inlet air air flow rates within a pilot scale fluidised bed granulator 137
6.13 Size characteristics for combined changes in process parameters . . . 138
6.14 Drying outputs from changes in combined process parameters within a pilot scale fluidised bed granulator 140
6.15 The Hellinger distance for each experimental subset 141
6.16 The measured flow rate out of the product stream for each experiment 142
6.17 The granule moisture content for experiments 1-8 143
6.18 The relative distance away from linear growth for all experiments . . 144

7.1 A comparison of the d_{10}, d_{50} and d_{90} of the experiment and model. . . 152
7.2 A comparison of the volume density distribution between the experiment and model. 154

7.3 A comparison of the absolute humidity between the experiment and model. 157
7.4 A comparison of the exhaust temperature between the experiment and model. 159
7.5 A comparison of the product flow rate between the experiment and model. 161
7.6 A comparison of the granule moisture content between the experiment and model. 164

A.1 Key size properties of the analytical growth model for varying liquid-to-solid ratios 173
A.2 Surface coating properties of the analytical model for varying liquid-to-solid ratios 174
A.3 Surface plots of the variations of gas temperature and humidity across the dimensionless bed height at multiple droplet scenarios 175
A.4 Mean gas temperature and humidity against the liquid-to-solid ratio at varying number of transfer units 176
A.5 Specific mass flow against the liquid to solid ratio 176

Chapter 1

Introduction

1.1 The Industrial Problem

Formulated products are ubiquitous to major industrial operations in the production of agrochemicals, pharmaceuticals, food products and more. For example, the global agrochemicals industry is estimated to be worth $304 billion dollars by 2025 [Phillips, 2020], with forecasts suggesting further increases year-on-year.

Fundamental to these industries are the unit operations which manufacture the formulated products. The unit operation must enable the manufacturer the ability to produce products with desireable properties. For example in the agrochemical industry, fertiliser which is produced in solid form should have; high bulk density to minimise packaging, high flowability and low friability for easier transport, and desireable functional properties such as the suspensibility and redispersion.

The unit operations which produce formulated products are often lumped as particulate processes. These can include granulators, dryers, mills, size classifiers, hoppers and more. Particulate processes are well known to be difficult to operate. Most are operated with empirical knowledge accumulated from years of operation. However, this empiricism rarely arms the operator with the appropriate knowledge to problem-solve. Problems which often arise when moving towards new formulations and process conditions. A typical industrial problem which industry has typically struggled to solve quickly is the scenario where two process plants which manufacture the same product producing vastly different outputs. The empirical knowledge used to troubleshoot may only satisfy one process plant, but, the other may result in a significantly worse output. As a result, this incurs heavy financial costs, loss of product and operating bottlenecks to meet consumer demand.

Fluidised beds are among the most prominently used units due to their flexibility, to act simultaneously as a granulator and dryer in either batch or continuous modes

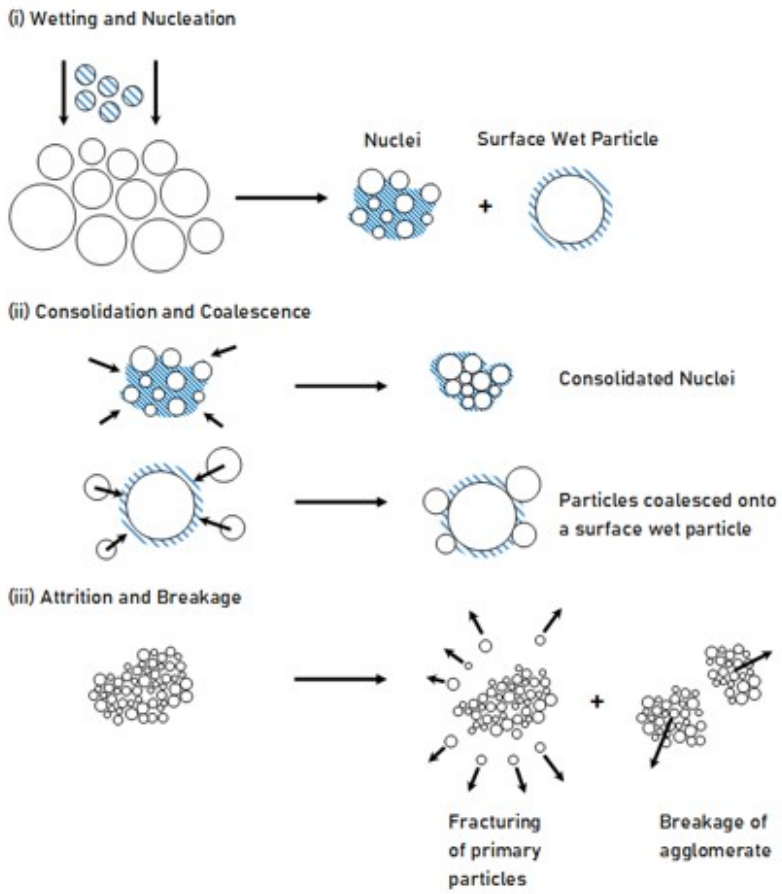

Figure 1.1: Schematic of the granulation mechanisms

[Cryer, 1999]. They are known to achieve high heat and mass transfer ratios, but, are often operated away from optimal points due to the limited mechanistic understanding of the process. As more industries begin to emphasise technical excellence, there is a push to integrate the state-of-the-art at the industrial scale; hence the drive to build towards a model-driven approach and the development of mechanistic models.

1.2 The Mechanisms of Wet Granulation

Wet granulation is a particle size enlargement process to form larger entities known as agglomerates by the mechanisms of layering and agglomeration. This size enlargement is achieved by the addition of a liquid binder into a particle bed assisted by some form of agitation. This agitation could be by impeller, rotation or fluidisation. Wet granulation can be classified into three core phenomena where this is shown on Figure 1.1.

The wetting and nucleation is the process of liquid binder interacting with primary

particles to form either surface wet particles or nuclei; a liquid dense entity composed of fine particles. Nucleation is usually categorised as either distributive, when the droplet diameter is much smaller than the primary particles, or immersion when the droplet diameter exceeds the primary particles. Distributive type nucleation often results in surface wet particles, where immersive results in nuclei.

Often by advective movement (for example by impeller or fluidised air) the nuclei or surface wet particle can interact with the rest of the bulk particle bed to consolidate and coalesce. In the case of nuclei, it will first consolidate and redistribute the internal liquid to the surface to form a surface wet particle, to then further coalesce with nearby particles.

If the particle-particle collision energies exceed an appropriate threshold, two modes of breakage can occur, attrition and breakage. Attrition often refers to "shaving off" small primary particles from the surface of an agglomerate structure. Breakage on the other hand is the separation of an agglomerate into several smaller agglomerates.

These mechanisms have been described in detail in Iveson et al. [2001] with the appropriate validation experiments referenced throughout this work. This framework was a significant step in developing a core understanding of granulation from a fundamental approach. Using this framework, various researches have linked core process parameters to the respective mechanisms; such as Tan et al. [2004a], Vreman et al. [2009], Bertin et al. [2011] and Rajniak et al. [2009] for fluidised beds. In practice, the studies are rarely integrated into industrial scenario due to the complexity of adapting to real industrial problems and issues. These problems can include, complex formulations, scaling from lab-scale batch to industrial-scale continuous, impractical process controls, and most importantly a poor cost value to test unknown steady-states. In essence, there are too many experiments required to find and test the new optimal operating position.

As a way to help optimise processes, modelling tools have been developed. The most popular tools include population balance models (PBM), discrete element models (DEM), computational fluid dynamics (CFD). In particular, population balance modelling has become popular due to the low computational costs to model macro-scale systems. This allows for population balance models to potentially be applicable to industrial-scale processes due to the low computational cost and the ability to scale-up across multiple operation plants.

1.3 Population Balance Modelling

The generic one-dimensional population balance model can be written as Equation 1.1.

$$\frac{\partial\left(Vn(x,t)\right)}{\partial t}+\frac{\partial\left(VGn(x,t)\right)}{\partial x}=\dot{Q}_{in}n(x,t)-\dot{Q}_{out}n(x,t)+VBn(x,t)-VDn(x,t) \quad (1.1)$$

Where V is the volume of the equipment, n is the number density of particles along the particle length co-ordinate x, G an appropriate differential growth function (often expressed as the function of $G=\frac{dx}{dt}$), $\dot{Q}_{in}$ is the volumetric inflow of particles, $\dot{Q}_{out}$ the volumetric outflow, B any generic birth function and D any generic death function.

The birth and death terms are fundamental to express the granulation rate mechanisms. Birth often refers to new agglomerates forming from two colliding particles, nuclei forming after interacting with a droplet and daughter particles from breakage events. On the other hand, death terms refer to the disappearance of smaller particles to form agglomerates and disappearance of an agglomerate after breakage. Layering of fine particles or liquid layered growth is dominated by the advective term where a mechanistic function is defined by the growth function G.

Many researches have focused on defining mechanistic birth and death rates, as well as growth functions for the granulation processes and have found success within their studies [Cameron et al., 2005]. However, when integrating these models at the larger scale, the accuracy of the model-space tends to fall short with varying process parameters; such as the liquid loading rates, initial particle size and spray dynamics [Iveson, 2002]. This issue has been discussed by many authors and is often attributed to the over simplification of the mixing zones and the lack of relevant granule properties within typical population balance models [Biggs et al., 2003, Cameron et al., 2005, Braumann et al., 2007, Li et al., 2012, Hussain et al., 2014, Barrasso, 2015, Liu et al., 2019].

As a result, plenty of effort has been placed into building multi-dimensional models and implementing compartmental models [Hounslow, 1998, Kumar et al., 2006, 2008, Li et al., 2012, Barrasso and Ramachandran, 2012, Chaudhury et al., 2014, Barrasso, 2015]. Multi-dimensional models extend the particle properties to particle size, liquid content and gas content; where previously only size would be modelled. As a result, multi-dimensional models have the potential to integrate more physically based rate models through the modelling of added granule co-ordinates.

While there is promising work demonstrating compartmentalised multi-dimensional models the computational costs are excessively high, such that it becomes aggressively unattractive for practical use. While multi-dimensional frameworks are available, the framework rarely integrate mechanistic rate models. This is either due to the lack of available models or the numerical complexity leading to instabilities. Therefore, its becoming an increasingly important question to ask:

- How many dimensions are necessary to model the process to a sufficient accuracy?
- What particle properties are necessary to develop a sufficient model to predict particle growth?
- What granulation mechanisms should be included to successfully predict process behaviour?
- How and what compartments are necessary to minimise the effects of the well-mixed assumption of the population balance model?

The following work aims to tackle these questions by developing a reduced-order multi-dimensional population balance model for a top-spray fluidised bed granulator. There will be an emphasis on developing and using physically representative multi-dimensional rate models which model the particle growth. Model compartmentalisation will be tested to identify the effectiveness on model accuracy to pilot-scale data of an industrial product.

1.4 Thesis Objectives

The objective of the thesis is to:

- Develop and implement mechanistic multi-dimensional rate models for agglomeration, liquid layered growth and drying that is physically representative of the granulation mechanisms within a top-spray fluidised bed granulator.
- Perform continuous pilot scale top-spray fluidised bed granulation studies using an industrial application. Key outcomes are to identify and quantify the effects of key operational parameters on particle size and drying.
- Integrate and implement a compartmental population balance model using mechanistic rate models and validate this model against the pilot-scale data.

Chapter 2

Literature Review

In the first section, this literature review aims to identify the core mechanisms which drive the granulation processes within a top-spray fluidised bed granulator. The second section will include the state-of-the-art of the current rate models available in literature. The final section will discuss how current modelling tools have been used within the literature, the key assumptions used and the accuracy to the model outputs. More specifically, there will be discussion on the effects of model outputs and properties by compartmentalised methods, and the integration of such methods into multi-dimensional population balance models.

2.1 Granulation Mechanisms of a Top-spray Fluidised Bed Granulator

The modern understanding of the granulation mechanisms was popularised by the works of Iveson et al. [2001] and Ennis and Litster [1997] who collated and demonstrated all fundamental rate mechanisms occurring within the current research at the time. It became an agreed understanding that granulation occurs by three core phenomena; wetting an nucleation, consolidation and growth, and attrition and breakage (discussed in Chapter 1). This was further accelerated by a popular modelling framework by Hounslow et al. [1988] who integrated the current understanding of nucleation, agglomeration and breakage into a single continuous integro-differential equation, formally known as the population balance. This framework has seen great success in works such as Hounslow [1998], Hounslow et al. [2001].

However more recently, there is a greater understanding that each type of granulator often have certain mechanisms emphasised (or which can be largely ignored) by the inherent virtue of the process design. Whether a mechanism can be made neg-

ligible, or be considered important, fundamentally relies upon the type of agitation of the particle bed, the location of spray, width of the spray and geometry of the equipment.

Thus, it is important to understand how process dynamics influence key granulation phenomena .This allows for both the operator and process engineer understand how key process parameters influence the outputs, whether by experimental empiricism or an appropriate model.

2.1.1 Process parameters and Rate Processes of Fluid Bed Granulation

There is a plethora of research which correlate process parameters with the properties of the product for fluidised beds [Kristensen and Schaefer, 1987, Michael and Michael, 1991, Kunii and Levenspiel, 1991, Nienow, 1995, Boerefijn and Hounslow, 2005]. These effects can be summarised in Table 2.1, which highlights the qualitative effects on key process parameters on particle properties.

Table 2.1: The effects of key operational process parameters on particle growth and fluidisation behaviour

Process Parameter	Effect at a low relative value	Effect at a high relative value	References	Comments
Spray rate	Layering dominant growth	Agglomeration dominant growth, eventual bed collapse	Cryer [1999], Tan et al. [2006], Boerefijn and Hounslow [2005], Bertin et al. [2011]	The effect of spray rate has been extensively studied by many authors and have consistently shown strong links to the growth behaviour of the particle bed.

Binder viscosity	Promotes more successful agglomeration	Blockage of the spray nozzle, poor distribution of binder throughout the particle bed	Tardos et al. [1997], Iveson et al. [2001], Zhai et al. [2009], Wade et al. [2020]	Studies involving binder viscosity are relatively limited and the effects are rarely isolated. The viscosity of the binder can result in functional operational issues as, in the case of it being too large, it would be too difficult to pump. It is typically a fixed property as part of the formulation, but, can be manipulated during processing to a more desirable value.
Fluidisation air flow rate	Maintain fluidisation and steady growth, increase in drying rate	Elutriation of fines to the head of the equipment, excessive breakage of particles, can result in spray-drying	Nienow [1995], Tan et al. [2006], Moraga et al. [2015]	Fluidisation air is typically controlled to maintain bed pressure drop. There is currently very little consideration for the interaction of the fluidisation air and the spray within both industry and the literature.

Fluidisation air temperature	Minor decrease in particle size	Sintering of particles, spray drying the spray, increase in breakage	Goldschmidt et al. [2002], Tan et al. [2006], Mörl et al. [2007], Bertin et al. [2011], Moraga et al. [2015]	The current literature is relatively inconsistent with regards to the effects of fluidisation air on the granule size. It's clear that the temperature of the bed as a multi-faceted effect on the collision behaviour, spray dynamics and growth. As a result, the effects measured have shown alternative behaviours depending on the operational envelope.
Primary particle size/droplet diameter	Reduction of agglomerates if primary particle size is greater than the droplet diameter	Complete reduction of agglomeration, increased demand of air flow rate to maintain fluidisation	Kunii and Levenspiel [1991], Goldschmidt et al. [2002, 2003], Tan et al. [2002], Kariuki et al. [2013], Villa et al. [2016], Rieck et al. [2016]	Most literature investigate primary particle size as an isolated experiment as opposed to the relationship with the droplet diameter. More recently studies have been performed characterising the ratio as an important parameter for experimental design and model development.

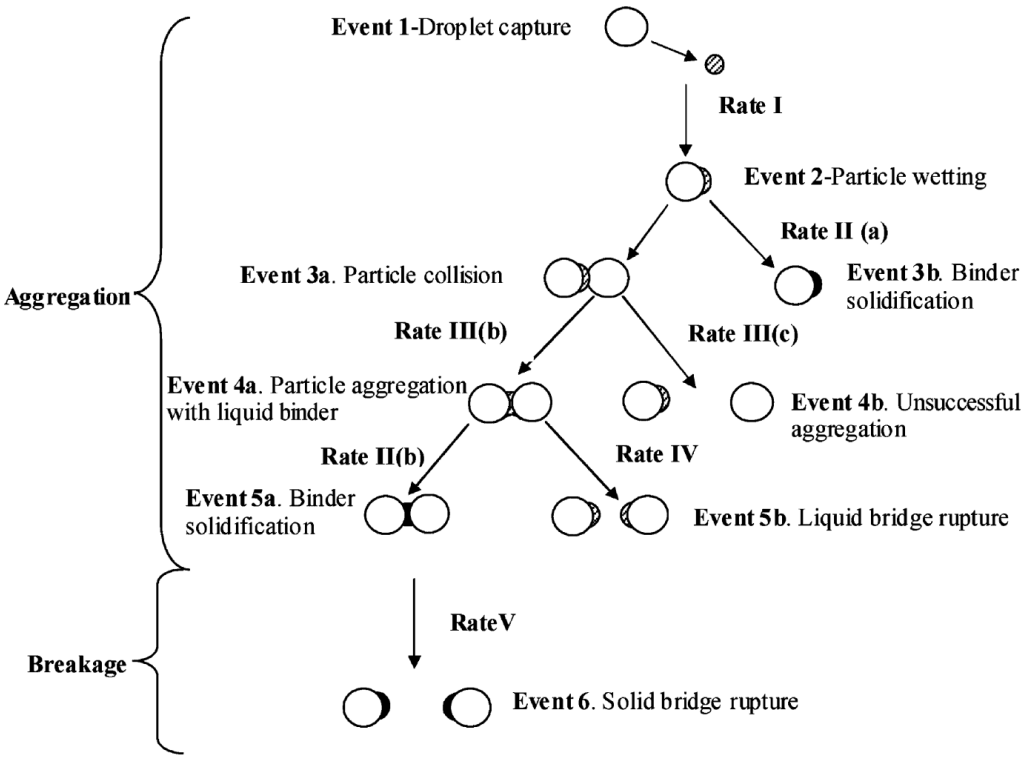

Figure 2.1: Rate process map proposed by Tan et al. [2006] for fluid bed melt granulation

Very little effort has been placed into adapting granulation phenomena into fluid bed granulation. Some of the earliest work in linking granulation phenomena was performed by Tan et al. [2006]. The author had proposed a generic rate process map for fluid bed granulation. Figure 2.1 shows the proposed scheme.

Here, the sequence of events is characterised into five rate processes. Rate (I) is the droplet capture process in which the droplet binder is captured onto the surface of the particle to form a smooth (and temporary) liquid layer. In this case, a broad assumption is made that the effects of nucleation by immersion is minimal. This generally holds true given that; a) the droplet diameter is much smaller than the particle bed and b) the bed is well fluidised such that the collision frequency of the particle bed is much greater than the rate of nucleation [Goldschmidt et al., 2002, Tan et al., 2002].

Once the particle captures the droplet, the particle is surface wet which can allow for the further rate processes of either binder solidification (Rate II(a) and (b)) or for event 3a where the surface wet particle collides with another local particle. If the collision is successful this will form a temporary aggregate.

The liquid bridge of the temporary aggregate can rupture to re-distribute the liquid phase over the two primary particles, or can solidify to form the final aggregate. The aggregate can then further go under a breakage event to reduce in size. The process map was well validated in the following works by the same author [Tan et al., 2002, 2004a,b, 2006, 2005].

Figure 2.1 provides a mechanistic model for a fixed envelope of a fluid bed granulation. However, there are clear omissions for some granulation phenomena, for example; particle attrition and nucleation. Furthermore, there is no clear indication within the proposed map that may lead to known operational issues such as the collapsing of the particle bed [Cryer, 1999, Vreman et al., 2009].

Therefore, for a mathematical model to be generalised for all the relevant operational design spaces; it is important that we define a model which unifies and generalises all known mechanisms.

2.1.2 Impact of the Spray and Process Geometry on Granulation Rate Mechanisms

The biggest advantage of adopting fluidised beds within any industrial circuit is the flexibility of the unit. This is particularly desirable for maximising the operational footprint of plant [Heinrich and Mörl, 1999, Peglow et al., 2007].

When designing a fluidised bed, a series of questions are often asked by the process designer; "where should the spray be placed?", "how many sprays are necessary?", "What type of nozzles should be used?" as well as other common questions such as whether it should be operated as batch, semi-batch or fully continuous [Kunii and Levenspiel, 1991]. Figures 2.2 and 2.3 provide a typical setup of a top-spray and bottom spray (Wurster type) arrangement respectively. While both processes are considered to be fluid bed granulation, the mechanisms and products outputs can vary significantly. This is surprising given that the difference is the location of the spray.

Often when equipment volumes become very large the distance from the fluidised particle bed and the spray can become significant. This often leads to partial spray drying of the spray which drives other core mechanisms such as layering (by primary particles) and agglomeration. A large spray-bed distance can also lead to a spray-drying dominated regime if the drying capacity of the inlet fluidisation air is large [Rajniak et al., 2009, Rieck et al., 2015]. A Wurster type arrangement can avoid this issue due to the spray and particle bed being in direct contact. Furthermore, the spray interaction often leads to higher bed velocities which in-turn leads

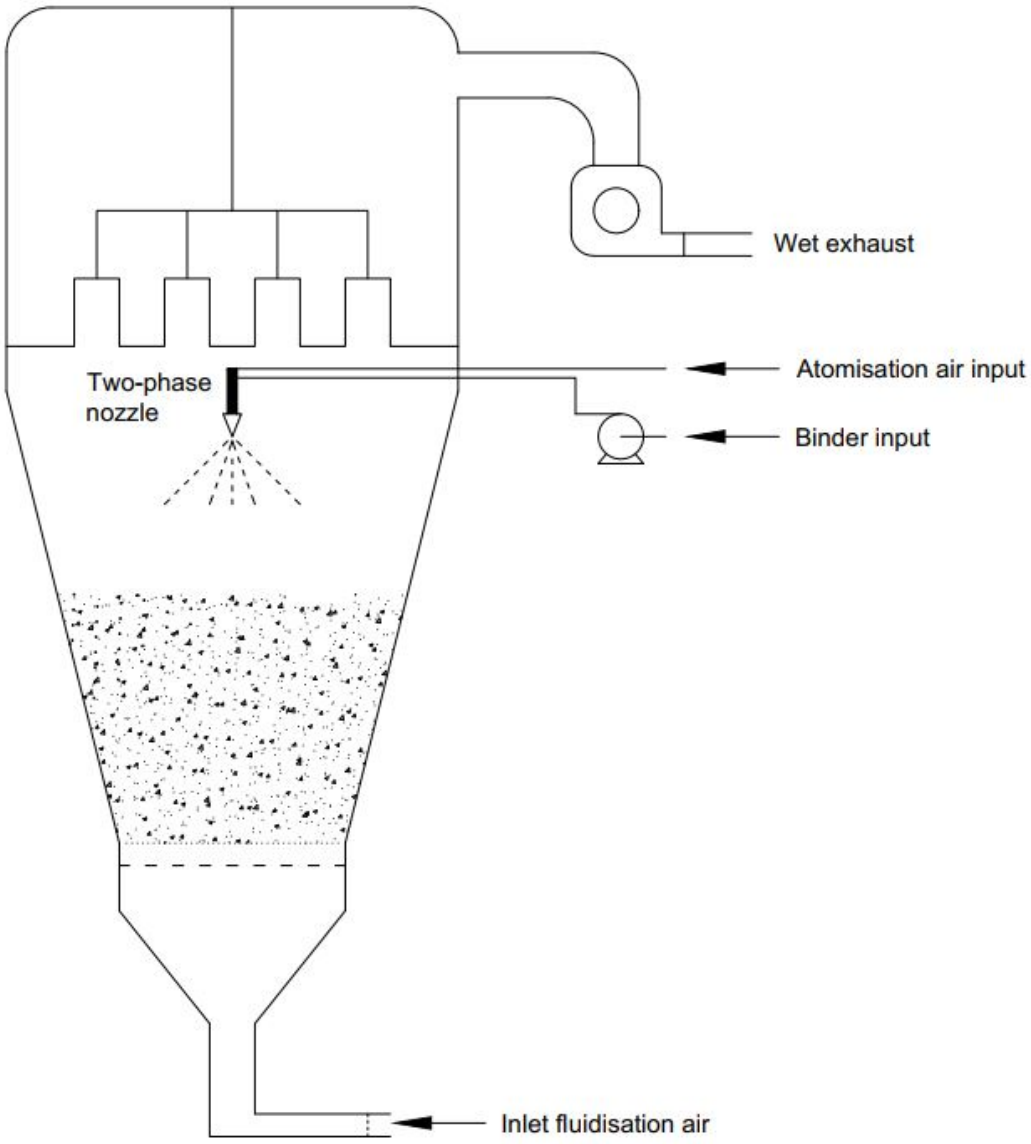

Figure 2.2: A typical setup for top-spray fluidised bed granulation

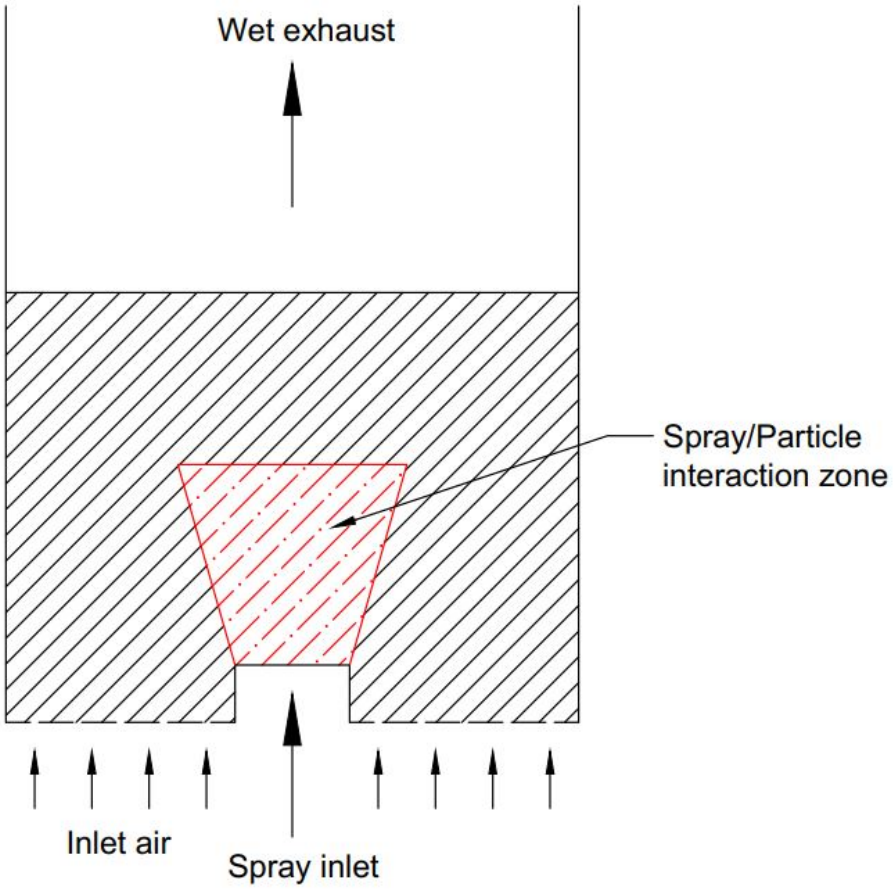

Figure 2.3: A typical setup for a bottom spray (Wurster) fluidised bed granulator

to less agglomeration [Cryer, 1999, Litster, 2016]. Often, this is the reason why bottom-spray arrangements are favoured for coating applications whereas top-spray for granulation/size-enlargement.

There is an important relationship between the spray and granulation mechanisms within the bed. The way in which the droplet interacts with the bed significantly influences the product output. Most literature tend to condense these mechanisms that are specific to the arrangement type, such as in the works of Michael and Michael [1991], Heinrich and Mörl [1999]) for bottom spray and Tan et al. [2004a], Peglow et al. [2007] for the top-spray arrangement. This means there is space within the current research to attempt to unify and generalise the rate processes.

2.1.3 Generalising the Rate Processes for Fluid Bed Granulation

To generalise the mechanisms we consider the three core phenomena; nucleation and wetting, consolidation and coalescence and finally breakage and attrition. We propose a rate process map which expands on the works of Tan et al. [2006] as Figure 2.4.

Here, the mechanisms are proposed from the onset of drop generation to the interaction in the particle bed and the respective processes within the bulk. It is proposed that the granulation mechanisms are driven by five events, droplet drying, nucleation, collisions, drying and eventually breakage. Within each event there are multiple processes which occur simultaneously. Rate processes which follow a solid black line show a specific rate process which must follow its predecessor. For example, rate I(b) follows directly into rate II(b). Whereas, processes in dashed lines suggest that the rate can "short-circuit" or skip a series of events based on the process geometry or conditions; for example rate II(a) which can skip to rate VI(a). Here, the intention is to show that rate processes can be successive or altered based on the process dynamics. Most of literature verify this, but, it is not explicitly described or shown.

Event 1: Droplet Drying is the event where the fluidisation air interacts with the travelling droplets from the spray to the particle bed. There are two outcomes, hence, two rates; Rate I(a) and Rate I(b). Rate I(a) is the rate process of droplet drying where the drying capacity of fluidisation air is large enough to change the

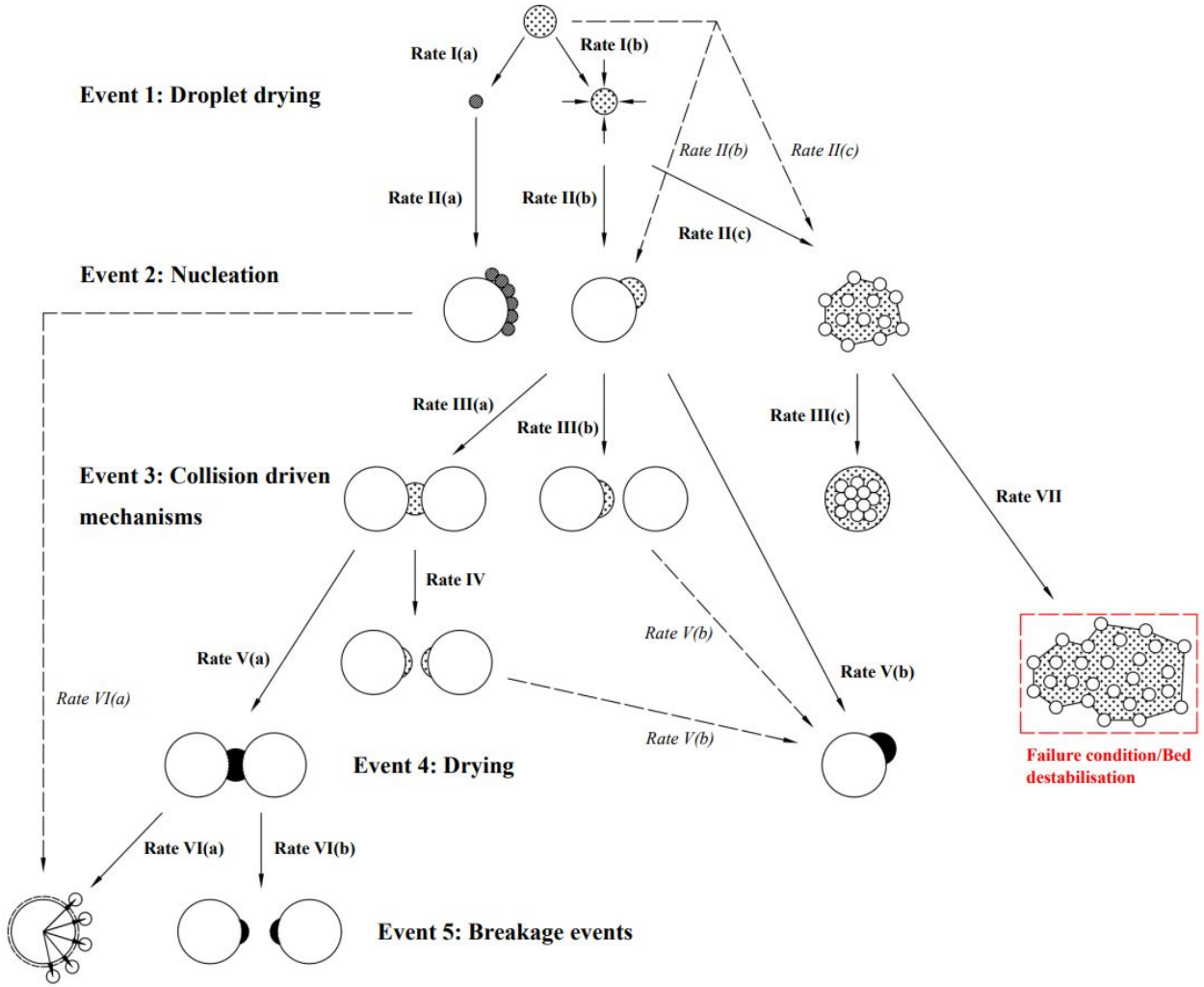

Figure 2.4: A proposed rate process map for fluidised bed granulation, adapted and modified from Tan et al. [2006]. The solid lines refer to processes which happen directly after the specific event, where dashed lines are those which may "short-circuit" based on specific geometries or process conditions.

droplet phase into the particle phase. Rate I(b) is the process of droplet shrinkage where the drying capacity is not sufficient for complete spray drying. There is a potential short-circuit into the nucleation phase to Rate II(b) where if the spray-to-bed distance is small, or the spray is in direct contact with the particle bed then the capacity to dry the droplets is non-existent.

Event 2: Nucleation describes the rate processes where the droplet (or spray dried particle) interacts with the particle bed. Rate II(a) follows the process where if the droplet has been spray-dried, it will interact with the particle bed to layer onto the surface of the particles of the bed. Rate II(b) is the distributive type nucleation where the droplet will interact with the particle to wet the surface, whereas, Rate II(c) follows the immersion type where the droplet wets the particle bed to form a liquid-dense nuclei. In this case, Rate II(b) and Rate II(c) are competitive with each other depending on the size ratio of the droplet versus the particle. If the droplet diameter is much smaller than the particle then Rate II(b) will be preferred and vice-versa.

Event 3: Collision Driven Mechanisms describes the set of processes where a wetted particle collides with the bulk of the particle bed. Rate III(a) is the agglomeration process where the surface wet particle forms a liquid-bridge with the adjoined particle as a temporary agglomerate. Rate III(b) describes the rebound process where the surface wet particle collides with the bulk to then immediately rebound. Rate III(c) is the process of nuclei consolidation, where the liquid dense nuclei collides with the equipment or neighbouring particles to densify and form a surface wet particle (which can further undergo processes of Rate III(a) and (b)). As an extension, following from Rate III(a) the process of liquid-redistribution/breakage of the temporary agglomerate can occur as Rate (IV). This results in two surface wet particles which can undergo Rates III(a) and (b).

Event 4: Drying describes the set of processes in which the bulk particle bed is dried by the inlet fluidisation air. Rate V(a) is the drying of the temporary agglomerate produced from Rate III(a) where the liquid-bridge is dried. Rate V(b) is the drying of any surface wet particle before it can interact with another particle to form an agglomerate. It is important to note the short-circuits where if the surface wet-particle cannot form a liquid-bridge before drying then there is preferential growth by liquid-layering.

Event 5: Breakage describes the final set of events where a dried particle can separate to form smaller particles (often referred to as daughter particles). In this case, Rate VI(a) is the attrition of small fines from the surface of the particle. Rate

VI(b) on the other hand is binary breakage of the agglomerate. From here, these particles can then re-enter the nucleation phase.

One rate process that sits outside the defined events is Rate VII which is the bed collapse. This rate process describes the over-wetting of the particle bed. If the spray rate is too large then the bed will de-fluidised and collapse. Often, this process is overlooked due to most rate process schematics ignoring the influence of the spray on the particle dynamics.

2.2 Modelling Granulation Rate Mechanisms

This section will expand on the current understanding of the granulation mechanism. There will be a deeper look into the state-of-the-art modelling techniques used to represent granulation phenomena by a series of continuous equations as part of population balance frameworks, while also discussing the limitations of these techniques, models and frameworks.

2.2.1 Nucleation & Wetting

Nucleation and wetting is the process which nuclei are formed from droplets interacting with a dry powder bed. Typically, liquid binder is introduced by atomised spray. The nucleation and wetting mechanism has become of recent interest as there has been a greater focus on the spray dynamics on the overall granulation phenomena [Schaafsma et al., 1999].

To characterise the influence of the spray on nucleation Litster et al. [2001] proposed the dimensionless spray flux, Ψ, as a tool to characterise the behaviour of nuclei formation across a moving powder bed. This is presented as Equation 2.1:

$$\Psi = \frac{3\dot{V}}{2\dot{A}d_d} \tag{2.1}$$

where $\dot{V}$ is the volumetric flow rate of binder from the nozzle, $\dot{A}$ is the powder surface flux passing through the spray area and d_d is the droplet diameter produced from the nozzle.

The dimensionless spray flux, Ψ, describes the rate at which droplets impact surface of the bed to the turnover rate of the powder bed. This allows for the characterisation of two regimes. If the spray flux is low then the bed turnover rate is sufficiently high such that any droplet which interacts with the bed will hit an area of non-wetted powder, on the other hand, at a high spray flux the droplets are more

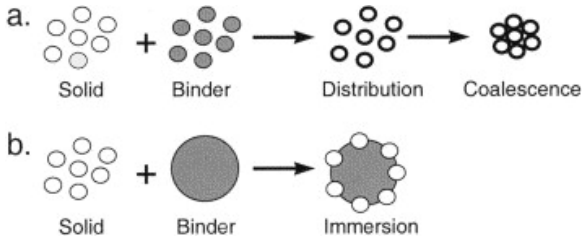

Figure 2.5: Visual representation of the two nucleation mechanisms (a) distribution and (b) immersion [Hapgood et al., 2003]

likely to overlap with wetted parts of the bed. Therefore, this allows for insight of the nucleation characteristics.

The droplets have a large influence on the type of nucleation. Hapgood et al. [2003] proposed two important nucleation regimes which relate to the droplet diameter; the immersion type and the distributive type. These nucleation types are drawn as Figure 2.5.

If the droplet is small relative to the impacting particle, distributive nucleation dominates whereas if the droplet is large compared to the particle size immersion nucleation dominates. The nuclei formed by distribution nucleation are surface wet particles coated by liquid binder whereas immersion-type nuclei are form liquid saturated nuclei that are proportional to the size of the droplet [Iveson et al., 2001, Hapgood et al., 2003].

The drop penetration time is an important thermodynamic property as this helps quantify whether the droplets have fully penetrated the bed before additional drops are introduced. Hapgood et al. [2003] defined the drop penetration time for droplets to fully penetrate the bed by Equation 2.2:

$$t_p = 1.35 \frac{{V_d}^{\frac{2}{3}} \mu_l}{R_{eff} {\varepsilon_{eff}}^2 \gamma^{lv} cos\theta} \tag{2.2}$$

where V_d is the volume of the droplet placed onto the powder bed, μ is the viscosity of the fluid, R_{eff} is the effective capillary size of the pores, ε_{eff} is the effective bed voidage, γ^{lv} is the liquid-vapour surface tension and θ is the contact angle [Hapgood et al., 2003].

Equation 2.2 has been well validated for hydrophilic, homogeneous, vapour-liquid systems, but, has shown limited performance with hydrophobic formulations [Mundozah et al., 2018, 2019]. By combining the dimensionless spray flux with the proposed dimensionless drop penetration time, Hapgood et al. [2003] was able to develop a regime

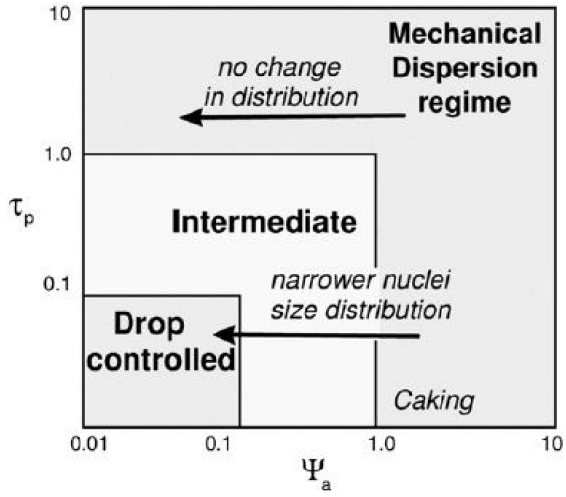

Figure 2.6: The nucleation regime map proposed in Hapgood et al. [2003] which plots dimensionless spray flux against the dimensionless drop penetration time.

map which quantifies nucleation types for a given process. The dimensionless drop penetration time is defined as:

$$\tau_p = \frac{t_p}{t_c} \tag{2.3}$$

where t_c is the residence (circulation) time for a quantity of powder to enter and leave the spray zone. With this definition, a regime map which proposes three distinctive regimes was developed (Figure 2.6).

The three regimes identified are the drop controlled regime, intermediate and mechanical dispersion regime:

1. The drop controlled regime is often described to be the preferential regime to design a process within [Litster, 2016]. This is because there is a one-to-one relationship with the drop size distribution of the nuclei size distribution, ensuring easily predictable growth behaviour.

2. The intermediate regime is currently poorly understood. The regime is sensitive to changes in process parameters or formulation thermodynamics, which can lead to significant changes to the nuclei size distribution and overall product output.

3. The mechanical dispersion regime is where the nuclei size and liquid distribution become independent to the spray conditions and is determined by the mechanical mixing conditions of the particle bed (for example by impeller) [Hapgood et al., 2003].

The regime map is a useful tool for understanding the process as it allows for insight on the current processing conditions and product formulation. The regime map is limited in developing any quantitative understanding around the final product after granulation. It is suggested that it is used as a tool exclusively for the nucleation behaviour to ensure reasonable bed and spray dynamics.

Hapgood et al. [2004] extended the work by adopting a Monte-Carlo method to model a spray which produces droplets which form nuclei. The model calculated the nuclei distribution through the drop controlled regime into the transition regime, providing quantitative analysis on the effects of spray and process parameters. The model is limited at high spray fluxes due to the statistical limitations of not encompassing droplet overlap behaviour [Wildeboer et al., 2005].

Further to this work, a nuclei size distribution model was proposed as the Poisson distribution model Hapgood et al. [2009]. The model incorporated the dimensionless spray flux as the core variable and is shown as Equation 2.4:

$$P_n = \exp(-4\Psi)\frac{-4\Psi^n}{(n-1)!} \tag{2.4}$$

where P_n is the probability of a nuclei to form by n drops. The nuclei diameter at any given time t is calculated from the following relationship in Equation 2.5; initially proposed by Hounslow et al. [2009] and is modified to include the number of drops for an immersion nucleation scenario:

$$d_n = nd_d\left(1 + \frac{1-\phi_{cp}}{\phi_{cp}}\sqrt{\frac{t}{t_p}}\right) \tag{2.5}$$

where d_n is the nuclei diameter, d_d is the droplet diameter, ϕ_{cp} is the critical packing liquid volume fraction and t_p is the drop penetration time. Equations 2.4 and 2.5 provides a framework to predict the nuclei size in any given system where the droplet size is much larger than the primary particle size. However, this model ignored the breakage and distribution of the nuclei. To include such phenomena, the Poisson distribution model (Equation 2.4) was expanded to include the Stokes deformation number as a controlling parameter for nuclei breakage [Liu et al., 2013]. The Stokes deformation number is defined as Equation 2.6:

$$St_{def} = \frac{\rho_g {v_c}^2}{2\delta_p} \tag{2.6}$$

where ρ_g is the granule density, v_c is the impact velocity and δ_p is the dynamic strength of the granule. The Stokes deformation number provides a criteria for nuclei

breakage. If $St_{def} > St_{crit}$ then this would lead to successful breakage. The nuclei size distribution function with breakage is defined as:

$$n(v) = \frac{\int_v^\infty (St_{def})^p u^{q-1} n'(u) du}{(St_{def})^p v^q} \tag{2.7}$$

where $n'(u)$ is the initial nuclei distribution, p and q are empirical fitting parameters. While this is certainly a step in the right direction to encompass greater detail in nuclei formation and distribution, it is arguable that as the model uses the Hapgood et al. [2009] model for nuclei formation probability, the inherent limitations of spray fluxes generally greater than $\Phi > 0.5$ were apparent. Further validation work is necessary for understanding the mechanical dispersion regime.

Up to now, the models that have been described detail the mechanistic behaviour for immersion-type nucleation only. Distribution nucleation has seen comparatively little work. Pioneering work by Kariuki et al. [2013] proposed a dimensionless number, the particle coating number, which quantifies the particle wetting behaviour during distribution nucleation. The particle coating number, ϕ_p, is shown as Equation 3.11:

$$\phi_p = \frac{6 x_{LS} a_d}{\pi d_p^3 \rho_d A_{SA}} \tag{2.8}$$

where x_{LS} is the liquid to solid ratio, A_{SA} is the specific surface area (of some given roughness and geometry) and a_d is the spherical area of a given particle with a diameter d. The coating number is the ratio of the theoretical area coated by droplets against the total surface area of the particle. The model was validated and provided numerical insight on the extent of coating for particles. The model has yet to seen use in any extensive population balance model, but, shows promising ability to help characterise whether distribution nucleation occurs during granulation.

Nucleation in population balance models is largely treated as a source term for small particles [Hounslow et al., 1988, Kumar and Ramkrishna, 1997]. In its simplest form, the population balance equation for nucleation can be trivially written as Equation 2.9:

$$\frac{dn(v,t)}{dt} = B_{nuc}(v) \tag{2.9}$$

Equation 2.9 simply represents the rate of change of number density at a rate of B_{nuc}. A common approach for nucleation is to consider it as a process which adds nuclei to the gridpoint of a given distribution. This is expressed as Equation 2.10 [Hounslow et al., 1988]:

$$B_{nuc}(v) = N_0 \delta(v - v') \tag{2.10}$$

where v' is the desired volume of particle (of usually the first gridpoint), δ is the dirac delta function and N_0 is the number of particles added to the size class. This expression suggests that any nuclei formed must be of the smallest size class and therefore are treated as some source into the smallest boundary. This expression has some considerable limitations. Given the current form, the nuclei input is fixed to a specific size class. Nuclei formed are often distributed in size, liquid content and powder content which this model cannot physically represent.

Hounslow et al. [2009] developed a mechanistic description for the growth of a nuclei as particles are "added" to a drop. For planar geometry, it is written as Equation 2.11:

$$v = \frac{v_l}{\phi_{cp}}\left(1 - \frac{1-\phi_{cp}}{1+\phi_{cp}}\exp\left(\frac{-4D_{eff}\phi_{cp}^2}{h_0^2}\right)\right) \tag{2.11}$$

where D_{eff} is the effective diffusivity, v_l refers to the liquid volume, v is the volume of the nuclei and h_0 is the initial thickness of the nuclei. The model is derived on the basis of deformation driven flow, where the liquid is driven to the surface by repeated deformation of the nuclei. This model was later validated in Pitt et al. [2018] showing good agreement between model predictions and experimental data. The limitations of the model are related to the high sensitivity in the critical packing factor, ϕ_{cp}, in addition to the absence of fundamental understanding on the parameter D_{eff} with regards to solid-liquid diffusive flow. In this case, these parameters are treated as adjustable and must be fitted.

Poon et al. [2008] developed a mechanistic nucleation model for the use in a three dimensional population balance by using a spreading coefficient analogy. This is written as Equation 2.12:

$$k_{nuc}(s,l,g) = A_0\dot{Q}e^{\lambda/RT} \tag{2.12}$$

In this equation, A_0 is an adjustable parameter, $\dot{Q}$ is the volumetric flowrate of the spray, λ is the spreading coefficient, R and T the ideal gas coefficient and gas temperature respectively. The model treated the primary particles and nuclei as separate phases. A mass balance was written as Equations 2.13 and 2.14 to describe the growth and disappearance of the nuclei and primary particle phases by two coupled population balance models:

$$\frac{dN_{nuc}}{dt} = k_{nuc}(s,l,g) \tag{2.13}$$

$$\frac{dN_{primary}}{dt} = -k_{nuc}(s,l,g)N_0 x(s,l,g) \tag{2.14}$$

where $N_{primary}$ is the number of primary particles, N_0 is the initial particle count and x is the fraction of primary particles within the nuclei. The model is limited due to the assumed dynamics of the liquid penetration and spreading, where some key assumptions are:

- The droplets are well spread and do not overlap.
- If existing particles are present in the system, they will only receive binder if the droplets do not wet the bed quickly and do not penetrate into the bed quickly.

As a result of the assumptions, the model does not describe the drop formation and spreading/penetration dynamics of nucleation, where authors have shown importance to these dynamics, i.e. Hapgood et al. [2003], Wildeboer et al. [2005].

Bellinghausen et al. [2019] proposed an alternative approach to predict the nuclei size distribution by expanding on the works of Hapgood et al. [2004] and Wildeboer et al. [2005]. The author suggested that the nuclei size distribution can be modelled using a log-normal distribution given as Equation 2.15:

$$f'_m(d'_n, \mu_n, \sigma_n) = \frac{1}{d'_n((s_1\sigma_x + s_2)\Psi_n + s_3)\sqrt{2\pi}} \times \exp\left(\frac{(\ln(d'_n - ((m_1\sigma_x + m_2)\Psi_n + m_3)))^2}{2((s_1\sigma_x + s_2)\Psi_n + s_3)^2}\right) \tag{2.15}$$

where f'_m is the dimensionless mass density of the nuclei, d'_n is the dimensionless nuclei diameter, σ_x is the deviation of the spatial drop distribution, Ψ_n the dimensionless nucleation number and $s_1, s_2, s_3, m_1, m_2, m_3$ are fitting parameters.

A Monte-Carlo method was used to fit the adjustable parameters of Equation 2.15, which was then compared to available data within the literature. This model showed more flexibility in modelling the nuclei size distribution than that of Hapgood et al. [2004], Wildeboer et al. [2005] and Hapgood et al. [2009] - which often struggled to predict outside the drop-controlled regime. What is particularly advantageous of the model proposed by Bellinghausen et al. [2019], is the ability to integrate into other process models such as the generic population balance. This was often the limiting factor for models such as Hounslow et al. [2009] and Poon et al. [2008] where both did not offer easy implementation.

Nucleation within population balance modelling appears to be understudied, and particularly the core issue may be related to the framework where nuclei are only considered as a feed source, as opposed to a dynamic particle. The available models which incorporate multiple dimensions are largely unimplemented in any commercial format of population balance models.

2.2.2 Layering & Agglomeration

Layering and Agglomerations broadly describes the mechanism in which particles collide and interact to form a single larger particle, where it is often attributed to agglomeration (synonymous to coalescence) and layering. Fundamentally, agglomeration of wet granules is a binary process. Layering is a differential growth process where coating of successive layers of melt, solution, slurry or fine particles onto a surface wet particle results in enlargement of the coated particle.

Layering is considered in two forms; growth by layering of the liquid on the surface of the particle or by small fines (or primary particles) which accumulate onto surface wet particles. For both types of layering the population balance equation can be written as Equation 2.16:

$$\frac{dn(v,t)}{dt} = -\frac{d[Gn(v,t)]}{dv} \tag{2.16}$$

Here, G represents the layering function which would describe the physical mechanism for layered growth.

For liquid layered growth a mechanistic model proposed by Heinrich and Mörl [1999] is commonly used among many researches, this is shown as Equation 2.17 [Bertin et al., 2011]:

$$G = \frac{2m_{spray}}{\rho_p A_{tot}} \tag{2.17}$$

where m_{spray} refers to the total mass spray rate, ρ_p is the particle density and A_{tot} total particle surface area within the system respectively.

Equation 2.17 assumes that the liquid from the spray will immediately interact with every particle within the bed, where clearly for systems with sprays the liquid will only see the surface/or some fraction of a particle bed. Key dynamics such as liquid dispersion and contact spreading are ignored or assumed negligible; although such mechanisms are known to be dominant in fluidised bed coating systems [Dewettinck and Huyghebaert, 1999, Hemati et al., 2003]. Despite the limitations, the biggest advantage here is the lack of adjustable parameters; a true mechanistic model.

Where most growth functions for liquid layered growth will include a term related to the spray rate, growth functions which describe layering by fines must then intuitively include a term that includes total mass of fines and particles. Cameron et al. [2005] proposed a mechanistic growth model for layering by fines as shown by Equation 2.18:

$$G = G_m \frac{M_{fines}}{kM_{granules} + M_{fines}} \exp[-a(x_w - x_{wc})^2] \tag{2.18}$$

Where G_m is the maximum growth rate of the system, M_{fines} is the total mass of fines, $M_{granulate}$ is the total mass of granules, x_w is the moisture content of the granule, x_{wc} is the critical moisture content of the granule and k and a are fitting parameters which relate to the kinetics.

Equation 2.18 describes the growth by layering to be proportional to the number of fines in the system in relation to the overall granule mass. This intuition makes sense and studies by Barrasso [2015] have shown that this model performs well for twin-screw granulation systems. Notably, this model also has a term for moisture content, hence, for this model to be useable it requires implementation within a multi-dimensional model with at least two granule co-ordinates, particle diameter and particle moisture content. The key weaknesses here are the use of fitting parameters to describe kinetic behaviour that may deviate from formulation and processes.

Sayin [2016] proposed a model as an extension of Cameron et al. [2005]. The model proposed is shown as Equation 2.19:

$$G = \begin{cases} k\lambda, & \frac{M_{fines}}{M_{total}} > w_{p,crit} \\ k\frac{M_{fines}}{M_{total}}\lambda & \frac{M_{fines}}{M_{total}} \leq w_{p,crit} \end{cases} \tag{2.19}$$

Where λ is the liquid height at the surface of a particle, k is the layering rate constant and $w_{p,crit}$ is the critical fine powder mass fraction. The model extends from Cameron et al. [2005] by taking into account the over-excess of fines in relation to the liquid availability. This allows for more dynamic behaviour with regards to powder input and growth, where if the critical fines fraction is exceed then the system will grow at the rate of the maximum, k. Still, in this case two fitting parameters are needed for k and $w_{p,crit}$.

Agglomeration has been rigorously studied with many models implmeneted into various forms of population balance models. Based on the fundamentals, for agglomeration to occur a criterion was determined by [Ennis et al., 1991] where the

phenomenon is controlled by the viscous Stokes number, St_v:

$$St_v = \frac{4\rho_g U_c d_g}{9\mu_l} \tag{2.20}$$

The viscous Stokes number is the ratio of viscous dissipation to the kinetic energy at a binary particle collision, where U_c is the collision velocity. The criterion for agglomeration is [Ennis et al., 1991]:

$$\begin{aligned} St_v < St_v^* \quad &\text{coalescence} \\ St_v > St_v^* \quad &\text{rebound} \end{aligned} \tag{2.21}$$

Where the St^* is the critical viscous Stokes number which is further defined as:

$$St_v^* = \left[1 + \frac{1}{e_r}\right] \ln\left(\frac{h_l}{h_a}\right) \tag{2.22}$$

The critical viscous Stokes number provides a minimum value which the rebound velocity between two particles during agglomeration is zero. In this scenario, the terms that drive this behaviour are: e_r which is the coefficient of restitution for the surface-wet particle, h_a which is some characteristic length scale of the surface asperities and h_l is the liquid layer thickness of the particle. The criterion develops some core insight with regards to the operation of a granulation process, though it is emphasised that this model assumes no deformation of the granule. Furthermore, the assumption suggests that the model is only suitable for low shear processes.

Suppose that the average collision velocity can be measured throughout the particle bed, three distinct regimes are observed when compared to the critical viscous Stokes number. The following regimes are:

1. Non-inertial regime: the scenario where the operational viscous Stokes number is sufficiently less than the critical Stokes number, or numerically where $St_v/St_v^* \to 0$. The non-inertial regime identifies a point of operation where all collisions are successful and thus, result in coalescence.

2. Inertial regime: the scenario where the operational viscous Stokes number is close to or equal to the critical Stokes number, $St_v/St_v^* \approx 1$. This regime tends to contain granules which are approaching the critical value. Within this regime, physical inputs such as bubbling gas velocity and impeller rotation play a key role in the success of collisions between granules through inertial input.

3. Coating regime: the scenario where the operational viscous Stokes number is larger than the critical Stokes number, in other words, $St_v/St_v^* > 1$. This regime is where granule collisions do not guarantee coalescence.

The aforementioned regimes do not describe the the entire particle space. In most cases, specific regions of the process unit could be operating in different regimes. This may be due to effects of segregation, poor mixing and/or poor distribution of liquid. This creates difficulty in evaluating the dominant growth regime within the system, hence limiting the effectiveness of the viscous Stokes number as a quantitative tool for understanding the operational behaviour.

Within population balance models, agglomeration is described as a birth and death term. Equations 2.23 and 2.24 shows this mathematically [Rumpf, 1958]:

$$\dot{b}_{coal} = \frac{1}{2}\int_0^v \beta(d_p, d_p')n(d_p - d_p')n(d_p')dd_p' \tag{2.23}$$

$$\dot{d}_{coal} = n(d_p, t)\int_0^\infty \beta(d_p, d_p')n(d_p')dd_p' \tag{2.24}$$

where $\beta(d_p, d_p')$ is the rate model which physically describes agglomeration. This often encompasses information about the powder formulation and process dynamics; d_p represents the particle diameter and d_p' is the diameter of a particle which is arbitrarily less than d_p. While the internal co-ordinate of particle length is used in this case, this can be any arbitrary intensive property which can be used to describe a granule.

The majority of currently literature has focused on developing agglomeration models where $\beta(d_p, d_p')$ is expanded into forms that are dependent on core granule properties, e.g. size and liquid content. The simplest model is assuming size independent growth where all particles agglomerate at a constant rate [Rumpf, 1958, 1973]. Analogies have been made with the viscous stokes number, where growth behaviours are separated by cases for values of St_v [Liu et al., 2000, Adetayo et al., 1995]. This was adapted as a mechanistic model in Liu and Litster [2002] which set cases for type I and type II coalescence; which characterises whether the granule collisions will lead to the surfaces of the colliding granules to meet to result in deformation. The model applies a mechanistic framework for the agglomeration rate, but, was not able to predict a priori due to the need to fit adjustable parameters.

A multi-dimensional model was developed which suggested that the rate of agglomeration is a component of the size of the particle and the fractional liquid content

of the particle [Madec et al., 2003]. The model relies on the assumption that the population balance equation solved is multi-dimensional that is at least two dimensional in solid volume and liquid volume. The model had some mechanistic basis where mass is conserved during collision and liquid agglomeration rate is a function against some experimentally determined "optimum" operating liquid-to-solid ratio. The model has been used by other authors such as Barrasso [2015], Chaudhury and Ramachandran [2013], Boukouvala et al. [2013] and Prakash et al. [2013]. The model has not been extensively validated but allows liquid content to be a contributor to the growth rate as opposed to the one-dimensional expressions that are currently in the literature. This was among the first agglomeration models to integrate multiple granule co-ordinates as part of the agglomeration rate, however, it is semi-empirical in nature thus lacking a physical basis to achieve reasonable predictions.

Further agglomeration models are provided in Table 2.2 with an associated discussion.

Table 2.2: Comparisons of various agglomeration models available in the current literature.

Coalescence model	Comments
β_0	*The size independent model* assumes that growth is independent of size or any other internal parameter. Therefore, this model is only viable for systems where all particles are of a similar size and growth is linear at all time stages. In most literature it is considered as some "fixing" parameter which fundamentally has mechanistic meaning but is treated as some calibration value [Rumpf, 1958, Hounslow et al., 1988].
$\beta_0 \frac{(v+v')^a}{(vv')^b}$	*The size dependent model* relates the coalescence rate with the size of the granule. The model describes the rate of growth being more preferential for larger particles rather than smaller [Kapur and Fuerstenau, 1969]. a and b are adjustable parameters that require experimental fitting. The coalescence model is largely empirical where experimental fitting is necessary thus not being a truly predictive model. The growth model was extensively tested against a pelletisation process which showed a good level of agreement. However, the estimation of the parameters was not well detailed.
$\beta_0(v^{2/3}+v'^{2/3})(\frac{1}{v}+\frac{1}{v'})$	*The Sastry [1975] size dependent model* considers that the rate of coalescence is due to the ratio of surface area to volume for two colliding particles. For particles that have low surface areas but a large volume will agglomerate slower than for the reverse case. However, due to no tracking of particle morphology, this is averaged across all size bins. In addition, one key assumption is that the (apparent) density does not change with time, which for high shear granulation or twin screw processes is certainly not true [Djuric and Kleinebudde, 2008, Gao et al., 2002].

$\beta = \begin{cases} \beta_0 & w < w^* \\ 0 & w > w^* \end{cases}$ where $w^* = \frac{(vv')^b}{(v+v')^a} = \frac{\pi}{6}\left(\frac{16\mu}{\rho v} St^*\right)^3$	*The cutoff model* states that after a given criteria granule growth becomes zero. In this case, a loose form of the Stokes criteria is given which is related to the Kapur and Fuerstenau [1969] size dependent model. This criteria is mechanistic in nature where it is understood that for granules to coalesce they must have the internal Stokes number less than the critical [Ennis et al., 1991].
$\beta_0(v+v')^{\frac{2}{3}}\sqrt{(\frac{1}{v}+\frac{1}{v})}$	*The equipartition of kinetic energy (EKE) model* is a mechanistic expression developed by [Hounslow, 1998] which adapts the kinetic theory of gases to model the collision frequency of the granules. This expression has been primarily used within fluid bed granulators [Tan et al., 2005, 2006] as there is convicing theory that the fluid bed dynamics resemble the behaviour [Deen et al., 2007]. The model is particular useful as this gives an approach to model collision frequency rather than the rate of coalescence. In further work by Tan et al. [2005] the EKE model is combined with a coalescence likelihood model which with experimental fitting produces a model that shows good agreement for granule growth.
$\beta_0(v+v')^{\frac{2}{3}}$	*The Smouluchowski shear model* is a model that assumes the particles are in a dilute phase which are carried by the fluid stream. This in reality is vastly different for dense phase particulate systems such as in a high shear mixer. The Smoluchowski shear model is likely to have greater applicability for dilute crystallisation systems or aerosol processes [Darelius et al., 2005].
. $\beta = \begin{cases} \beta_1 & \text{Type I coalescence} \\ \beta_2 & \text{Type II coalescence} \\ 0 & \text{Rebound} \end{cases}$	This model was developed and validated in Liu and Litster [2002] within a drum granulation process. For Type I and Type II coalescence the rate of agglomeration is different given the viscous Stokes criteria further detailed in Liu et al. [2000]. The model is mechanistically based and generally has found good agreement with experiments, albeit, overestimating the oversized particles.

$\beta_0 \int_{-\infty}^{St^*} f(\phi, t) d\phi$	This model was originally developed for an industrial continuous fluid bed by Cryer [1999]. The model translates the calculations of particle size into a distribution of viscous Stokes number ($f(\phi, t)$), where the critical viscous Stokes number is a variable that transitions over time by a parameterised function. The model is semi-mechanistic in the sense that it states that all particles under the critical stokes number can agglomerate, but empirical as the viscous Stokes number is given a normal distribution through a polynomial chaos expansion. This expansion was also performed of the particle diameter (where the harmonic mean between a two particle collision is not an average of the mass) and the collision velocity.
$\beta_0(v + v') \cdot$ $\left(\left(l(v) + l(v') \right)^a \left(1 - \frac{l(v) + l(v')}{2} \right)^b \right)^a$	*The Madec et al. [2003] model* is a multi-dimensional model which considers the growth rate by particle size and liquid composition. the parameter b is a consolidation term and a is a random variable where both parameters are experimentally fitted. This model is quite powerful in that it combines the growth rates from two major contributors in particle growth the size and liquid content. Though in this case, the liquid content is only the composition. No account for surface liquid is considered. Though for suspension processes, this model is more likely applicable (as this was originally developed for such processes) due to the over-saturation of liquid within the particle geometry. It is necessary to use a population balance which tracks both size and liquid for this model to be used.

$\beta_0 \psi_{i,j} d_{p,4,3}^{\gamma} (v + v')^{\frac{2}{3}} \sqrt{\left(\frac{1}{v} + \frac{1}{v'}\right)}$	The model developed by Rajniak et al. [2009] combines multiple aspects which contribute to the likelihood for coalescence. The parameter $\psi_{i,j}$ is the success factor which is composed of a geometric likelihood function and a physical success function that is related to the viscous Stokes criteria. By incorporation of some key mesoscale phenomena, the model is rather sophisticated but requires a lot of inputs from external calculations. The author, Rajniak et al. [2009], utilised a coupled CFD model to calculate some of these core physical parameters, where if a pure population balance model is used a majority of these parameters will become unknown variables.

2.2.3 Breakage & Attrition

Differential size reduction is attributed to attrition. Attrition is the process of small fragments that are chipped from the surface which reduces the effective volume of the particle, but in this case further small particles are added into the particle population which is often treated as internal nucleation.

In population balance models, attrition is considered to be the opposite of differential growth. An analogous form can be written as Equation 2.25 [Bertin et al., 2016]:

$$\frac{dn(v,t)}{dt} = \frac{d[G_{attr}n(v,t)]}{dv} \tag{2.25}$$

The function G_{attr}, like layered growth, is the function which defines the physical form of the phenomena within the population balance framework. The typical form which G_{attr} takes is written as Equation 2.26 [Tan et al., 2004b]:

$$G_{attr} = \frac{dv}{dt} = -S(v)\varphi \tag{2.26}$$

where S(v) is the apparent attrition rate of granule size v and φ is the average mass of an attrition fragment.

The average mass of an attrition fragment is considered to be distributed property, and has been frequently chosen to be the initial primary particle distribution [Hounslow et al., 1988, Heinrich et al., 2002, Tan et al., 2004b, Bertin et al., 2016]. Tan et al. [2004b] justifies the assumption by stating that attrition particles are often at sizes comparable to the primary particles. Consequently, $S(v)$ can be rewritten in terms of particle length in which the fragmentation function $S(v)$ can be defined by the initial size distribution. This is written as Equation 2.27:

$$S(v) = \frac{S_0\bar{d}_{p0}(\bar{d}_{p0}^{\,2} + 3\sigma_0^2 l^{q-2})}{3} \tag{2.27}$$

given that S_0 is some breakage rate constant, $\bar{d}_{p0}$ is the mean granule diameter of the initial particle size distribution, σ_0 is the standard deviation of the length based particle size distribution and q is a parameter that signifies the order of size dependence.

The resulting mass of fragments will result in the initial particle size distribution of equal mass to the fragments. This effectively results in some apparent nucleation term (this can also be read as a mass input). In doing so, a semi-mechanistic form for attrition is developed.

Breakage or fragmentation are modelled by a birth and death term within population balance models. This form of breakage is not considered as a differential size reduction, as the breakage will result in a significant size reduction with the production of fragments, where the volume is typically assumed to be conserved. Following this assumption, the birth term and death for breakage is written as Equation 2.28 and 2.29 respectively:

$$\dot{B}_{break} = \int_{v}^{\infty} \beta_{break}(v')b(v', v)n(v', t)dv' \tag{2.28}$$

and

$$\dot{D}_{break} = \beta_{break}(v)n(v, t) \tag{2.29}$$

where β_{break} is the breakage rate constant and $b(v', v)$ is the resulting breakage fragment distribution function.

These two parameters define the breakage behaviour within population balances models, where largely empirical models have been developed [Austin et al., 1976, Austin and Klimpel, 1984, Hounslow et al., 2001, Vogel and Peukert, 2004]. Most of these models were initially proposed for milling processes. Currently, breakage in literature is still often treated as an analogy from milling. This has inherent limitations due to the normal operation of mills being dry, where for wet granulation the strength of the granule is dictated by a large amount of factors, in particular; the viscous forces of the liquid bridges and processing environment that is largely different to that of mills. Hounslow et al. [2001] performed tracer studies within a high shear mixer to validate a simple breakage model. The model suggested that mother particles would break and result in two equally sized daughter particles; essentially being among the simplest breakage models available in the current literature for granulation. Despite the simplicity, it was found to be effective in predicting breakage behaviour in works of Tan et al. [2004b, 2005].

Many additional breakage models have been proposed recently, in works such as Ramachandran et al. [2009], Pradhan et al. [2017], Hayashi and Watano [2019], Wang et al. [2020, 2021]. These have seen plenty of success within high shear and twin screw granulators. Modern fluidised bed models tend to ignore breakage, or use the simple linear breakage model as proposed by Tan et al. [2004b].

2.2.4 Co-dynamics of Rate Mechanisms

Population balance models integrate the granulation mechanisms by combining all the relevant birth and death terms into a single continuous form. Emphasis is placed

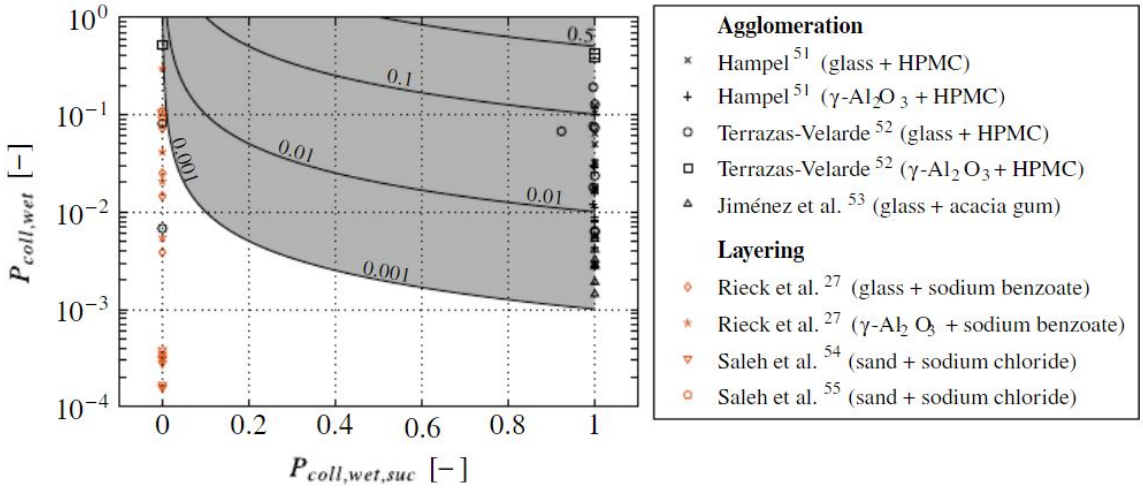

Figure 2.7: Probability of wet collisions versus the probability of successful wet collisions from Rieck et al. [2020].

into choosing a rate model for the birth and death terms which best describes the type of growth or breakage. This results in a model framework where terms such as agglomeration and breakage plug-in and out rate equations without much thought on how these rate models affect one another. If we consider the fluidised bed granulator, if the inlet fluidisation air is increased to a large value then it is expected that the rate of breakage and attrition is increased, the rate of agglomeration decreases. With the current state of rate models and the way they are used, most cannot represent those respective changes; which in the current state of the literature, is because of the lack of physically based multi-dimensional models and framework.

Ensuring a model can physically represent co-dynamic mechanisms are important to maintain flexibility of the model design space. This is particularly important for granulation where mechanisms such as liquid-layered growth or agglomeration compete with one-another depending spray and drying conditions. As such, the rate models must encompass those effects to accurately predict whether the system should; take off due to agglomeration or grow slowly by layering.

Rieck et al. [2020] pioneered an approach to determine the dominant growth mechanism within a fluidised bed process. Here, it was suggested that if the Stokes criterion is used (see Equation 2.21) to predict the likelihood of coalescence, and if the frequency of wet collisions is known then the probability of successful collisions can be calculated. Rieck et al. [2020] proposed that if the probability exceeds 0.001 then agglomeration would become dominant. Figure 2.7 shows how experimental data from the literature compares to the predictive model.

The work is still limited in terms of integrating this format into the population balance framework. The probability of collision here was treated as an adjustable value where the successful collisions were calculated on the basis of the Stokes criterion. To integrate the ability to model the co-dynamics, there is a need to ensure both the collision rate and success are calculated as part of the rate model. This can open the avenue to model the co-dynamics of layering and agglomeration as competitive processes. To achieve this would require the appropriate population balance framework that is multi-dimensional in at least particle length and liquid volume.

2.3 Multi-dimensional Population Balance Models

This section will cover the overall framework of multi-dimensional population balance models and the implementation within current literature. A key focus will be on the chose granule co-ordinates the authors have chosen to model as well as the rate models used to simulate the process.

2.3.1 Framework of a Multi-dimensional Population Model

Multi-dimensional population balance models have become increasingly popular due to larger computational resources becoming more available. Multi-dimensional models are typically considered to be superior to that of a one-dimensional model due to the ability to track multiple distributed granule properties and therefore can model more complex phenomena and behaviours [Iveson, 2002]. Examples of the types of properties tracked are described in Ramkrishna [2000] and is listed as; the particle length, liquid volume of a particle, gas volume of a particle, masses of the components within a granule, the age of the particle, shape and potentially more.

Commonly, multi-dimensional population balance models tracks the mass of solid, liquid and gas as these are the most commonly observable properties of granule; by measurement of mass, moisture content and porosity. The general form of the three-dimensional population balance for a framework such as this is written as Equation 2.30 [Litster, 2016]:

$$\begin{aligned}\frac{\partial n(s,l,g,t)}{\partial t} + \frac{\partial \left[G_{layer} n(s,l,g,t)\right]}{\partial s} + \frac{\partial \left[G_{wetting} n(s,l,g,t)\right]}{\partial l} \\ + \frac{\partial \left[G_{cons} n(s,l,g,t)\right]}{\partial g} = \dot{B}(s,l,g,t) - \dot{D}(s,l,g,t)\end{aligned} \tag{2.30}$$

where s is the total solid mass, l is the total liquid mass and g is the total gas mass of the granule, $n(s, l, g, t)$ is the population density of the granule described by the respective component property over time, and $\dot{B}$ and $\dot{D}$ are the birth and death terms which would represent the granulation phenomena agglomeration, breakage and nucleation. The three growth terms would represent the differential growth phenomena such as solid layering, wetting (liquid layering) and gas consolidation [Immanuel and Doyle Iii, 2003, Poon et al., 2008, Ramachandran and Barton, 2010, Sen and Ramachandran, 2013, Barrasso, 2015].

The volume of the granule (and therefore length) can be calculated by taking the additive sum of all three masses and dividing the total mass by the composite density [Barrasso and Ramachandran, 2012, Barrasso, 2015, Muddu et al., 2018]. This is shown as Equation 2.31:

$$v = \frac{s + l + g}{\rho_{comp}} \tag{2.31}$$

where v in this case is the volume of the granule which is composed of s, l, g and ρ_{comp} is the composite density.

This framework has been implemented for multiple types of granulation processes and have shown to be a robust approach to modelling multiple granule dimensions [Immanuel and Doyle Iii, 2003, Poon et al., 2008, Li et al., 2012, Barrasso, 2015, Chaudhury et al., 2015, Ismail et al., 2020b]. However, this is at the expense of significant computational costs.

Importantly, a multi-dimensional population balance model is capable of modelling the differential growth processes independently of the respective granule component as opposed to the summative result used in one-dimensional population balance models. This is advantageous as it allows for the isolation of, and emphasis to, the respective mechanisms across the particle distribution.

To model agglomeration, Equation 2.23 is expanded to include all distributed granule co-ordinates. The general form for the birth and death equation for the three-dimensional agglomeration model is written as Equation 2.32 and Equation 2.33 [Ramkrishna, 2000, Barrasso, 2015]:

$$\begin{aligned} \dot{B}_{agglom} = \frac{1}{2} \int_0^s \int_0^l \int_0^g \beta(s - s', l - l', g - g', s', l', g') \\ \times n(s - s', l - l', g - g', s', l', g', t) n(s', l', g', t) dg' dl' ds' \end{aligned} \tag{2.32}$$

$$\dot{D}_{agglom} = n(s,l,g,t)\int_0^\infty\int_0^\infty\int_0^\infty \beta(s-s',l-l',g-g',s',l',g') \times n(s',l',g',t)dg'dl'ds' \tag{2.33}$$

where s, l, g maintain the same definition and s', l', g' is the particle which is arbitrarily smaller than s, l, g of the respective granule co-ordinate.

The framework here allows for more physically representative models to be implemented as it allows tracking of properties which are relevant to the granule mechanism [Iveson, 2002]. Many reseaches suggest that liquid content is an important property to include within an agglomeration model; which a one-dimensional model is unable to achieve [Hemati et al., 2003, Tan et al., 2006, Vreman et al., 2009, Bertin et al., 2011, Barrasso and Ramachandran, 2012, Chaudhury et al., 2014] .

Similarly, breakage can be expanded into a multi-dimensional framework by expanding on Equations 2.28 and 2.29. This forms both Equations 2.34 and 2.35:

$$\dot{B}_{break} = \int_0^\infty\int_0^\infty\int_0^\infty \beta_{break}(s',l',g')b(s',l',g's,l,g)n(s',l',g',t)dg'dl'ds' \tag{2.34}$$

$$\dot{D}_{break} = \beta_{break}(s,l,g)n(s,l,g,t) \tag{2.35}$$

This framework was applied by various authors and validated against experimental data for multiple granulation processes and have found success in predicting the size distribution [Braumann et al., 2007, Li et al., 2012, Barrasso and Ramachandran, 2012, Chaudhury et al., 2014, 2015]. However, there was less success in tracking such as moisture content and porosity. This is attributed by the authors to the lack of physically representative models available in literature and poor validation tools which cannot measure the respective distributed properties [Barrasso and Ramachandran, 2012, Barrasso, 2015, Muddu et al., 2018].

2.3.2 Model Reduction of Multi-dimensional Models

Multidimensional models are computationally intensive and are difficult to use [Ramachandran and Barton, 2010]. From an industrial stand-point, complexity is unattractive for internal integration. Biggs et al. [2003] proposed a multi-dimensional population balance model which retained aspects of the traditional multi-dimensional model, but, could be solved as a series of one-dimensional population balance equations; a reduced order model. To convert the multi-dimensional model to a series of coupled one-dimensional equations, a two assumptions are necessary:

- The granule property is equally distributed over all granules for any given size range, and
- The granule property is equally distributed within any granule

With these assumptions, the reduced order form for size and any other intensive granule property can be written as Equation 2.36 and Equation 2.37:

$$\frac{\partial n(v,t)}{\partial t} = -\frac{\partial [Gn(v,t)]}{\partial v} + \dot{B}(v,t) - \dot{D}(v,t) \tag{2.36}$$

$$\frac{\partial M(v,t)}{\partial t} = -\frac{\partial [M(v,t)]}{\partial v}\frac{dM(v)}{dt} + \dot{B}(v,t) - \dot{D}(v,t) \tag{2.37}$$

where $n(v,t)$ represents the number distribution as a function of size and time, and $dM = M(v,t)$ is the mass of the intensive property (such as liquid volume or gas volume) within the size range $(v, v+dv)$ [Biggs et al., 2003].

The particular advantage here is that we retain the ability the model the multiple dimensions of a granule but at a computational cost which is similar to that of a one-dimensional model. Notably, we also retain the ability to model the differential growth of each individual component separately; layering, wetting and consolidation are treated as separate growth properties within their respective lumped distributions. Hounslow et al. [2001] advises against using the intensive properties to model the rates. However, this framework has seen success in predicting the intensive properties in works such as Biggs et al. [2003], Barrasso [2015], Bellinghausen et al. [2019], Bellinghausen [2021]. The authors suggest that the framework is appropriate given that the rate models physically represent the intensive properties that are relevant to the granulation mechanisms.

2.3.3 Compartmentalised Frameworks

Population balance models are often assumed that the particles are well-mixed within the space of the equipment. This means that phenomena such as segregation and internal mixing are ignored entirely [Hounslow, 1998]. In recent literature, an approach known as model compartmentalisation has become increasingly popular as a way circumvent the well-mixed assumption to emphasise rate processes which depend on spatial properties [Li et al., 2012, Liu and Li, 2014, Lee et al., 2017, Wang et al., 2021].

Compartmentalisation is the method of distributing the spatial co-ordinates of the bed into discrete points. In fact, this is analogous to the concept of how a plug

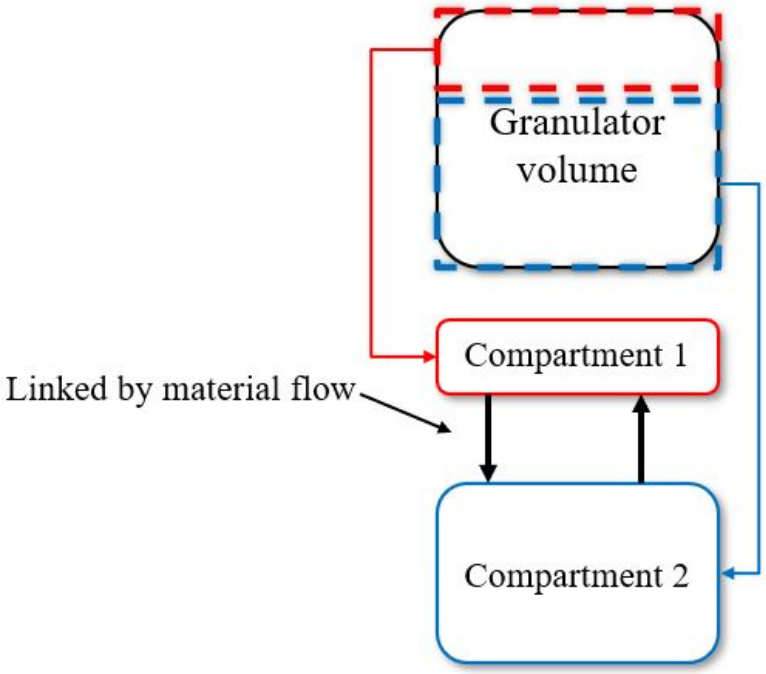

Figure 2.8: Generic process of compartmentalisation an equipment volume into two discrete compartments

flow reactor can be treated as an infinite series of stirred tank reactors [Chaturbedi et al., 2017, Ismail et al., 2020a]. Figure 2.8 shows how a single granulator volume can be converted into two discrete regions, compartment one and two.

Compartmental models have seen plenty of success in validating experimental studies in works such as Börner et al. [2013], Hussain et al. [2014], Barrasso [2015], Muddu et al. [2018]. These authors repeatedly discussed that by separating the volume of the particle bed which interacts with the spray, the model tends to perform better in predicting agglomeration. In particular, Kaur et al. [2019] shows that by manipulating the volume of the compartment, the effect of mechanisms such as agglomeration and breakage can have dramatic changes on the model outputs; which introduces a new parameter to improve model accuracy.

Compartmentalisation allows for the improved treatment of rate processes for a given equipment volume. However, most models fail to treat the spray with appropriate attention, and often, most current literature fail to integrate more than one granulation mechanism within a compartmental framework [Li et al., 2012, Lee et al., 2017, Liu and Li, 2014].

Figure 2.9 suggests three main compartments, spray drying, wetting and bulk particle bed. Here, the spray drying compartment would encompass the volume of

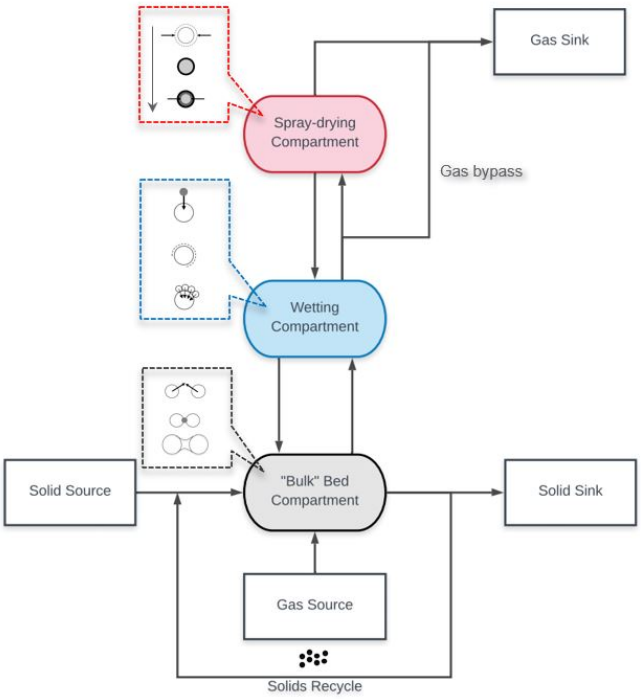

Figure 2.9: A proposed approach for a three-compartmental model of top-spray fluidised bed granulation

the spray and the mechanisms of spray drying. The wetting compartment would include the volume of the particle bed that is in contact with the spray and would include any wetting or layering mechanisms that are part of the droplet/particle mechanisms. The bulk particle bed would then include the volume of the remaining particle bed in addition to all other relevant mechanisms such as agglomeration, drying and breakage. The material flow rate from the bulk particle bed compartment to the wetting compartment is more difficult to define. Börner et al. [2013] and Kaur et al. [2019] suggest describing the flow based on the relative volume of two compartments. This can be calculated by Equations 2.38 and 2.39:

$$\alpha = \frac{V_1}{V_1 + V_2} \tag{2.38}$$

$$t_1 = \frac{V_1}{\dot{Q}}, \quad t_2 = \frac{V_2}{\dot{Q}} \tag{2.39}$$

where α is the volume ratio of the compartments, V_1 and V_2 are the volumes of the individual compartments, t_1 and t_2 are the respective residence times, and $\dot{Q}$ is the volumetric flow rate of the particle. If the volume ratio is set as an adjustable parameter, then appropriate value for the volumetric flow rate is necessary. For any

fluidised bed this can be satisfied by a turbulent free model found in Truckenbrodt [2008] and Börner et al. [2013].

2.4 Conclusion

There has been significant progress in developing a mechanistic understanding of the rate processes which drive fluid bed granulation. The understanding of the process tends to be overly-specific, as the growth mechanisms studied tend to be fixed by the process conditions. This has lead to limited attempts to unify the mechanisms to build a generalised model; in which there must be significant improvements.

Population balance frameworks are moving quickly away from the classical one-dimensional framework to a multi-dimensional framework. This is primarily due to improved computing resources and valuable tools to simplify and reduce complexity. While the modelling framework can integrate more intensive granule properties as part of the rate models, there has been very little effort in developing rate models which include these intensive properties. Therefore models within the current literature choose continue to use one-dimensional rate models. There is a strong demand to integrate a multi-dimensional, physically relevant rate model for all granulation mechanisms.

Compartmentalisation is particularly popular to help reduce the effects of the well mixed assumption. Most models use two-compartmental approaches to discretise the particle bed, but, very little focus on the spray. One compartment typically involves the mechanisms which the particle-spray interacts and the other bulk drying, breakage and agglomeration. Compartmental models show strong promise in modelling agglomeration and breakage systems where additional control is provided by the volume of the compartments. A particular issue is determining the material flow between compartments where this knowledge can be limited for specific granulators. In the case of a fluidised bed, there are a plethora of studies which investigate flow and are readily available. Building a compartmental model for the spray has yet to be studied and integrated within the literature and should be a focus to improve the understanding of equipment dynamics.

Chapter 3

Development of a Mechanistic Growth Model for Liquid Layering in Fluid Bed Granulation

3.1 Introduction

Within the domain of population balance modelling, growth by liquid layering, or equally, by primary particles is described by an analogous advection equation in one dimension. This is shown as Equation 3.1:

$$\frac{dn(v,t)}{dt} = -\frac{d[Gn(v,t)]}{dv} + \dot{Q}_{in}n(v,t) - \dot{Q}_{out}n(v,t) \tag{3.1}$$

The volume density function is represented by $n(v,t)$ for any reasonable internal co-ordinate v (typically solid, gas, liquid), G is the kinetic growth model and $\dot{Q}$ is the volumetric flowrate of the particle either in or out of the system. The kinetic function, G, can be further expressed as Equation 3.2:

$$G = \frac{dv}{dt} \qquad G(n) = 0 \tag{3.2}$$

where the final boundary of v is 0 given n grid co-ordinates (to ensure there is no growth out of the grid).

The issue among a majority of kinetic growth models is the reliance on the assumption that the spray will interact with all size classes of the particle bed at equal rates, in other words, the interaction is well-mixed. A well-mixed assumption is not capable of capturing the physical phenomenon that is observed in many practical industrial scenarios. However, the necessity to make such an assumption lies with the inherent population balance framework. As a majority of published models dynamically calculate the distributed solid volume/mass key granule properties, such

as liquid and gas content, are not available as functional properties for a physically representative kinetic model.

3.2 Multi-dimensional Population Balance Model For Layering

To track multiple dimensions of a granule, a class of population balance equations have been proposed by multiple authors [Barrasso and Ramachandran, 2012, Biggs et al., 2003, Ding et al., 2006, Ramkrishna, 2000]. The form of a three-dimensional population balance, which encompasses the solid, liquid and gas volumes of the granule can be represented by Equation 3.3:

$$\frac{\partial n(s,l,g,t)}{\partial t} = -\left[\frac{\partial n(s,l,g,t)}{\partial s}\frac{ds}{dt} + \frac{\partial n(s,l,g,t)}{\partial l}\frac{dl}{dt} + \frac{\partial n(s,l,g,t)}{\partial g}\frac{dg}{dt}\right] + \dot{Q}_{in}n(s,l,g,t) - \dot{Q}_{out}n(s,l,g,t) \tag{3.3}$$

Where $n(s,l,g,t)$ is the population density which describes the granule of the vector $[s,l,g]$, where s, l, g are the solid, liquid and gas volumes respectively. A multi-dimensional model is capable of calculating all the granule co-ordinates as a distributed properties; for increased computational costs. Studies performed by Barrasso [2015] showed that for each individual co-ordinate added to the granule vector, the time taken to compute the result increased ten-fold per ten gridpoints. Therefore, it is often discussed that the conventional multi-dimensional population balance model is quite impractical for industrial use.

Hounslow et al. [2001] proposed a reduced-order scheme to calculate multiple dimensions of a granule while having the computational cost similar to a one-dimensional model. A reduced order model, calculates the multiple dimensions by coupling sets of one-dimensional population balance equation. For each granule co-ordinate, one set of population balance equations are added. The framework assumes that within a single granule size class, all granules would share the same liquid content, gas content and/or similar. Therefore, a simplification of the multi-dimensional population balance can be achieved. The mathematical form of a reduced order form follows in Equation 3.4:

$$\begin{aligned}\frac{\partial n(v,t)}{\partial t} &= -\frac{\partial[Gn(v,t)]}{\partial v} + \dot{Q}_{in}n(v,t) - \dot{Q}_{out}n(v,t)\\ \frac{\partial M(v,t)}{\partial t} &= -\frac{\partial[GM(v,t)]}{\partial v} + \dot{Q}_{in}M(v,t) - \dot{Q}_{out}M(v,t)\end{aligned} \tag{3.4}$$

Where $n(v,t)$ is the population distribution of co-ordinate v (often solid volume, mass or length) and $M(v,t)$ is the secondary distribution of the secondary granule co-ordinate, e.g. liquid volume or gas volume. While the model solution is simplified, it is not equivalent to the full multi-dimensional form and multiple authors warn against using additional granule co-ordinates for the use in kinetic models and rate expressions [Biggs et al., 2003, Barrasso, 2015]. However, the balance between computational cost and speed of a reduced-order model provides a good platform for wide-spread implementation.

3.3 Model Development and Implementation

The fluid bed granulator was discretised into a three co-ordinate system with a set of coupled one-dimensional population balance equations. By modifying Equation 3.4 the internal granule co-ordinates which are modelled are the solid, liquid and gas volumes.

$$\frac{\partial s(v,t)}{\partial t} = -\frac{\partial [G_{layer} s(v,t)]}{\partial v} + \dot{Q}_{in} s(v,t) - \dot{Q}_{out} s(v,t) \tag{3.5a}$$

$$\frac{\partial l(v,t)}{\partial t} = -\frac{\partial [G_{wetting} l(v,t)]}{\partial v} + \dot{Q}_{in} l(v,t) - \dot{Q}_{out} l(v,t) \tag{3.5b}$$

$$\frac{\partial g(v,t)}{\partial t} = -\frac{\partial [G_{cons} g(v,t)]}{\partial v} + \dot{Q}_{in} g(v,t) - \dot{Q}_{out} g(v,t) \tag{3.5c}$$

Here $s(v,t)$, $l(v,t)$ and $g(v,t)$ are the solid, liquid and gas distributions against the gridpoints of size classes v. G here is separated into the three respective growth processes relevant to the granule dimension. For this model, as we are interested in the liquid layered growth over the particle surface, $G_{wetting}$ is the function we integrate which takes the form of $\frac{dl(v)}{dt}$ [Hounslow et al., 2001, Biggs et al., 2003]. Equations 3.5a - 3.5c provide the individual component balances for the properties of the granule. Therefore, the granule should be a vector of the individual components, as represented by Equation 3.6:

$$v(s,l,g,t) = \begin{bmatrix} s \\ l \\ g \end{bmatrix}^T \tag{3.6}$$

where the total volume of the granule is simply the additive sum of the individual components at a given grid point as shown in Equation 3.7:

$$v = s + l + g \tag{3.7}$$

and hence the particle diameter, d_p:

$$d_p(s,l,g) = \frac{6v}{\pi} \tag{3.8}$$

3.3.1 Development of a Kinetic Model for Liquid Layered Growth

The velocity at which the granule grows in size is dependent upon many factors. For a system which grows by an accumulation of liquid layers the key factors are:

- The size and surface area of the particle that is in contact with the spray.
- The total mass flow rate entering the particle system by spray and the distribution of the mass over the total particle bed.
- The solid composition and rheology of the liquid phase which contributes to the surface growth.
- Surface thermodynamics such as wet-ability and contact angle.

We choose to a set a control volume around a particle which has made contact with a droplet and has reached some level of surface coating. Figure 3.1 provides a schematic representation of the control volume. To develop a mass balance we must make a set of assumptions:

1. The droplet diameter is much smaller than the particle diameter such that $d_d << d_p$.
2. We assume that the liquid which enters the system by spray is a two-phase mixture of some solids and liquid content.
3. The mass distribution of the spray across the particle size distribution is only a function of the visible surface area of the particle, that is, particles of a greater surface area have a greater tendency to interact with the spray.
4. The external available liquid can be expressed purely by some critical pore saturation.

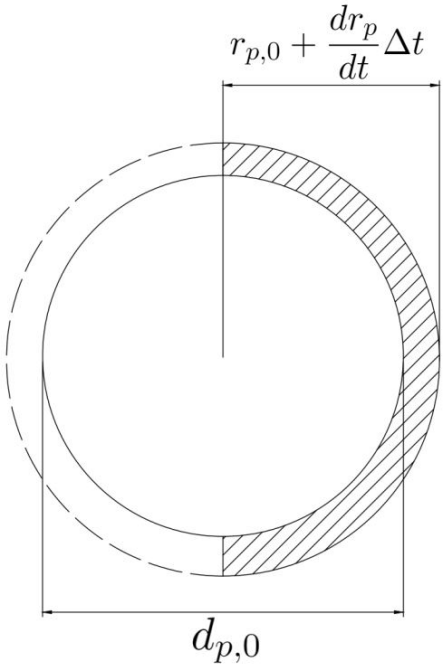

Figure 3.1: Schematic representation of the control volume for liquid layered growth around a partially wet surface [Mörl et al., 2007]

The mass balance around the wetted portion of the particle at size class v can be written as Equation 3.9:

$$\frac{dm_p(v)}{dt} = \frac{\sigma_p(v,t)A_p(v,t)}{\pi \int_0^\infty \sigma_p(v,t)d_p(t)^2 dv}\dot{M}_{spray} \tag{3.9}$$

Here, σ_p is the fraction of surface area wetted by liquid, A_p is the area of the particle, v the diameter of particle, $\dot{M}_{spray}$ the total mass flow rate of the spray entering the system and x_{spray} is the fraction of the total solids content within the liquid phase. The reader should note that the numerator refers to the total wetted surface area within a single size class across a distributed population, whereas, the denominator expresses the total wetted surface area across the entire distribution. Here, it is also considered that all of the liquid from the spray contributes to the growth of the particle, in reality, drying will be occurring simultaneously which evaporates the solvent phase of the spray. While not extensively elaborated within this section where an ideal scenario is assumed, this phenomenon is studied in-depth further in the forthcoming chapters.

The rate of change in diameter can therefore be determined by a conversion to a volume balance through the application of the appropriate chain-rule. The final

result is shown as Equation 3.10:

$$G_{wetting} = \frac{dl(v,t)}{dt} = \frac{2\sigma_p(v,t)}{\pi\rho_p \int_0^\infty \sigma_p(v,t) d_p(t)^2 dv} \dot{M}_{spray} \tag{3.10}$$

It is now necessary to define the function which determines the surface wetness of the particle, $\sigma(v,t)$. This is calculated by adapting the results from Kariuki et al. [2013] and the appropriate derivation for the proposed particle coating number, ϕ_p. From Kariuki et al. [2013] the particle coating number is defined as Equation 3.11:

$$\phi_p(v,t) = \frac{6x_{LS}a_d}{\pi d_d^3 \rho_d A_{SA}} \tag{3.11}$$

Where x_{LS} is the total external liquid on the surface of the particle, a_d is the contact area of the droplet interacting with the particle, d_d is the droplet diameter and A_{SA} is the specific surface area of the particle.

By inspection, the particle coating number indicates the ratio of area covered by droplets over the total particle area [Kariuki et al., 2013]. However, it should be noted that a_d is not simply the visible surface area of the droplet ($\frac{\pi}{4}d_d^2$) and it must therefore be further defined. The expression provided Clarke et al. [2002] for the contact area can be used if the assumption that the effects of the surface curvature is minimal. The contact area a_d is calculated by Equation 3.12:

$$a_d = \left(\frac{3V_d\sqrt{\pi}\sin^3(\theta)}{2 - 3\cos(\theta) + \cos^3(\theta)} \right)^{\frac{2}{3}} \tag{3.12}$$

Given that, V_d is the droplet volume and θ is the contact angle of the droplet with the particle surface. As it is already assumed that $d_d << d_p$ this function can be safely applied within this scenario.

Finally, to determine the fraction of the surface coating another result from Kariuki et al. [2013] is used. This follows as Equation 3.13:

$$\sigma_p(v,t) = 1 - e^{-\phi_p(v,t)} \tag{3.13}$$

The external liquid to solid ratio is a critical parameter to the model philosophy. The liquid that is available in the granule array is assumed to be either within the pores or available at the surface of the granule. An approach is adapted from Pohlman [2015] to calculate the external liquid volume, this is shown as Equation 3.14:

$$l_{ex}(v,t) = l(v,t) - g(v,t)\Phi \tag{3.14}$$

Given that l_{ex} is the external liquid, Φ is the critical pore saturation fraction and $l(v,t)$ and $g(v,t)$, as previously mentioned, are the volume of liquid and gas volume of the granule within the gridpoint v. The critical pore saturation is effectively the parameter which determines the total maximum volume which can be occupied within the granule. In reality, this saturation fraction is a function of the granule morphology, pore radius and the surface thermodynamics of the liquid-gas-solid phases. In the absence of a model to determine this parameter mechanistically, it is assumed that this value remains constant throughout the entire simulation duration.

From Equation 3.14 it is possible to calculate the external liquid to solid ratio around any gridpoint by Equation 3.15:

$$x_{LS} = \frac{l_{ex}(v,t)\rho_l}{s(v,t)\rho_s + g(v,t)\rho_g} \tag{3.15}$$

3.3.2 Discretisation Strategy

A simple first-order upwind finite volume scheme was implemented to transform the component PDEs of Equations 3.5a-3.5c into a set of ordinary differential equations.

The set of equations were directly implemented into the gProms Formulated Products 2.0.0 custom modelling platform. The scheme discretises all length co-ordinate differentials, to transform the partial differential equations into ordinary differential equations. All time differentials are solved by the inbuilt DAEBsolver where the intermediate mid-points along the grid vector are linearly interpolated.

3.3.3 Model Initialisation

A logarithmic grid was used to represent the length vector d_p. Furthermore, as part of the initial condition at $t = 0$, a log normal distribution was used to pre-allocate the particles into the respective size classes. The log-normal distribution was initialised with a mean value, $\bar{v}$ and a standard deviation σ. A log-normal distribution was chosen to remain consistent in respect to the chosen grid discretisation. The mean value and standard deviation of the log-normal distribution are given within Table 3.1.

All further model parameters and initial values are summarised in Table 3.1.

3.3.4 Experimental Method

To test whether the model behaves reasonably, a small set of experiments were performed with a lab-scale top-spray fluidised bed (Aeromatic Fielder, GEA Pharma

Table 3.1: Table of parameters

Parameter Name	Symbol	Value
Spray mass flow rate	$\dot{M}_{spray}$	0.1-3 kg/hr
Initial bed mass	M_{bed}	3 kg
Granulator volume	V_{eq}	1 L
Minimum particle size	v_{min}	5 μm
Maximum particle size	v_{max}	1000 μm
Number of size classes	N	20
Mean particle size	$\bar{v}$	250 μm
Standard deviation	σ	90 μm
Initial solid composition	x_s	0.95 kg/kg
Initial liquid composition	x_l	0.05 kg/kg
Intra-particle void fraction	x_g	0.1 m^3/m^3
Density of solid phase	ρ_s	1500 kg/m^3
Density of solvent phase	ρ_l	1000 kg/m^3
Density of gas phase	ρ_g	1.2 kg/m^3
Simulation duration	t	4000 s
Droplet diameter	d_d	15-100 μm
Solid composition of the spray	x_{spray}	0.5 kg/kg
Contact angle	θ	30-60°
Critical pore saturation	Φ	0.5 m^3/m^3

Systems Ltd.) using an industrial spray application by mixing an industrial placebo with water to form a slurry. The slurry is a Newtonian mixture which has a viscosity of $0.025 Pa.s$. The fluidised bed is conical in geometry with a base (tray) diameter of 0.108m to a maximum expanded diameter of 0.3m across a 0.5m height. The particle bed when fluidised would typically occupy an average bed diameter of 0.16 m for a inlet air flow rate of 0.055 m^3/s. The experimental setup is shown on Figure 3.2. The bed was charged with 600g particles composing of the industrial placebo with a mean size of $226 \mu m$ and initial bulk density of $780 kg/m^3$. The fluidisation air was pre-heated to a temperature of 60° which, during operation, maintained a bed temperature of $30 - 40°$. The aim was to maximise drying of the slurry in the bulk whilst minimising drying of the spray as much as reasonably achievable. Temperatures greater than 70° were found to produce an excess of dust while below 60° resulted in insufficient drying. Two experiments were performed under the same conditions which had a total duration of 24 minutes.

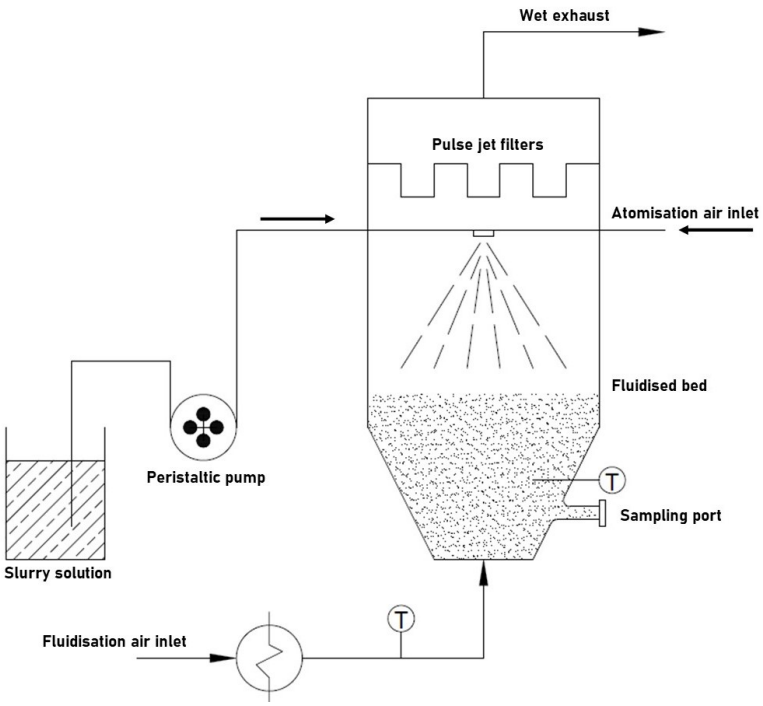

Figure 3.2: Experimental setup for the fluidised bed process

The bed was pre-fluidised before the start of each experiment. The particle bed was sprayed with the slurry for fixed duration while samples were taken from the sampling port every 4 minutes. The slurry was sprayed for a total of 780 seconds at a mass flow rate of 10 g/min with a further 660 seconds to dry the solvent. To account

Table 3.2: Standard experimental conditions

Experimental Parameter	Value
Slurry spray rate, g/min	10
Initial bed mass, kg	0.6 ($226\mu m$)
Atomisation pressure, bar	1.5 ($14.7\mu m$)
Gas temperature, $°C$	60
Bed temperature, $°C$	30-40
Solid loading of slurry, (kg/kg)	0.5
Superficial air velocity, m/s	2.73

for the removed solvent it is assumed in the model that all the solvent is removed at all timepoints, therefore, $\dot{M}_{spray}$ in Equation 3.10 is multiplied by the solid mass fraction of the solid in the slurry, which in this case is 0.5. The size distribution of these samples was analysed by a optical imaging technique - QicPic (Sympatech GmbH).

The droplet diameter was measured using a laser diffraction method (VisiSize N60, Oxford Lasers, UK) externally from the fluidised bed. The droplet diameter was measured as $14.7\mu m$ but is expected to be marginally lower due to drying effects. As the droplet diameter has a minimal effect on the overall growth, the effect of droplet drying within the bed is considered to be negligible.

The standard experimental conditions are detailed in Table 3.2.

3.4 Batch Fluid Bed Granulation

This section follows the study where the model is modified to simulate a batch fluid bed granulator. This is achieved by defining a single inflow stream which adds liquid mass and setting all outflow streams to 0.

A parametric study was performed to analyse the sensitivity of the model against the key process inputs. The growth and surface coating of the particle bed was analysed against three key input properties relating to the proposed model; the mass flow rate of the spray, the mean droplet size of the spray and the contact angle of the droplets against the particle.

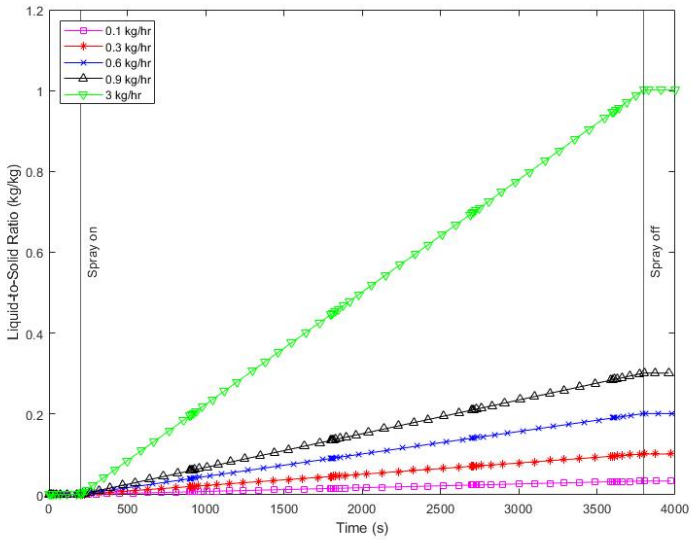

Figure 3.3: The change in the liquid-to-solid ratio for varying spray rates over a one hour period.

3.4.1 Effect of Spray Rate

The growth of the granules and surface wetting was studied at four different spray rates. The spray was initialised as a step-increase and decrease over a chosen spray period. The effect on the total liquid-to-solid ratio of the bed can be shown for the various scenarios on Figure 3.3:

From Figure 3.3 the total mass of spray added and the liquid-to-solid ratio are consistent with each other verifying the mass balance. It should be highlighted that the spray is composed of two components, some solid phase component and some solvent phase component. The model treats both components to be within the liquid phase, thus contributing to the liquid mass of the overall liquid-to-solid ratio. This treatment is necessary when agglomeration and drying is considered and is further elaborated later in Chapter 4 and 5.

Figure 3.4a shows how the average particle size of the granulator varies for multiple mass spray rates over a spray period. The model captures the aspect where layered growth occurs only when spray is added to the bed, which is physically represented at the appropriate plateaus before and after the spray is turned on/off. The curve, while initially appears linear, shows slight curvature for all spray rates where this is more emphasised at higher spray rates. Equally, Figure 3.4b shows how the distribution changes with increasing spray rates. The model follows the typical advective growth pattern; with a translation across the grid and a slight widening of the distribution

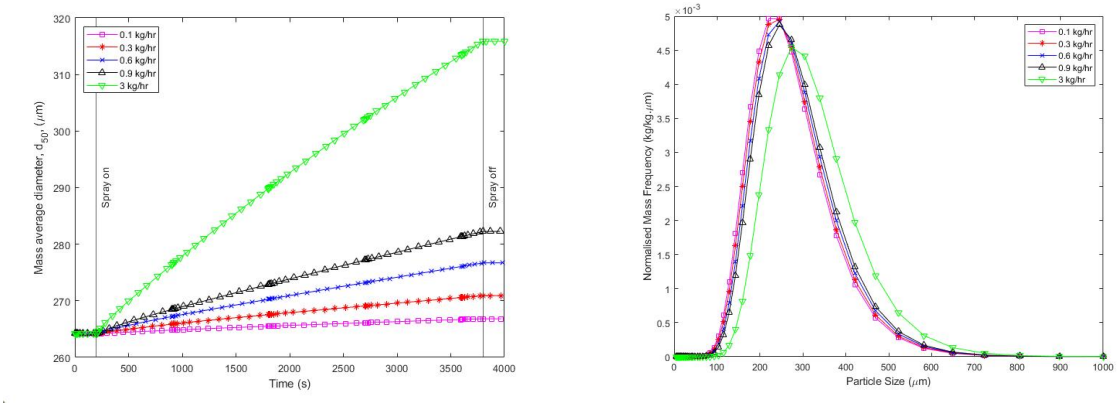

(a) (b)

Figure 3.4: (a) The variation in the mass-averaged mean particle size with respect to time over the spray period; (b) The particle size distribution at varying mass spray rates.

which is a typical characteristic to a mass based distribution. In particular, there is slight emphasis that larger particles grow quicker than that of smaller particles, capturing the physical behaviour of larger particles being more likely to interact with the spray than smaller particles. The model shows limitations with regards to the present liquid-to-solid ratio, where in this scenario growth will always occur regardless of the mass spray rate. In this case, $3kg/hr$ represents a final liquid-to-solid ratio of 1, which would be an unrealistic scenario for a well-posed process.

Figure 3.5(a) shows that with an increase in mass spray rate, the average surface coated by spray increases. The average coating of the distribution is calculated by taking the mean of the coating fraction distribution ($\bar{\sigma}_p = \int_0^\infty d_p \phi_p(d_p, t) dd_p$). The model asymptotes to a maximum value of one for all spray rates. The only key difference is the speed at which the model reaches the asymptote, which for higher mass spray rate is attained faster. Furthermore, larger particles also reach a full surface coating quicker than that of smaller particles

The distribution of surface wetness is shown by Figures 3.5(b) and 3.5(c) which identifies that with an increase in spray rate the overall distribution of surface wetness approaches some steady-state value. Here at the 0.1 kg/hr scenario only a select few bins see the most liquid as the model preferentially adds more liquid to those size classes which have theoretically more visible area to interact with the spray. As the spray rate increases, the distribution flattens indicating an evenness of spread where the particles of all size classes are evenly coated relative to one-another.

Clearly, as more liquid is added over the spray period the surface wetness of all size

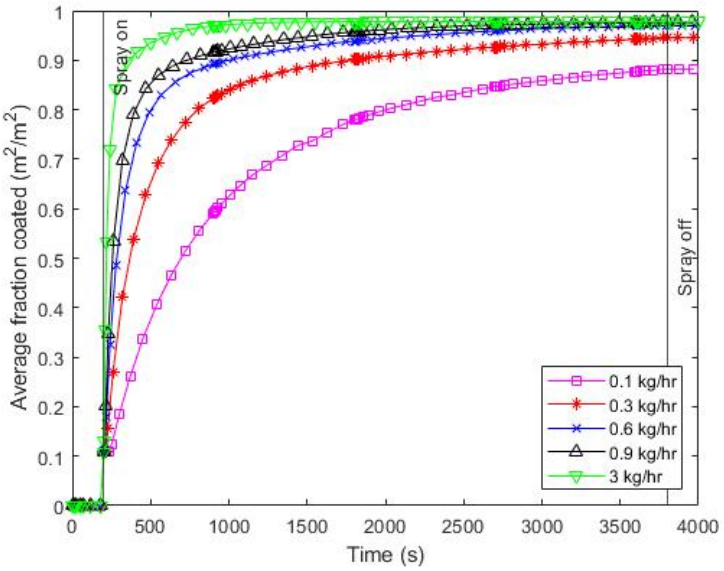

(a)

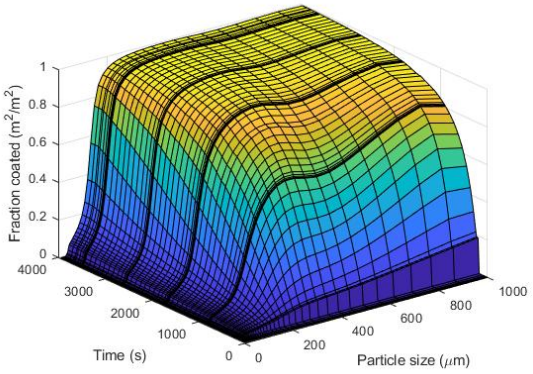

(b)

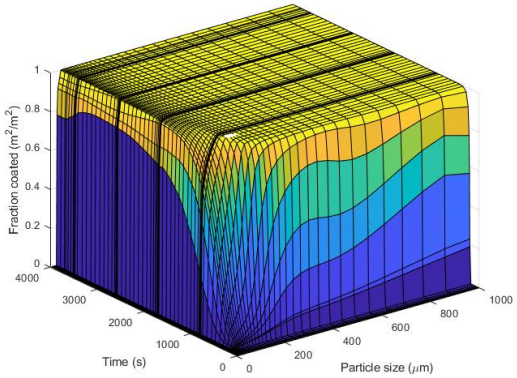

(c)

Figure 3.5: (a) The variation in the average surface coating versus time at varying mass spray rates.; (b) A surface plot of how the coating fraction varies for the distribution over the simulation duration for the 0.1 kg/hr mass spray rate scenario; (c) A surface plot of how the coating fraction varies for the distribution over the simulation duration for the 3 kg/hr mass spray rate scenario

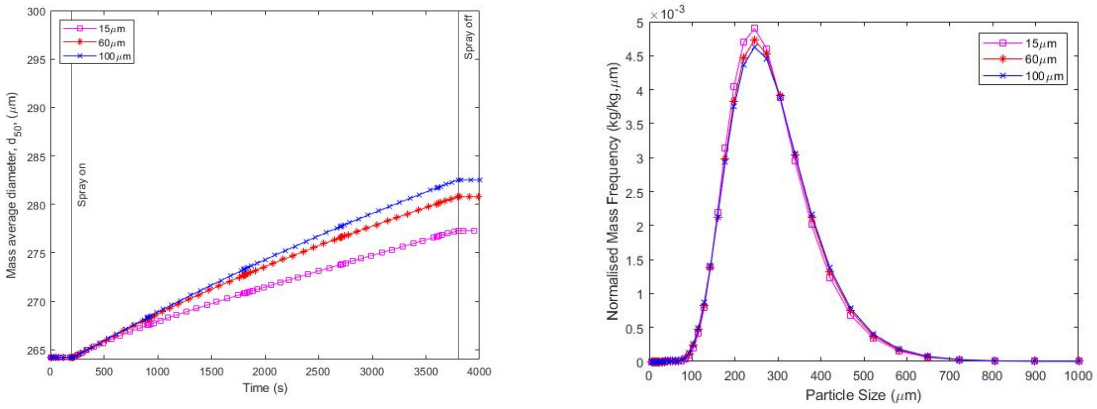

(a) (b)

Figure 3.6: (a) The variation in the mass-based average particle size for varying droplet diameters. (b) the particle size distribution for varying droplet diameters

classes increases. For the grid points which have the most associated liquid mass, the fractional coating values approach the maximum rapidly, but, fail to reach a value of one. This is not surprising due to the exponential nature of Equation 3.13 requiring a spray time of $t \to \infty$ to reach this value. However, the fractional coating values for the most coated size classes are within $0.9 - 0.96$ indicating a surface wetness that is practical to industrial coating.

3.4.2 Effect of Droplet Size

The droplet size primarily dictates the number of droplets available per unit volume of spray and the contact area of the individual droplet over the particle size. The droplet size was varied at values of 15, 60 and 100 μm. In a single droplet event, this corresponds to a ratio of the droplet volume against the initial particle volume, v_d/v, of $0.014, 0.890, 4.100\%$ respectively.

Figure 3.6a shows that with an increase in droplet diameter the average particle size also increases. The overall differences result in a $\pm 4\mu m$ between the droplet sizes, where primarily, this is due to the surface area dependency of the model. As there are less droplets at larger droplet sizes, these droplets have a greater tendency to interact with particles of the larger size class, hence, larger particles grow ever slightly faster than that of the smaller size classes. This is further emphasised by Figure 3.6b where the distribution shows less growth of particles over the smaller size classes, albeit, marginally.

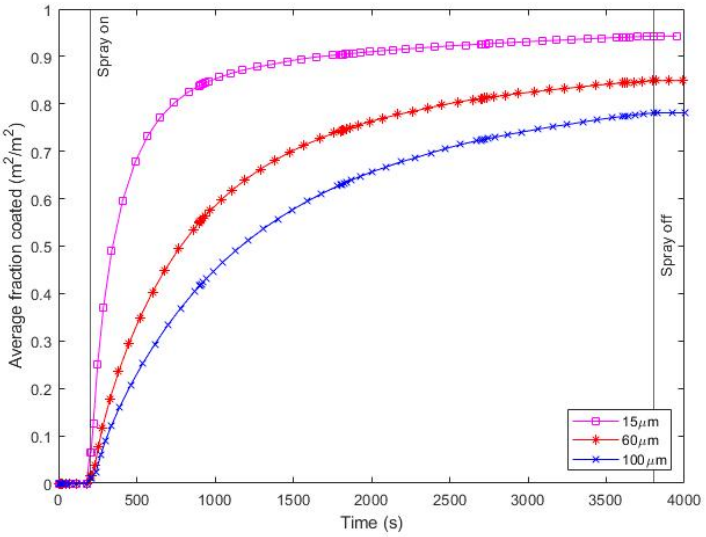

Figure 3.7: The variation in the average surface coating versus time at varying droplet diameters.

Figure 3.10 shows that the larger the droplet diameter the lower the surface coating of the distribution. With larger droplets the number of droplet events is reduced. With a lower number of droplet events, the probability that these droplets will interact with the entire distribution is reduced, hence, less uniform coating. The respective surface plots agree with this statement where Figure 3.8(a) shows much greater uniformity across the distribution in comparison to Figure 3.8(b) and Figure 3.8(c).

3.4.3 Effect of Contact Angle

The contact area in which the droplet coats over a single particle is a function of the contact angle. The effect of varying contact angle was analysed primarily to understand how the change in droplet contact area affects the overall size distribution and coating quality. The contact angle was varied at three values, 30°, 45° and 60°.

The contact angle has minimal effect on the overall growth of the size distribution. Figure 3.9 shows that there is no significant change in the distribution profile.

The effect on the average surface coating for varying contact angle is more significant. The larger the contact angle the poorer the coating. Generally, large contact angles translates into smaller droplet footprints per droplet (see Figure 3.10, therefore, reducing the overall coating per droplet event. Some scrutiny is necessary, the model assumes that the effects of the particle curvature is minimal which is true for $d_d << d_p$. If this assumption does not hold it is expected that the dependency of the

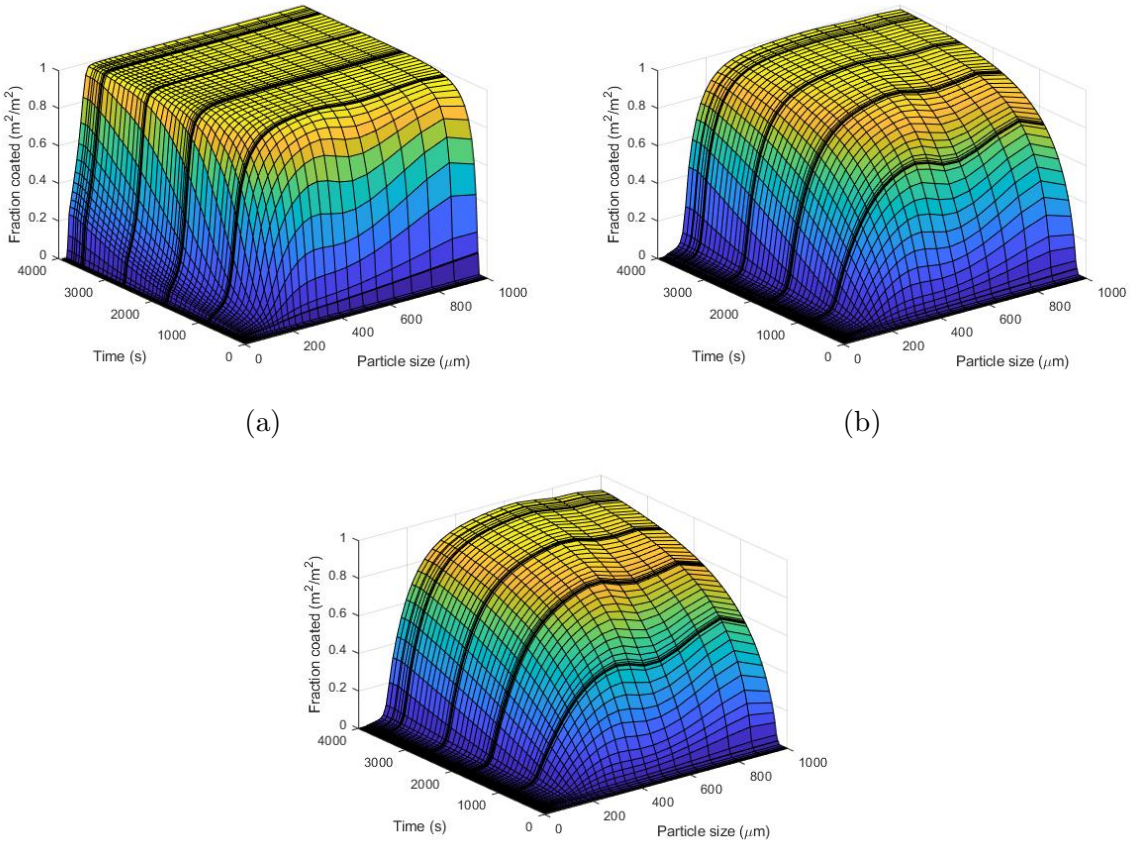

Figure 3.8: The surface plot of coating distribution with respect to time for a droplet diameter of (a) $15\mu m$ (b) $60\mu m$ (c) $100\mu m$

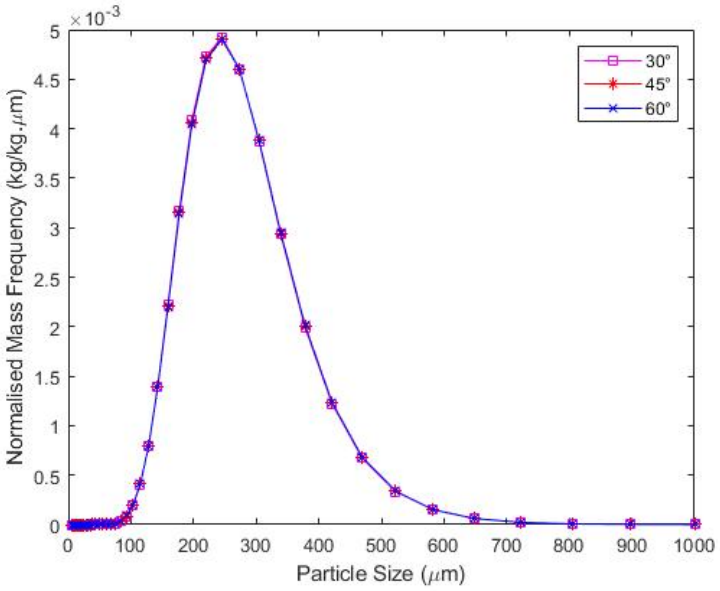

Figure 3.9: The particle size distribution for varying contact angles

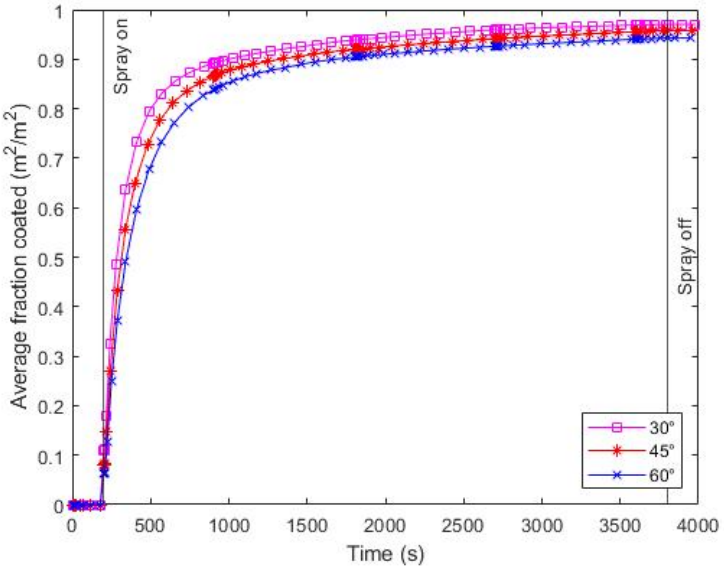

Figure 3.10: The variation in the average surface coating versus time at varying droplet diameters.

contact angle would be more prevalent by greater surface wetting over the curvature of the particle.

3.4.4 Experimental and Model Comparisons

Plots of the size distribution and the d10, d50, d90 for the individual samples taken across the experimental duration against the model outputs. Based on Figure 3.11, the model shows good agreement with the experiments performed especially given that there are no adjustable parameters. As the time progresses, the overall distributions for both the experiments and model show growth in the positive direction along the axis. Generally, the predicted size distributions are slightly broader than those measured experimentally, but, the difference is small. The fit is particularly impressive given that the model uses no adjustable parameters. This does allude to layering as a process regime that is "optimal-to-predict" as it can be well estimated through a simple mass balance driven model.

The comparisons of the d_{10}, d_{50} and d_{90} distribution parameters are shown as Figure 3.12. Again, the model shows good agreement. There is scatter observed among the experimental data, likely as a result of sampling inconsistencies from the port. Given that the model simulates the spray period as a fix time step, growth is only seen during this period and stops once the drying phase of the experiments begin. There is some suggestion of growth after the spray period in the experiments, particularly for the lower size classes, which suggests some form of agglomeration persists throughout.

These results show that a 1-D coupled approach for granulation modelling is adequate for modelling a layered growth process. This has many practical advantages suggesting that lower-dimensional models are sufficient for model accuracy, capturing the necessary granule parameters for use in complex rate models, with cheaper computational costs compared to those of higher-dimensional models. In terms of deploying the model in an industrial scenario, this is likely a more viable method than the true multi-dimensional models.

3.5 Conclusion

A mechanistic growth equation is derived and implemented into a reduced-order multi-dimensional scheme and studied at varying key parameter scenarios. By the implementation of the particle coating number, ϕ_p, the mal-distribution of liquid across a distributed domain can be modelled, analysed and quantified. Of three chosen

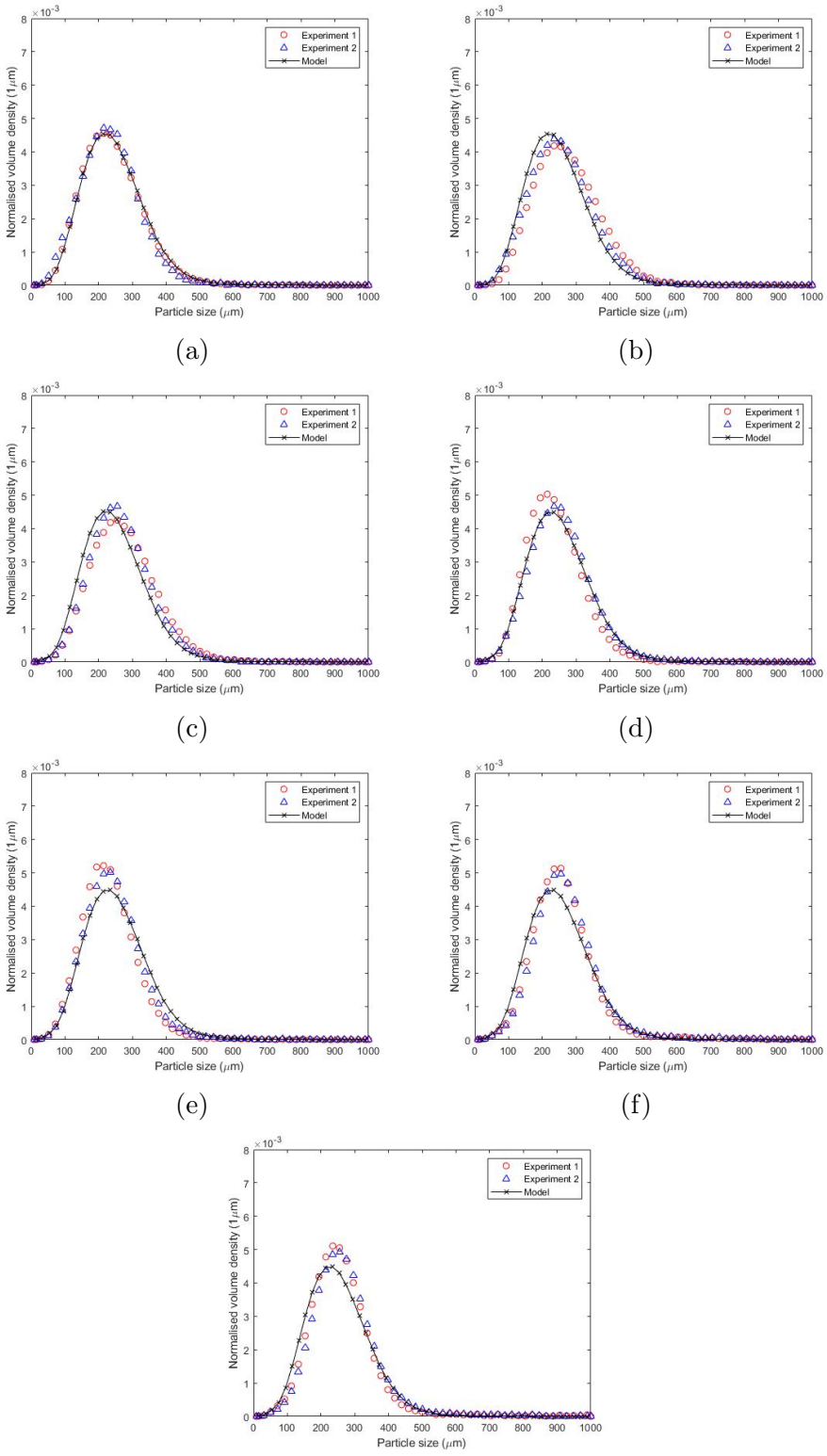

Figure 3.11: Comparisons of the normalised volume density distributions at each sampling point for both experiments against the model

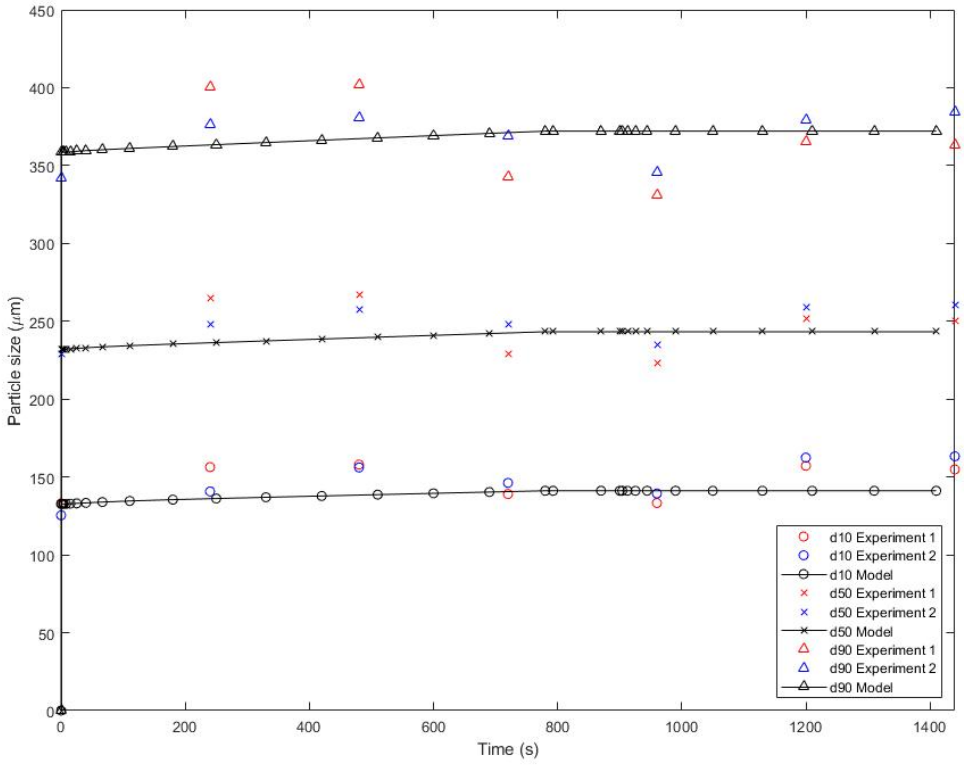

Figure 3.12: Comparisons of the d10, d50 and d90 of the model versus the experiments

parameters, the spray rate, droplet diameter and the contact angle, the spray rate showed the most dominant contribution to growth and surface coating of the particle bed. The model showed good agreement to experimental data demonstrating that the model is both reasonable and accurate. Therefore, if the bed can be controlled purely within the layering regime, the growth of the particle is easily predictable. This allows for some determination of the coating quality during the process design stage.

Chapter 4

Development of a Mechanistic Agglomeration Model for Fluid Bed Granulation Processes

4.1 Introduction

Population balance equations are commonly used to model particulate processes as the method is effective in tracking distributed properties. This is particularly useful for granulation and powdered processes as size, liquid content and porosity are distributed properties over a granule sample. Hounslow et al. [1988] developed a convenient discretised framework to model granulation to include, nucleation, agglomeration and breakage; a framework which provided some of the earliest studies on dynamic particle growth via agglomeration. The agglomeration rate process is defined as an integro-differential equation. The one-dimensional form is shown as Equation 4.1:

$$\frac{dn(v,t)}{dt} = \int_0^v \beta(v,v')n(v,t)n(v',t)dv' - \int_0^\infty \beta(v,v')n(v',t)dv \tag{4.1}$$

where $n(v,t)$ is the distribution function of the solid volume v, $n(v,t)$ is the volume density function, v' is the particle volume which is arbitrarily smaller than v and $\beta(v,v')$ is the agglomeration kinetic rate equation; often times referred to as the agglomeration kernel [Ramkrishna, 2000].

Significant effort has been placed into developing a representative agglomeration rate equation. Authors in the past have defined one dimensional expressions which depend only on the size of the colliding particles [Hounslow, 1998, Adetayo and Ennis, 1997, Ramkrishna, 2000, Tan et al., 2004a]. A majority of these models have shown good accuracy for the envelope of experiments performed within these researches.

However, universally it is often commented that these models are unsuitable because the models do not scale effectively with changes in process dynamics. As a result, there is a continuous drive within the current literature to develop agglomeration models which are more physically representative. To achieve this, it is necessary to include further particle dimensions which cannot be expressed in a one-dimensional framework. Dimensions such as the particle liquid content, porosity and for some cases the shape.

With the rise in computing power, multi-dimensional frameworks are becoming increasingly popular [Barrasso, 2015]. With the ability to track multiple particle properties, agglomeration models have been proposed which include properties such as the liquid content and particle porosity. Madec et al. [2003] proposed a multi-dimensional agglomeration model which incorporate the liquid fraction as a component to the agglomeration rate. It was clearly demonstrated within the work of Madec et al. [2003] that non-mechanistic models such as the sum and product models were insufficient and multi-dimensional models allow for improvements of the envelope of accuracy. However, the model proposed by Madec et al. [2003] was limited with regards to the physical representation of the particle-liquid interactions. Further models have been proposed since [Darelius et al., 2005, Goodson et al., 2004, Pohlman, 2015].

Currently, there is still a lack of mechanistic agglomeration models that are useable within a population balance framework. Models which can accurately describe the role of liquid binder between two-colliding particles. Often, over-simplifications are made and/or semi-empirical models are employed to describe such interactions [Rajniak et al., 2009]. Mechanistic models have been developed to describe such interactions within Monte-Carlo methods [Braumann et al., 2007, Rieck et al., 2020], but, very little for continuous methods. Monte-carlo methods have the advantage to describe each particle interaction explicitly whereas for continuous methods the particle properties are lumped per gridpoint; a limitation that is difficult to circumvent.

The following work aims to fill this gap by proposing a mechanistic agglomeration model which includes a modelling framework to describe the liquid-particle interaction of colliding particles within a continuous population balance framework.

4.2 Model Development and Implementation

Equation 4.1 is modified into a series of four coupled population balance equations to incorporate the solid, liquid, gas and solid in liquid phases. The overall population balance equations are shown as Equations 4.2-4.5:

$$\frac{\partial s(v,t)}{\partial t} = \int_0^v \beta(v,v')s(v,t)s(v',t)\partial v' - \int_0^\infty \beta(v,v')s(v',t)\partial v + \dot{Q}_{in}s(v,t) - \dot{Q}_{out}s(v,t) \quad (4.2)$$

$$\frac{\partial l(v,t)}{\partial t} = \int_0^v \beta(v,v')l(v,t)l(v',t)\partial v' - \int_0^\infty \beta(v,v')l(v',t)\partial v + \dot{Q}_{in}l(v,t) - \dot{Q}_{out}l(v,t) \quad (4.3)$$

$$\frac{\partial g(v,t)}{\partial t} = \int_0^v \beta(v,v')g(v,t)g(v',t)\partial v' - \int_0^\infty \beta(v,v')g(v',t)\partial v + \dot{Q}_{in}g(v,t) - \dot{Q}_{out}g(v,t) \quad (4.4)$$

$$\frac{\partial s_{liq}(v,t)}{\partial t} = \int_0^v \beta(v,v')s_{liq}(v,t)s_{liq}(v',t)\partial v' - \int_0^\infty \beta(v,v')s_{liq}(v',t)\partial v + \dot{Q}_{in}s_{liq}(v,t) - \dot{Q}_{out}s_{liq}(v,t) \quad (4.5)$$

where $s(v,t)$, $l(v,t)$, $g(v,t)$, $s_{liq}(v,t)$ refers to the density distribution of the respective components, solid, liquid, gas and solid in liquid phase of particles with a volume v while $s(v',t)$, $l(v',t)$, $g(v',t)$, $s_{liq}(v',t)$ refers to the distribution of the particles with a volume arbitrarily smaller than v.

4.2.1 Development of the Agglomeration Model

To define the kinetic model for agglomeration, we assume that the agglomeration of two particles is a function of two key physical interactions; the frequency of collision and likelihood of coalescence and rebound [Cameron et al., 2005]. Explicitly, this can be defined as Equation 4.6:

$$\beta(v,v') = \Psi_{coll}\Omega_{coal} \quad (4.6)$$

where $\beta(v,v')$ is the agglomeration rate model, Ψ_{coll} is the collision function and Ω_{coal} is the coalescence likelihood function.

The frequency of collision within fluidised beds is determined by the hydrodynamic properties of the bed. Tan et al. [2004a] showed that if the bed is well fluidised, then the collision frequency can be defined by the equipartition of kinetic energy model [Hounslow et al., 1988]. Assuming that the interactions are non-deformable, we choose to define the collision frequency as Equation 4.7:

$$\Psi_{coll}(d_p, d'_p) = \beta_0 (d_p + d'_p)^2 \sqrt{\frac{1}{d_p^3} + \frac{1}{d_p'^3}} \tag{4.7}$$

where β_0 is an adjustable rate constant and d_p is the particle diameter. β_0 is typically a parameter which is fitted against experimental data and would represent mechanistic properties such as formulation characteristics, shape, equipment geometry and more.

If we assume that the interaction between any two particles are like those proposed by Ennis et al. [1991], we can then characterise the coalescence likelihood as a function of the surface liquid of a particle. The coalescence likelihood can therefore be quantified by the viscous Stokes number as shown by Equation 4.8:

$$St_v = \frac{8\rho_p U_c \tilde{d}_p}{9\mu_l} \tag{4.8}$$

where St_v is the viscous Stokes number, ρ_p is the particle density, U_c is the relative velocity of the two colliding particles, $\tilde{d}_p$ is the harmonic mean diameter of the colliding particles and μ_l the apparent viscosity of the liquid binder.

We can express the harmonic mean diameter of the colliding particles as Equation 4.9:

$$\tilde{d}_p = \frac{2 d_i d_j}{d_i + d_j} \tag{4.9}$$

where d_i and d_j indicate the diameter of two particles i and j. To calculate the bubble properties a standard approach is used from Kunii and Levenspiel [1991]. The approach is detailed in Appendix B.

To quantify the relative velocity of the colliding particles a well-known empirical approach is used and adapted from Kunii and Levenspiel [1991]. The relative velocity is estimated by Equation 4.10:

$$U_c = \frac{6 U_b \tilde{d}_p}{\bar{d}_b} \tag{4.10}$$

where U_b is the bubble rise velocity and $\bar{d}_b$ is the mean bubble diameter across the length of the bed.

Ennis et al. [1991] suggests that the viscous Stokes number can be used to determine whether coalescence or rebound can occur. The boundary for both phenomena is characterised by the critical Stokes number which is defined as Equation 4.11:

$$St_{crit} = \left(1 + \frac{1}{e}\right) \log\left(\frac{h}{h_0}\right) \tag{4.11}$$

where e is the coefficient of restitution, h the liquid layer thickness on the surface of the particle and h_0 the characteristic length of the surface asperities. To estimate the liquid layer thickness the external surface liquid must be known. Taking the approach applied in Section 3.4 we can calculate the external liquid volume in the exact same manner and further transform this value into a characteristic length. The liquid layer thickness for an individual particle can therefore be defined as Equation 4.12:

$$h = l_{ex}/(\pi d_p^2) \tag{4.12}$$

where h is the liquid layer thickness and l_{ex} the external liquid volume. For the interaction of two particles, the average liquid thickness is taken in calculating the critical Stokes number for this interaction. Therefore, the liquid layer thickness of two colliding particles as the arithmetic mean which is simply defined as Equation 4.13:

$$\bar{h} = \frac{h_i + h_j}{2} \tag{4.13}$$

For coalescence to occur the viscous Stokes number must be below the critical, $St_v < St_{crit}$; and for rebound, $St_v \geq St_{crit}$.

The models discussed and proposed are those which currently exist in the literature. However, there is a fundamental underlying limitation. There is a universal assumption that the particles are fully surface wet. Realistically, particles are partially wet. Therefore, there is a need to extend the inclusion of partial wetting to support the Stokes criterion model.

In this study, we use the particle coating number to extend the current models to include partial wetting. Adapting the same methodology as Section 3.3.1, the particle coating number can be used to quantify the surface wetting; which can be incorporated into the agglomeration model. This allows for the calculation of the probability for a single particle to interact with a wet-surface of another particle. This interaction can be classified as three types, a wet-wet, wet-dry and dry-dry particle collision. Intuitively, any dry-dry particle collisions will result in no agglomeration,

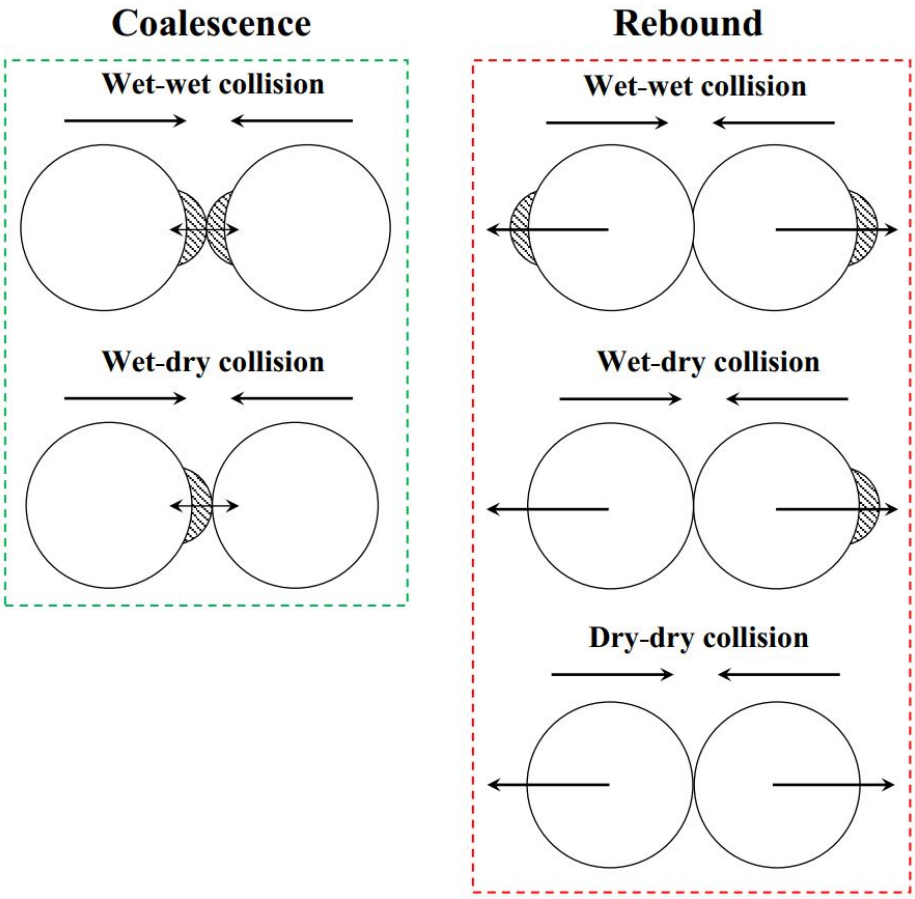

Figure 4.1: Types of coalescence interactions for wet-wet, wet-dry and dry-dry particles.

but, for wet-wet and wet-dry there are some subtleties needed to be considered. These modes of interaction are shown visually on Figure 4.1.

Figure 4.1 shows that while we can achieve coalescence with both wet-wet and wet-dry particles, there is a chance of these two particles to meet at the dry surfaces which would lead to rebound. Integrating this aspect into the agglomeration model is the primary focus for this work.

If the probability of interacting with the wet surface of a particle is given by the fractional coating, and if it is assumed that the overlapping of two-liquid layers has no impact on the probability, the overall probability of each interaction mode can be expressed as Equation 4.14:

$$\eta_{eff} = \begin{cases} (1-f_i)f_j + f_i f_j + f_i(1-f_j) & \{f_i, f_j\} > 0 \\ 0 < f_k \; k \in \{i,j\} & f_k = 0, k \in \{i,j\} \; i \neq j \\ 0 & f_i = f_j = 0 \end{cases} \tag{4.14}$$

Here, η_{eff} is the effective probability for partially wet particles to interact at a wet surface and f represents the fractional coating of the two interacting particles i and j which is defined by:

$$f_i = 1 - e^{-\phi_p} \tag{4.15}$$

where ϕ_p is the particle coating number which is given by Equation 4.16:

$$\phi_p(v,t) = \frac{6x_{LS}a_d}{\pi d_d^3 \rho_d A_{SA}} \tag{4.16}$$

The product of η_{eff} and the Stokes criterion gives the coalescence probability function. This is shown as Equation 4.17:

$$\Omega_{coal} = \eta_{eff} \times \begin{cases} 1 & St_v < St_{crit} \\ 0 & St_v \geq St_{crit} \end{cases} \tag{4.17}$$

What this function demonstrates is that for any particle that isn't within the criterion no agglomeration would occur, and in the case that it does, the probability of agglomeration becomes a function of the total surface wetting of the colliding particles.

Therefore, by substituting Equation 4.7 and 4.17 into Equation 4.6 we get the final explicit form as Equation 4.18:

$$\beta_{agg} = \beta_0 \eta_{eff} (d_p + d_p')^2 \sqrt{\frac{1}{d_p^3} + \frac{1}{d_p'^3}} \times \begin{cases} 1 & St_v < St_{crit} \\ 0 & St_v \geq St_{crit} \end{cases} \tag{4.18}$$

and in terms of volume v:

$$\beta_{agg} = \beta_0 \eta_{eff} (v + v')^{\frac{2}{3}} \sqrt{\frac{1}{v} + \frac{1}{v'}} \times \begin{cases} 1 & St_v < St_{crit} \\ 0 & St_v \geq St_{crit} \end{cases} \tag{4.19}$$

4.2.2 Model Parameters and Initialisation

The population balance equations are solved simultaneously within gFormulate 2.0.0 using the powder processing library. The agglomeration model is a custom-defined sub-model using the available custom template and is given by Equation 4.19. The population balance equations are discretised via a finite volume method along the particle length vector and a finite differences approach for any time differential. A numerical solver, DAEsolver, is used to solve the respective set of discretised equations using a variable step approach to solve the time domain. Details of the solver scheme

Table 4.1: Table of parameters

Parameter Name	Symbol	Value
Spray rate	$\dot{m}_{spray}$	0.5-1.5 kg/hr
Number of size classes	N	10
Mean particle size	μ	350 μm
Standard deviation	σ	50 μm
Initial Bed mass	M_{bed}	5 kg
Initial solid composition	x_s	0.99 kg/kg
Initial liquid composition	x_l	0.01 kg/kg
Density of solid phase	ρ_s	1300 kg/m^3
Density of liquid phase	ρ_l	1000 kg/m^3
Density of gas phase	ρ_g	1.2 kg/m^3
Droplet diameter	d_d	15 μm
Solid composition of the spray	x_{spray}	0.5 kg/kg
Contact angle	θ	30°
Bed Diameter	d_{bed}	0.15 m
Inlet fluidisation air flow rate	$\dot{M}_g$	10-100 kg/hr
Rate constant	β_0	varies $\frac{1}{s}$
Simulation duration	t	3 hours

can be found in great detail by the following authors Vassiliadis et al. [1994a,b], Oh and Pantelides [1996]. Further parameters necessary to initialise the model are given in Table 4.1.

4.3 Numerical Study

In the following sections a parametric study is performed to analyse model behaviour and performance against key process parameters. In this case, the mass spray rate, fluidisation air flow rate is varied to quantify the effects of the outlet product parameters such as particle size, distributions, Stokes number and key hydrodynamic properties. The mass spray rate and fluidisation air flow rate are linearised into the spray rate to bed mass ratio and the superficial to minimum velocity ratio.

4.3.1 Model Analysis

The spray rate to bed mass ratio was varied from a value of 0.1 kg/kg.hr to 0.3 kg/kg.hr within a 5kg batch fluidised bed. This ratio was calculated from the current

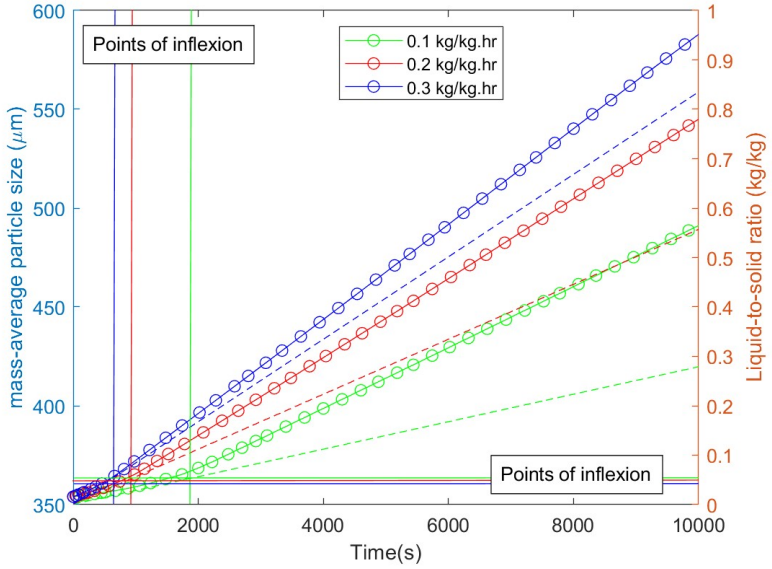

Figure 4.2: The effect of the spray rate/bed mass ratio on the growth for the agglomeration model and the liquid-to-solid ratio (in dashed lines), where the lines of inflexion are drawn for each respective ratio.

spray rate divided by the total bed mass, $\frac{\dot{m}_{spray}}{M_{bed}}$. Figure 4.2 shows that with increasing spray rate the overall growth of the particle bed increases. This is consistent experimental literature which suggests that with the greater volumes of liquid, there are more likely successful collisions which would lead to growth.

Interestingly, there are points of inflexion where growth shifts from a slow growth regime to an rapid agglomeration dominant regime. The time in which the growth regime shifts is slower at a lower spray rate. This indicates that with increasing spray rate, the time taken to reach the point where the bulk of the particle bed meets the criterion for agglomeration reduces. Similarly, we also see that for a lower spray rate the required liquid-to-solid ratio to reach the point of inflexion for agglomeration is higher, though minimal.

Figure 4.3 shows how the normalised mass distribution evolves with time. With increasing spray rate the distribution grows quicker with more large particles in the bed. At early time stages growth is shown to slow. It increases rapidly during later stages of growth. Here, most particles initially do not have the necessary surface wetting to achieve the Stokes criterion for growth and as the spray continues, the Stokes criterion is met in the bulk and growth initiates.

Figures 4.4(a)-(j) and 4.5(a)-(j) show how the agglomeration probability coefficient, η_{eff}, changes for the given spray scenario of 0.1 kg/kg.hr and 0.3 kg/kg.hr. In

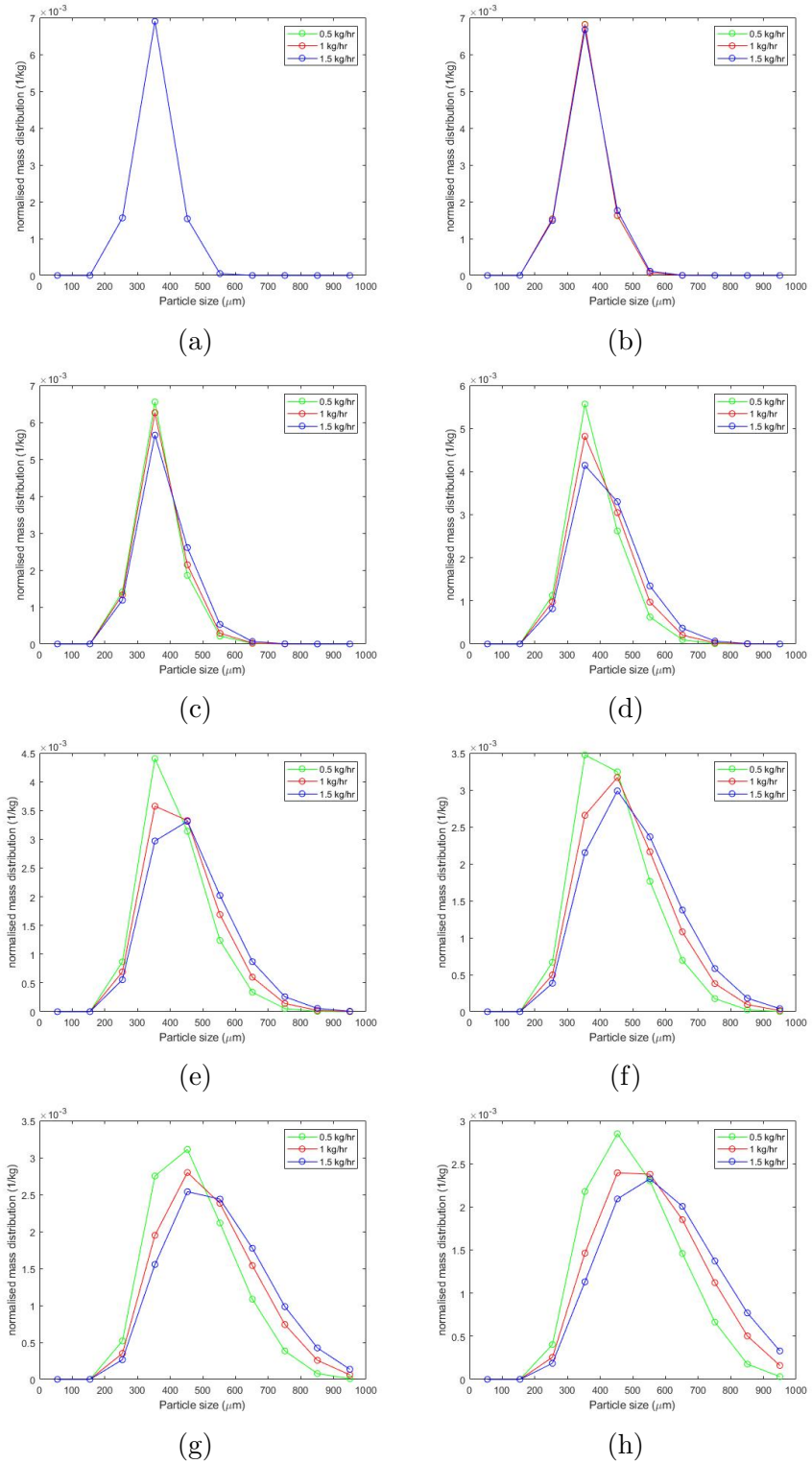

Figure 4.3: The evolution of the normalised particle size distributions for the spray scenarios of 0.1 kg/kg.hr, 0.2 kg/kg.hr and 0.3 kg/kg.hr at specific time intervals of (a) $t = 0s$, (b) $t = 320s$, (c) $t = 1320s$, (d) $t = 2940s$, (e) $t = 2940s$, (f) $t = 4680s$, (g) $t = 6380s$, (h) $t = 8140s$, (i) $t =$ final

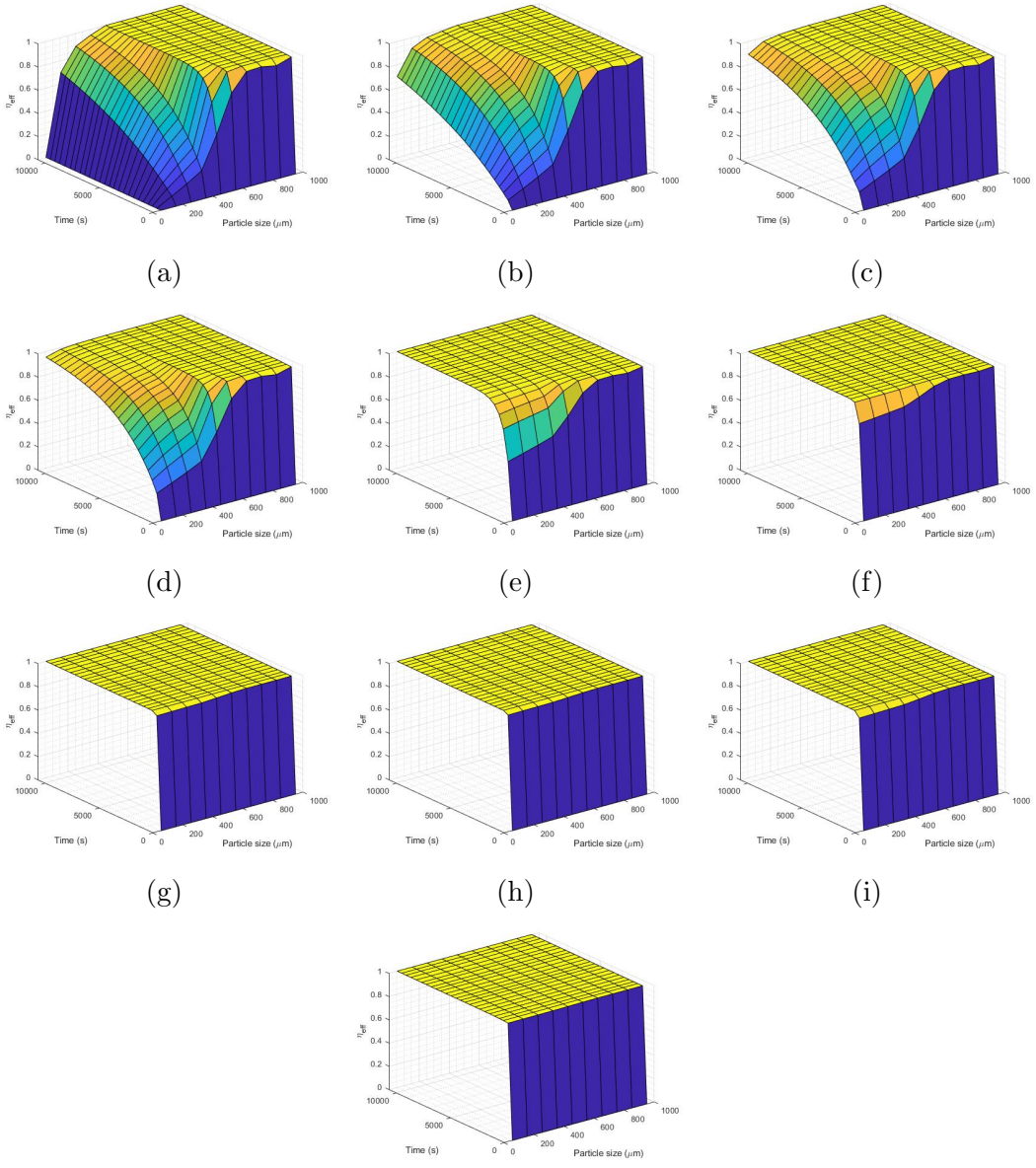

Figure 4.4: The coalescence likelihood coefficient, η_{eff}, for a spray scenario of 0.1 kg/kg.hr for particles of sizes (a) 54.75 μm (b) 154.25 μm (c) 253.75 μm (d) 353.25 μm (e) 452.75 μm (f) 552.25 μm (g) 651.75 μm (h) 751.25 μm (i) 850.75 μm (j) 950.25 μm

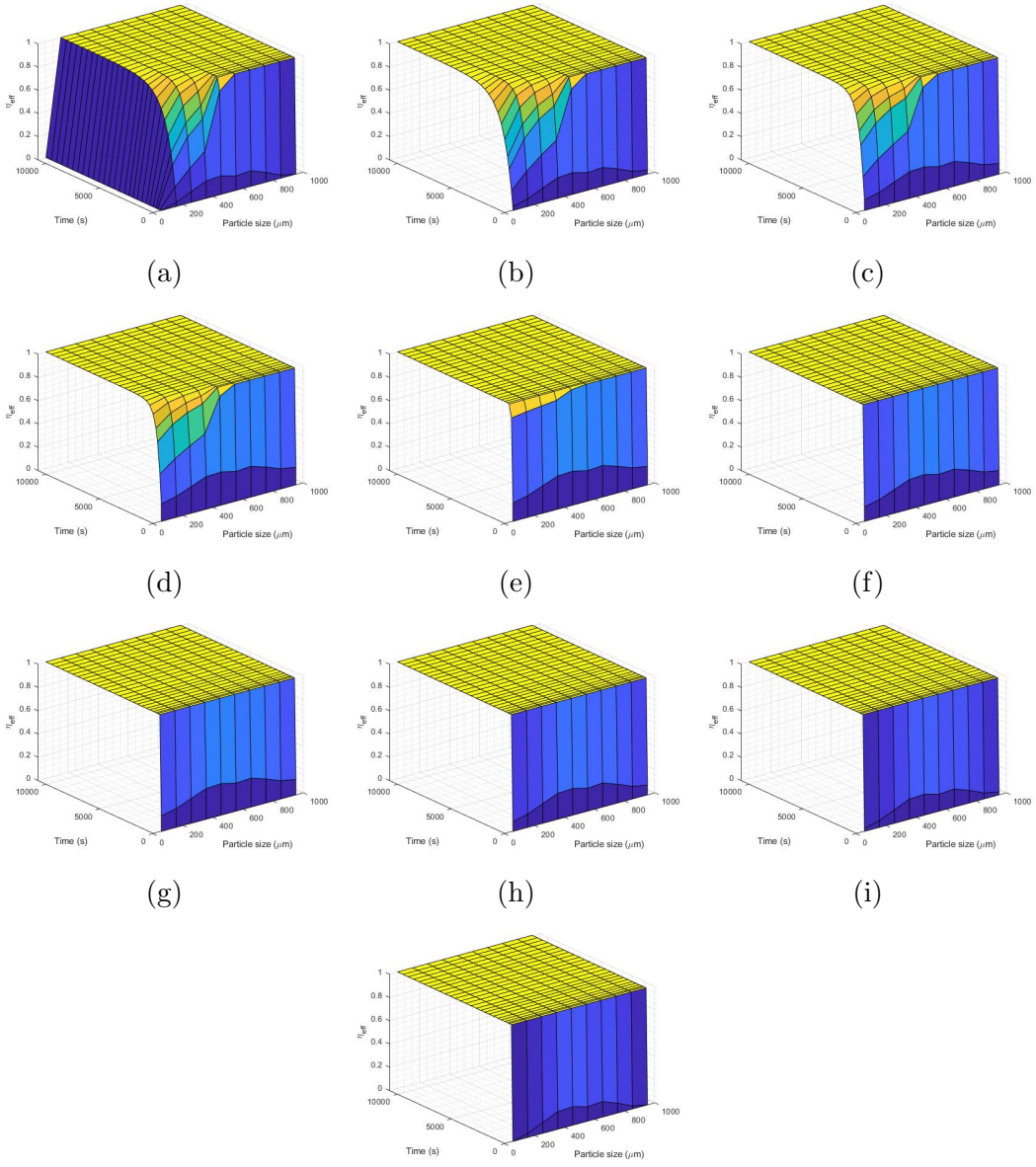

Figure 4.5: The coalescence likelihood coefficient, η_{eff}, for a spray scenario of 0.3 kg/kg.hr for particles of sizes (a) 54.75 μm (b) 154.25 μm (c) 253.75 μm (d) 353.25 μm (e) 452.75 μm (f) 552.25 μm (g) 651.75 μm (h) 751.25 μm (i) 850.75 μm (j) 950.25 μm

this case, the sub-figures (a)-(j) represent the probability of agglomeration with other respective particles for a given size. Small particles, especially for sub-figures (a)-(c), show a slower approach to unity. This indicates that for a small particle to become sufficiently surface wet to agglomerate effectively with other small particles, the bed must requires a large availability of liquid distributed throughout the bed.

On the other hand, large particles are not limited by the liquid availability. Larger particles have a greater surface area and are more likely to interact with the spray, therefore becoming surface wet quicker than the smaller particles. This is true for both spray scenarios, indicating that if the bed has sufficient liquid loading, the agglomeration of large particles are not limited by the liquid availability.

Figures 4.6 and 4.7 shows the variation in the Stokes criterion for the two spray scenarios and 0.1 kg/kg.hr and 0.3 kg/kg.hr respectively. The Stokes criterion is a binary number, 1 if the criterion is met and 0 if not. The value of 0.3 kg/kg.hr indicates that a greater number of agglomeration possibilities leads meet the Stokes criterion, hence, why it is observed that the inflexion for agglomeration from Figure 4.2 occurs earlier.

Smaller particles also show that they are more likely to meet the Stokes criterion as opposed to larger particles; generally less than half of the agglomeration possibilities meet the Stokes criterion for the largest particle size. The Stokes criterion is proportional to the size of the particle and given that the viscous Stokes number must be below a critical value, smaller particles are therefore likely to sit below this critical value.

This provides surprising contrast to the parameter η_{eff}, where smaller particles inherently hold lower values. This supports the idea that if the bed does attain a sufficient level of liquid loading and/or the spray conditions are met, agglomeration is predominantly limited by the collision behaviour as opposed to the viscous dissipation.

Figure 4.8 shows the how the average particle size changes with the fluidisation ratio. The flow rates used were 10 kg/hr, 50 kg/hr and 100 kg/hr which corresponded to a ratio against the minimum fluidisation velocity of 1.05, 5.27 and 10.6. At a ratio of 1.05 the growth is slowest, where the growth diminishes rapidly across the duration of the simulation. This does indicate that the particles do not satisfy the minimum fluidisation criteria and hence the the Stokes criterion [Ennis et al., 1991]. As a result, this culminates in less overall growth which reflects uniquely as a function of this model.

Interestingly a ratio of 10.6 shows slightly less growth than that of 5.27. Here the the internal kinetics of the particle exceed the critical Stokes value so rebound type

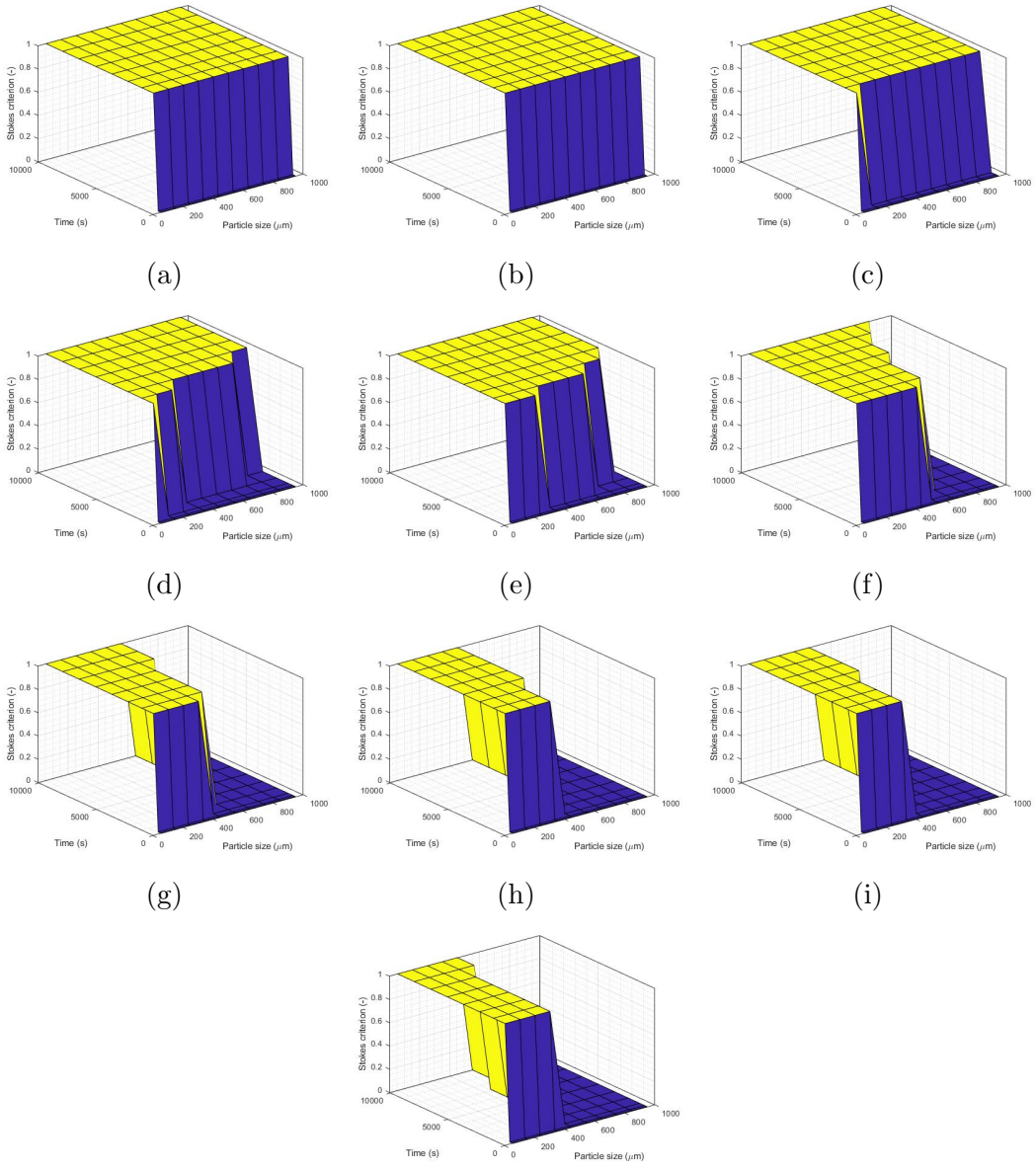

Figure 4.6: The condition of the Stokes criterion for a spray scenario of 0.1 kg/kg.hr for particles of sizes (a) 54.75 μm (b) 154.25 μm (c) 253.75 μm (d) 353.25 μm (e) 452.75 μm (f) 552.25 μm (g) 651.75 μm (h) 751.25 μm (i) 850.75 μm (j) 950.25 μm. One would refer to successful coalescence and zero would be unsuccessful

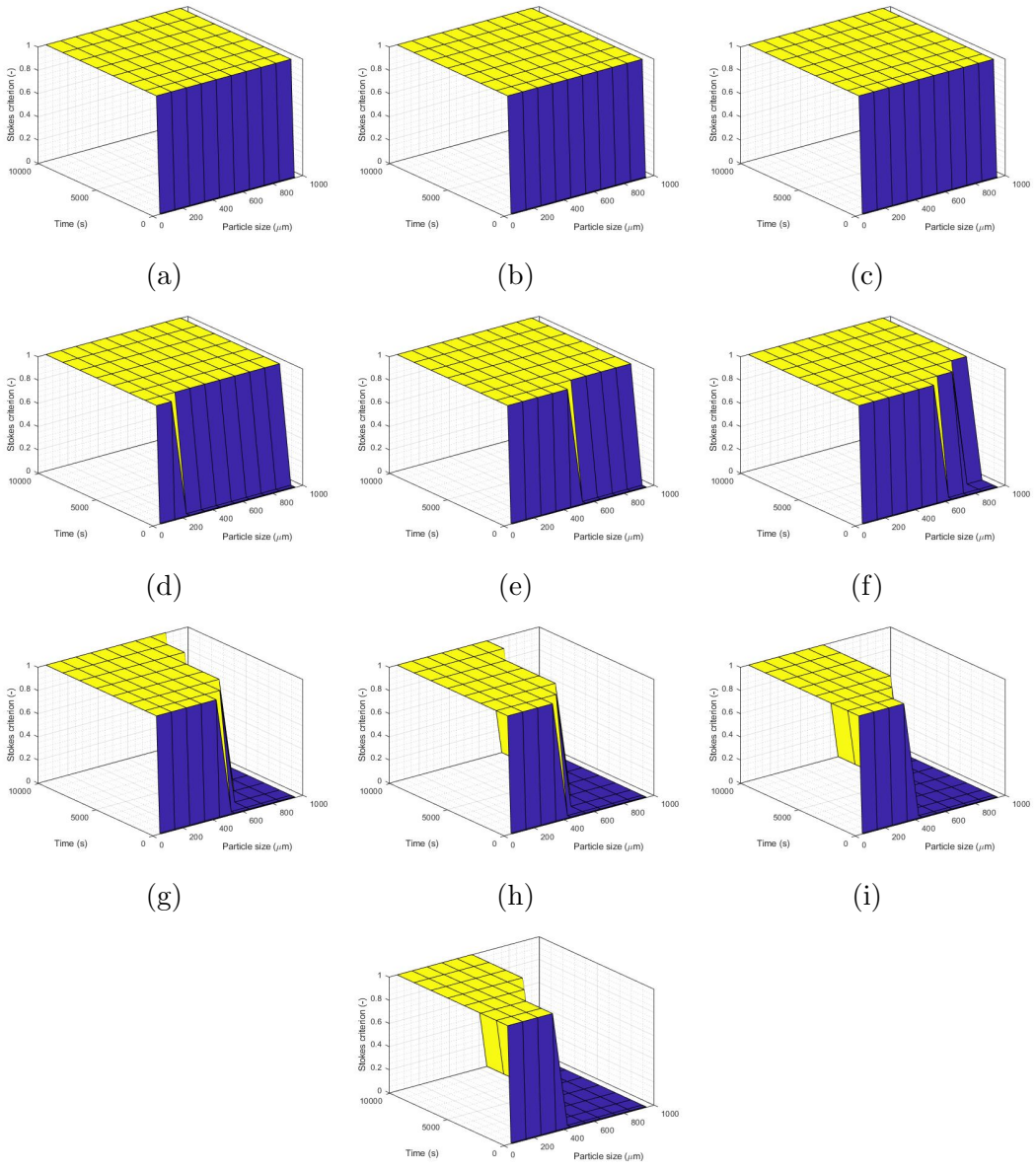

Figure 4.7: The condition of the Stokes criterion for a spray scenario of 0.3 kg/kg.hr for particles of sizes (a) 54.75 μm (b) 154.25 μm (c) 253.75 μm (d) 353.25 μm (e) 452.75 μm (f) 552.25 μm (g) 651.75 μm (h) 751.25 μm (i) 850.75 μm (j) 950.25 μm.

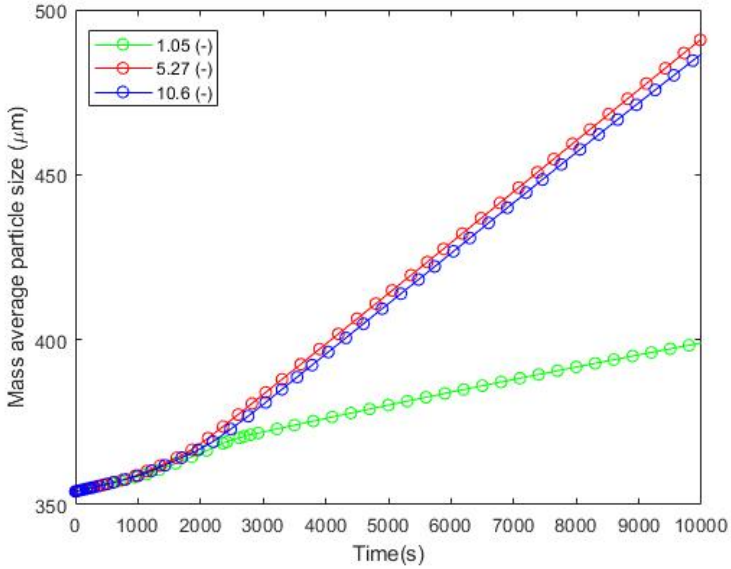

Figure 4.8: The effect of the ratio of the superficial gas velocity over the initial minimum fluidisation, $\frac{u_0}{u_{mf}}$, on the mass-based average particle diameter

collisions are occurring more frequently. The model captures the over-fluidisation of the bed which does imply some optimal value for agglomeration must sit below this value. During real operation, a fluidisation air flow rate of this value for the given bed diameter would most definitely lead to extensive elutriation of the fines and breakage of the particles. It would be expected that there would be an even greater reduction of particle size due to the contributions of breakage and attrition.

Figure 4.9 shows how the changing fluidisation ratios affect the distribution. Growth is more pronounced at the larger granule size distributions for ratios of 5.27 and 10.6. Comparatively, for a ratio of 5.27 and 10.6 the lower value showed more growth, particularly of the smaller particles as there is more growth into the larger bins. This shows how larger fluidisation ratios can lead to more rebound of small particles.

For a ratio of 1.05 there is initial growth for the larger particles grow but reduces at later time stages. This suggests that for the scenario of 1.05 some particles were below the minimum fluidisation velocity, resulting in no possibility for agglomeration by collision (see Figure 4.10). The minimum increases with time and increases faster when the average particle diameter of the bed increases. This is unsurprising as larger particles demand more air flow to overcome a greater gravitational drag. In the case of the fluidisation ratio of 1.05, as the minimum fluidisation velocity increases above the superficial, the growth by agglomeration diminishes entirely and returns

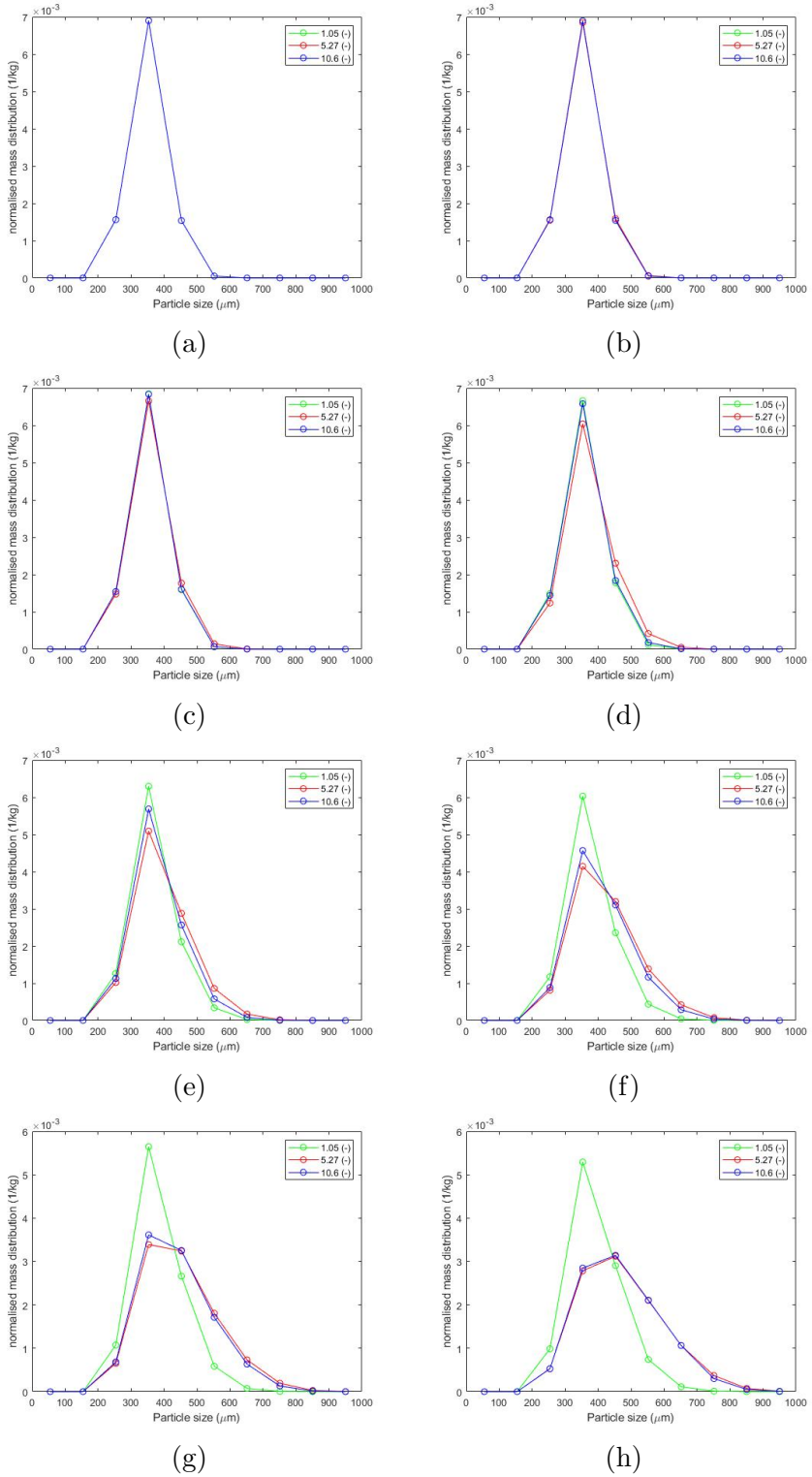

Figure 4.9: The evolution of the normalised particle size distributions for the fluidisation ratios of 1.05, 5.27 and 10.6 where (a) $t = 0s$, (b) $t = 320s$, (c) $t = 1320s$, (d) $t = 2940s$, (e) $t = 2940s$, (f) $t = 4680s$, (g) $t = 6380s$, (h) $t = 8140s$, (i) $t = \text{final}$

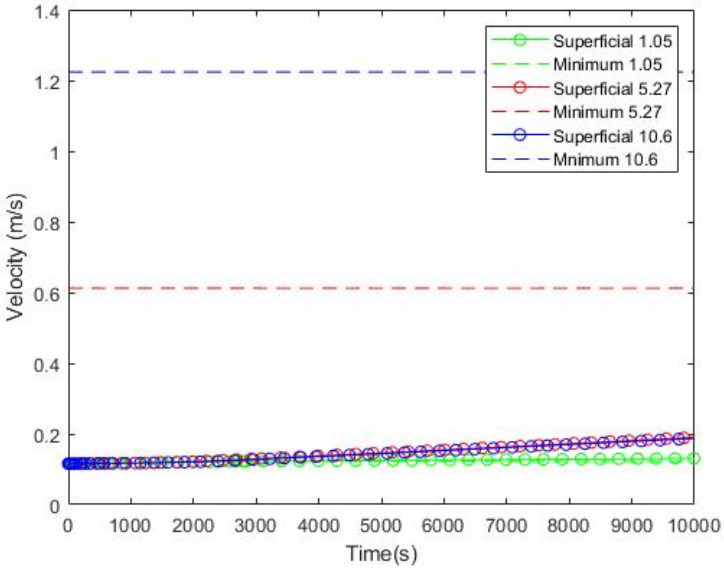

Figure 4.10: The variation of the superficial and minimum fluidisation velocities with time

to the linear rate of liquid addition. Though reality might suggest that the bed has collapsed; we would normally see formation of over-wetted large lumps. The model does not capture this specific phenomenon but still retains the aspect of the minimum fluidisation velocity which results in zero agglomeration.

4.3.2 Determining dominant growth mechanisms

To quantify the point at which agglomeration dominates the growth mechanism of a particle bed, an agglomeration number is defined as Equation 4.20:

$$AN = \frac{1}{2N} \int_0^\infty \eta_{eff}(d_p, d'_p, t) St_{cond}(d_p, d'_p, t) dd_p \tag{4.20}$$

where AN is the agglomeration number, N is the total number of gridpoints, St_{cond} is the Stoke's criterion and the rest as previously defined.

The agglomeration number provides a scalar value which varies from 0 to 1 and indicates the fraction in which the bed is in the "agglomeration state". This provides a theoretical basis to predict the position at which agglomeration type growth dominates the bed. The time-point of inflexion in growth would suggest a specific value for when the bed would shift from a layered-growth regime to one of agglomeration. Applying Equation 4.20 to the previous spray and flow rate scenarios, we can observe how the agglomeration number varies with time as Figure 4.11

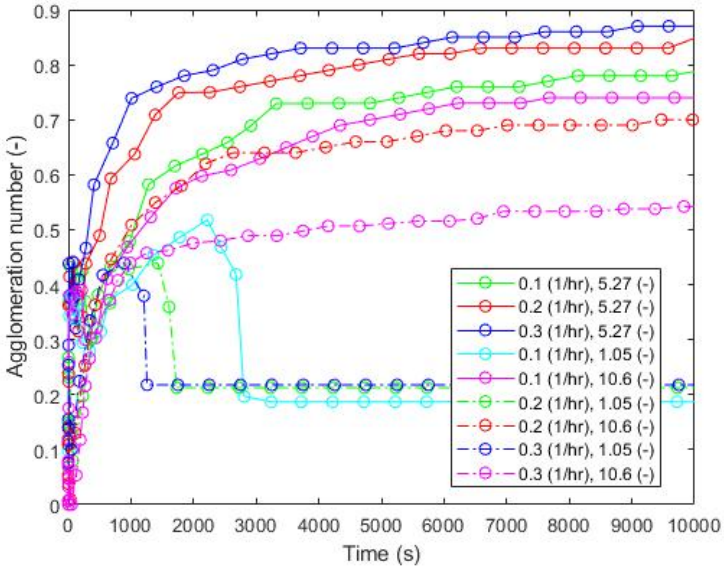

Figure 4.11: The variation of the agglomeration number with time for the spray and air flow rate ratios

Figure 4.11 reflects similar information as that of particle growth. The greater the agglomeration number the greater the growth, indicating that a greater total of particles are within the satisfactory regime to agglomerate. At early stages, the number appears to be convoluted for all scenarios, suggesting that there is some instability in the growth regime approaching agglomeration. Perhaps, this is a transition phase of a combination of variables approaching a critical value, such as the liquid layer thickness, particle velocity and size. Though once through this transition phase the number stabilises and approaches an asymptotes.

The agglomeration number is calculated at the inflexion points of the particle growth. This way, it is possible to identify the critical number for which agglomeration dominates within this theoretical scenario. These values are shown in Table 4.2.

From Table 4.2 it suggests that the point at which agglomeration becomes noticeable is when the proposed agglomeration number is roughly ≈ 0.45 based on the closeness from all scenarios where agglomeration took place. For scenarios where agglomeration did not take place (flow ratio of 1.05) showed a closeness at the point of inflexion to 0.45, but never exceeding the value. This provides some valuable insight as the proposed agglomeration number does suggest that the position at which growth rapidly increases can be related to a single value.

Table 4.2: The values of the agglomeration number at the points of inflexion for particle growth for the given scenarios

Spray-to-bed mass ratio	Ratio above minimum fluidisation	Value
0.1	5.27	0.4529
0.2	5.27	0.4525
0.3	5.27	0.4525
0.1	1.05	0.4424
0.1	10.6	0.4569
0.2	1.05	0.4384
0.2	10.6	0.4564
0.3	1.05	0.4389
0.3	10.6	0.4531

4.4 Conclusion

A reduced-order multi-dimensional agglomeration model was developed and implemented. The model took the form of a 1-D coupled population balance model which simulated a batch fluidised bed granulator. The model combines a coalescence likelihood function with a collision frequency function to provide a novel formulation of an agglomeration model.

The model showed sensitivities to both the spray rate and fluidisation air flow rate which resulted in changes to the particle growth. The agglomeration model responded similarly to experimental literature for both process parameters; which is unique to this model. The model demonstrated that it was possible to identify the positions when agglomeration-type growth would become dominant; an aspect which most current modelling literature has not clearly demonstrated.

The agglomeration number was proposed which combines the parameters, η_{eff} and St_{cond} to characterise the agglomeration behaviour throughout the bed. The number showed similar trends to growth and was consistent to the expectations of the definition. The value was calculated at the points of inflexion for growth to characterise the change from linear growth to agglomeration. It was found that at these inflexion points a similar value was calculated at ≈ 0.45 suggesting that when this value is exceeded, agglomeration is the dominant behaviour.

Chapter 5

Integrated Models for Fluid Bed Granulation

In the previous chapters, the focus was on understanding and developing mechanistic models to incorporate into a reduced order multi-dimensional framework which physically represent growth and agglomeration for fluidised beds. However, to fully encapsulate the mechanisms of a fluidised bed there are a few phenomenon which are necessary to be considered. On top of the models proposed so far, there is an inclusion of particle drying, spray drying and simple bed hydrodynamics to describe material discharge and flow.

This section aims to integrate layered growth, wetting, agglomeration, drying and spray drying into a unified framework via well-mixed and compartmentalised approaches.

5.1 Introduction

To build a framework that unifies the proposed models we draw a similar diagram to that of Figure 2.4 and simplify. This is shown as Figure 5.1.

Figure 5.1 reduces to Figure 2.1 by simplifying the aspects of nucleation and breakage, but, broadly considers similar aspects of spray drying, wetting, agglomeration and drying. Importantly, to model these mechanisms they must be framed in a way which reflects the real process. These considerations can include:

- Is the spray single-phase or two-phase?
- Is the spray above or below the bed?
- What is the shape of the bed? Cylindrical, conical, square, etc..?

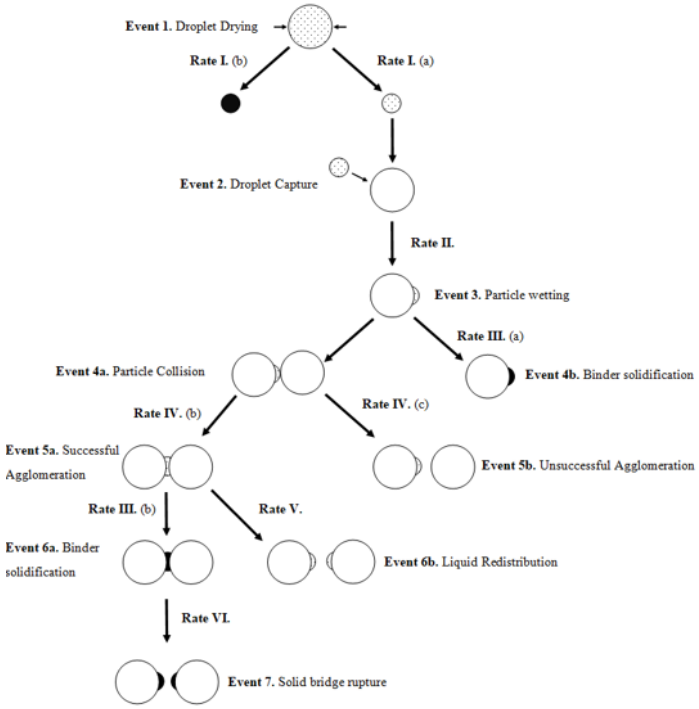

Figure 5.1: A rate process diagram for fluid bed granulation, simplified from Section 2.

- Is the bed continuous or batch? How are the granules discharged as a result?

Often these practical aspects have been overlooked which industrial operators and engineers would naturally consider important [Heinrich and Mörl, 1999, Heinrich et al., 2002, Tan et al., 2002, 2004a, Vreman et al., 2009, Fries et al., 2013, Börner et al., 2013, Chaudhury et al., 2013, Bück et al., 2016, Neugebauer et al., 2017, Diez et al., 2018]

Including all the discussed considerations is difficult. Lower dimensional models aren't sophisticated enough to mathematically incorporate the necessary information to integrate the real physical process parameters, whereas, higher dimensional models are difficult to solve and are numerically unstable. From a modelling perspective, there must be a trade-off when building a framework so that the most important mechanisms are considered, in addition to the important process parameters which influence those mechanisms.

5.2 Framework for Fluid Bed Granulation

A model framework in two parts is proposed as Figure 5.2. The model considers a single well-mixed model which encompasses the mechanisms as a single solution block.

An alternative two-compartment model is also proposed, which separates the spray and the bulk particle bed. Ultimately, both approaches will share similar population balances, kinetic models and treatment of the particle space. The key differences will be the way which the spray interacts with the particle bed. Figure 5.2 differentiates between the well-mixed formulation and the two-compartment model through the "orange" and "red" process lines. For the example in Figure 5.2, when the well-mixed model is chosen, the model de-activates the red pathways and uses the ones in orange, and vice-versa.

The model is formulated together through series of sub-models which dictate key physical behaviours of a fluidised bed. The model links the population balance model with other sub-models such as bed hydrodynamics and drying to determine the growth, drying and fluidisation performance. This approach expands upon modern frameworks proposed by Chaudhury et al. [2015] and Neugebauer et al. [2017].

In many cases, some of these models are simplified to ensure numerical stability. Despite the simplicity, the framework still provides a platform which incorporates the relevant mechanisms. This ensures that there is room to expand to use other coupling techniques to model a few of the sub-models.

5.3 Model Development for the Integrated Fluidised Bed Granulation Model

In this section, the overall balances and kinetic equations for a one-compartment and two-compartment fluidised bed models will be proposed. The intention by the end of this section is to provide the framework to build four models which will be studied during Section 5.5. These models are a: one compartment model with no recycle, one compartment model with a recycle, a two compartment model with no recycle, and a two compartment model with a recycle.

5.3.1 Mass and Energy Balances

The heat and mass transfer of the fluidised bed is described using a heterogenous model similar to that found by Burgschweiger et al. [1999] and Bertin et al. [2011]. The particle space is considered well-mixed and the gas phase is distributed across the length of the bed. First, we derive the overall mass and energy balances for the solution block. The overall mass balance is given by Equation 5.1:

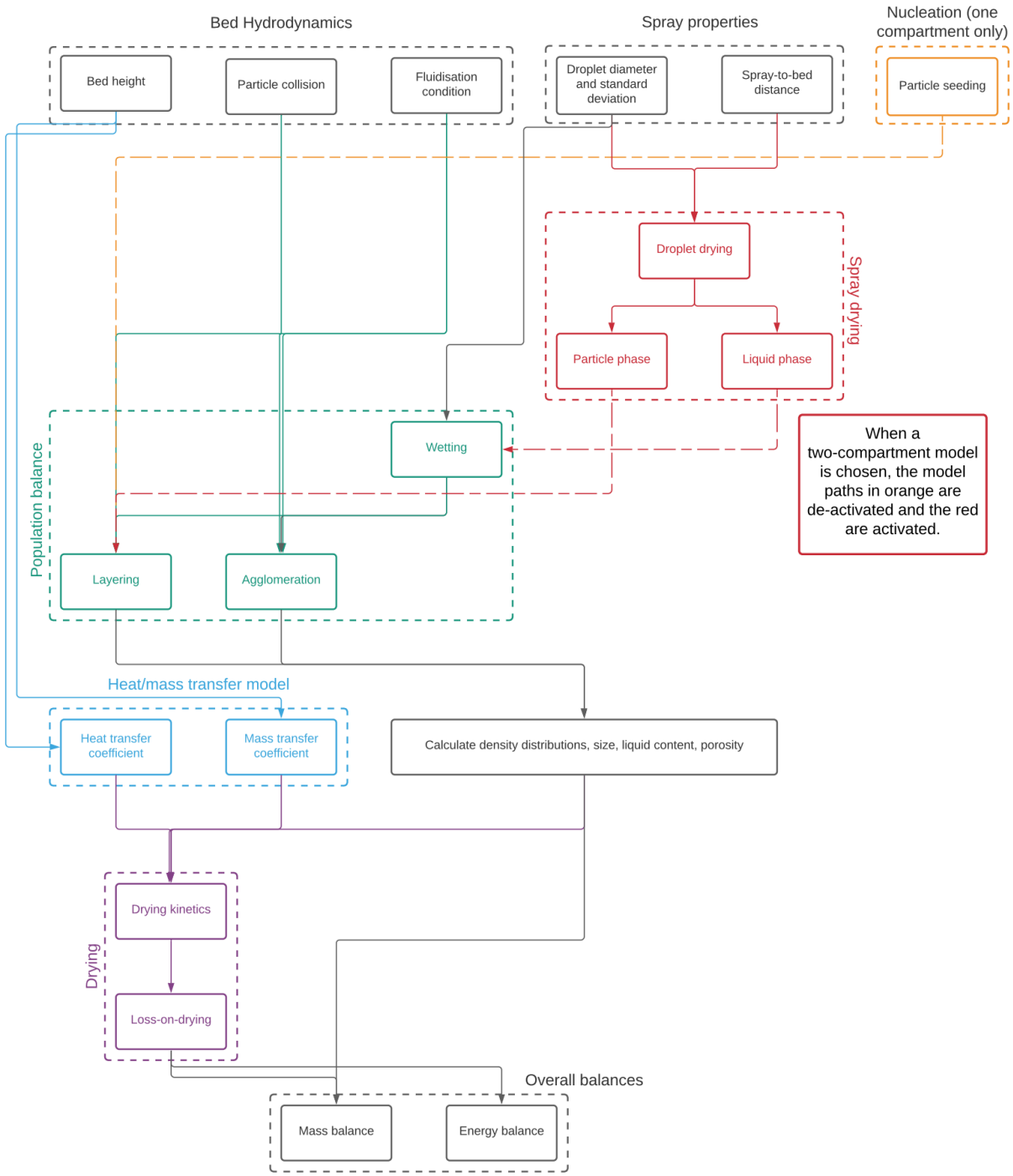

Figure 5.2: The proposed model framework for a fluidised bed granulator.

$$\frac{d(\rho V)}{dt} = \sum_{i}^{inlets} \dot{M}_{in,i} - \sum_{j}^{outlets} \dot{M}_{out,j} \quad \{i,j\} = 1,2,3...N \tag{5.1}$$

where ρ is the composite density of the holdup, V the volume of the holdup, N being the number of streams entering and leaving the fluidised bed, $\dot{M}_{in}$ is the mass flow rate of the inlet streams into the fluidised bed granulator and $\dot{M}_{outlet}$ is the mass flow rate of the outlet streams.

The energy balance is written similarly as Equation 5.2:

$$\frac{dH}{dt} = \sum_{i}^{inlets} \dot{H}_{in,i} - \sum_{j}^{outlets} \dot{H}_{out,j} \quad \{i,j\} = 1,2,3...N \tag{5.2}$$

where H is the enthalpy of the system, $\dot{H}_{in}$ is the total enthalpy entering the system through the inlet streams and $\dot{H}_{outlet}$ is the total enthalpy leaving.

To avoid convoluting the granule phase and the gas phase when calculating the volumetric holdup, we choose to write separate balances for both. From Figure 5.4 and we can derive the mass balances for the particle and gas phases for a typical industrial continuous fluidised bed granulator. The mass balances for the one-compartment particle and gas phases are:

$$\frac{d(\rho_p V_p)}{dt} = \dot{M}_{in} + \dot{M}_{recycle} + \dot{M}_{spray} - \dot{M}_{evap} - \dot{M}_{out} \tag{5.3}$$

$$\dot{M}_g \frac{dY_g}{dt} = -\dot{M}_{evap} + \dot{M}_{g,in} Y_{g,in} - \dot{M}_{g,out} Y_{g,out} \tag{5.4}$$

and the mass and gas balance for the two-compartment form:

$$\frac{d(\rho_p V_p)}{dt} = \dot{M}_{in} + \dot{M}_{recycle} + \dot{M}_{spray} - \dot{M}_{evap} - \dot{M}_{out} + r\dot{M}_g(Y_{spray,in} - Y_{spray,out}) \tag{5.5}$$

$$\dot{M}_g \frac{dY_g}{dt} = -\dot{M}_{evap} + \dot{M}_{g,in} Y_{g,in} - \dot{M}_{g,out} Y_{g,out} + r\dot{M}_g(Y_{spray,out} - Y_{spray,in}) \tag{5.6}$$

where ρ_p is the composite density of the particle, V_p the volume of the particles and Y_g is the moisture content of the evaporating phase.

The mass inlets and outlets for the particle phases can change depending on how we choose to define the fluidised bed granulator. This can be more easily understood by a series of typical scenarios.

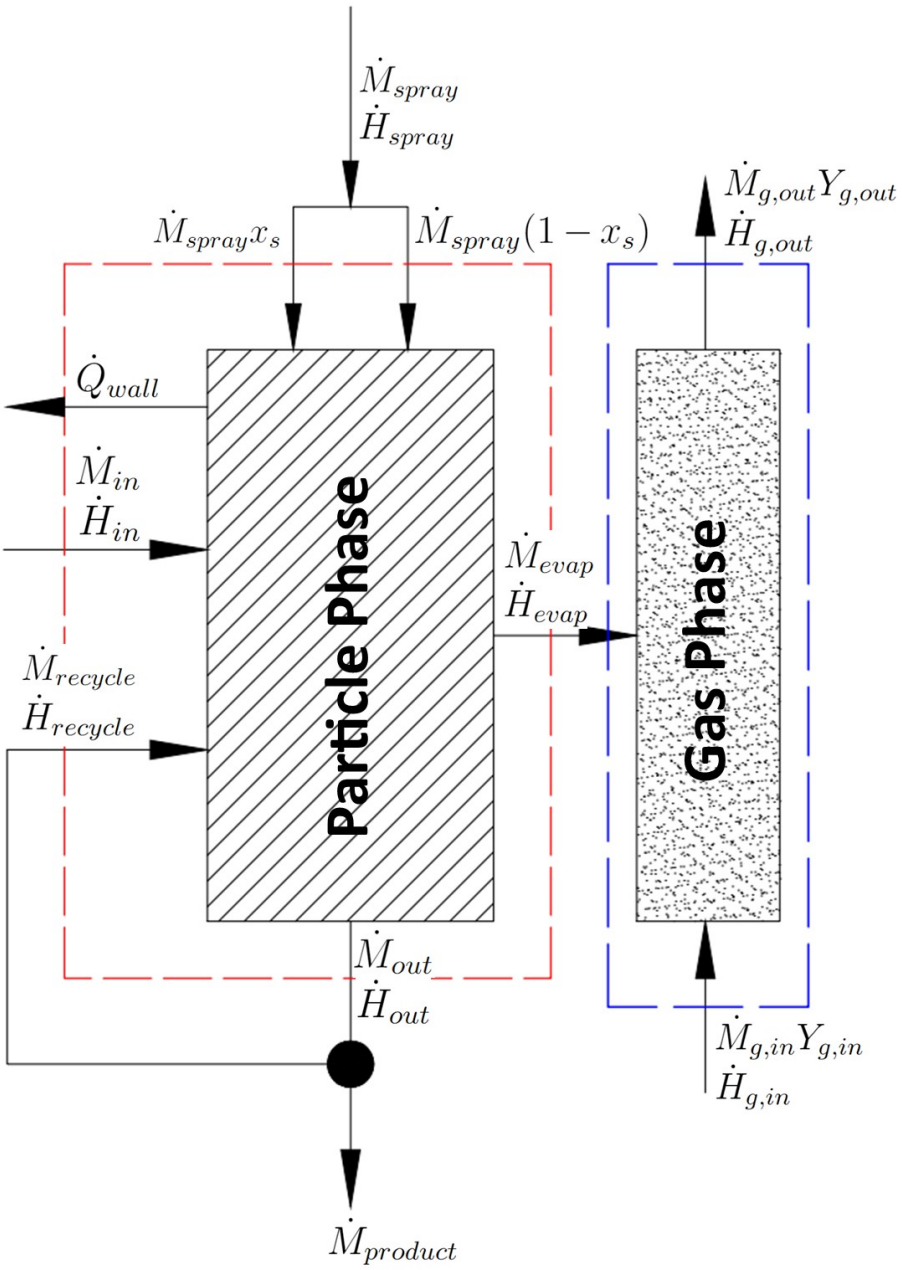

Figure 5.3: The control volume of the one-compartment fluidised bed granulator for the particle and gas phases

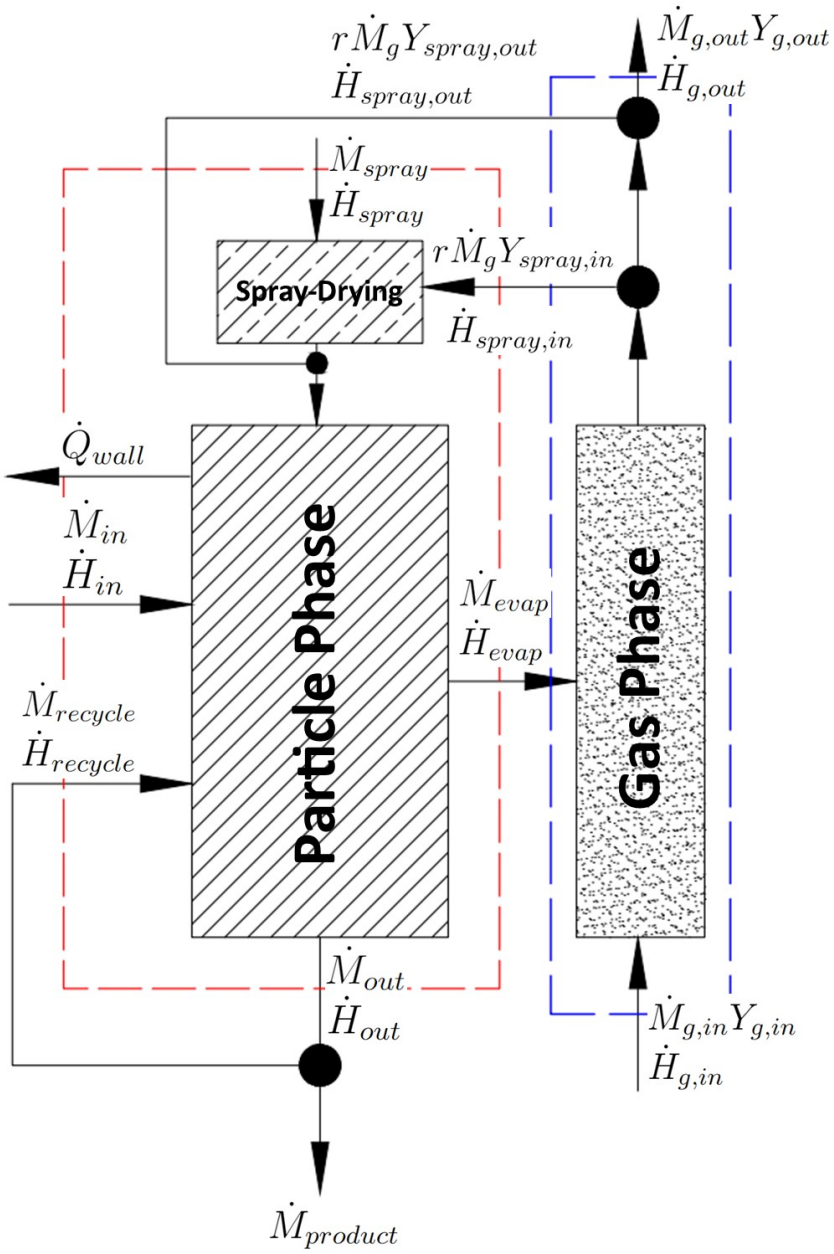

Figure 5.4: The control volume of the two-compartment fluidised bed granulator for the particle and gas phases

Scenario 1: Batch fluid bed granulation with a single phase spray: This would mean that $\dot{M}_{in}$, $\dot{M}_{out}$ and $\dot{M}_{recycle}$ are set to 0. This is the simplest formulation of the model, as there is no consideration of the spray outside of the growth mechanics of the particles.

Scenario 2: Continuous fluid bed granulation and single phase spray: For this scenario, all the mass flows proposed in Equation 5.3 and 5.5.

Scenario 3: Continuous fluid bed granulation and a two-phase spray and recycle: In this scenario, we set $\dot{M}_{in}$ to 0 and separate the spray into two components for the one compartment model. One component as $\dot{M}_{spray}x_s$ to represent the solid content, where x_s is the solids weight fraction of the spray, and, $\dot{M}_{spray}(1 - x_s)$ which is the solvent fraction of the spray (see Figure 5.4). In essence, the one compartment model needs to treat the solid's addition through the spray as a "false nucleation" term. The two compartment model requires a small change by including a bypass of the gas phase air into the spray-drying compartment. The two compartment model does not require the separation of the solids fraction in the spray. The two-compartment model can drive the nucleation through spray drying, whereas, the one-compartment model does not have this benefit. This final scenario is of the most interest for the rest of this work as this replicates the system described in Chapter 6, and as a result, the integrated models which are formulated will be structured on this scenario with and without a recycle.

The energy balances for the system can be written as:

$$\frac{dH_p}{dt} = \dot{H}_{in} + \dot{H}_{recycle} + \dot{H}_{spray} - \dot{H}_{evap} - \dot{H}_{out} - \dot{Q}_{wall} \tag{5.7}$$

$$\frac{dH_g}{dt} = \dot{H}_{evap} + \dot{H}_{g,in} - \dot{H}_{g,out} \tag{5.8}$$

and the enthalpy balance for the two compartment form:

$$\frac{dH_p}{dt} = \dot{H}_{in} + \dot{H}_{recycle} + \dot{H}_{spray} - \dot{H}_{evap} - \dot{H}_{out} - \dot{Q}_{wall} + \dot{H}_{spray,in} - \dot{H}_{spray,out} \tag{5.9}$$

$$\frac{dH_g}{dt} = \dot{H}_{evap} + \dot{H}_{g,in} - \dot{H}_{g,out} - \dot{H}_{spray,in} + \dot{H}_{spray,out} \tag{5.10}$$

Where H_p is the accumulated enthalpy of the particle phase and H_g is the enthalpy of the gas phase. The specific enthalpies of the particle and gas phases are given as Equations 5.11 and 5.12:

$$\dot{H}_p = \rho_p \int_0^\infty n(v,t) \left[\sum_i^{components} x_i c_{p,i} \right] T_p dv \tag{5.11}$$

$$\dot{H}_g = c_{p,g} T_g + Y_g (c_{p,w} T_g + \Delta h_v) \tag{5.12}$$

where x_i is the weight fraction of component i in the particle phase, $c_{p,i}$ is the specific heat capacity of component i, T_p and T_g the temperature of the particle and gas phases and Δh_v the latent heat of evaporation of the vaporising solvent (where the latent heat is calculated at $T_g = T_{out}$).

5.3.2 Population Balance

A coupled 1-D population balance equation which considers wetting and agglomeration for a four co-ordinate granule system is proposed. The co-ordinates chosen is the solids, solids in the liquid phase, the solvent and the gas fractions, which are additive. Therefore, m the mass of a granule, can be calculated as:

$$m = s + s_{liq} + l + g \tag{5.13}$$

where s is the mass of the solid in the particle phase, s_{liq} the mass of the solid in the liquid phase, l the mass of the solvent and g the mass of gas by the inherent porosity of the granule.

The overall population balance equations for each individual component, including the respective stream flows from the inlets and outlets, is given as Equations 5.14-5.17:

$$\begin{aligned} \frac{\partial [s(v,t)]}{\partial t} = &- \left[\frac{ds}{dt} \frac{\partial s(v,t)}{\partial v} \right] + \frac{1}{2} \int_0^v \beta(v,v') s(v,v',t) s(v',t) dv' \\ &- s(v,t) \int_0^\infty \beta(v,v') s(v',t) dv' + \dot{M}_{in} s(v,t) + \dot{M}_{recycle} s(v,t) \\ &+ \dot{M}_{spray} x_s s(v,t) - \dot{M}_{out} s(v,t) \end{aligned} \tag{5.14}$$

$$\begin{aligned} \frac{\partial [s_{liq}(v,t)]}{\partial t} = &- \left[\frac{ds_{liq}}{dt} \frac{\partial s_{liq}(v,t)}{\partial v} \right] + \frac{1}{2} \int_0^v \beta(v,v') s_{liq}(v,v',t) s_{liq}(v',t) dv' \\ &- s_{liq}(v,t) \int_0^\infty \beta(v,v') s_{liq}(v',t) dv' + \dot{M}_{recycle} s_{liq}(v,t) \\ &+ \dot{M}_{spray} (1 - x_s) s_{liq}(v,t) - \dot{M}_{out} s_{liq}(v,t) \end{aligned} \tag{5.15}$$

$$\frac{\partial[l(v,t)]}{\partial t} = -\left[\frac{dl}{dt}\frac{\partial l(v,t)}{\partial v}\right] + \frac{1}{2}\int_0^v \beta(v,v')l(v,v',t)l(v',t)dv' - l(v,t)\int_0^\infty \beta(v,v')l(v',t)dv' + \dot{M}_{in}l(v,t) + \dot{M}_{recycle}l(v,t) + \dot{M}_{spray}l(v,t) - \dot{M}_{out}l(v,t) - \dot{M}_{evap}l(v,t) \quad (5.16)$$

$$\frac{\partial[g(v,t)]}{\partial t} = -\left[\frac{dg}{dt}\frac{\partial g(v,t)}{\partial v}\right] + \frac{1}{2}\int_0^v \beta(v,v')g(v,v',t)g(v',t)dv' - g(v,t)\int_0^\infty \beta(v,v')g(v',t)dv' + \dot{M}_{in}g(v,t) + \dot{M}_{recycle}g(v,t) + \dot{M}_{spray}g(v,t) - \dot{M}_{out}g(v,t) \quad (5.17)$$

where $s(v,t)$, $s_{liq}(v,t)$, $l(v,t)$ $g(v,t)$ are the mass density distributions of the respective components along the length vector, $\beta(v,v')$ is the rate model which describes agglomeration, $\partial s(v,t)$, $\partial s_{liq}(v,t)$, $\partial l(v,t)$, $\partial g(v,t)$ are the differential growth functions which would represent layering, wetting and consolidation respectively.

The population balance framework provides the ability to model multiple intensive properties of a granule while maintaining the computational intensity of a one-dimensional model. This is advantageous as this allows for the incorporation of these intensive properties in the kinetic models, but, with the disadvantage of assuming that the properties are averaged over the size class. Another disadvantage is that when compartmentalising the particle bed, there is no clear improvement of the model's ability to capture the distribution of wetted particles which have recently entered the spray zone [Bellinghausen, 2021].

5.3.3 Wetting

The rate of particle wetting is dictated by differentials given in Equations 5.15 and 5.16. Before the model is defined, it is important to characterise the liquid-to-solid ratio specific to each individual properties. This is given as Equations 5.18 and 5.19 for the component of solid in liquid phase and the solvent phase respectively:

$$x_{s_{liq}} = \frac{s_{liq}}{s + s_{liq} + l + g} \quad (5.18)$$

$$x_l = \frac{l}{s + s_{liq} + l + g} \quad (5.19)$$

where the overall liquid-to-solid ratio is given by the addition of both:

$$x_{LS} = \frac{s_{liq} + l}{s + s_{liq} + l + g} \tag{5.20}$$

The wetting rates for each component can then be given as Equations 5.21 and 5.22:

$$\frac{ds_{liq}}{dt} = \frac{2f_{s_{liq}}(v,t)}{\frac{\pi}{4}\rho_p \int_0^\infty f_{s_{liq}}(v,t) d_p^2 dv} \dot{M}_{spray} x_{s_{liq}} \tag{5.21}$$

$$\frac{dl}{dt} = \frac{2f_l(v,t)}{\frac{\pi}{4}\rho_p \int_0^\infty f_l(v,t) d_p^2 dv} \dot{M}_{spray} x_l \tag{5.22}$$

where $f_{s_{liq}}$ and f_l is the surface wetting fraction of the respective components. Both these properties can be given by the particle coating number, where we substitute the liquid-to-solid ratio with the respective ratio for each individual component.

The advantage of separating the liquid phase into two-components for a two-phase spray is that this allows us to track the spray properties over the granule phase easier. It is simpler to assume that liquid which enters from the spray is predominantly part of the external film of the granule. This allows for the characterisation of; the total surface coating of the active ingredient of the spray, the total drying rate of solvent from the liquid film, the crust formation and eutectics of the liquid film on the granule surface. While only some of these advantages are implemented within the model, this does provide a platform for expanded use in the future.

5.3.4 Agglomeration

To define the rate of agglomeration within the particle bed, the model proposed in Chapter 4 is used. This is given as Equation 5.23:

$$\beta_{agg} = \beta_0 \eta_{eff} (v + v')^{\frac{2}{3}} \sqrt{\frac{1}{v} + \frac{1}{v'}} \times \begin{cases} 1 & St_v < St_{crit} \\ 0 & St_v \geq St_{crit} \end{cases} \tag{5.23}$$

where η_{eff} is given by Equation 5.24:

$$\eta_{eff} = \begin{cases} (1 - f_i) f_j + f_i f_j + f_i (1 - f_j) & \{f_i, f_j\} > 0 \\ 0 < f_k \ k \in \{i, j\} & f_k = 0, k \in \{i, j\} \ i \neq j \\ 0 & f_i = f_j = 0 \end{cases} \tag{5.24}$$

The agglomeration model physically describes how the surface wetting and collision characteristics lead to agglomeration which is driven by the dimensionless numbers η_{eff} and St_v respectively.

To calculate the surface wetting of each individual particle, the overall liquid-to-solid ratio (as given by Equation 5.20) is considered and is substituted into the particle coating number. This is more explicitly shown as Equation 5.25:

$$\phi_p(v,t) = \frac{6x_{LS}a_d}{\pi d_d^3 \rho_d A_{SA}} \tag{5.25}$$

The methodology for calculating St_v and the external surface liquid which are necessary for the agglomeration model are given in Chapters 3 and 4.

5.3.5 Drying

The Burgschweiger et al. [1999] model is adapted and implemented as the drying model for the bulk particle bed. As stated by the author, a set of assumptions are made to formulate the kinetic expressions:

- The particle phase is well-mixed.
- All particles are considered to be spherical.
- The particle phase and gas phase interact by heat and mass transfer.
- The particle phase is not spatially distributed, hence, neither is the heat loss through the wall.
- There is no back-mixing of gas along the length of the fluidised bed.
- The fluidised bed is well insulated such that $\dot{Q}_{wall} = 0$.

To describe the mass and heat transfer between the particle and gas phases, a kinetic expression first proposed by Groenewold and Tsotsas [1997] is used. The evaporation rate of the liquid solvent can be given as Equation 5.26:

$$\dot{M}_{evap} = \dot{\nu_g} \rho_g \beta_{p\to g} A_p \left(Y_{eq}(X, T_p) - Y_g\right) \tag{5.26}$$

where $\dot{\nu_g}$ is the relative drying rate due to the influence of the sorptivity of the particle, as frist described by Burgschweiger et al. [1999], $\beta_{p\to g}$ is the mass transfer coefficient between the particle and gas phase, A_p the surface area of the particle, Y_{eq} is the equilibrium moisture content and Y_g is the moisture content of the gas phase.

The equilibrium moisture content is given by Equation 5.27:

$$Y_{eq} = \frac{\tilde{M}_w}{\tilde{M}_g} \left(\frac{p_{sat}(T_p, X)}{P_{tot} - p_{sat}(T_p, X)} \right) \tag{5.27}$$

where $\tilde{M}_w$ is the molecular weight of the solvent, $\tilde{M}_g$ is the molecular weight of the drying gas, p_{sat} is the partial pressure of the solvent in the gas phase and P_{tot} is the total pressure of the gas phase.

The relative drying rate, $\dot{\nu_g}$ is a property that is related to the ratio of the actual drying rate over the drying rate of the first period - a property of the characteristic drying curve. This is given as Equation 5.28:

$$\dot{\nu_g} = \frac{\dot{M}_{evap}(\eta)}{\dot{M}_{evap,1st}(\eta)} \tag{5.28}$$

whereby the drying rates are related to the normalised particle moisture content, η. This is given as Equation 5.29:

$$\eta = \frac{X - X_{eq}(RH)}{X_{critical} - X_{eq}(RH)} \tag{5.29}$$

where $\dot{M}_{evap,1st}$ is the drying rate during the first drying period, X the particle moisture content, X_{eq} the equilibrium moisture content of the particle phase and $X_{critical}$ is the critical moisture content which is the moisture content which the particle shifts from the first drying period to the second.

Functionally, the relative drying rate takes the value 1 when the normalised moisture content is greater than 1, and as a function of η when the normalised moisture content is less than 1. This is more explicitly shown as Equation 5.30:

$$\dot{\nu_g} = \begin{cases} 1 & \eta > 1 \\ f(\eta) & \eta < 1 \end{cases} \tag{5.30}$$

To determine the equilibrium moisture content, a sorption isotherm is used. This relates the relative humidity of the gas phase with the equilibrium moisture content. The relative humidity can simply be given as:

$$RH = \frac{p}{p_{sat}} \tag{5.31}$$

such that p is the partial pressure of the solvent in the gas phase.

This modelling approach requires two experimental inputs: the characteristic drying curve which is necessary to determine the relative drying rate and the sorption isotherm. This ensures that the model is responsive to changes in input formulation as the drying kinetics is severely dependent on the isotherm and drying curve properties. This has advantages in maintaining model accuracy for changes in formulation, but, requires accurate experimental inputs to initialise the framework.

5.3.6 Bed Hydrodynamics

The model combines the work of Werther [1977], Kunii and Levenspiel [1991] and Goldschmidt et al. [2002] by building a framework which estimates key bed properties such as; fluidisation condition, bulk collision velocities, bed height, heat and mass transfer properties and discharge rates.

To determine these properties, we first need to determine the minimum fluidisation velocity of a particle size d_i within the particle bed. This is shown as Equation 5.32:

$$\frac{1.75}{\varepsilon_{mf}^3 \phi_s}\left(\frac{d_{3,2} u_{mf} \rho_g}{\mu_g}\right)^2 + \frac{150(1-\varepsilon_{mf})}{\varepsilon_{mf}^3 \phi_s^2}\left(\frac{d_{3,2} u_{mf} \rho_g}{\mu_g}\right) = \frac{d_{3,2}^2 \rho_g (\rho_p - \rho_g) g}{\mu_g^2} \tag{5.32}$$

where u_{mf} is the minimum fluidisation velocity, $d_{3,2}$ is the sauter mean particle size, ϵ_{mf} is the initial bed porosity, Φ_s is the shape factor of the particle, μ_g the gas viscosity, ρ_g the gas density and ρ_p the granule skeletal density.

The expanded bed porosity is a function of the superficial and elutrition gas velocities as shown by Equation 5.33 [Kunii and Levenspiel, 1991, Richardson and Zaki, 1997]:

$$\varepsilon^n = \frac{Re_0}{Re_{elu}} \tag{5.33}$$

where ε is the expanded bed porosity, n is an exponent, Re_0 the superficial Reynolds number and Re_{elu} is the elutriation Reynolds number. These two dimensionless numbers are calculated by Equations 5.34 and 5.35:

$$Re_0 = \frac{u_0 d_p (\rho_p - \rho_g)}{\mu_g} \tag{5.34}$$

$$Re_{elu} = \sqrt{\frac{4}{3} Ar} \tag{5.35}$$

where Ar is the Archimedes number

$$Ar = \frac{g \rho_g d_{p,i}^3}{\mu_g} \frac{\rho_p - \rho_g}{\rho g} \tag{5.36}$$

the variable n can be related by both the minimum Reynolds number and the elutriation. This is given by Equation 5.37:

$$n = \frac{\ln\left(Re_{mf}/Re_{elu}\right)}{\ln\left(\varepsilon_{mf}\right)} \tag{5.37}$$

To calculate the heat and mass transfer between the composite particle phase and fluidisation gas, we adapt the approach of Gnielinski [2009] as described in Ammar and Park [2020] and Peglow et al. [2007]. The approach is given by Equations 5.38a through 5.38g:

$$Sc = \frac{\mu_g}{D_{eff,g}} \tag{5.38a}$$

$$Sh_{lam} = 0.664 Re^{0.5} Sc^{0.33} \tag{5.38b}$$

$$Sh_{tur} = \frac{0.037 Re^{0.8} Sc}{1 + 2.44 Re^{-0.1}(Sc^{2/3} - 1)} \tag{5.38c}$$

$$Sh_{single} = 2 + \sqrt{Sh_{lam}^2 + Sh_{tur}^2} \tag{5.38d}$$

$$Sh = [1 + 1.5(1 - \varepsilon_{mf})] Sh_{single} \tag{5.38e}$$

$$Nu = ShLe^{-1/3} \tag{5.38f}$$

$$Le = \frac{\lambda_g}{c_{p,g} \rho_g D_{eff,g}} \tag{5.38g}$$

where Sc is the Schmidt number, Sh the Sherwood number, Nu the Nusselt number and Le the Lewis number.

To determine the discharge rate of the fludised bed, we take a coefficient of discharge approach which relates the height of the bed with the opening outlet. This is given as Equation 5.39:

$$\dot{m}_{discharge} = C_d A_0 \rho_{bed} \sqrt{2 g H_{bed}} \tag{5.39}$$

where C_d is the coefficient of discharge (set to 0.5 as suggested by Bertin et al. [2011]) A_0 is the discharge outlet area within the vessel, ρ_{bed} is the overall bed density and H_{bed} is the bed height. The bed density can be given by Equation 5.40 and the bed height by Equation 5.41:

$$\rho_{bed} = (1 - \varepsilon)\rho_p + \varepsilon \rho_g \tag{5.40}$$

$$H_{bed} = \frac{M_{bed}}{\rho_{bed} A_{bed}} \tag{5.41}$$

5.3.7 Nucleation (one compartment only)

In a one compartment model the droplets cannot be dynamically modelled. This means that we need to treat the nucleation of the small particles which would be

spray dried as a nucleation term which feeds small particles into the bed. Assuming a log-normal distribution of a particle with mean size $d_{nuc,m}$ and a standard deviation of σ_{nuc} we can write the nucleation rate as Equation 5.42:

$$\dot{M}_{nuc} = x_s \dot{M}_{spray} \int_0^{\infty} \frac{1}{\sqrt{2\pi}\sigma_{nuc}} \exp\Big[- \frac{(\ln(d_{nuc} - d_{nuc,m}))^2)}{2\sigma_{nuc}^2} \Big] dd_{nuc} \tag{5.42}$$

5.3.8 Spray Drying (two compartment only)

The final component of the model includes modelling the drying of the spray within the fluidised bed. Key components include: predicting the initial droplet size, drying of the droplets, droplet temperatures and residence time. To develop the equation set, a few assumptions are made:

- The spray is treated as a well-mixed zone, therefore, effects of counter-current flow are ignored.
- The material feed through the spray is two-phase; of a solvent and solid phase.
- Agglomeration and breakage of droplets is not considered.
- There is no accumulation of solid, liquid or gas within the spray drying zone.
- The droplet is distributed log-normally by one standard-deviation.

The mass balance for the evaporating phase in the spray inlet is given as Equation 5.43:

$$r\dot{M}_g \frac{dY}{dt} = r\dot{M}_g(Y_{in} - Y_{out}) + \int_0^{t_{max}} \dot{M}_{evap} dt \tag{5.43}$$

where t_{max} is the maximum residence time of the droplet and r is the recycle ratio of the inlet fluidisation air into the spray drying compartment. The property r is effectively the result of a gas bypass which indicates that not all of the fluidisation air would be en-trained into the spray.

The droplet dries over the distance between the nozzle and the particle bed over some residence time. Therefore, the total mass lost through drying will be the integral of the evaporation rate across the residence time domain. The mass balance for the droplet phase is given as Equation 5.44:

$$\dot{M}_{spray} \frac{\partial X}{\partial t} = -\dot{M}_{evap} \tag{5.44}$$

where t represents the residence time domain of the droplet. The heat balance for the gas and solid phases are given as Equations 5.45 and 5.46:

$$\frac{dH}{dt} = r\dot{M}_g \sum_{i}^{components} x_{in,i} c_{p,i} T_{inlet} - r\dot{M}_g \sum_{i}^{components} x_{out,i} c_{p,i} T_{outlet} c_{p,w} \left(\int_0^{t_{max}} M_{evap} dt \right) T_{out} - h_{d\rightarrow air} \int_0^{t_{max}} A_d (T_{out} - T_d) dt \quad (5.45)$$

$$\dot{M}_{spray} \left(c_p + x_w c_{p,w} \right) \frac{dT_d}{dt} = h A_d T_{out} - \Delta h_v \int_0^{t_{max}} \dot{M}_{evap} dt \quad (5.46)$$

The kinetic expression for drying is exactly the same as Equation 5.26. To predict the heat and mass transfer coefficients between the droplet phase and gas phase a simple Ranz-Marshall correlation is taken as Equation 5.47:

$$Nu = Sh = 2 \quad (5.47)$$

To model the distribution of droplets from the nozzle a normal distribution model is used. This is given as Equation 5.48:

$$n(d_d) = \frac{\dot{M}_{spray}}{\sqrt{2\pi}\sigma} \exp\Big[- \frac{(\ln(d_{3,2} - d_{3,2,m}))^2)}{2\sigma^2} \Big] \quad (5.48)$$

where $d_{3,2}$ is the Sauter diameter of the droplet, $d_{3,2,m}$ is the Sauter mean diameter of the droplet and σ the standard deviation.

To calculate the droplet shrinkage an approach suggested by Oakley [2004] is used. If we suppose that the droplet shrinks until the critical moisture content, we can write the change in diameter as:

$$\frac{dd_d}{dt} = \begin{cases} f(d_d) & X \geq X_{cr} \\ 0 & X \leq X_{cr} \end{cases} \quad (5.49)$$

where d_d is the droplet diameter, $f(d_d)$ is the size change function, X the droplet moisture content and X_{cr} the critical moisture content. We define the size change function as suggested by Oakley [2004] as Equation 5.50:

$$d_d = d_{d,0} \left(\frac{\rho_{solid}}{\rho_d} \right)^{\frac{1}{3}} \left(\frac{\rho_d}{\rho_{dry}} \right)^{\frac{1}{3}} \quad (5.50)$$

where $d_{d,0}$ is the initial droplet diameter, ρ_d is the density of the droplet and ρ_{solid} is the density of the droplet's solid phase.

To calculate the density of the droplet, it is calculated as a weighted average as shown in Equation 5.51:

$$\frac{1 + \sum_i^{components} X_i}{\rho_d} = \frac{1}{\rho_{dry}} + \sum_i^{components} \frac{X_i}{\rho_i} \tag{5.51}$$

5.4 Model Implementation

Four models were implemented within the gFormulate 2.3.0 environment (Seimens PSE ltd.) using a custom library for the agglomeration, drying, heat transfer, bed hydrodynamics and spray drying. These are:

1. A one compartment continuous fluidised bed model which includes all the previously discussed models with the exclusion of spray drying and a product recycle.

2. A one compartment continuous fluidised bed model which includes all rate models and a product recycle. This model excludes spray drying.

3. A two compartment continuous fluidised bed model which includes all rate models and spray drying. This excludes a product recycle.

4. A two compartment continuous fluidised bed model which includes all rate models, spray drying and a product recycle.

The internal library model "fluidised bed granulator with population balance" was used as the supporting hierarchical structure as this already integrates the proposed population balance framework. To implement the product screen for the product recycle, the screen model was used directly from the formulated products library. This model was not customised and was used as featured within the 2.3.0 version.

The internal gProms DAEBDF solver was used with the default tolerances for the relative and absolute errors. Details for the solver can be found within the gProms documentation and in the works of Vassiliadis et al. [1994a,b], Oh and Pantelides [1996].

A table of parameters used to initialise the model is provided as Table 5.1.

Table 5.1: Table of parameters for the integrated models

Parameter Name	Symbol	Value
Spray rate	$\dot{m}_{spray}$	45-55 kg/hr
Number of size classes	N	15 (-)
Mean particle size of the bed	μ	230 μm
Standard deviation of the bed	σ	90 μm
Initial bed mass	M_{bed}	10-25 kg
Solid composition of the spray	x_s	0.5 w/w
Initial moisture content of the bed	x_l	0.01 kg/kg
Density of solid phase	ρ_s/ρ_{dry}	1300 kg/m^3
Density of liquid phase	ρ_l	1000 kg/m^3
Density of gas phase	ρ_g	1.2 kg/m^3
Initial droplet diameter	$d_{d,0}$	100-200 μm
Droplet standard deviation	σ_d	10 μm
Droplet residence time	t_d	2 s
Discretisation points for spray drying	N_d	10 (-)
Nuclei diameter	d_{nuclei}	100-200 μm
Standard deviation of the nuclei	σ_{nuc}	10 μm
Solid composition of the spray	x_{spray}	0.5 kg/kg
Critical moisture content	X_{cr}	0.3 kg/kg
Bed diameter	d_{bed}	0.5 m
Inlet fluidisation air flow rate	$\dot{M}_g$	1200-1300 m^3/hr
Initial fluidisation gas temperature	$T_{g,0}$	85 °C
Initial bed temperature	$T_{b,0}$	25 °C
Inlet spray temperature	$T_{spray,0}$	25 °C
Inlet relative humidity	RH_0	1 % w/w
Latent heat of evaporation	δh_v	2570 $\frac{kJ}{kg.K}$
Vapour thermal conductivity	λ_g	0.024 $\frac{W}{m.K}$
Gas viscosity	μ_g	1e-5 $Pa.s$
Rate constant	β_0	1e-16 $\frac{1}{s}$
Contact angle	θ	35°
Surface asperity length	h_0	1e-6 m
Coefficient of discharge	C_d	0.5 (-)
Discharge area	A_0	0.03 m^2 (15% of the area)
Recycle ratio	r	0.9 (-)
Minimum fluidisation porosity	ε_{mf}	0.43 (-)
Screen aperture size	-	200 μm
Range below which the aperture is non-ideal	-	30 μm
Simulation duration	t	3 hours

5.5 Numerical Study

This section will perform a numerical study on understanding the influence of the initial bed mass, the spray rate, droplet size, fluidisation air flow rate and temperature on key product properties. These properties include the; particle size and distribution, vapour moisture content and temperature, granule moisture content, mass holdup and the outlet flow rate from the bed and the screen.

5.5.1 Effect of Initial Bed Mass

For the simulations within this section, the initial bed mass was varied at initial values of 10 kg and 25 kg. The mass spray rate was fixed at 50 kg/hr with a droplet nuclei diameter of 30 μm. The agglomeration rate constant was fixed to a value of $1e-16s^{-1}$ in addition to the inlet fluidisation air temperature and flow rate of 85 $^{\circ}C$ and 1300 $\frac{m^3}{hr}$ respectively.

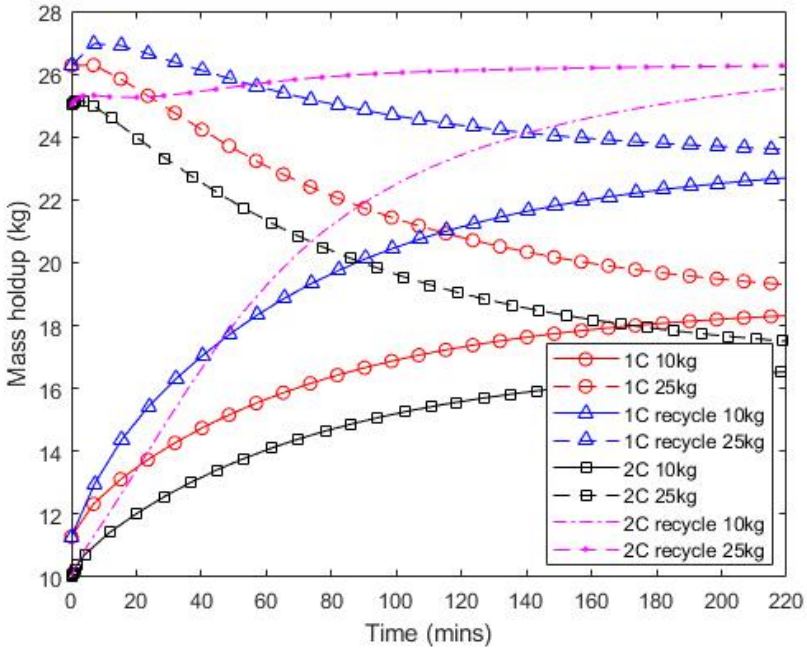

Figure 5.5: The effect of the initial bed mass on the mass holdup

From Figures 5.5 and 5.6 we see how the four granulator models vary with changes in the initial bed mass. The models which contain a recycle show that the total mass holdup within the bed is higher and that the total discharge from the granulator is also higher. This is expected as the undersize recycle contributes to the overall bed mass (as seen on Figure 5.7). Interestingly for the models which do not include a recycle, the

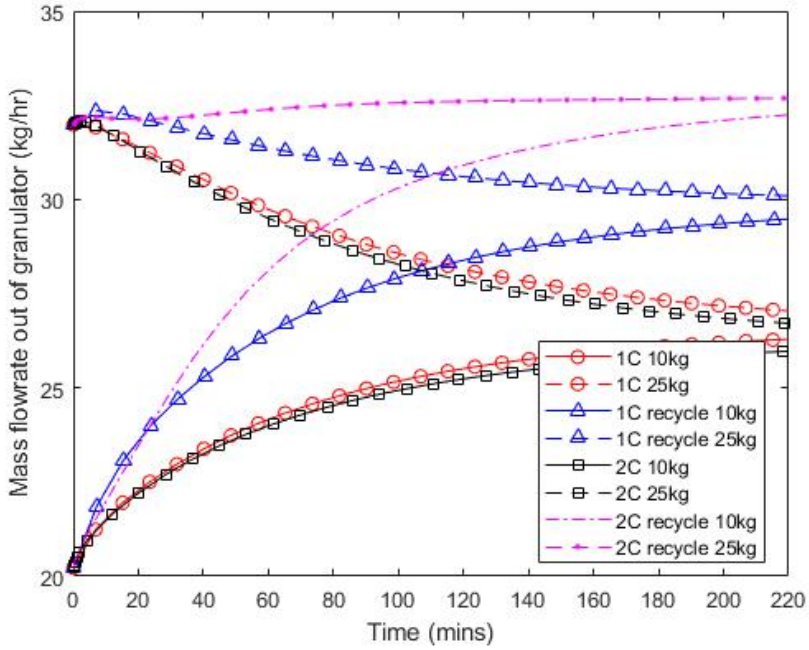

Figure 5.6: The effect of the initial bed mass on the outlet mass flow rate from the granulator

holdup in the two compartment model is lower than that of the one compartment. Whereas for the models which do include as recycle, the two compartment model shows a greater mass holdup than that of the one compartment. This observation is replicated in the outlet flow rate from the granulator.

The mass holdup and outlet flow rate reaches steady-state quicker depending on how close the initial properties are to the steady-state. This can be seen for the two compartment recycle model at 25 kg where the steady-state holdup and flow rate is seemingly close to the initial value compared to the other models. This is consistent with works by Cryer [1999], Vreman et al. [2009], Bertin et al. [2011] who observed similar effects within their experiments; though as stated in Cryer [1999] this is common practice for operators to seed the bed at the expected steady-state (though without any physical reasoning). Timescale in which the models approach steady-state differ, the change in initial bed mass does not change the final steady-state.

From Figure 5.8 the average particle size does vary with the initial bed mass. Both the two compartment and one compartment model show that they are both approaching the same steady-state. Comparing the one compartment and two compartment models, there is less growth in a two compartment model due to evaporation of spray

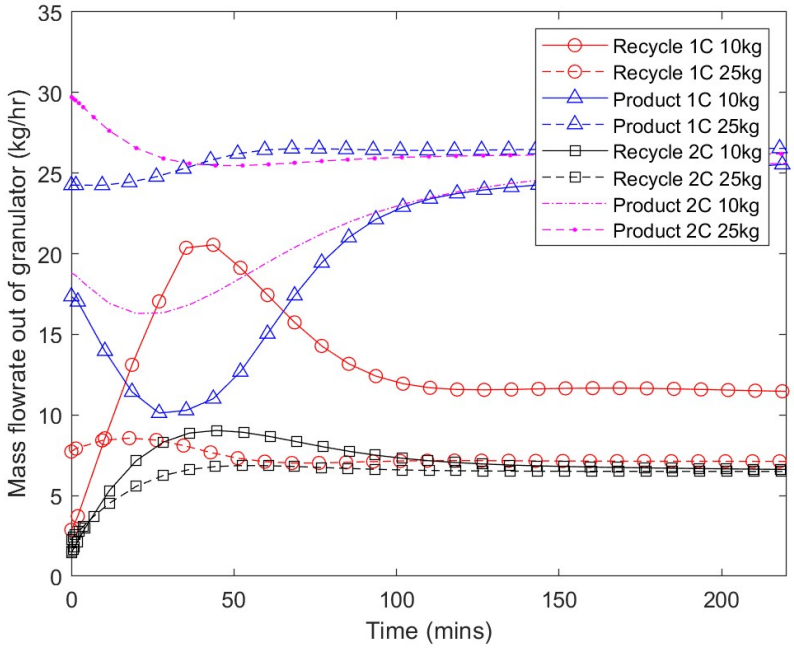

Figure 5.7: The effect of the initial bed mass on the product and recycle streams from the screen

leading to less liquid for growth.

Figure 5.10 shows the normalised mass density distributions are dominated by the entering nuclei. The one compartment models generally show more growth with the addition of a recycle also widening the distributions. The reason for why a two compartment model shows less growth is likely due to the evaporation of the spray resulting in less availability of liquid throughout the bed, hence less agglomeration. The recycle ensures that small particles re-enter which increases the chance to agglomerate, and therefore widening the distribution.

5.5.2 Effect of Mass Spray Rate

For the simulations within this section, the mass flow rate from the spray was varied at 45-55 kg/hr. The initial bed mass was fixed at 25 kg with a droplet and nuclei mean diameter of 100 μm. The agglomeration rate constant was fixed to a value of $1e-16\frac{1}{s}$ in addition to the inlet fluidisation air temperature and flow rate of 85 $^{\circ}C$ and 1300 $\frac{m^3}{hr}$ respectively.

Figure 5.11 showed that with an increase in the mass flow rate through the spray, we see more overall growth. This is the expected as the increase in liquid content results in more agglomeration. The models which recycle the product output also

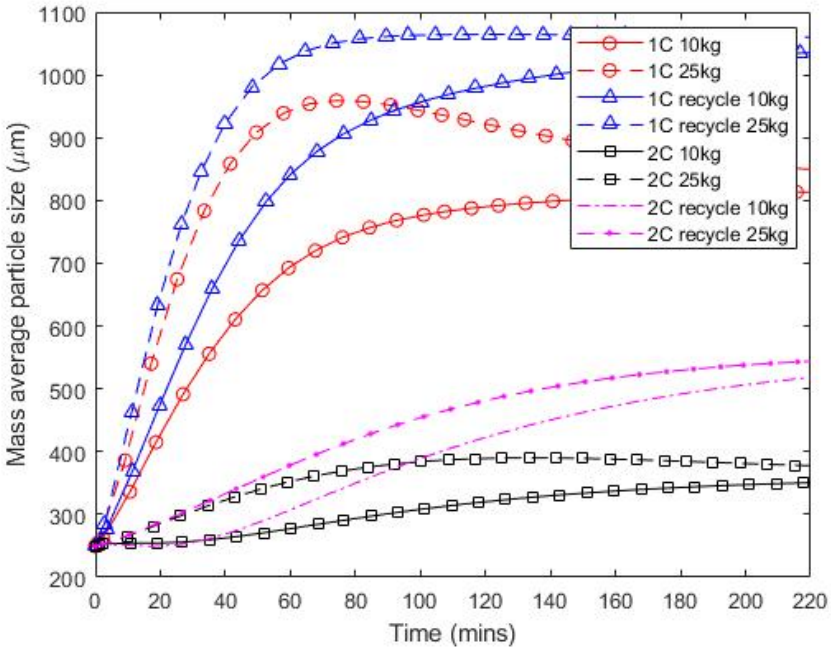

Figure 5.8: Evolution of the average particle size in the fluidised bed outlet for varying bed masses.

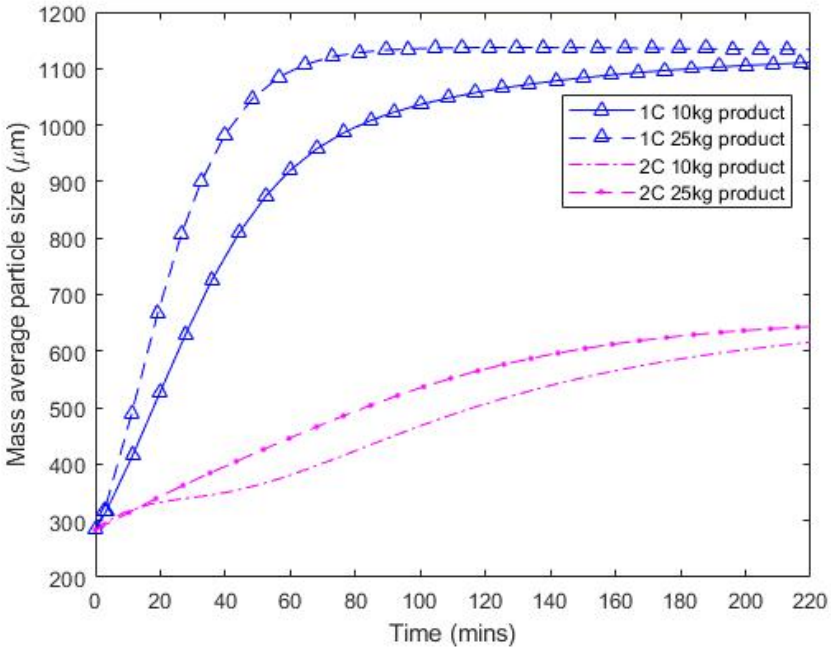

Figure 5.9: Evolution of the average particle size in the product stream of the recycle circuits.

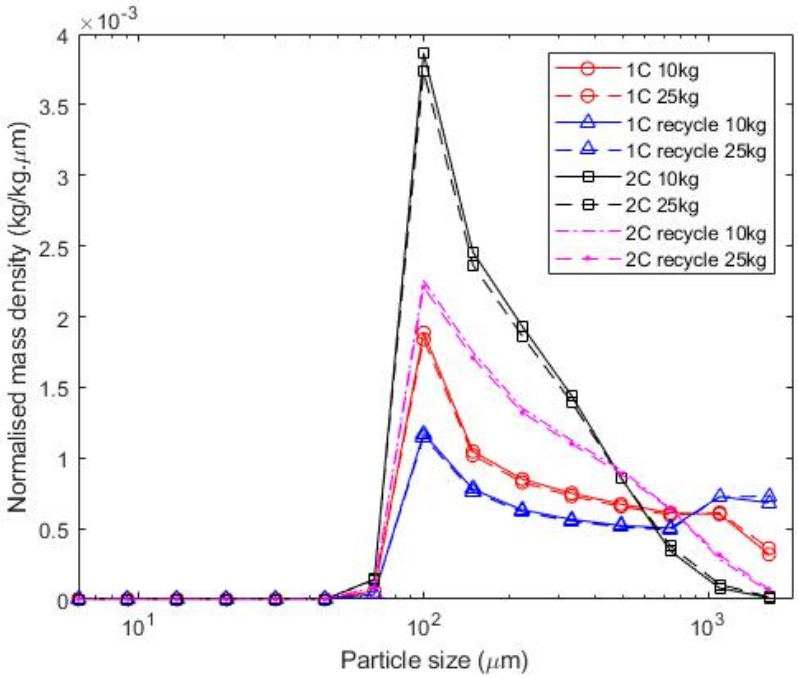

Figure 5.10: The normalised mass density distribution at $t = 3$ hours

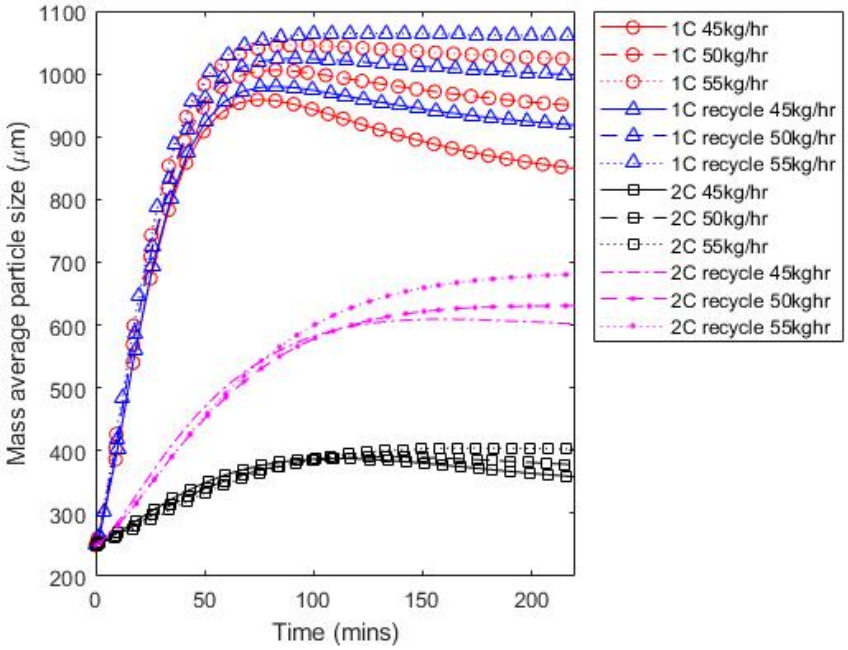

Figure 5.11: The evolution of the mass averaged particle diameter for spray mass flow rates of 45, 50 and 55 kg/hr.

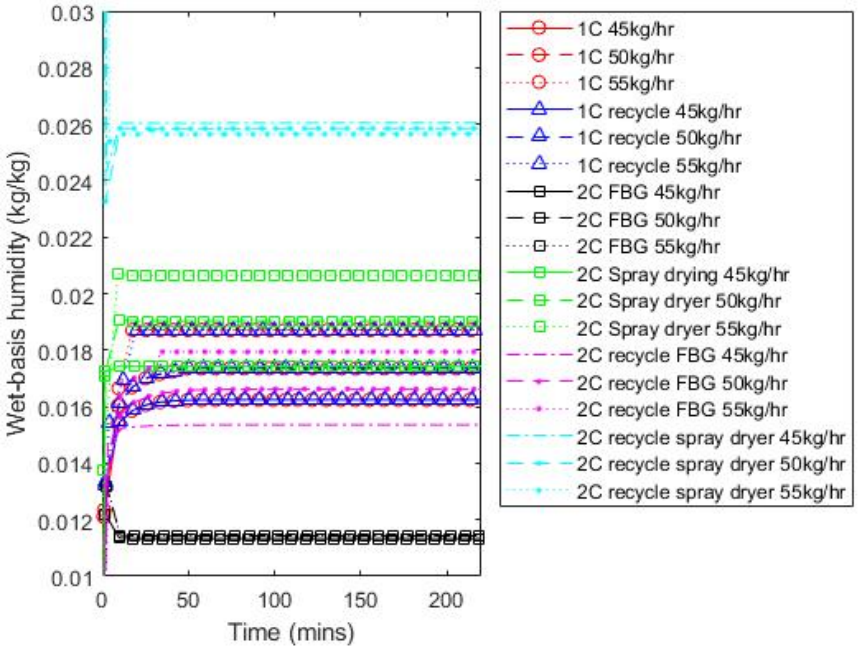

Figure 5.12: The outlet humidity for the four model formulations. For the two compartment scenarios the outlet humidity from the fluidised bed and the outlet from the spray drying compartment are included also.

show more growth as we are maximising the growth of small particles by increasing the residence time through the bed.

Figure 5.12 shows that with an increase in mass flow rate through the spray we see an increase in the overall outlet humidity. With more liquid available (and given that the inlet air streams are not saturated) there is an increase of evaporation.

We see that for a one compartment model that there is little difference between the outlet humidities of the models with and without recycle. This suggests that for a compartment system that the drying is independent of bed mass, but rather, the capacity of drying within the fluidisation air. This is not observed within a two compartment model. There is a difference in the outlet humidity from both the fluidised bed and spray drying compartment. The outlet humidity from the spray drying compartment is shown to be generally larger than that of the fluidised bed. This is expected, as the exhaust from the fluidised bed is recycled into the spray drying compartment which ensures there is greater mass transfer into the air stream.

In the two compartment model with recycle, we see that the lower the spray rate the greater the outlet humidity is from the the spray compartment. This is likely due to the unique circumstance where the outlet temperature at lower spray rates

being higher, hence, a greater capacity to hold moisture. As the drying gas isn't saturated at the bed due to the lower mass flow rate through the spray, it enters the spray compartment at a higher temperature. The difference is marginal but is an interesting scenario.

We see a numerical artifact for the two compartment recycle model, where there is a sharp incline in the exhaust humidity from the initialised value. While the final steady state is reached there is perhaps a numerical issue during the early stages of the simulation. This issue however seems to be isolated to within the spray drying compartment and for early time values between 0-10 seconds of simulated time. Therefore, this effect is negligible.

5.5.3 Effect of Droplet/Nuclei Diameter

All properties except the droplet/nuclei diameter were kept the same as previous during these sets of simulations. The droplet/nuclei diameter was varied between 100 and 200 μm.

Figure 5.13 shows that with an increase in the nuclei and droplet diameter we see more growth overall. As we are continuously seeding the bed with larger particles, they agglomerate to grow even larger. Furthermore, larger droplets dry slower which increases the overall liquid content within the bed. This allows for more agglomeration. Interestingly, the models which recycled the output show that the average size tends towards a similar asymptote despite differences in the droplet and nuclei diameter. While they do tend towards a similar size, Figure 5.14 shows that the mass density of the size classes vary significantly. The nuclei/droplet diameter is often shown as the modal peak along the distribution, where for the models with a recycle show wider distributions.

We see how the droplet size distribution changes on Figure 5.15. In general, changes seem minimal and the droplets largely enter the bed at a size slightly smaller than that of the initial. The largest change is seen in the two compartment with no recycle model where there is a notable reduction from the modal peak of 200 μm. However, this seems almost exclusive to the 200 μm scenario as the 100 μm shows almost no change. This can likely be attributed to the larger droplet diameter having a larger area for heat and mass transfer hence more drying. This clearly diminishes as the droplet reduces in size.

Figure 5.16 shows relative humidity and temperature for the spray compartment. The recycle models show that the relative humidity in the outlet is considerably lower than the model without recycle. The increase in bed mass within the recycle models

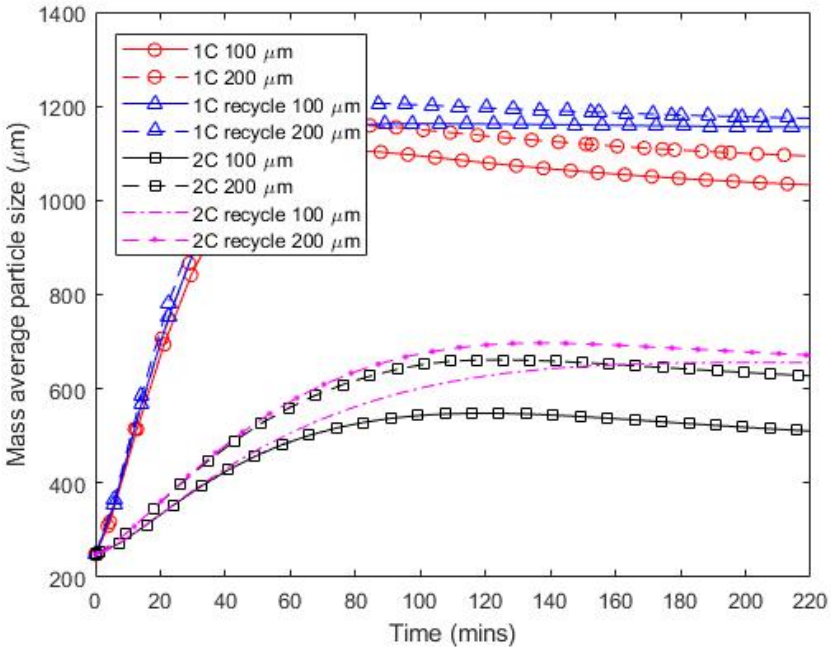

Figure 5.13: The mass average particle size for changing droplet/nuclei diameter for all four model formulations.

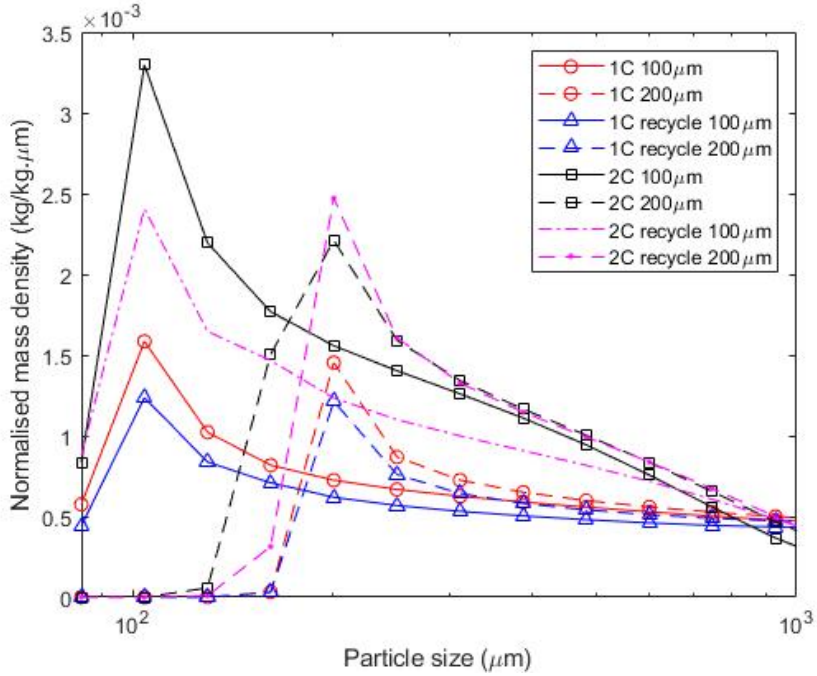

Figure 5.14: The mass density distribution for changing droplet/nuclei diameter for all four model formulations at $t = 3$ hours

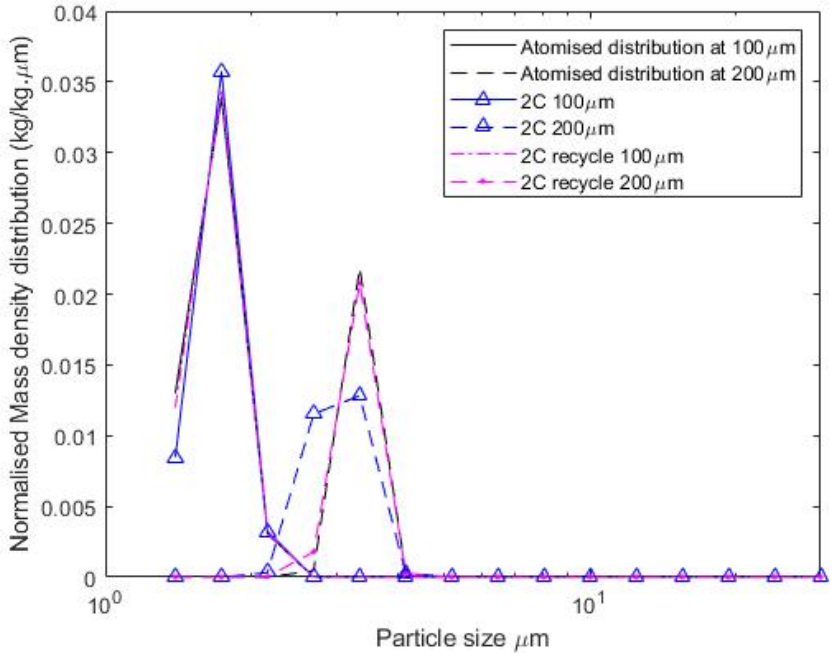

Figure 5.15: The droplet size distribution of the atomised droplets in the spray drying compartment for the two compartment models.

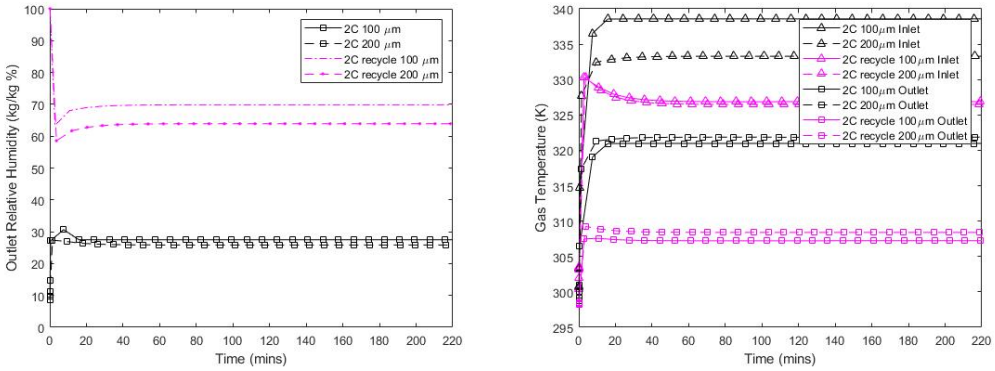

(a) (b)

Figure 5.16: The (a) relative humidity and (b) temperature for the spray drying compartment in the two compartment model for varying droplet diameters.

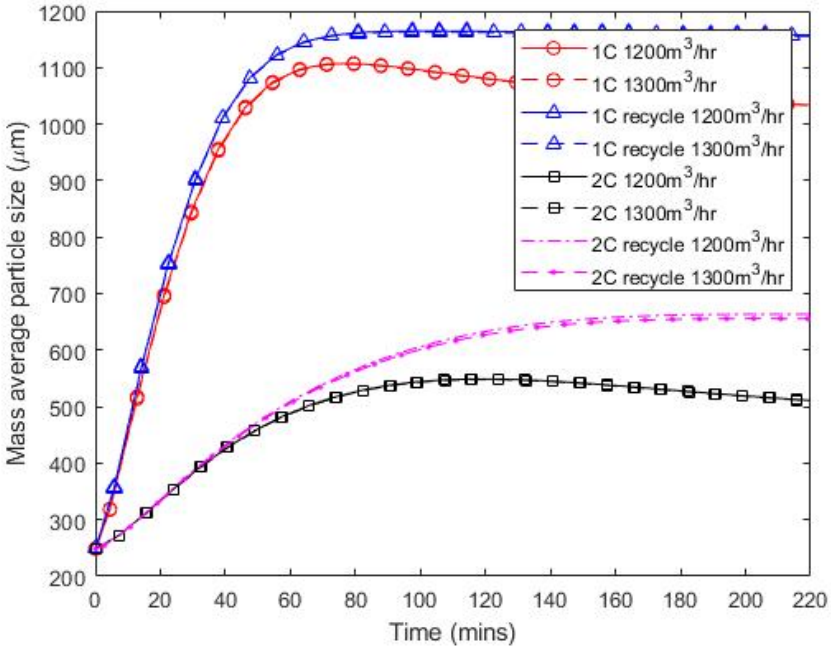

Figure 5.17: The mass average particle size for changing fluidisation air flow rate for all four model formulations.

leads to more drying of the bed and ultimately reducing the temperature and drying capacity of the gas. This is supported by Figure 5.16(b) where we can see that the streams enters the spray compartment at a lower value for the recycle model where after drying it reduces significantly, such that the drying capacity reduces and the relative humidity increases.

5.5.4 Effect of Inlet Fluidisation Flow Rate

Figure 5.17 shows that there is very little sensitivity to the inlet fluidisation flow rate with regards to the average particle size. Numerically, the changes are roughly $\approx 2\mu m$ where the greatest change is observed in the two compartment recycle model. The fluidisation flow rate is often regarded as a process parameter which influences breakage and drying [Werther, 1977, Hemati et al., 2003]. For the proposed model we ignore breakage, so it is unsurprising that there is little change. The expected changes would be in the behaviour of the Stoke's criterion and liquid availability.

The models without a recycle show lower average particle size to the recycle variant. The difference is likely related to re-nucleating the bed with particles from the recycle which promotes more growth given there is available liquid.

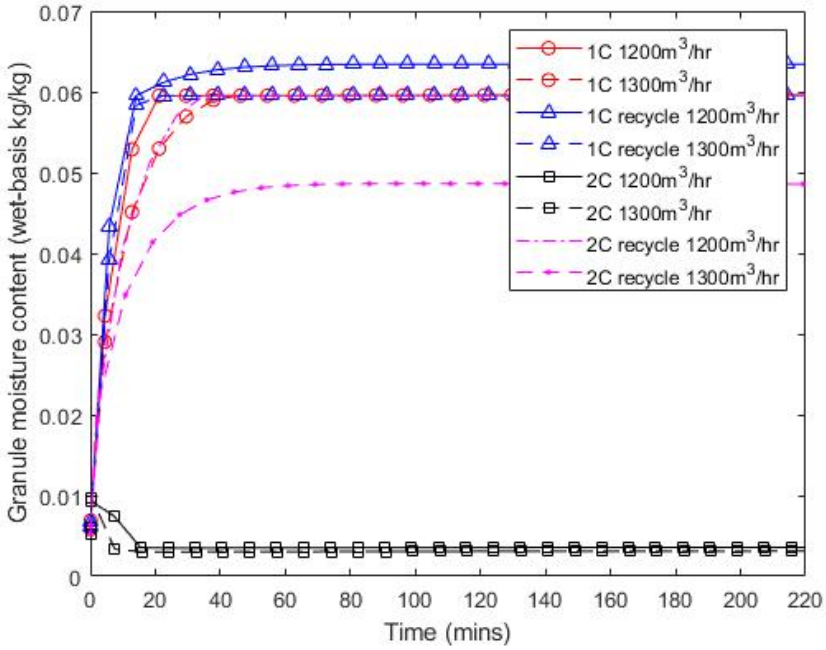

Figure 5.18: The granule moisture content within the granule bed for all four model formulations.

From Figure 5.18 we see the granule moisture content for the lower fluidisation flow rates to be higher. With less air flow through the bed, the overall drying rate reduces. An anomaly is seen for the two compartment model, where the moisture content remains fixed at a value that seems unreasonable compared to the other formulations. We hypothesise that the issue is related to the two compartment nature of the model. As the air flows through the bed, there is initial drying, which then further dries within the spray drying compartment. With a continuous flow out of the bed the part of the available moisture leaves through this stream. With a reduced moisture within the bed, this amplifies the capacity to dry in the spray compartment; which then results in less liquid entering the bed. This results in an positive feedback loop where the drying increases until the minimum equilibrium solid's moisture content is reached. This is clearly erroneous and is possibly a product of the simulation parameters. This issue is avoided by the addition of a recycle as we ensure liquid which leaves the bed re-enters through the recycle stream. For the models which include a recycle we can see a clear sensitivity to the inlet drying air, whereas, the no recycle models show that they reach an equilibrium quickly. We see from Figure 5.19 that there is a large change both the bed mass and discharge which is likely destabilising the drying phenomena. This highlights a key issue when formulating

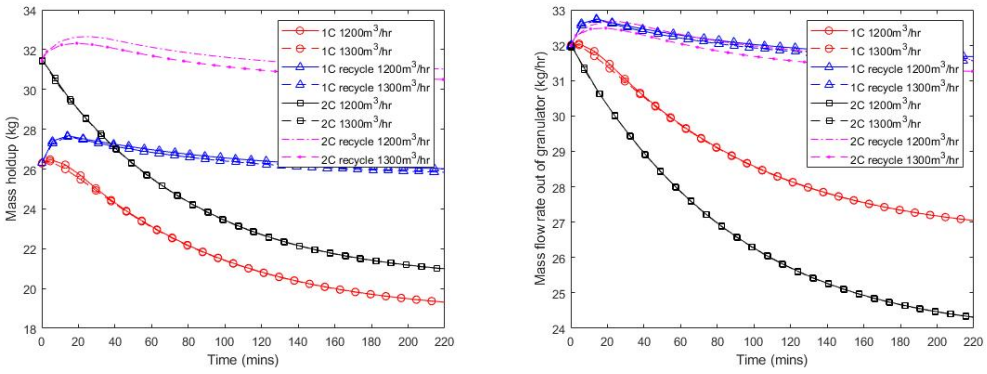

(a) (b)

Figure 5.19: The (a) total mass holdup within the particle bed and (b) the discharge rate from the particle bed for all four model formulations.

a two-compartment model for a continuous system - the model is very sensitive to changes in the bed and drying conditions.

5.5.5 Effect of Inlet Fluidisation Temperature

Figure 5.20 shows that with an increase in fluidisation air temperature the average particle size decreases slightly. Similar to the previous parameters, this is most emphasised in the two compartment model with a recycle. Increasing the temperature reduces the overall liquid availability in the bed, which results in slightly less agglomeration. For the two compartment model, we see no change which is infact consistent with the previous study as it was identified that the liquid availability was already extremely low for the simulation conditions.

The temperatures for the solid, vapour and the spray drying compartment are shown on Figure 5.21, where as expected, an increase in temperature leads to an overall temperature increase for all phases. Importantly, the vapour phase sits at temperatures slightly above the solid phase which confirms that the energy balance is consistent. An interesting aspect of the model is the approach for which the temperature increases for the vapour phase. As the simulation proceeds, the approach is from below at 25°C to the steady-state. The system is initialised to treat the initial holdup of vapour to be at the same temperature as the solid-phase, that is all phases initially within the fluidised bed are the same temperature. Therefore, it should be expected that the approach to steady-state is initially from below.

The moisture content decreases with an increase in temperature. With an increase in the drying potential more moisture is removed from the granule phase. Within the

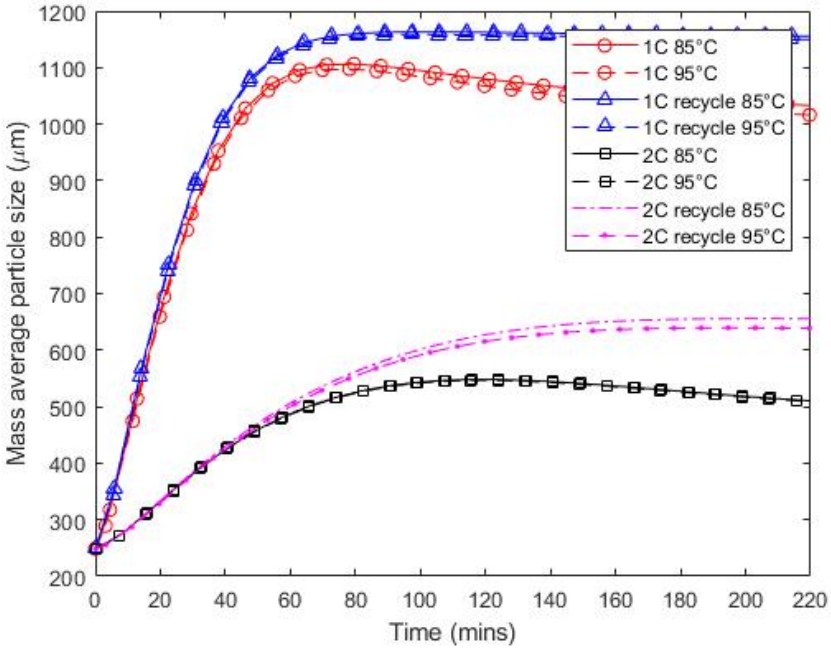

Figure 5.20: The mass average particle size for changing inlet fluidisation air temperature for all four model formulations.

spray drying compartment, for the two-compartment model with a recycle the change in temperature only provided a small change in the moisture content of the droplets. The two-compartment model without recycle remains almost unchanged, which given the previous observations, ensures that the model is consistent.

5.6 Conclusion

A sensitivity analysis is performed on four model formulations to investigate how key physical parameters influence the output for key outputs. Based on the results, the model shows consistency with what is expected in literature; where the greatest change to particle growth was influenced by the mass spray rate. The fluidisation flow rate and temperature did hold some influence to growth, but, provided a more dominant change to the drying conditions. The proposed model provides a stable framework to model continuous fluidised bed granulators which can model to a steady-state, which is particularly relevant to many industrial systems.

A clear limitation to the one compartment model is the dominance of nucleation within the distributions, and the two-compartment model showing great sensitivity to changes in the drying conditions. The issue with the nucleation rate is that the

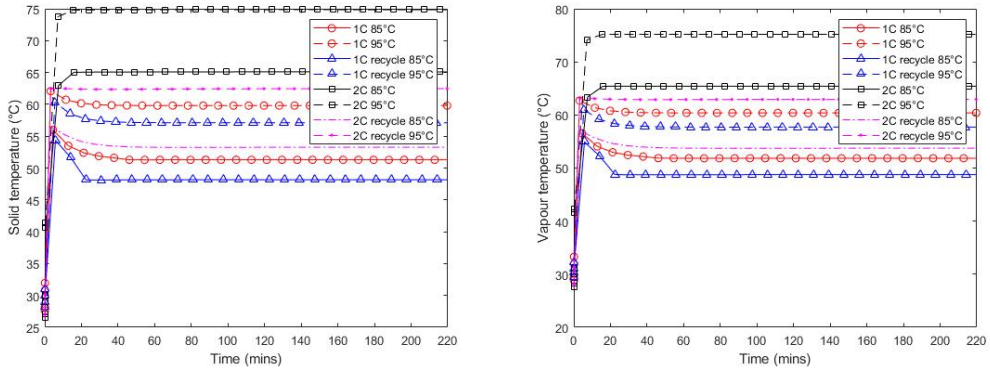

(a)

(b)

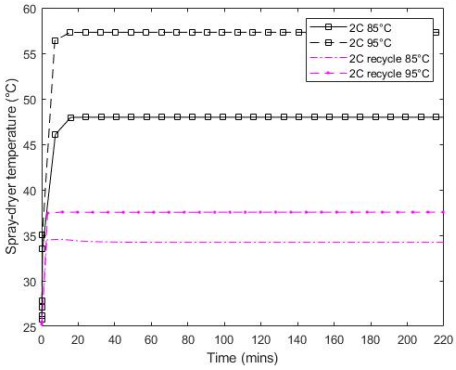

(c)

Figure 5.21: The (a) solid temperature, (b) the vapour temperature and (c) the temperature within the spray drying compartment

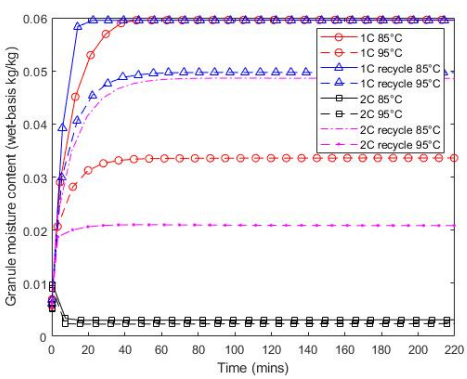

(a)

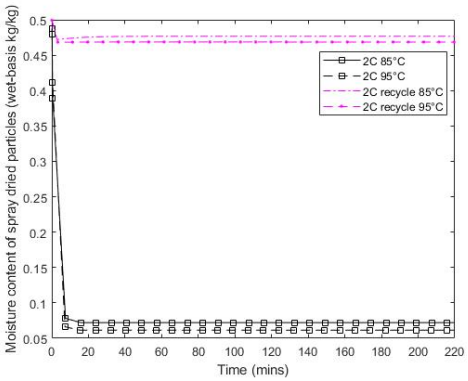

(b)

Figure 5.22: The (a) granule moisture content of the four model formulations and (b) the moisture content of the droplets in the spray drying compartment for the two compartmental models.

particles are added to the gridpoint but show little growth. This leads to a large peak around the nuclei particle diameter, where intuitively, we should expect these nuclei to agglomerate immediately. This is a product of a couple issues; the coupled population balance approach, in addition to, the sensitivity of wetting rate to the size of the particles. As the liquid which is added to each gridpoint is averaged over all the particles, we lose the immediate information from the spray-drying compartment that the particle is wet. When combined with the wetting rate we see that the model prefers large particles; the droplets which enter the smaller gridpoints don't receive enough liquid to ensure rapid growth.

Chapter 6

Experimental Studies of a Pilot-scale Top-spray Fluidised Bed

6.1 Introduction

In this chapter, experimental studies on a pilot-scale top-spray fluidised bed granulator are performed to develop a mechanistic understanding of the influence of the mass spray rate, the fluidisation air temperature and the fluidisation air flow rate. These three parameters are commonly varied to troubleshoot process anomalies, often without much scientific understanding. Therefore, there is value in understanding the influence of these process parameters on the granulation mechanisms to; validate the proposed granulation rate process framework and to enhance the process operator's ability to troubleshoot.

The overall goal is to provide a quantitative analysis on the effects of the key process parameters on the product output, such as the average particle size, the size distribution and moisture content of the granule.

6.2 The Pilot-scale Fluidised Bed Granulator

A flow diagram of the continuous pilot-scale fluidised bed granulator is provided as Figure 6.1. The fluidised bed has a tray diameter of 0.5 m and a top-spray arrangement with an internal nozzle diameter of 4 mm. The material discharges through a screw conveyor which roughly encompasses 10% of the tray area. The screw conveyor aims to maintain a constant pressure drop across the bed through a PID control loop which correlates to a constant bed mass. The PID responds to changes in sensors P11 and P17 and adjusts the rotation speed of the rotary valve accordingly. The fluidised bed product enters an over and undersize sieve, sized at 1600 μm and 200

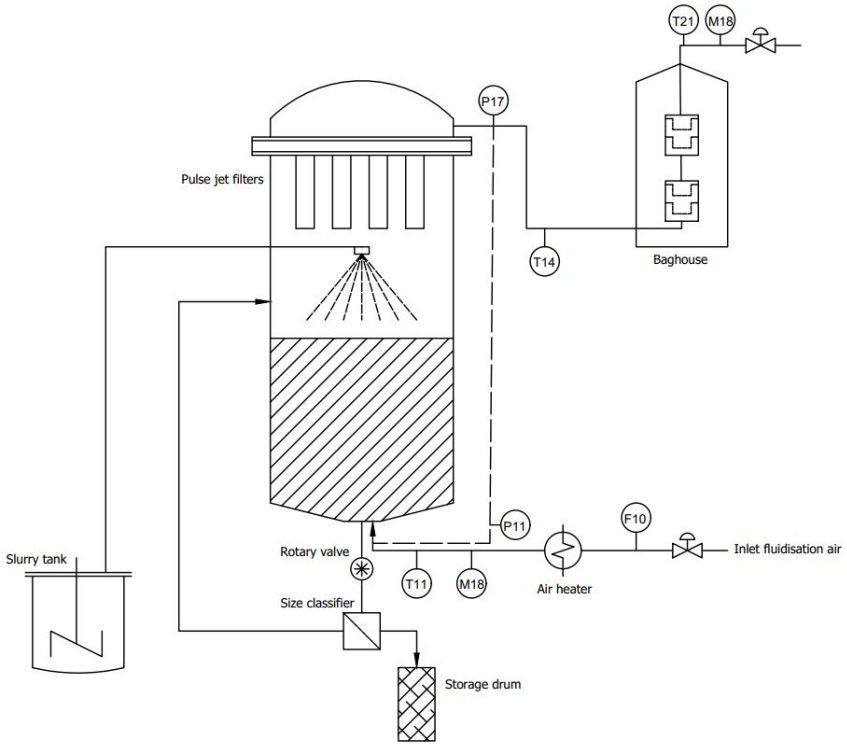

Figure 6.1: Flow diagram of the pilot scale unit.

μm respectively. The product stream is discharged into a material drum which sits on top of a gravimetric scale. Once the material drum is full it is removed, stored and replaced. The undersize is pneumatically transported back into the bed and the oversize is normally returned back into the slurry tank, though this functionality was not available during the period of this study. The unit is fitted with pulse jet filters and a bag house to minimise the escape of small fines through the air stream. The unit has an estimated maximum throughput of 500 kg/hr.

The author's primary role was to design the experimental approach. The key responsibilities was to decide what spray rates, air temperatures, air flow rates, the choice of measurement technique, what measurements and sampling frequency. The experiments were performed and managed by the Syngenta process engineers and operators. They would set-up and clean the equipment, perform the appropriate maintenance checks and perform all manual measurements. The manual measurements include sampling from the bed, sampling from the product stream, performing the size measurements, performing the moisture measurements and exporting the sensor measurements.

6.3 Materials and Methods

A placebo formulation was used as the granule material. This formulation shares similar processing characteristics to trademarked products of Syngenta. It is relatively cheap to manufacture and was readily available as a substitute to a "real" industrial product. As the placebo formulation is commonly used internally, key properties such as size, densities, viscosity profiles and thermal properties are readily known; which is a key advantage over using a manufactured formulation. Though for future work, it is advised to move away from the placebo formulation to a a real API to test validity and rigour of the experimental hypothesis. Due to disclosure agreements, the composition of the placebo will not be detailed and from hereon will be referred to as Placebo A7946T.

6.3.1 Size Characteristics

To characterise the size and distribution of the Placebo A7946T powder, a Malvern Mastersizer 3000 with a dry cell (Malvern Panalytical Ltd.) was used. A sample mass of 4 g was fed into the top hopper, which would vibrate and promote a flow of particles into the analysis compartment. The equipment measures the intensity of the light scattered as the dispersed, flowing particles, fall through the analysis region. From the scattered patterns, this is converted into a size (as from the work of Rawle [2003]). Three samples were measured to provide a volume based frequency. The grid was initialised with fifty points from a minimum value of 0.01 to 3500 μm across a logarithmic scale. The distribution properties are shown as Figure 6.2:

The methodology and samples show high reproducibility. All three curves show a small peak at $\approx$30 μm which may indicate the capture of dust from the pulse jet filter. Furthermore, additional size information is given on Table 6.1 which provides values on the d_{10}, d_{50}, d_{90} and $d_{3,2}$.

Table 6.1: The d_{10}, d_{50}, d_{90} and $d_{3,2}$ for the Placebo A7946T.

Sample	$d_{10}(\mu m)$	$d_{50}(\mu m)$	$d_{90}(\mu m)$	$d_{3,2}(\mu m)$
1	123	207	338	183
2	121	206	337	182
3	119	200	325	177

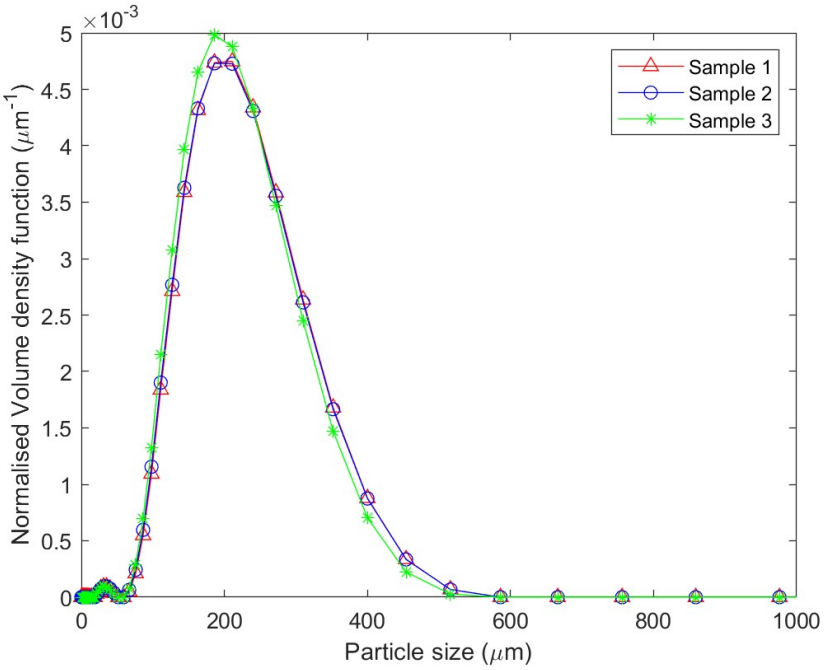

Figure 6.2: The initial size distribution of Placebo A7946T, (a) the volume density

6.3.2 Bulk Density

The bulk density is measured using the CIPAC MT 186 method, a standard cross-industry method. Detailed information of this method can be found within the formulated pesticide handbook [Ashworth et al., 1970]. A value of 653 kg/m^3 was measured.

6.3.3 Specific Heat Capcity

Given the specific nature of Placebo A7946T, calibrating a calorimeter is practically difficult. An estimate of the specific heat is calculated based on the composition of Placebo A7946T. From this calculation a specific heat value of 1.26 $J/kg.K$ is attained.

6.3.4 Granule Moisture Content

To measure the granule moisture content a coulometric Karl-Fischer titration method was used. A two samples of 100 mg was placed into the measuring cell of the Titrator Compact V10S (Mettler Toledo Solutions) that contains a solution of methanol, sulphur dioxide and iodide. The equipment is initially calibrated to remove the effects of ambient moisture. The moisture of the granule sample reacts with the iodide to form

iodine, which flows by a voltage differential provided by an anode and cathode. Once the measured voltage dramatically drops, this indicates the end of the experiment as all the contained water within the sample has reacted. The moisture content is then calculated by measuring the current needed to electrochemical generation of Iodine to iodide.

6.3.5 Desorption Isotherms and Drying Curves

To determine the isotherms and drying curves a dynamic vapour sorption (DVS) technique was used. A slurry composed of 60% Placebo A7946T and 40% water was placed in the DVS equipment, the DVS Endeavour (SMS Ltd.). The equipment is loaded with ≈15mg of the solution which is set to sweep relative humidities of 0% to 90%. Steps of 10% were chosen. The equipment was set to shift to the next interval after a percentage mass change, at the given humidity, reached a value of 0.0012 s^{-1}. After the measurement at 90% relative humidity was measured, it would return back to 0 in steps of -10% through a similar manner. The desorption isotherm is of interest here, based on the suggestion by Burgschweiger et al. [1999] and Peglow et al. [2007]. This is because the particle undergoes desorption-like kinetics during drying. A third-order polynomial fit was used to generate a line of best fit for the experimental data. The isotherm was measured at three different temperatures, 40°C, 50°C and 60°C. Figure 6.3 shows the desorption isotherms which shows some dependence on temperature. The value at 100% relative humidity is interpolated from the line of best fit.

To determine the single particle drying curve, the slurry was placed in a metal cylinder and inserted into the DVS equipment. The slurry was exposed to a fixed temperature where the loss-on-weight was measured. The air inlet was set to attain a target partial pressure of 0% (bone-dry air) and was passed over the slurry at creeping flow. To estimate the critical moisture content from the drying curve, a linear interpolation is carried out on a polynomial fit. Once the rate of change of the gradient is less than 5% the critical moisture content is estimated from this position. This was carried out over three temperatures, 40°C, 50°C and 60°C. Figure 6.4 shows the data. The critical moisture content is measured at 40°C to be 0.246 (as shown on Figure 6.4), at 50°C a value of 0.278 and at 60°C a value of 0.463.

6.4 Experimental Method and Design

There are three key phases in the experimental process. These are:

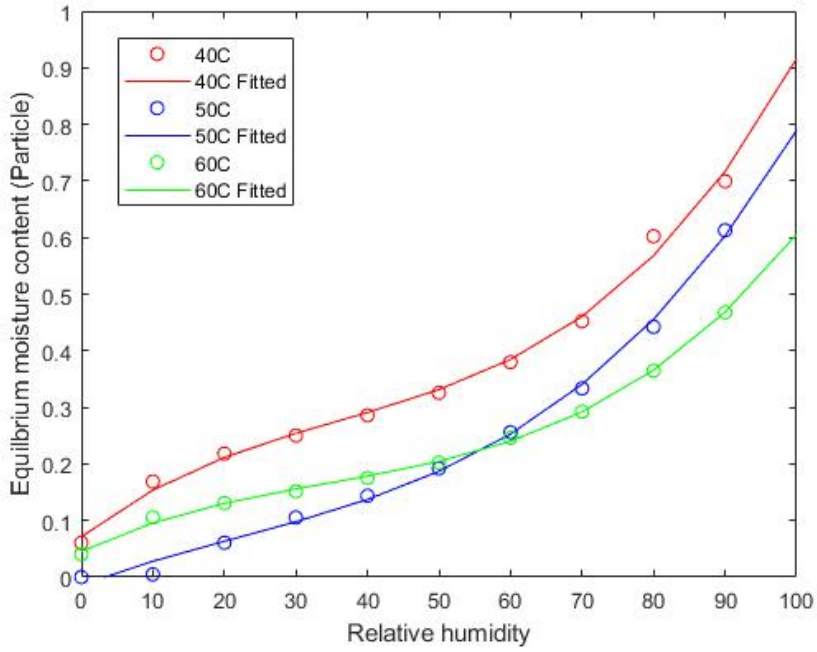

Figure 6.3: The desorption isotherm of the Placebo A7946T slurry.

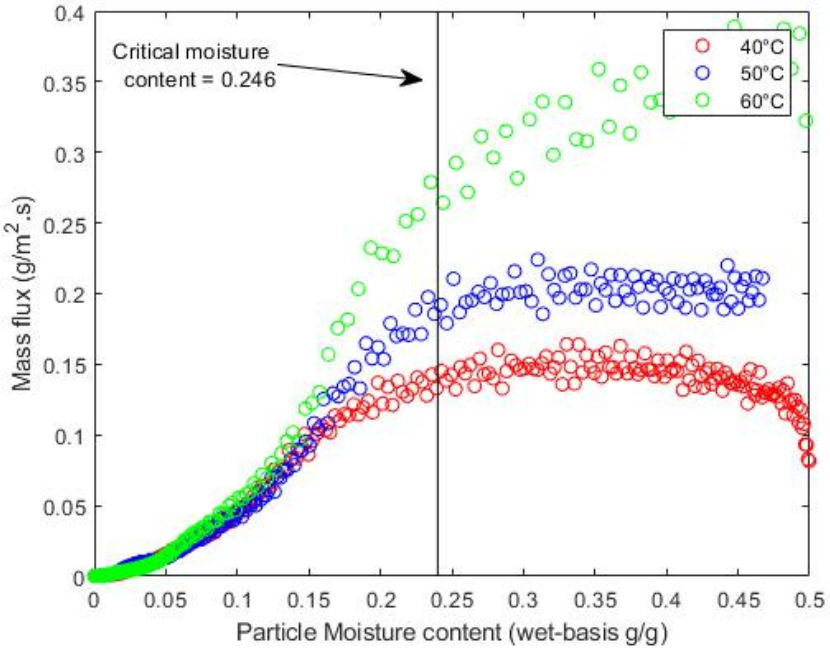

Figure 6.4: Experimental drying curves.

1. Preparing and mixing the slurry
2. Grinding of the slurry
3. Granulation and sampling

To prepare the slurry, the constituent components of Placebo A7946T were mixed in a cooled vessel with a tooth disc stirrer. The contents were stirred until all the components were completely dissolved and were homogeneously dispersed; this was left to stir for at least 30 minutes.

The slurry was then placed into a colloid mill with an initial throughput of 150 kg/hr which ramped up to 250 kg/hr. Samples were taken every 10 minutes. The target diameter of the colloid was $d_{50} \leq 2.5\mu m$, where grinding would continue until this criteria was reached. The discharge from the colloid mill was then pumped to a slurry tank where it is continuously mixed by a flat blade impeller at 450 RPM.

Each experiment initially starts by passing the inlet fluidisation air at the desired flow rate and temperature through an empty bed. The bed is kept empty until the exhaust temperature reaches steady-state. Once the air temperature reaches a steady-state, the bed is seeded via a feed nozzle with 25 kg of Placebo A7946T and is initially mixed at the experimental inlet air flow rate and temperature (as set by Table 6.3). Three samples are taken via the feed port which is then passed through the Mastersizer 3000 to characterise the initial size properties.

The slurry is pumped from the slurry tank to a two-phase nozzle to the set point of the experimental design. To minimise the effects of the droplet diameter when changing spray rates, the liquid pressure to gas pressure ratio was kept constant. The reasoning for this is related to the many works which suggest that maintaining a constant Weber number results in similar droplet sizes [Negiz et al., 1995, Tan et al., 2006, Cotabarren et al., 2018]. Table 6.2 shows the flow rates passed through the nozzles to maintain a constant ratio.

As the experiment proceeds, the material discharge passes via the screw conveyor to the over-and-under sieve. The product is discharged into a collection drum. During the experiments, no oversized particles were formed. Therefore, the typical operational method of passing the oversized particles back into the slurry tank to be re-mixed was not considered during operation. The under-size particles were fed back into the bed via pneumatic transport. The discharge flow rate was measured every 30 minutes during sampling time using a "stopwatch and bucket" method. The mass over 5 minutes was measured to determine the mass flow rate for that period.

Table 6.2: Nozzle parameters to maintain constant a constant ratio of liquid-to-gas pressure.

Spray rate (kg/hr)	P_{liquid} (barg)	$\dot{M}_{air}$ (kg/hr)	$\dot{Q}_{air}$ (Nm^3/hr)	P_{liquid}/P_{air} (-)
50	1.8	36.93	30.68	0.7387
40	1.225	29.55	24.54	0.7387
60	2.371	44.32	36.81	0.7387

Samples of approximately 5g were taken every 30 minutes via the sampling port of the bed. Three samples were collected and then immediately measured with the Mastersizer 3000 and then later stored. Each experiment lasted approximately 4 hours. At the end the bed is discharged into the drum and the bed cleaned out. This systematic process was repeated whereby the inlet air and spray parameters were set to the desired value and the bed were seeded again. Each experiment took one entire work day; from the generation of seeds and slurry, to the fluidisation experiments.

The process conditions were measured by sensors located at key points (as shown on Figure 6.1). The sensor values were internally recorded as part of the automated documentation system. The sensors are as follows: the inlet temperature (T11), the inlet flow rate (F10), the inlet humidity (M18), the outlet temperature before the baghouse (T14) , the outlet temperature after the baghouse (T21), outlet moisture content (M21) and the pressure drop between the inlet air stream and the exhaust (P11-P17).

A central-composite like experimental design was used. This approach was chosen as it benefits in two ways; we develop an understanding of the product output with changes in a single process parameter, and, we generate data which varies multiple parameters which is valuable to rigour test the integrated model. Figure 6.5 visually shows the design matrix and Table 6.3 provides the values for each individual experiment. Experiments 1-7 are the central component of the composite design, where the spray rate, inlet air temperature and inlet air flow rate would vary linearly and independently from the initial value.

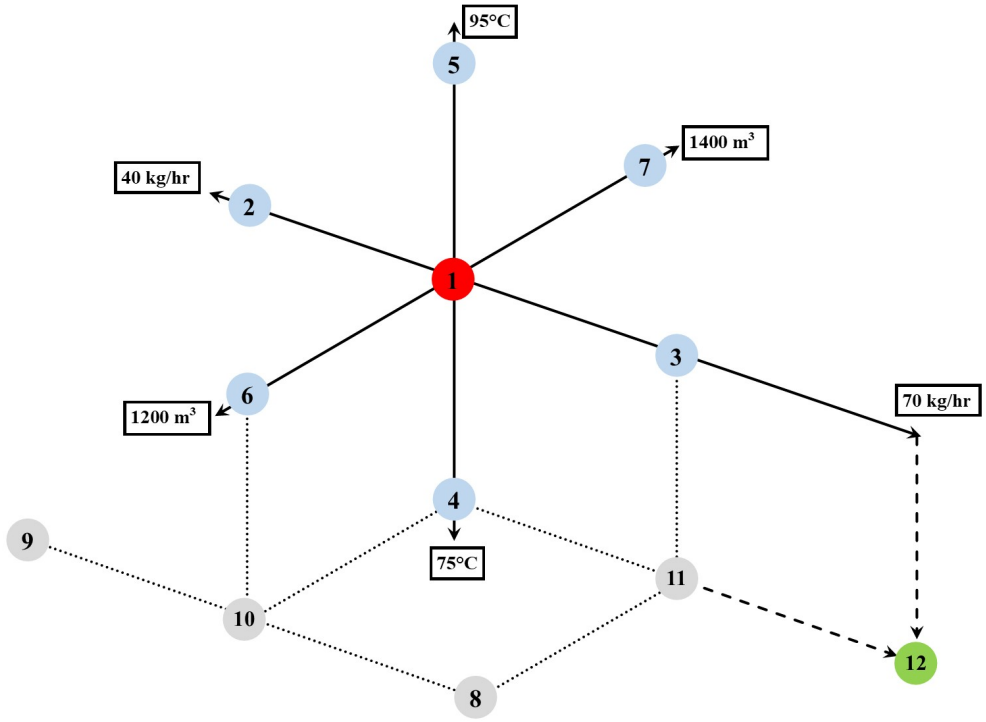

Figure 6.5: The experimental design matrix performed on the continuous pilot plant

Table 6.3: Table of experiments performed on the pilot scale fluidised bed.

Experiment No.	Spray rate (kg/hr)	Air temperature ($^{\circ}C$)	Air flow rate (m^3/hr)
1	50	85	1300
2	40	85	1300
3	60	85	1300
4	50	75	1300
5	50	95	1300
6	50	85	1200
7	50	85	1400
8	60	75	1200
9	40	75	1200
10	50	75	1200
11	60	75	1300
12	70	75	1300

From experiments 8-11 there is a deviation to the typical central composite design. As the experimentation was time-limited and increasingly intensive, there was a conscious decision to emphasise agglomeration as much as reasonably possible. This resulted in focusing on maximising the spray rate, minimising the air temperature and minimising the air flow rate. This maintains a relatively rigorous statistical set of experiments which would complete the vertex of a composite box. Experiments 8-11 reflect this by making adjusted changes in those parameters. Experiment 12 was an additional experiment, where unlike the other experiments which would start from a seeded bed, was a step-change during experiment 11 to gauge a general understanding of how such a change would influence the transient towards the next steady-state.

Despite the limited experimentation, this design provides three points of insight; the influence of the chosen process parameters, the influence of the process parameters in a hypothetical agglomeration dominated regime and an understanding of how a step change influences the steady-state and the transient change from one steady-state to another.

6.4.1 Calibrating the Moisture Sensor

The pilot plant is old, some sensors were poorly calibrated. The moisture sensor M21 was not reading the correct levels of moisture in the outlet stream. As a quick solution, a calibration curve was determined. Air of a known moisture content was

Table 6.4: Moisture sensor calibration experiments

Moisture set point ($^{\circ}Cdp$)	Actual value ($^{\circ}Cdp$)	Outlet temperature ($^{\circ}C$)	Outlet moisture measured (% RH)	Outlet moisture expected (% RH)
-5	-5.11	42.81	0	4.85
0	-0.64	40.29	2.31	7.75
5	5.53	41.34	3.78	11.42
10	10.22	43.24	8.35	14.27
20	19.79	43.6	16.29	26.08

passed through the empty bed where the outlet moisture content and temperature after steady-state was recorded. Table 6.4 shows the experimental results and Figure 6.6 shows the line of best fit used as the calibration curve.

6.4.2 Quantification of the Statistical Impact on the Particle Size Distributions

To compare the distributions between the "normal" and the deviations, the Hellinger distance is used. The Hellinger distance measures the likeness of two normalised distributions. This is a common method used within statistics and is often referred to as the minimum Hellinger distance estimation [Tamura and Boos, 1986]. The Hellinger distance is given as Equation 6.1:

$$H(f,g) = \sqrt{1 - \int_0^{\infty} \left(\sqrt{f(x) \times g(x)}\right) dx} \tag{6.1}$$

where f(x) and g(x) are normalised distributions describing the frequency against size and H the Hellinger distance.

This is a particularly convenient approach to quickly, and cheaply, understand which parameter had the greatest influence on the distribution and size. A value of 1 indicates that the distributions do not overlap, whereas a value of 0 quantifies that the distributions are exactly the same.

6.4.3 Fraction of Solvent Evaporated

The fraction of solvent evaporated is a useful property to check whether the mass balance of the system closes reasonably, in addition to, quantifying whether any

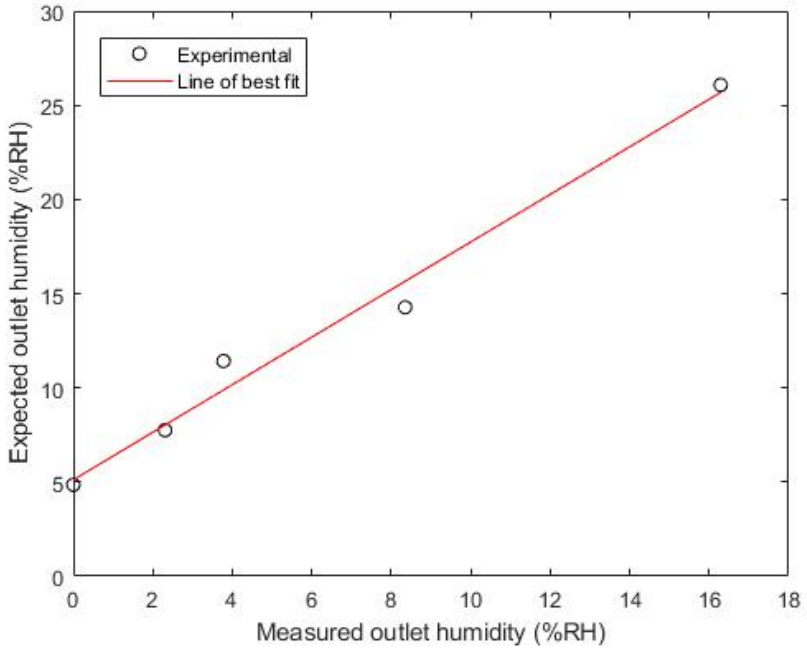

Figure 6.6: Calibration curve for the moisture sensor fitted with a first order polynomial, $y = 1.2629x + 5.112$

sensors are providing poor data. This can be calculated with Equation 6.2:

$$X_{evap} = \frac{(Y_{out} - Y_{in}) \times \dot{m}_{air}}{\dot{m}_{spray} \times x_l} \tag{6.2}$$

where Y_{out} is the outlet humidity, Y_{in} the inlet humidity, $\dot{m}_{air}$ the mass flow rate of the inlet fluidisation air, $\dot{m}_{spray}$ the mass spray rate and x_l the solvent fraction of the spray.

6.4.4 Relative Distance From Linear Growth

Another useful metric to quantify the growth behaviour is to check the relative distance of the mean particle size from an estimated linear growth model. A linear growth model has been formulated similarly to that of Appendix A. We can formulate similar assumptions:

1. The number of particles within the bed is constant.
2. The particle bed is initially mono-sized.
3. The spray evenly distributes liquid across the entire particle bed.

A big emphasis must be made, this is not an attempt to model the system, but rather, a check on the relative distance away from ideal layered growth. As a result, the model over-simplifies the dynamics of the bed and the treatment of particle size. The important detail the comparison does provide is understanding the extent of breakage and agglomeration within the measured outputs.

Based on the above assumptions, the model is shown as Equation 6.3:

$$d_{p,layering} = d_{p,0} + \frac{2\dot{m}_{spray}(1 - x_l) + \dot{m}_{spray} x_l X_{evap}}{\pi \rho_p d_{p,0}^2 M_{bed}} \tag{6.3}$$

where $d_{p,0}$ is the initial particle diameter (the Sauter mean diameter is used in this case), X_{evap} the fraction of solvent evaporated, ρ_p the particle density (taken to be 1535 kg/m^3 and M_{bed} the bed mass. To determine the bed mass a simple mass balance is formulated and used:

$$M_{bed} = M_{bed,initial} + (\dot{m}_{spray}(1 - x_l) + \dot{m}_{spray} x_l X_{evap}) - \dot{m}_{out} \tag{6.4}$$

where $\dot{m}_{out}$ is the product flow rate.

The relative distance can therefore be simply defined as:

$$\text{Relative distance} = d_{p,exp} - d_{p,layering} \tag{6.5}$$

6.5 Results and Discussion

A summary of the final size, granule moisture content and the exhaust temperature is provided on Table 6.5. As a statistical design of experiments used, these values can be used to perform typical Design-of-experiment tests, e.g. ANOVA. While this will not be performed as part of the work to follow, the author feels it is useful to provide the data upfront.

6.5.1 Influence of Spray Rate

Figure 6.7 shows the key size characteristics of experiments 1-3 which varied the spray rate between 40-60 kg/hr. In general, particles showed more growth with an increase in spray rate. Figure 6.7(a)-(c) shows the d_{10}, d_{50}, d_{90} respectively where the steady-state values (the horizontal black lines) are placed highest for 60 kg/hr.

The samples from the tower and product do not show any major difference and generally sit at similar steady-states. Within experiments 1-3 it is unlikely that there was any significant formation of agglomerates. Figure 6.7(d) supports this by showing

Table 6.5: Summary of the final measured size, granule moisture and exhaust temperature within the fluidised bed tower.

Experiment No.	d_{10} (μm)	d_{50} (μm)	d_{90} (μm)	X_w (kg/kg %)	$T_{exhaust}(C)$
1	159	260	409	2.74	47.6
2	139	232	372	2.23	49.0
3	180	305	490	3.58	40.2
4	151	262	416	3.62	38.7
5	138	236	375	2.22	50.2
6	156	270	438	3.295	41.3
7	137	232	375	2.66	45.7
8	330	581	964	5.43	31.9
9	138	236	380	-	39.5
10	200	374	633	-	33.9
11	193	362	596	-	37.1
12	394	688	1137	-	33.2

that the distributions translate smoothly across the x-axis with some widening of the distribution, as you would typically observe for volume distributions which undergo layered growth. As a result, the growth is tight and linear.

Figure 6.8 shows that with an increase in spray rate, the outlet relative humidity increases. This is consistent with the observed model sensitivities in Chapter 5 which suggested that the greater liquid availability allowed for more drying to occur. Figure 6.8 shows that the total evaporated solvent is slightly higher for the experiment 2 at 40 kg/hr. This could be a consequence of less liquid availability at lower spray rates which saturates the drying air less, consequently maintaining a greater capacity to hold liquid. Figure 6.8(c) and (d) shows that the capacity of drying available at the lower spray rate is much higher given that both the exhaust temperature is higher and the relative humidity is lower. There is clearly a balance between experiments 1 and 3. Despite having differing temperatures and relative humidities, the overall solvent evaporated is the same.

6.5.2 Influence of Inlet Air Temperature

Figure 6.9 shows that increasing the inlet air temperature we see a decrease in the overall particle size. As we increase the temperature, the drying rate of the solvent in the spray and bed dries increases, which leads to less liquid availability, hence, a decrease in both agglomeration and layered growth. The volume density distribution,

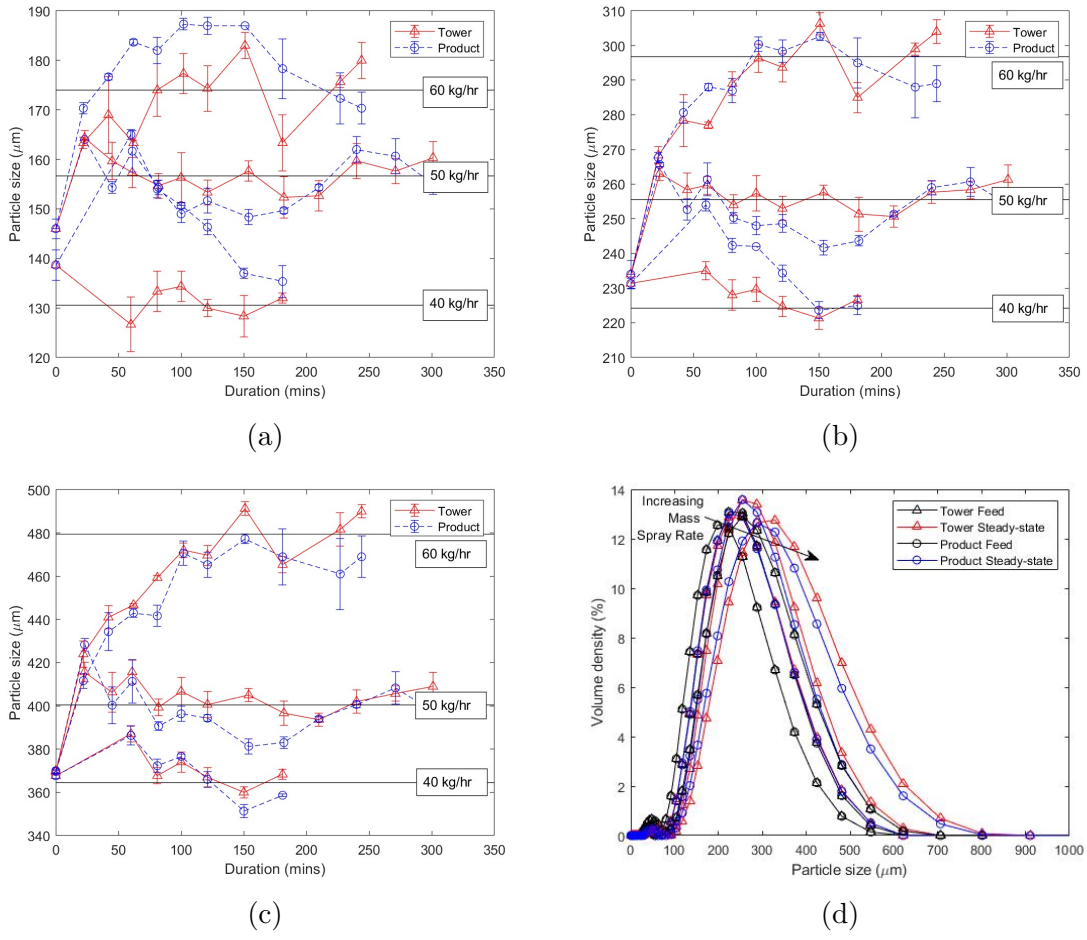

Figure 6.7: Size characteristics of varying spray rates within a pilot scale fluidised bed granulator where (a) is the d_{10}, (b) d_{50}, (c) d_{90}, (d) the volume density distribution

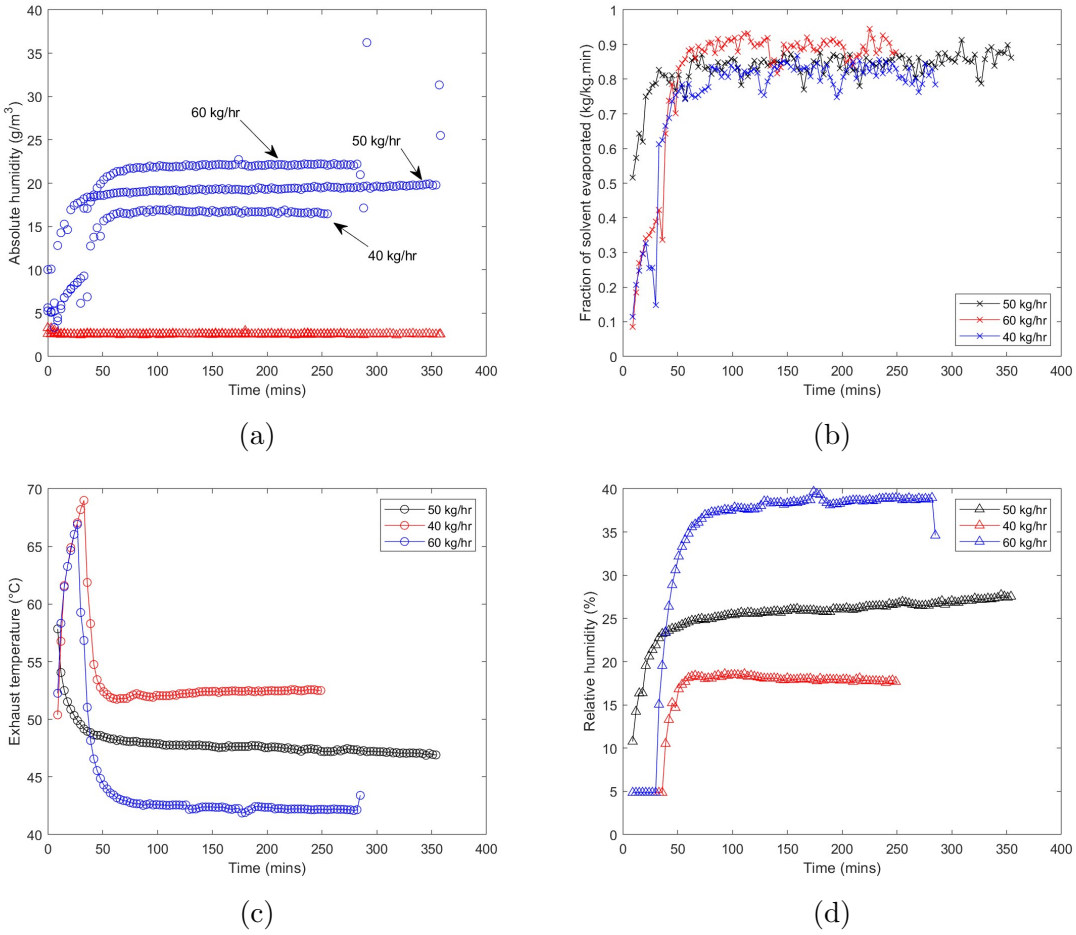

Figure 6.8: Drying characteristics of varying spray rates where (a) is the outlet humidity and (b) is the total solvent evaporated after correction with the calibration curve, (c) is the exhaust temperature and (d) the relative humidity of the exhaust.

as shown by Figure 6.9(d), does not show any significant changes which might indicate agglomeration. The translation of the density distribution across the size grid is smooth.

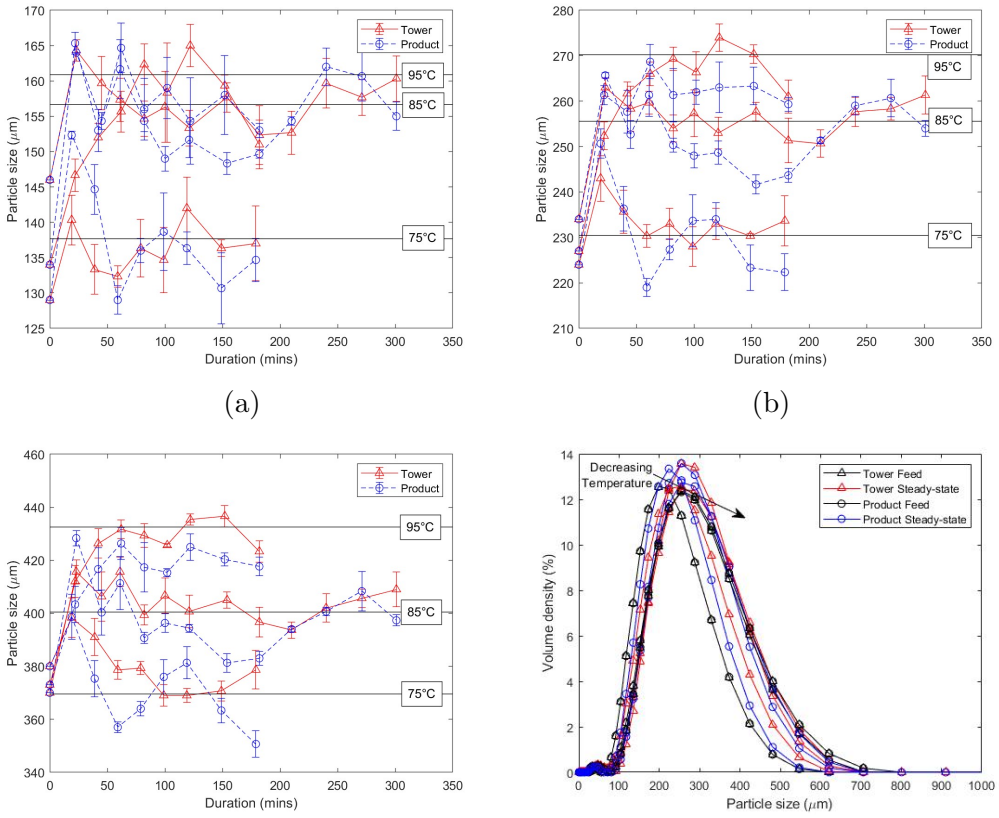

Figure 6.9: Size characteristics of varying inlet air temperatures where (a) is the d_{10}, (b) d_{50}, (c) d_{90} and (d) the volume density distribution

Surprisingly, there is not an obvious correlation between the outlet humidity and inlet air temperature. Figure 6.10(a) and (b) have similar outputs, where normally we would expect that the absolute humidity at 95°C to be greater than that of 85°C. This may be an artifact of the calibration curve being poorly designed for higher temperatures; as this curve was initially calibrated at 50°C. However, we do see the expected trends on Figures 6.10(c) and (d) where the temperature correlates with the inlet air temperature linearly, and the relative humidity inversely.

6.5.3 Influence of Inlet Air Flow Rate

Decreasing the inlet fluidisation air flow rate increases the particle size. Figure 6.11 shows the most growth for 1200 m^3/hr and the least for 1400 m^3/hr. As we reduce

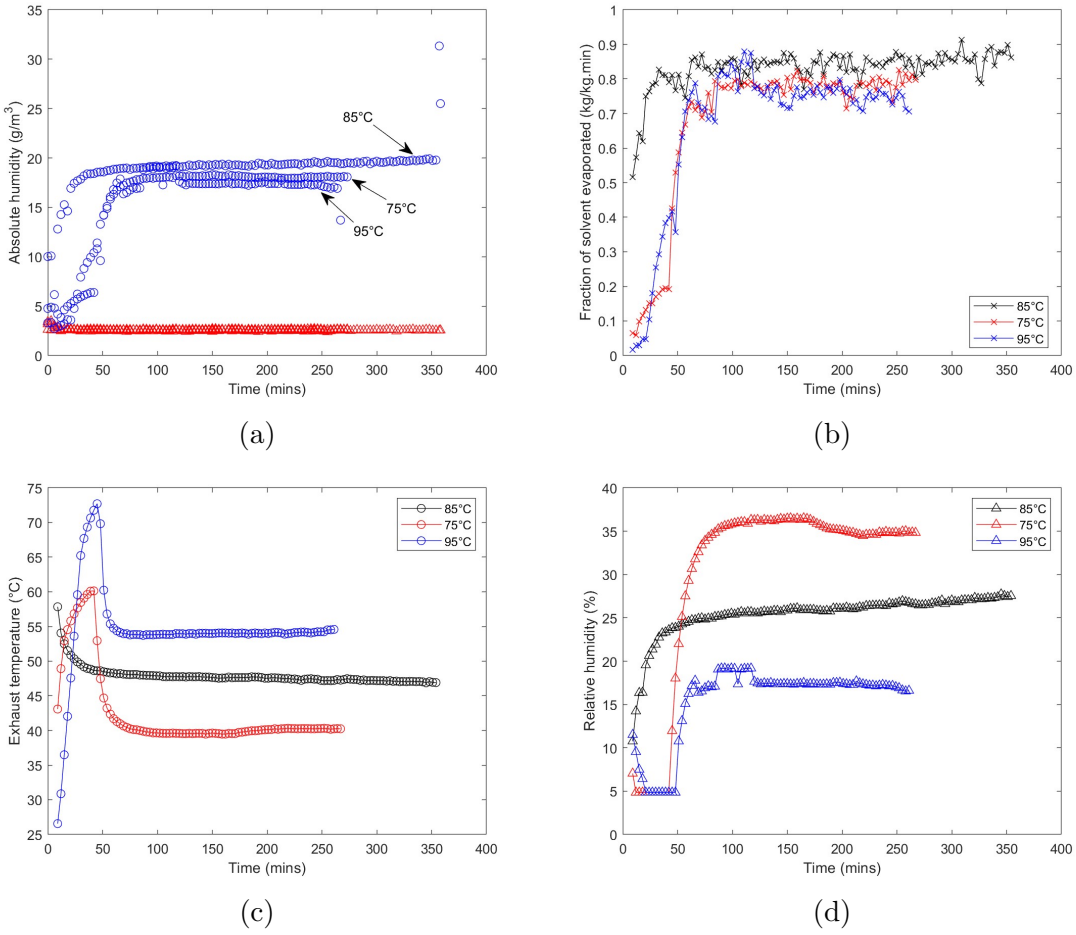

Figure 6.10: Drying characteristics of varying inlet air temperatures where (a) is the outlet humidity and (b) is the total solvent evaporated, (c) is the exhaust temperature and (d) the relative humidity of the exhaust.

the inlet air flow rate, the drying rate and particle collision velocity decreases which can lead to less breakage and more liquid availability to promotes growth.

Figure 6.12 shows the drying characteristics for the varying inlet air flow rates. We see that an increase in air flow rate lead to a lower uptake of solvent, a higher exhaust temperature and consequently a lower relative humidity. Increasing the air flow decreases the absolute humidity in the air stream, likely a result of greater air volumes and mass transfer limitations by an increased gas by-pass. Interestingly, the fraction of solvent evaporated shows similar values to 1300 m^3/hr, with a slight anomaly at $t = 146$ minutes. The anomaly is a result of a measurement error in the mass spray rate. Figure 6.12(d) shows that the relative humidity increases with a decrease in the flow rate, suggesting that there is more saturation of the drying air. There is a lower volume of air flowing through the unit and less drying capacity as a

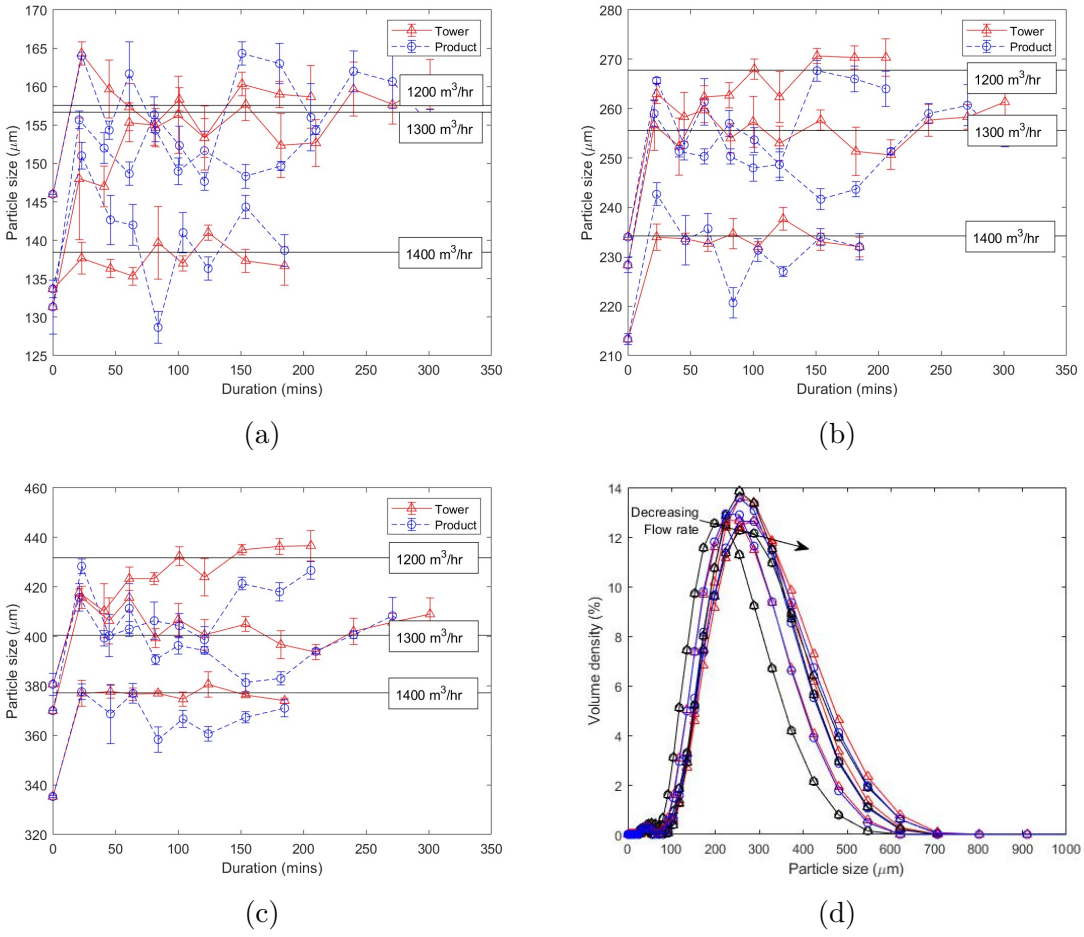

Figure 6.11: Size characteristics of varying inlet air flow rates where (a) is the d_{10}, (b) d_{50}, (c) d_{90} and (d) the volume density distribution

result.

6.5.4 Influence of Combined Process Parameters

The only experiment to consistently show less growth than the base case of experiment 1 was experiment 9 (as seen on Figure 6.13). There were two competing effects, a decrease in spray rate, which leads to less growth, and a decrease in temperature, which emphasises more growth. In this case, the decrease in spray rate is more impactful in controlling the size, though, the differences are small relative to experiment 1.

Figure 6.13 shows that both experiments 8 and 12 show large growth up until the bed collapses. Both show a significant difference from the sample within the tower and the sample within the product stream. The samples taken from the product

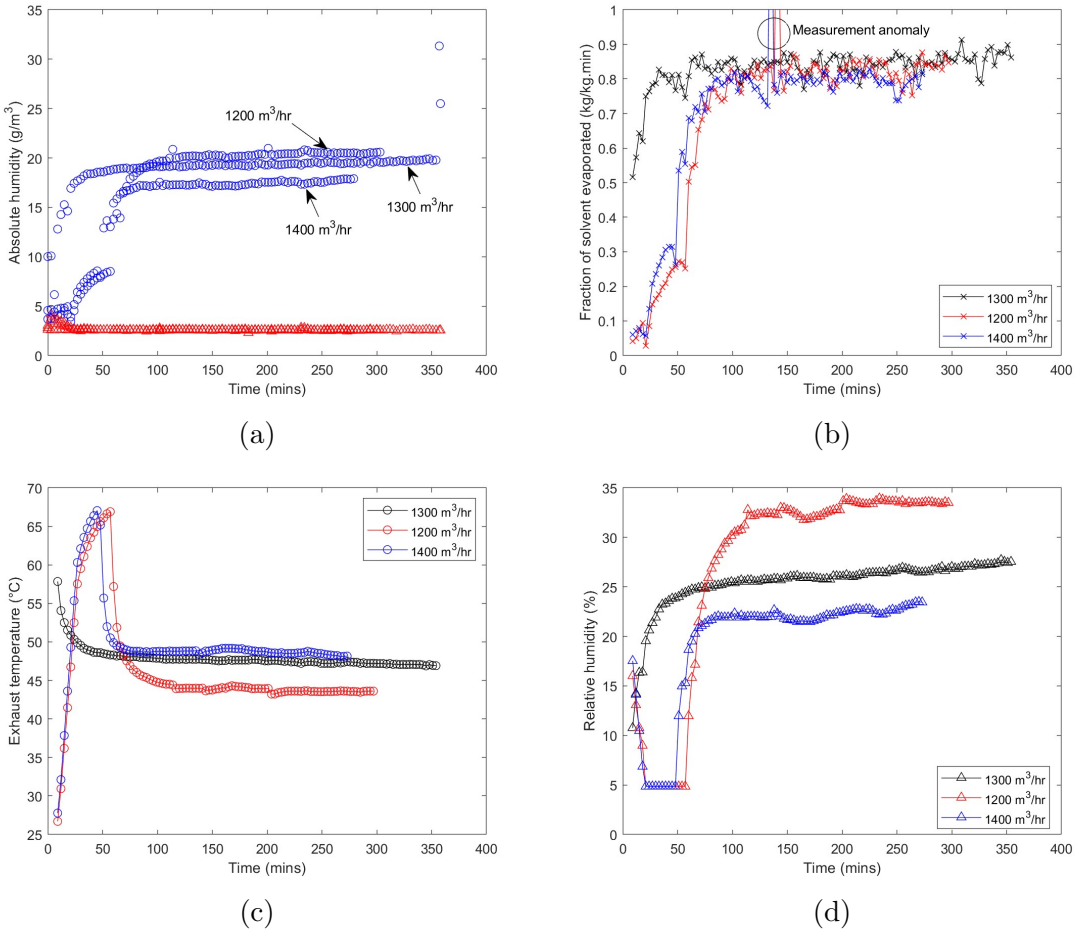

Figure 6.12: Drying characteristics of varying inlet air flow rates where (a) is the outlet humidity and (b) is the total solvent evaporated, (c) is the exhaust temperature and (d) the relative humidity of the exhaust.

stream appear to be smaller than that within the tower. This is attributed to the fact that large wet particles flow poorly which results in a segregation of particles as smaller particles have a tendency to flow out the discharge. Experiments 8 and 12 were the only two experiments to cause a collapse of the fluidised bed. The rapid growth and wetting of the bed resulted in gradual blockage of the discharge, where eventually the bed collapses.

Experiment 12 shows a significant change from experiment 11, where after the ramp increase to the next spray rate the particle growth showed an almost immediate response. This is made clear on Figures 6.13(a)-(c) where after the transition line the growth shows an immediate change. This is quite surprising as given most of literature such as Cryer [1999], Heinrich et al. [2002] and Vreman et al. [2009] show that there is lag from a change to an input to the measured output. Perhaps the sensitivity of

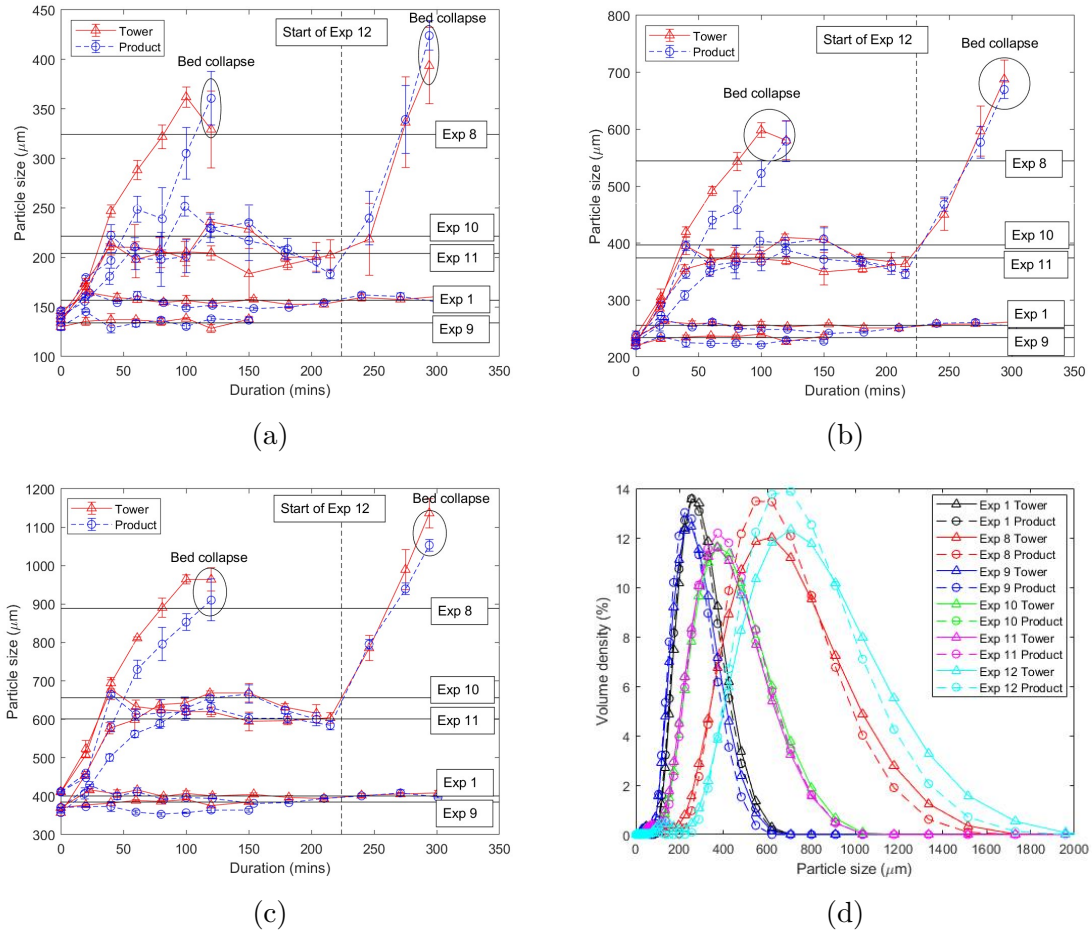

Figure 6.13: Size characteristics for combined changes in process parameters where (a) is the d_{10}, (b) d_{50}, (c) d_{90}, (d) the volume density distribution. The transition from experiment 11 to 12 is shown as a vertical dashed line position at $t = 224$ minutes.

the equipment is related to both the recycle and the spray; the mentioned researches added nuclei and binder through separate streams in a continuous system where this process drives nucleation and growth primarily through the spray.

Surprisingly, experiment 10 showed more growth than experiment 11. Experiment 10 compares to experiment 11 by having a lower inlet fluidisation air flow rate and a lower spray rate. It's clear here that the combined change in the inlet air flow rate and inlet air temperature, resulted in slightly more growth than a change in spray rate and inlet air temperature. Given that experiment 10 showed less drying (as shown by the results of Figures 6.14(b) and (c)) which ensures there is more liquid available in the bed for agglomeration. It seems there is a careful balance when optimising for growth; a change in air temperature and flow rate can have a larger influence than a change in spray rate.

Similar to the particle growth profiles of experiment 12, the drying properties also show a near immediate response when the system is ramped to the new steady-state. Again, this highlights that the system is sensitive to changes in process parameters.

Figure 6.15 shows the Hellinger distance for each experimental subset. The Hellinger distance is used as an alternative method to ANOVA which would use other distribution parameters such as the d_{10}, d_{50} and d_{50}. Both experiment 8 and 12 showed the greatest deviation away from experiment 1. This is unsurprising given that significant growth occurred during these two experiment. By quantifying the Hellinger distance, clearly highlights the differences between the product and tower. In most cases, the distribution within the tower showed the greatest distance away from experiment 1. On the other hand, the product stream for experiment 8, 11 and 12 showed the greatest deviation. This is likely the result of the recycle contributing less to the product distribution, shifting the distribution further along the grid and reducing the total overlap.

For influences of a single parameter, the increase in spray rate showed the greatest impact further highlighting the importance of the spray rate as a controlling factor for growth. This is followed by the increase temperature and then an increase in air flow rate. This indicates that controlling the drying and bed dynamics has a significant impact on the shape of the distribution.

6.5.5 Product Flow Rate Control

The fluidised bed was operated in a way to maintain a constant differential pressure across the entire bed by controlling the flow rate out of the bed. This is a common method within industry to maintain a constant bed mass. Figure 6.16 shows how the

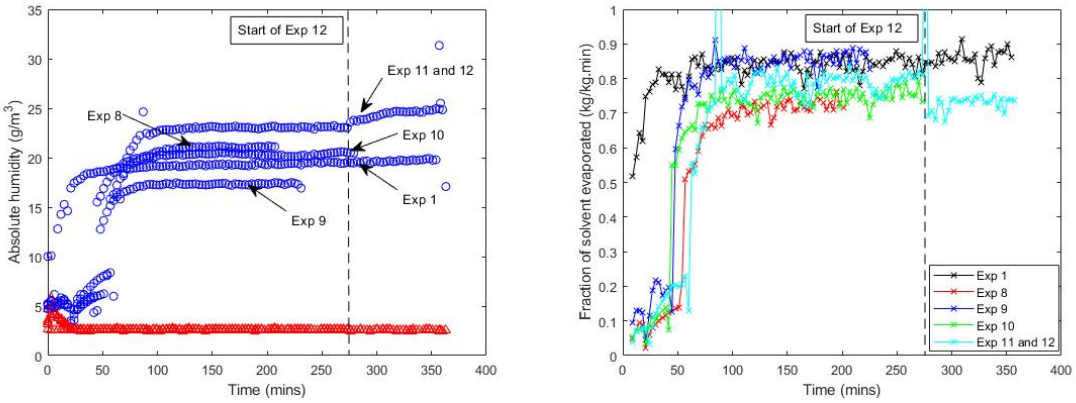

(a) (b)

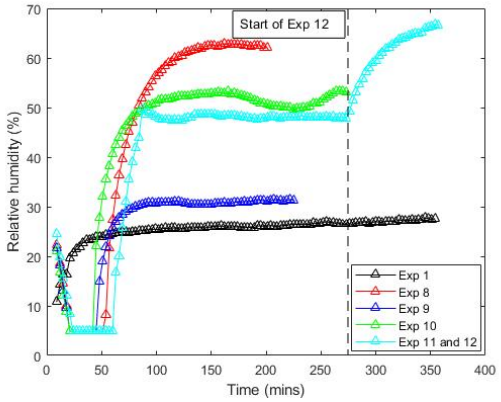

(c)

Figure 6.14: Drying characteristics of changes in combined process parameters where (a) is the outlet humidity and (b) is the total solvent evaporated and (c) the relative humidity of the exhaust. The position which the experiment 11 shifts to 12 is shown as a vertical dashed line at $t = 273$ minutes (an added compensation of the $\approx$1 hour later start compared to the particle size measurements).

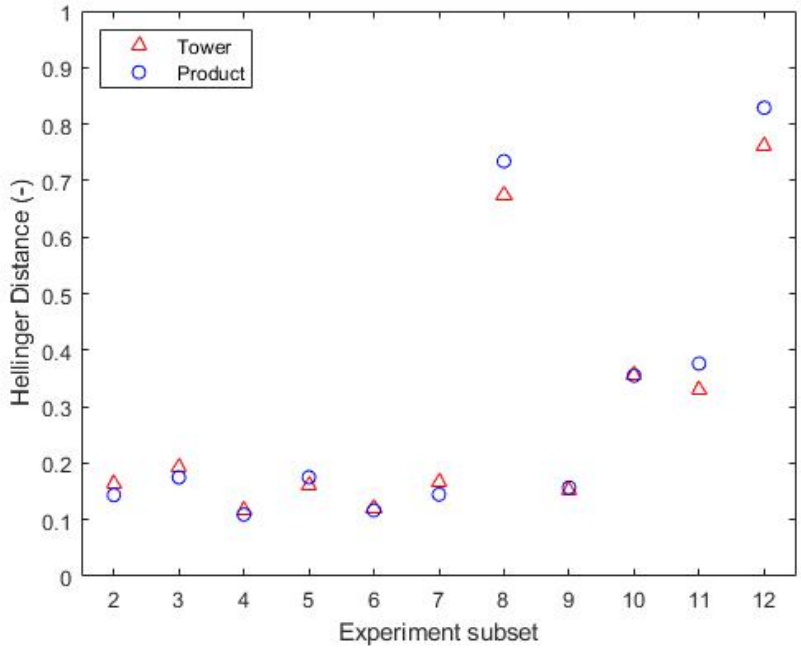

Figure 6.15: The calculated Hellinger distance for each experiment subset when compared to experiment 1.

measured flow rate varied for each experiment. Generally, the spray rate influenced the product flow rate the most as experiments 3, 8, 10 and 11 show that they are approaching a similar steady-state. In the case of experiment 8, as the bed destabalises and collapses the product flow rate diminished significantly towards the end of the sampling period. The other process parameters showed very little influence individually where the results sit roughly between 25-28 kg/hr.

6.5.6 Granule Moisture Content

Figure 6.17 shows the measured granule moisture content for experiments 1-8. Experiments 2 and 5, which corresponds to a decrease in spray rate and increase in temperature respectively, show a lower granule moisture content when compared to the base case of experiment 1. This is consistent with expectations. Reducing the spray rate reduces the available liquid throughout the bed, whereas, an increase in temperature increases the drying rate within the particle bed.

An incease in the spray rate and decreases in the air temperature and inlet air flow rate shows an increase in the granule moisture content. Again, this is expected as changes in these process dynamics promotes more liquid availability by either increased spray rates, or reduced rates of drying.

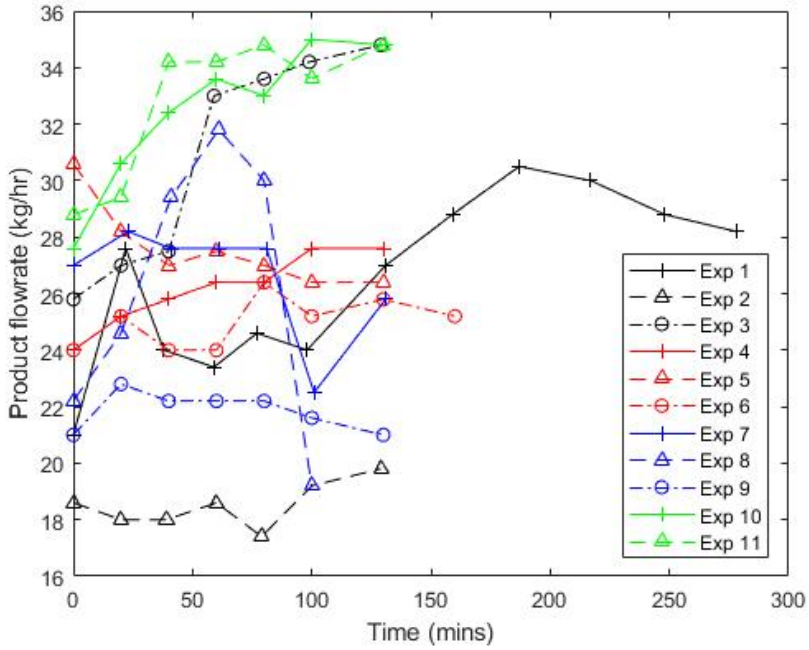

Figure 6.16: The measured flow rate out of the product stream for experiments 1-11. Experiment 12 was not measured.

With regards to experiment 7, an increase in the inlet air flow rate had a marginal decrease in the granule moisture content. This may suggest that the drying rate within the bulk particle bed was not significantly increased, which may be due to mass transfer limitations by a bubble gas bypass.

6.5.7 Relative Distance Against Linear Growth

Figure 6.18 quantifies the distance between a simple growth model and the experiments. The growth model is considered "simple" as this considers the growth of a mono-sized particle by layering. This can clarify the extent of agglomeration.

A negative value for the relative distance is calculated for experiments 2, 5 and 9. The differences are small and could be attributed to a small degree of particle breakage. Experiments 2 and 9 had reduced spray rates which may suggest that the rate of breakage may have been slightly more dominant than the rate of growth. This is further supported by Experiment 5 as the inlet air flow rate was increased, suggesting an increased probability in particle breakage. Though for these experiments, it is clear that breakage does not occur in excess.

Experiments 8 and 12 shows that there was large amounts agglomeration as the relative distance value exceeds 300 μm. For experiments 3, 10 and 11 the distances

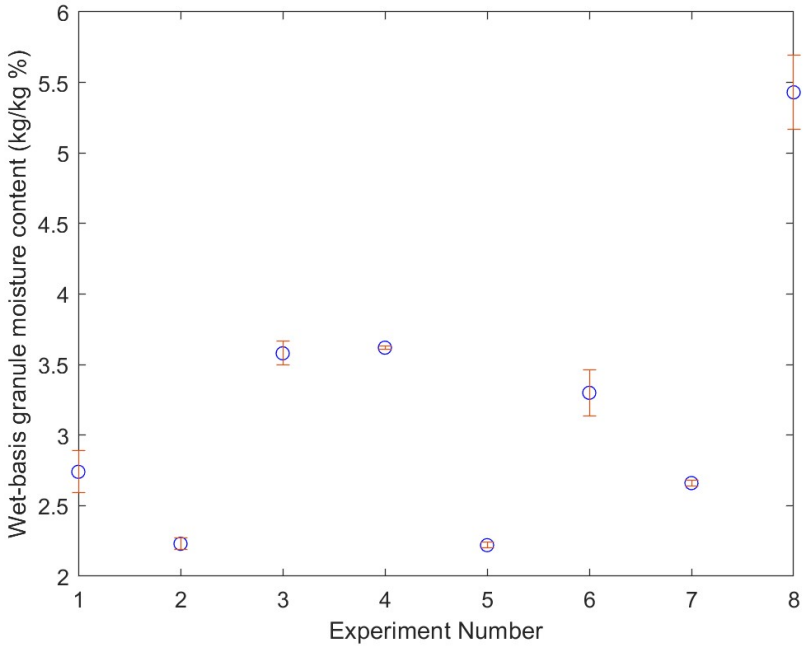

Figure 6.17: The granule moisture content for experiments 1-8.

are roughly 50-80 μm which might suggest that some agglomeration occurred but not enough to dominate the bed.

6.6 Conclusion

Experiments were performed on a continuous pilot scale fluidised bed where the influence of spray rate, inlet fluidisation air temperature, inlet fluidisation air flow rate and select combinations of these parameters were performed. From the study, it was found that the spray rate showed the greatest impact on the particle size distribution. This was quantified by a Hellinger distance estimation for the distribution and the relative distance against linear growth.

The measured particle sizes were consistent against the anticipated theory where increasing the spray rate, decreasing the inlet air temperature and decreasing the inlet air flow rate all resulted in more overall growth of the particle bed. While the growth measurements appear to be reliable, the outlet humidity, relative humidity and solvent evaporated may show inherent errors due to poor calibration of the moisture sensor/and overall measurements. This was particularly emphasised at higher temperatures which demonstrated poor consistency.

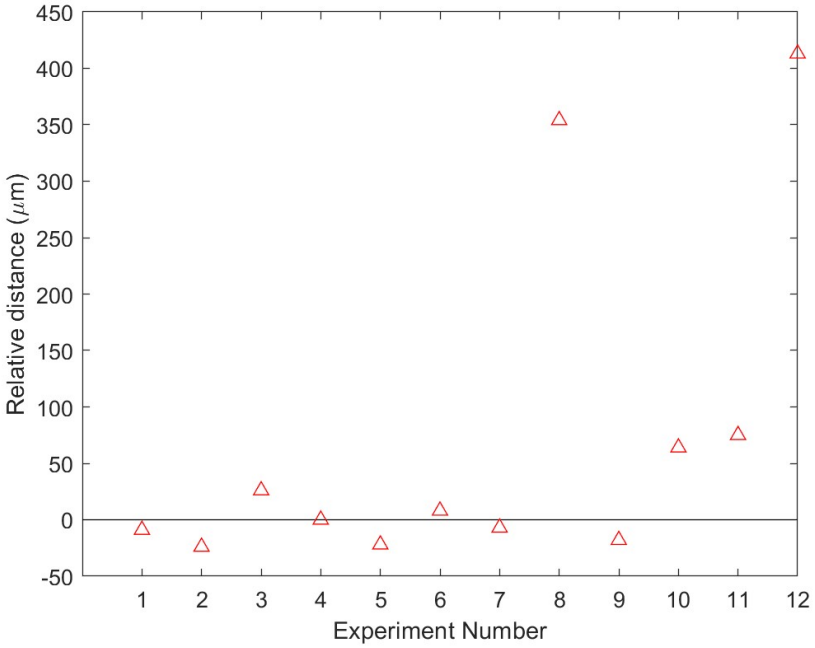

Figure 6.18: The calculated relative distance for all experiments when compared to a simple linear growth model. The product flow rate used to calculate the linear growth rate is estimated to be the same as experiment 11.

When the spray was increased by a large amount it was found that agglomeration dominates the bed. Over duration of the experiments the bed would begin to destabalise and eventually collapse. This was clearly indicated by the rapid growth in the particle size distribution and the gradual reduction flow rate of the product. The over-wetting of particles leads to uncontrolled growth which would defluidise and block the discharge, ultimately causing the bed to collapse.

The product flow rate didn't show much sensitivity to the inlet air temperature and the inlet air flow rate. The spray rate resulted in the most change as the discharge rate was a function of the total mass holdup and the pressure drop within the bed.

Overall, this work has provided analysis and data for a continuous pilot scale fluidised bed which uses a two-phase nozzle to drive nucleation and growth. This is novel among the literature and provides an experimental link to characterise process behaviour with granulation mechanisms.

Chapter 7

Validation of a two-compartment integrated population balance model using pilot plant data

7.1 Introduction

The literature has rarely delved into modelling continuous fluidised beds, especially one which drives nucleation and growth by a two-phase spray. Whilst most modern models introduce multi-dimensional properties, these models are not physically representative and most have not been extensively validated outside of lab-scale batch processes.

This chapter's goal is to validate the model formulated in Chapter 5 and critically analyse the performance of a coupled 1-D population balance framework. The key parameters against which the model is tested are the ability in predicting the size and drying characteristics of the experimental results from Chapter 6, a pilot-scale continuous fluidised bed granulator. The experimental table is repeated below as Table 7.1 and the model was set to the respective process conditions to attempt to predict the; size properties, the moisture content of the granule, the product flow rate out of the granulator and the absolute humidity of the outlet.

7.2 Model Formulation and Validation Strategy

The model is formulated in the same manner as Chapter 5, where the two-compartment model with recycle framework is used. Excluding the physical properties of the gas, liquid and particle phases, and the process inputs, the model requires a set of inputs to initialise. In some cases these parameters require estimation, but, others can be

Table 7.1: Table of experiments performed on the pilot scale fluidised bed.

Experiment No.	Spray rate (kg/hr)	Air temperature ($^{\circ}C$)	Air flow rate (m^3/hr)
1	50	85	1300
2	40	85	1300
3	60	85	1300
4	50	75	1300
5	50	95	1300
6	50	85	1200
7	50	85	1400
8	60	75	1200
9	40	75	1200
10	50	75	1200
11	60	75	1300
12	70	75	1300

derived either from literature or by lab-scale experiments. These parameters are listed on Table 7.2 with the value and acquisition method.

The model has four parameters that require estimation, that is the agglomeration rate constant, the droplet properties for the spray and the spray bypass ratio; the gas that is entrained into the spray drying compartment from the bed compartment. The droplet properties should be measured directly through common techniques such as laser diffraction, but, given the throughput and the size of the spray nozzle this is practically difficult. Therefore, the easiest method in this case is to estimate the properties. Drying properties such as the drying curve and isotherms are necessary to initialise the drying model, primarily to quantify the relative drying rate. Properties such as the minimum fluidisation porosity, discharge coefficient and surface asperities height are values taken directly from literature as recommended, or due to the relatively low sensitivity on the model outputs.

To estimate the parameters a maximum likelihood estimator is used. This has particular advantages of considering the standard error relative to multiple experiments in addition to solving dynamic and steady-state problems. The maximum likelihood objective function is given as Equation 7.1:

$$\chi = \frac{N_{exp}}{2}\ln(2) + \frac{1}{2}\min\left(\sum_{i=1}^{NE}\sum_{j=1}^{NV_i}\sum_{k=1}^{NM_{ij}}\left[\ln(\sigma_{ijk}^2) + \frac{(\tilde{z}_{ijk} - z_{ijk})^2}{\sigma_{ijk}^2}\right]\right) \tag{7.1}$$

Table 7.2: Table of parameters to initialise the model excluding physical properties.

Parameter Name	Symbol	Type	Value
Agglomeration rate constant	β_0	Estimation	-
Droplet diameter	$d_{d,0}$	Estimation	-
Standard deviation of droplets	σ_d	Estimation	-
Spray bypass ratio	r	Estimation	-
Contact angle	Ψ	Experiment	34°
Characteristic drying curve	-	Experiment	-
Critical moisture content	X_{cr}	Experiment	0.278
De-sorption isotherm	-	Experiment	-
Minimum fluidisation porosity		Literature	0.43(-)
Discharge coefficient	C_d	Literature	0.5(-)
Surface asperities height	h_0	Literature	1e-6 (m)

where N_{exp} is the number of measurements for all experiments, NE the number of experiments performed, NV_i the number of variables measured of the i_{th} experiment, NM_{ij} the number of measurements of the j_{th} variable of the i_{th} experiment, σ^2_{ijk} is the variance of the k_{th} measurement, $\tilde{z}_{ijk}$ is the k_{th} measured value of variable j in experiment i and z_{ijk} is the k_{th} model-predicted value of variable j in experiment i.

To initialise the estimation problem there are three requirements, an initial guess, a variance model and the experimental inputs. Choosing an initial guess is critical to the stability of the estimation problem [Barrasso, 2015]. Currently, there are no any reasonable strategies to choose the initial value. Therefore, a value which is known to result in a stable solution is chosen for the estimated parameters. A simple relative variance model is used as this is simple and stable approach. A value of 5% is used. The size distribution and humidity data of experiment 1 was used to fit these parameters. The philosophy of only using one experiment for fitting is paramount to test the model's ability to provide true predictions of changes in process parameters. If the model can reasonably predict the other experiments with only one initial experiment, then this would provide significant cost savings when compared to other models available in the literature.

Table 7.3 shows the results of the estimation problem. The parameter estimator would result in solutions in more than one decimal point and these values were rounded up to the closest one decimal point and/or integer as this would result in a more stable simulation. Another minor point to discuss is that the upper grid boundary was kept at 800 μm for all simulations except experiments 8 and 11-12 as

Table 7.3: Initial value and final estimated values

Parameter Name	Symbol	Initial Value	Final Value
Agglomeration rate constant	β_0	5e-17 s^{-1}	1.5e-16 s^{-1}
Droplet diameter	$d_{d,0}$	180 μm	226 μm
Standard deviation of droplets	σ_d	30 μm	54 μm
Spray bypass ratio	r	0.2	0.1 *(0.0976)* (-)

the growth in these experiments exceeded the maximum value of 800. To avoid the growth being limited by the grid the upper boundary was set to 1500 μm for these simulations. In addition, for experiment 11-12 the simulation duration was increased to 5 hours as this experiment exceeded 4 hours.

Finally, to complete the formulation of the model the physical properties and parameters necessary to initialise the numerical problem is given by Table 7.4.

7.3 Results & Discussion

Figures 7.1(a)-(k) show the comparison of the key size distribution values, the d_{10}, d_{50} and d_{90}. Overall, the model shows good fit the experiments, particularly for the dynamics and steady-states of the d_{10} and d_{50}. Generally, the values the d_{90} show poor dynamics during the early stages and often exceed the final steady-state value towards the end. It is clear that the model is overtuned for the growth of large particles. This could be attributed to the preferential wetting of large particles by the wetting function ultimately resulting in rapid agglomeration.

This can also be attributed to the numerical method, as the liquid component is not internally distributed. As growth continues, the liquid which is added is distributed over the current particle domain, any liquid in the lower particle size grid also grow towards the final grid where the particles would see more liquid which would realistically be attainable. As the agglomeration function is dependent on liquid content, this results in the large particles being larger than measured.

The poor dynamics at the early stages can be explained by the model continuously discharging granules that have the same distribution as within the bed. This may also be another aspect of the model which is overtuned as the dynamics of the experiments show that the large particles have a long residence time initially which allows these particles to grow quickly before being regularly discharged at the steady-state. The

Table 7.4: Table of parameters for the continuous fluidised bed model

Parameter Name	Symbol	Value
Number of size classes	N	15 (-)
Grid type	-	Logarithmic
Lower grid boundary	d_{min}	75 (μm)
Upper grid boundary	d_{max}	800 (μm)
Initial bed mass	M_{bed}	25 kg
Solid composition of the spray	x_s	0.6 kg/kg
Initial moisture content of the bed	x_l	0.01 kg/kg
Density of solid phase	ρ_s	1289 kg/m^3
Bulk density of solid phase	ρ_{bulk}	653 kg/m^3
Density of liquid phase	ρ_l	1000 kg/m^3
Density of gas phase	ρ_g	1.2 kg/m^3
Droplet residence time	t_d	2 s
Discretisation points for spray drying	N_d	10 (-)
Bed diameter	d_{bed}	0.5 m
Initial bed temperature	$T_{b,0}$	25 °C
Inlet spray temperature	$T_{spray,0}$	25 °C
Inlet relative humidity	RH_0	2 % w/w
Latent heat of evaporation	Δh_v	2570 $\frac{kJ}{kg.K}$
Vapour thermal conductivity	λ_g	0.024 $\frac{W}{m.K}$
Gas viscosity	μ_g	1e-5 $Pa.s$
Minimum fluidisation porosity	ε_{mf}	0.43 (-)
Undersize Screen aperture size	-	200 μm
Discharge area	A_0	0.02 m^2 ($\approx$ 10% of plate area)
Range below which the aperture is non-ideal	-	100 μm
Simulation duration	t	4 hours

model treats the particle residence times for all particle sizes equally, which means that the large particles are ejected as quickly as the small particles; which are unlikely to return to the bed as they are sieved out.

The worst fits are Figures 7.1(h) and (j). The comparison against Figure 7.1(h) is perhaps unfair as during the experiment the discharge valve was blocked due to operational error which resulted in the bed being operated as a batch granulator. This accelerated growth rapidly before collapse. The model demonstrates that agglomeration does occur later during the simulation but the operational aspects of the are not considered in this case. For Figure 7.1(j) its clear that the model shows slow growth towards the steady-state which might indicate that some aspects of the model are over-damped.

The normalised volume density distributions are given by Figures 7.2(a)-(k). Similar to the d_{10}, d_{50} and d_{90} values, there is good agreement between the model and the measured density distributions, especially for experiments which did not have excessive agglomeration. This is particularly true for Figures 7.2(h), (j) and (k). The large particles of the distribution continue to grow to the boundary, whereas the smaller particles show very little growth across the grid. This again could be a factor relating to the numerical method having little preference to retain liquid within the smaller size classes.

The model responds well to all changes in the process parameters. This demonstrates that a 1-D coupled population balance model, that is frameworked to consider the relevant mechanisms, is capable of encompassing the mechanistic changes of granulation and the related process parameters. In some cases this is done well and in other cases not as well.

The model shows very good accuracy in predicting the absolute humidity of the exhaust air as shown by Figures 7.3(a)-(k). Generally, the model slight under-predicts the humidity in most cases.

The experiments show that there isn't a clear transient increase towards steady-state, whereas the model jumps to the steady-state almost immediately. This is in contrast to the growth results which showed that it was over-damped; in this case we see that the drying is slightly under-damped.

What is re-assuring is that on Figure 7.3(k) we see that as the model switches from the conditions of experiment 11 to 12 (a shift in spray rate of 60 to 70 kg/hr) that we see a slight increase in the absolute humidity as a response to a new steady-state. This is in contrast to Figure 7.1(k) which does not show any significant change in the

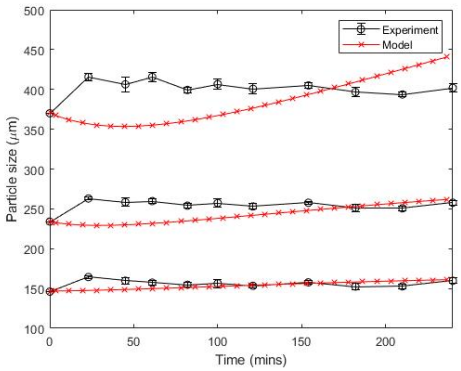
Experiment
Model
Particle size (μm)
Time (mins)

(a)

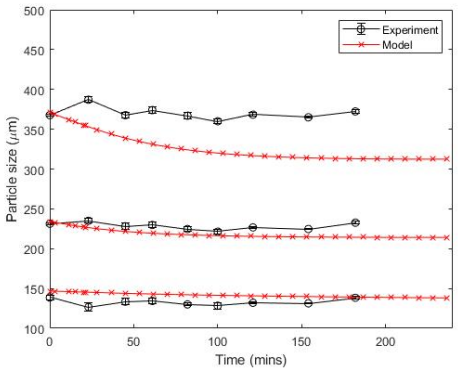
Experiment
Model
Particle size (μm)
Time (mins)

(b)

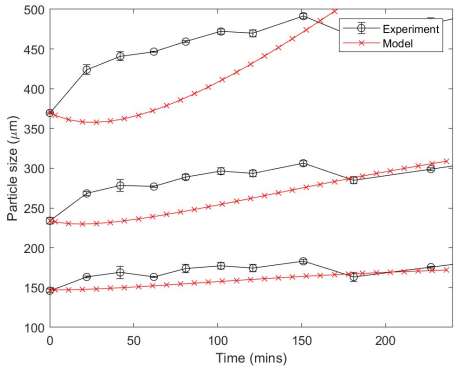
Experiment
Model
Particle size (μm)
Time (mins)

(c)

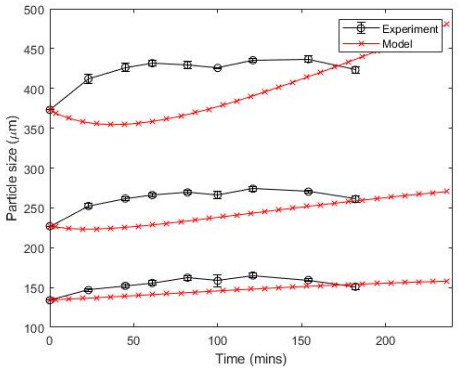
Experiment
Model
Particle size (μm)
Time (mins)

(d)

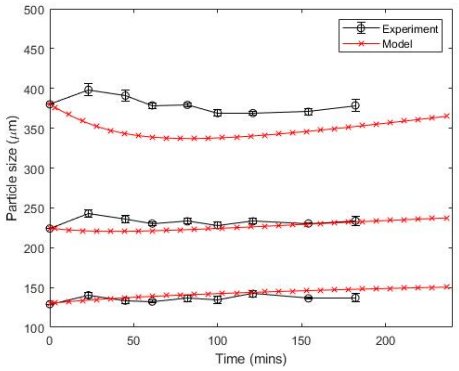
Experiment
Model
Particle size (μm)
Time (mins)

(e)

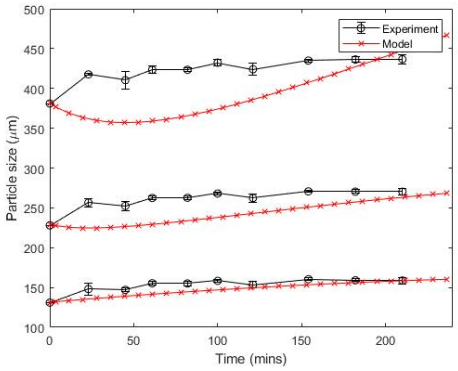
Experiment
Model
Particle size (μm)
Time (mins)

(f)

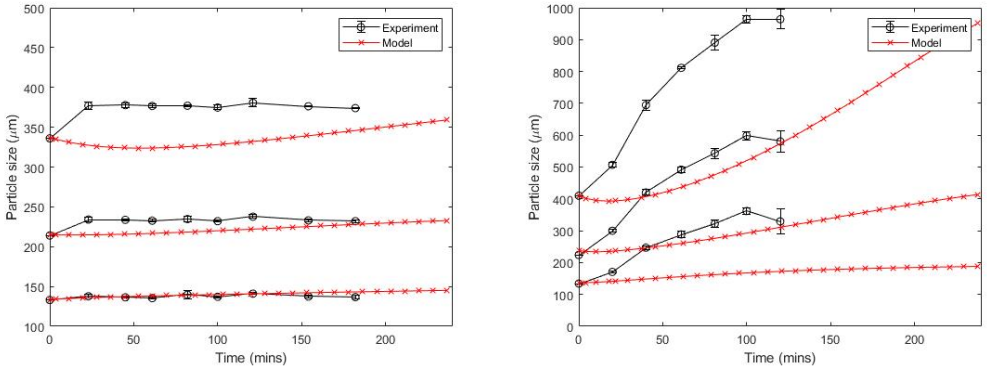

(g)

(h)

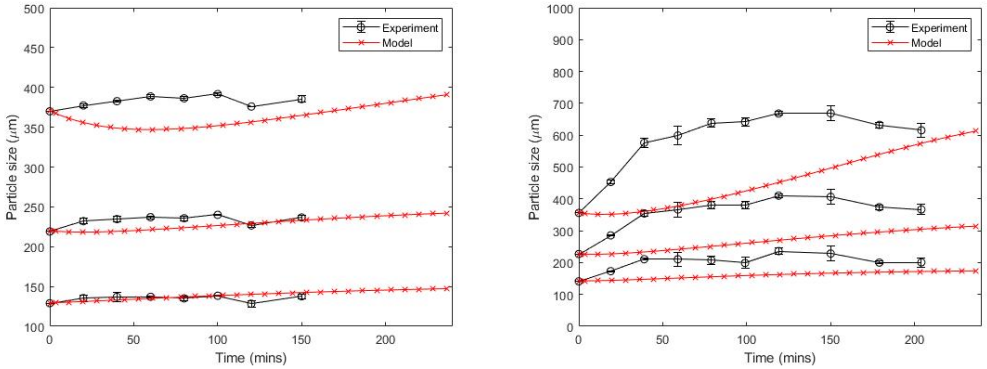

(i)

(j)

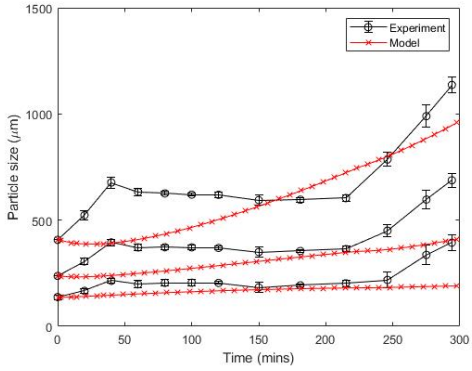

(k)

Figure 7.1: A comparison of the d_{10}, d_{50} and d_{90} between the experiment and model where subfigures (a)-(j) are experiments 1-10 and subfigure (k) is both experiment 11 and 12, where experiment 12 initiates after 224 minutes.

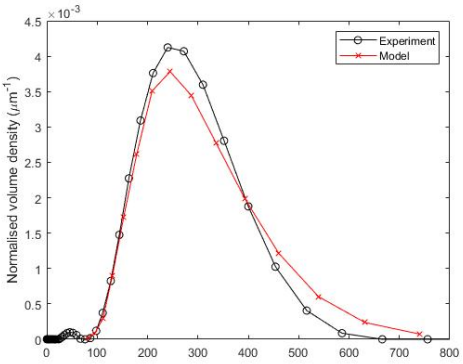
Experiment
Model
Normalised volume density (μm^{-1})
$\times 10^{-3}$

(a)

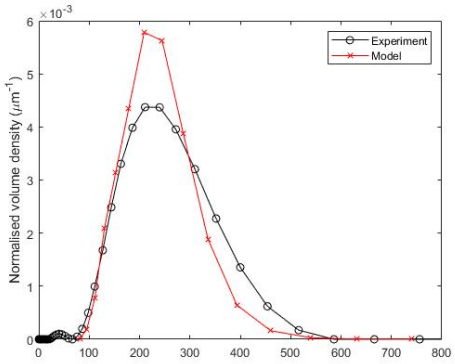
Experiment
Model
Normalised volume density (μm^{-1})
$\times 10^{-3}$

(b)

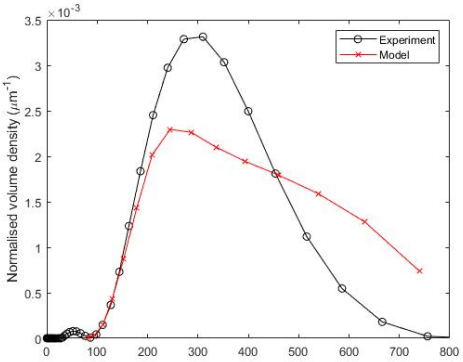
Experiment
Model
Normalised volume density (μm^{-1})
$\times 10^{-3}$

(c)

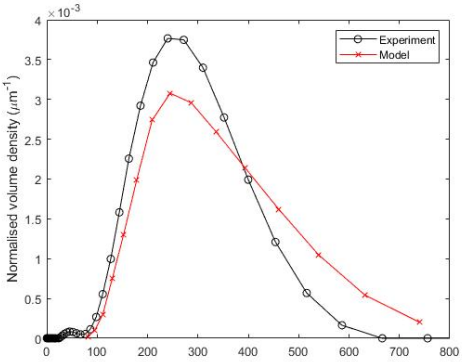
Experiment
Model
Normalised volume density (μm^{-1})
$\times 10^{-3}$

(d)

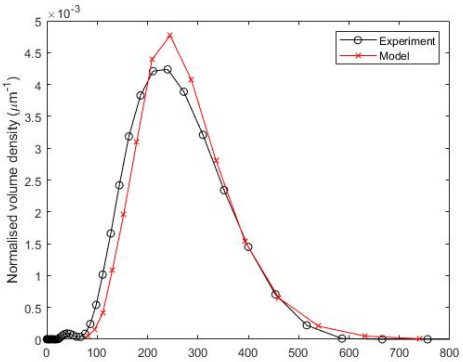
Experiment
Model
Normalised volume density (μm^{-1})
$\times 10^{-3}$

(e)

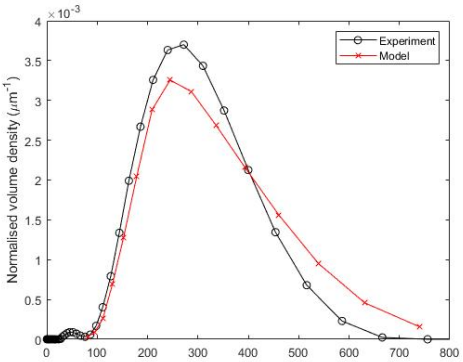
Experiment
Model
Normalised volume density (μm^{-1})
$\times 10^{-3}$

(f)

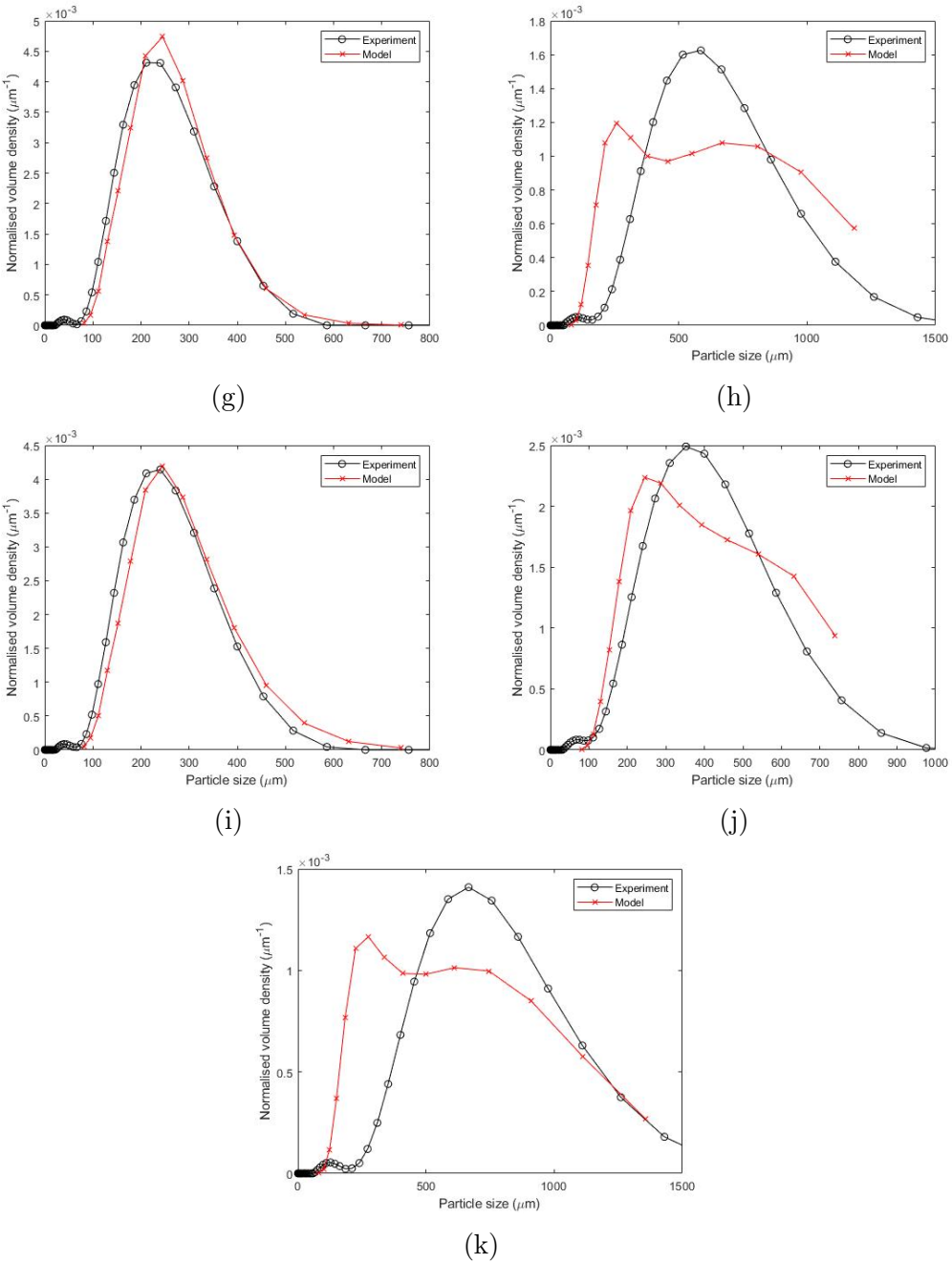

Figure 7.2: A comparison of the volume density distribution between the experiment and model where subfigures (a)-(j) are experiments 1-10 and subfigure (k) shows the final size distribution of experiment 12

modelled growth after the change in spray rate. This indicates that the drying model is well adjusted to the set process conditions.

Figures 7.4(a)-(k) shows how the exhaust temperature compares to the experimentally measured data. At first glance, it seems that the model is offset consistently for every experiment. This is not surprising considering that the exhaust air goes through both a pulse jet filter and a baghouse before measurement. We can reasonably expect heat losses at both these points which would result in a lower experimentally measured temperature. The model assumes that the exhaust leaves the bed adiabatically. As part of the future work, a heat loss model should be included if this model is to be successful in predicting the temperature of the exhaust.

Perhaps the weakest aspect of the model is the prediction of the product flow rate (as shown on Figures 7.5(a)-(k)). The model is slow to reach steady-state, where the experimental data shows that steady-state is attained very quickly. When the model reaches steady-state, the values are close to that of the experiment. This similarly suggests that the model is over-damped and perhaps an alternative discharge model should be used to replicate the screw-conveyor used in the experiments.

The comparisons of the predicted moisture content of the granules when compared to the measurements of experiments 1-8 are shown on Figure 7.6(a)-(f). For some cases the model shows good agreement, such as on Figures 7.6(a),(d) and (f). The model otherwise under-predicts on Figures 7.6(b),(e) and (g) whereas it over-predicts on Figures 7.6(c) and (j).

The inaccuracy can be attributed the spray bypass ratio. For experiments 2 and 3 (Figures 7.6(b) and (c)) we would expect a change in the amount of air which would bypass the spray zone. As detailed in Section 5, the model is incredibly sensitive to the granule moisture content with regards to the extent of spray drying. A large excess of air would lead to significant spray drying and a very dry bed, whereas, a small bypass ratio would lead to very wet particles in the bed and less overall spray drying. As the bypass ratio was fixed at a value of 0.1, this did not take into account the change in spray dynamics as a result of change in spray rate, temperature or air flow rate. For example, in experiment 2 (Figure 7.6(b)) as the spray is dropped to 40 kg/hr we would expect less spray coverage and less entrainment of the air. This would result in smaller value of the bypass ratio, hence less spray drying and ultimately more wet granules within the bed; which would result in a more accurate result.

This interaction is in fact a very interesting result. This provides a clear link with the process dynamics and spray dynamics to the moisture content of the granule, a

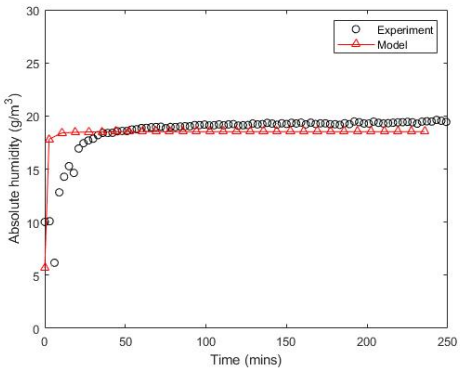
Experiment
Model
Absolute humidity (g/m^3)
Time (mins)

(a)

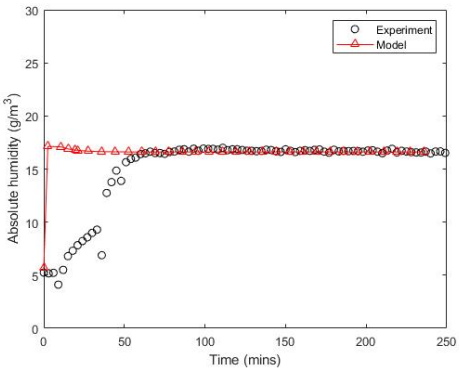
Experiment
Model
Absolute humidity (g/m^3)
Time (mins)

(b)

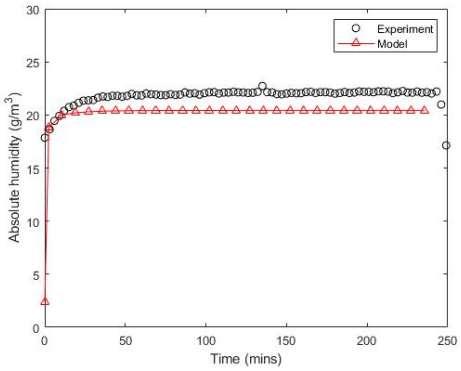
Experiment
Model
Absolute humidity (g/m^3)
Time (mins)

(c)

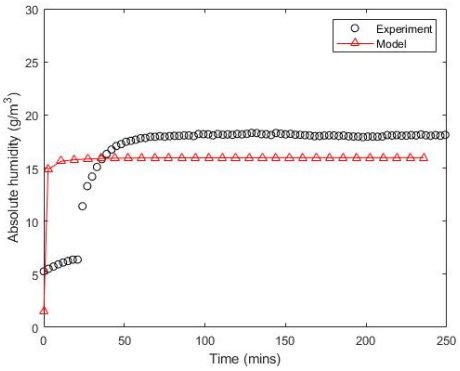
Experiment
Model
Absolute humidity (g/m^3)
Time (mins)

(d)

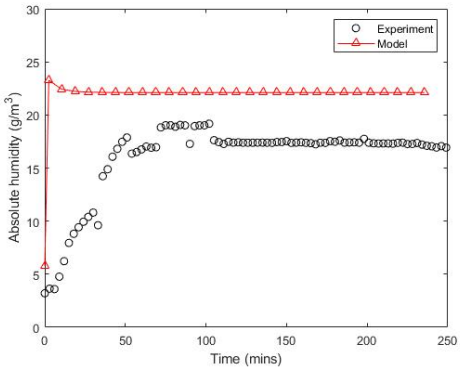
Experiment
Model
Absolute humidity (g/m^3)
Time (mins)

(e)

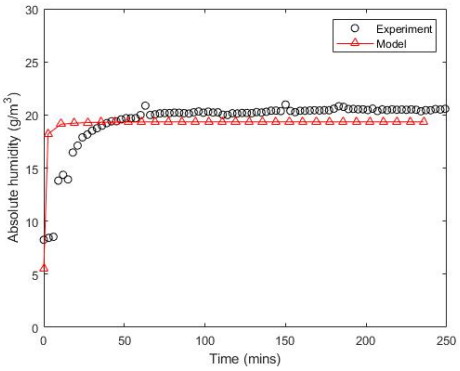
Experiment
Model
Absolute humidity (g/m^3)
Time (mins)

(f)

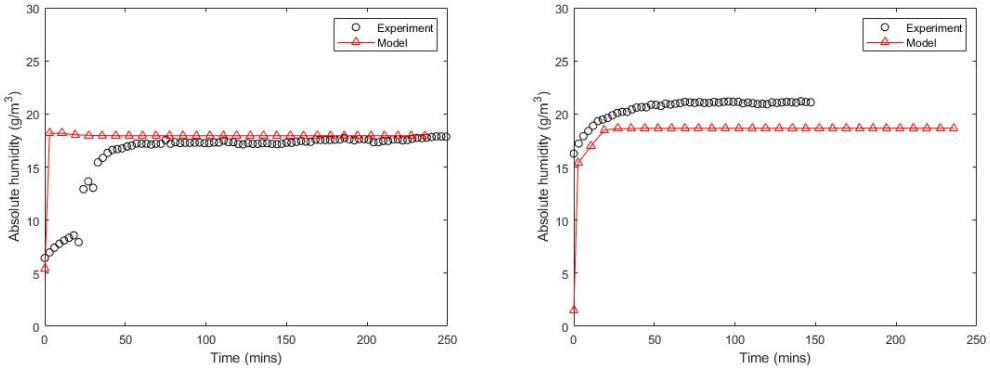

(g)

(h)

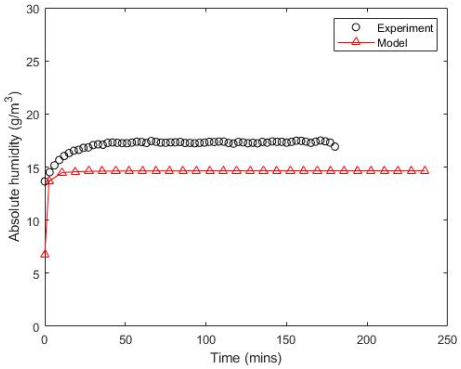

(i)

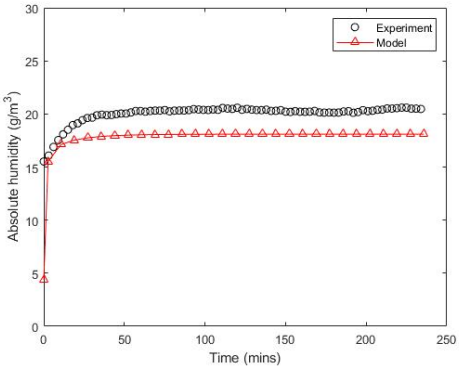

(j)

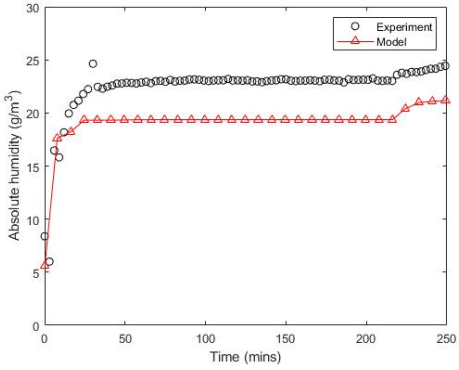

(k)

Figure 7.3: A comparison of the absolute humidity between the experiment and model where subfigures (a)-(j) are experiments 1-10 and subfigure (k) is both experiment 11 and 12, where experiment 12 initiates after 224 minutes.

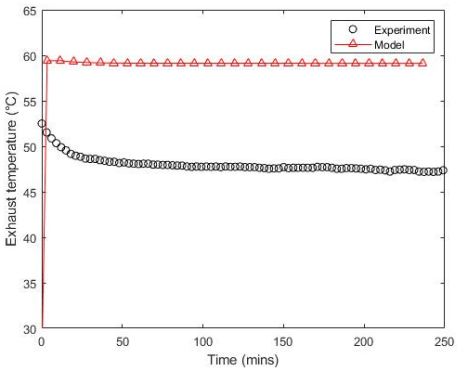
Experiment
Model
Exhaust temperature (°C)
Time (mins)

(a)

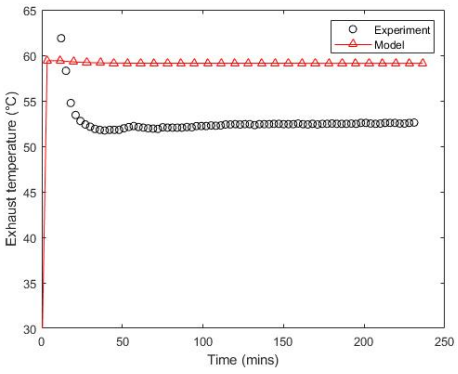
Experiment
Model
Exhaust temperature (°C)
Time (mins)

(b)

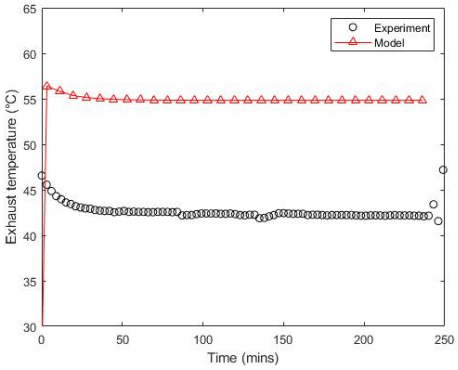
Experiment
Model
Exhaust temperature (°C)
Time (mins)

(c)

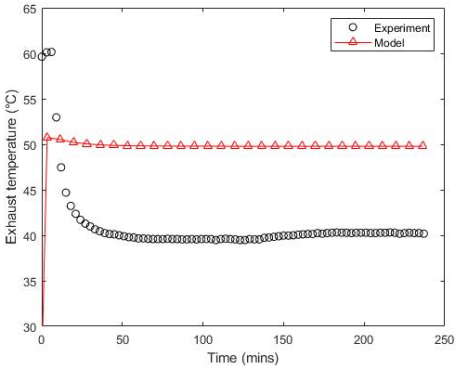
Experiment
Model
Exhaust temperature (°C)
Time (mins)

(d)

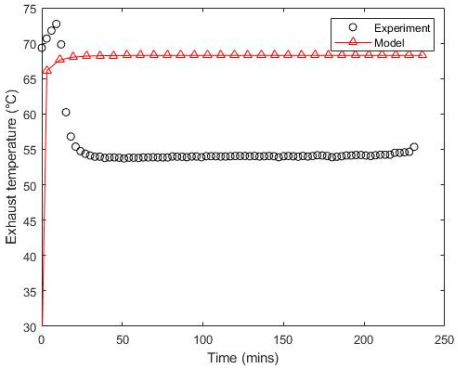
Experiment
Model
Exhaust temperature (°C)
Time (mins)

(e)

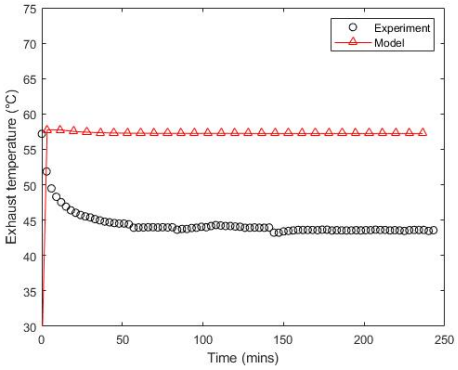
Experiment
Model
Exhaust temperature (°C)
Time (mins)

(f)

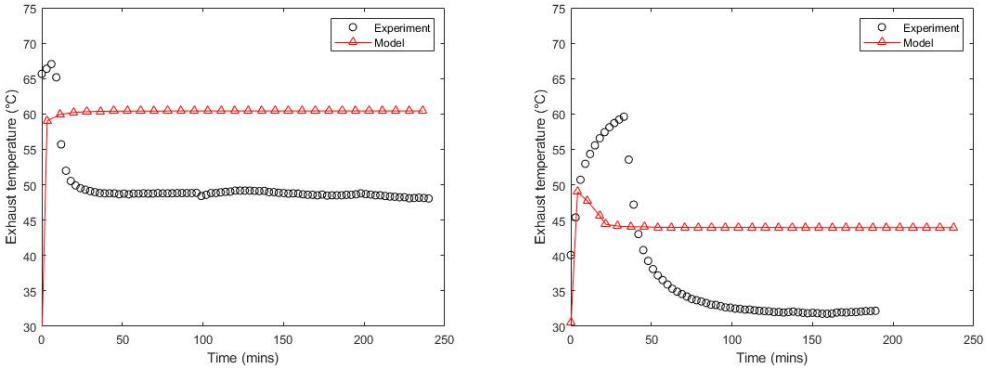

(g)

(h)

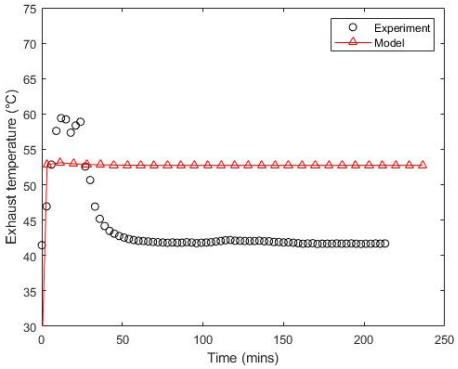

(i)

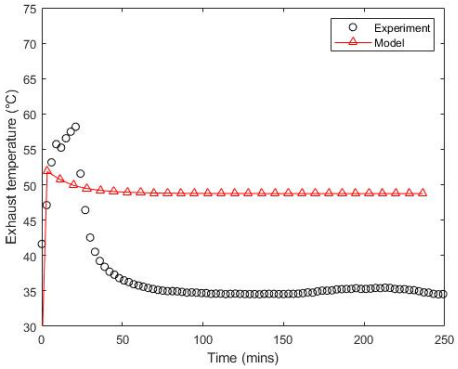

(j)

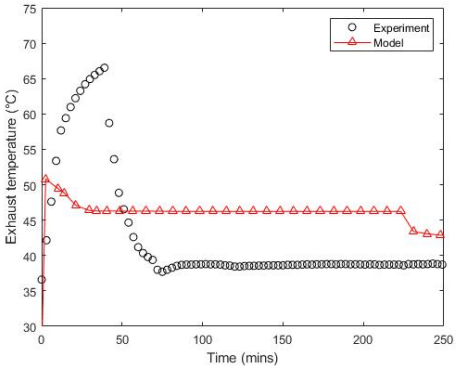

(k)

Figure 7.4: A comparison of the exhaust temperature between the experiment and model where subfigures (a)-(j) are experiments 1-10 and subfigure (k) is both experiment 11 and 12, where experiment 12 initiates after 224 minutes.

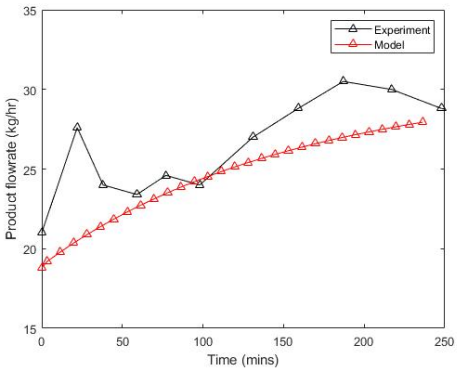
Experiment
Model
Product flowrate (kg/hr)
Time (mins)

(a)

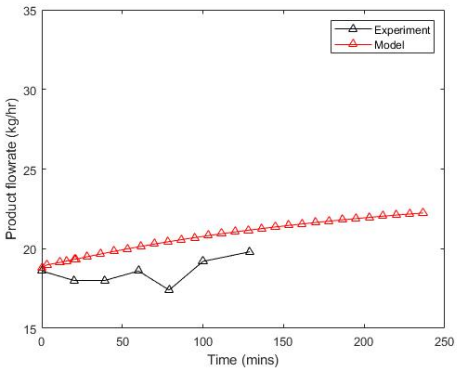
Experiment
Model
Product flowrate (kg/hr)
Time (mins)

(b)

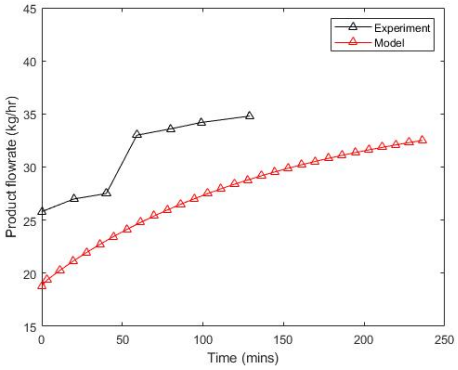
Experiment
Model
Product flowrate (kg/hr)
Time (mins)

(c)

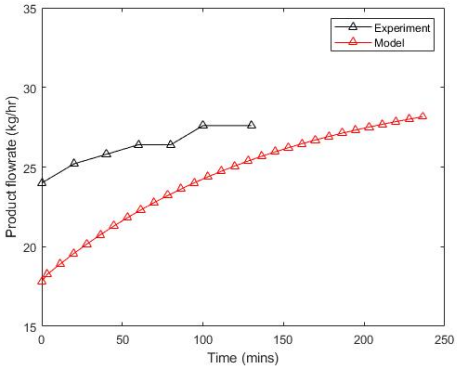
Experiment
Model
Product flowrate (kg/hr)
Time (mins)

(d)

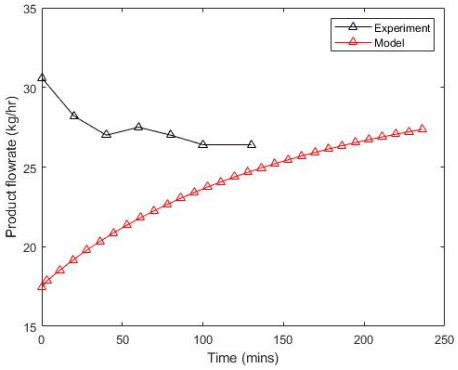
Experiment
Model
Product flowrate (kg/hr)
Time (mins)

(e)

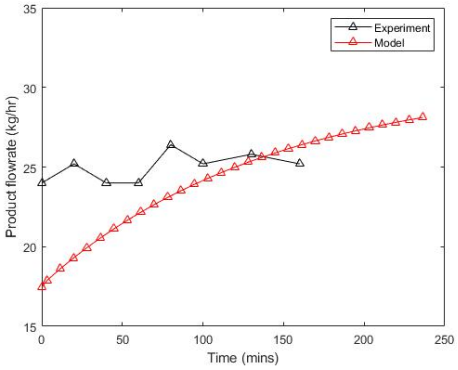
Experiment
Model
Product flowrate (kg/hr)
Time (mins)

(f)

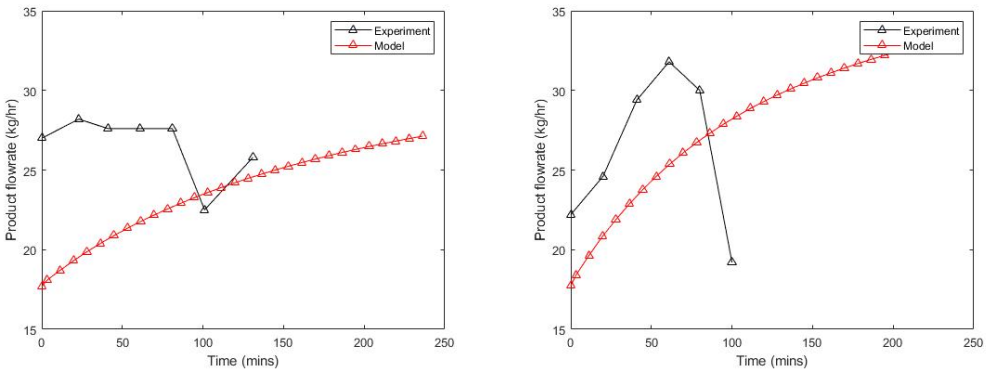

(g)

(h)

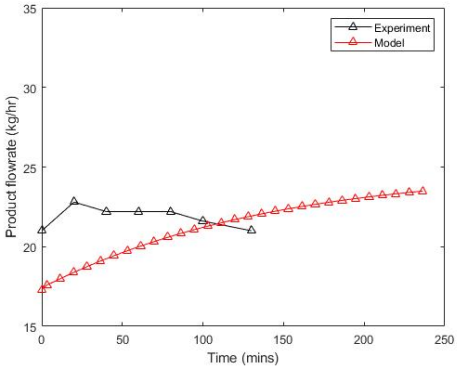

(i)

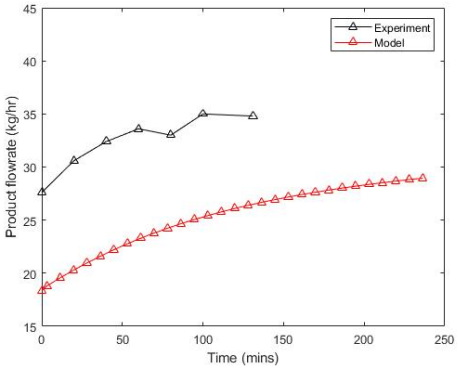

(j)

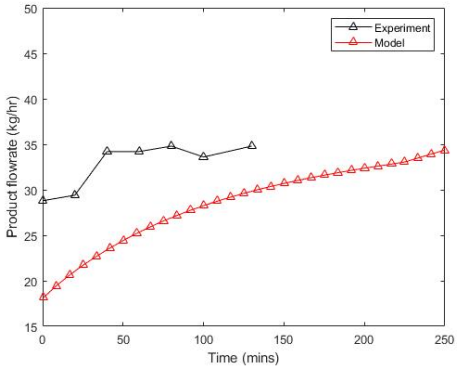

(k)

Figure 7.5: A comparison of the product flow rate between between the experiment and model where subfigures (a)-(j) are experiments 1-10 and subfigure (k) is experiment 11 only as no further measurements were made during experiment 12.

behaviour that isn't well documented in the current literature.

7.4 Conclusion

Validation of a two-compartment coupled 1-D population balance was performed against a pilot scale fluidised bed granulator. The model impressively showed accurate changes to growth and drying with changes in the spray rate, the inlet air temperature and inlet air flow rate - something that the current literature has not clearly demonstrated.

Growth was generally found to be over-damped as there was poor transience towards the steady-state. The experimental data showed a very quick approaches towards steady-state, and when the model attained a steady-state, showed a good agreement. The growth predictions were weakest at demonstrating the extent of agglomeration, as growth was heavily favourable for the larger particles, likely a limitation of the wetting model and the numerical framework of a 1-D coupled population balance model.

The model showed good agreements in predicting the outlet absolute humidity, however, under predicting the result in most cases. The predicted exhaust temperature was shown to be offset from that of the experimental data, but, was attributed to the experimental data having major heat losses through a pulse jet filter and a bag house. The model treats the exhaust adiabatically, which therefore, made comparisons difficult. The predict moisture content showed good agreement in most cases, however, it was identified that the spray bypass ratio (the extent at which the air is entrained into the spray drying compartment) held a key role in achieving better predictions of the moisture content of the bed. Process parameters which would have a significant influence over the spray dynamics, such as the spray rate, would lead to different values of the spray bypass ratio. This means that fixing the initial value of spray bypass ratio was not the appropriate strategy and should have been a variable which varies between process conditions.

Certainly, the weakest aspect of the model was the prediction for the product flow rate. The model showed over-damped behaviour and was very slow to reach a steady-state. The author suggests avoiding a height based discharge model for a screw-conveyor type product discharge.

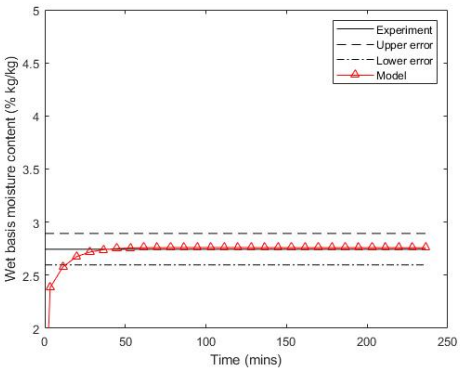
Experiment
Upper error
Lower error
Model
Wet basis moisture content (% kg/kg)
Time (mins)

(a)

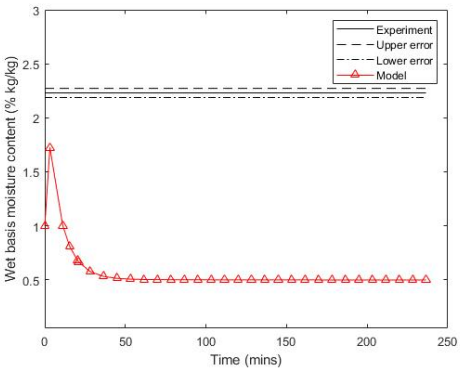
Experiment
Upper error
Lower error
Model
Wet basis moisture content (% kg/kg)
Time (mins)

(b)

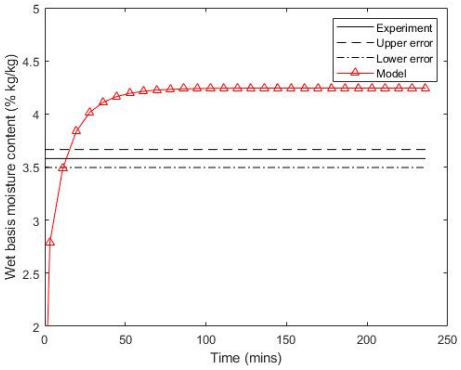
Experiment
Upper error
Lower error
Model
Wet basis moisture content (% kg/kg)
Time (mins)

(c)

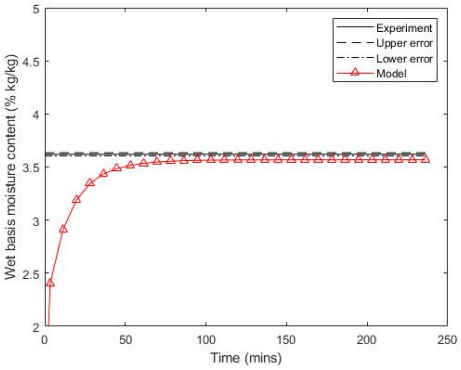
Experiment
Upper error
Lower error
Model
Wet basis moisture content (% kg/kg)
Time (mins)

(d)

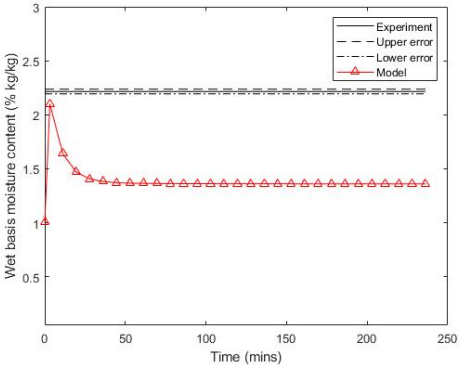
Experiment
Upper error
Lower error
Model
Wet basis moisture content (% kg/kg)
Time (mins)

(e)

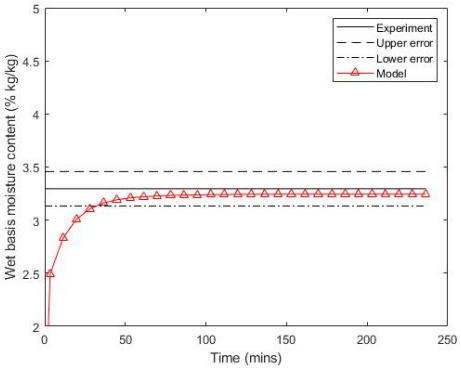
Experiment
Upper error
Lower error
Model
Wet basis moisture content (% kg/kg)
Time (mins)

(f)

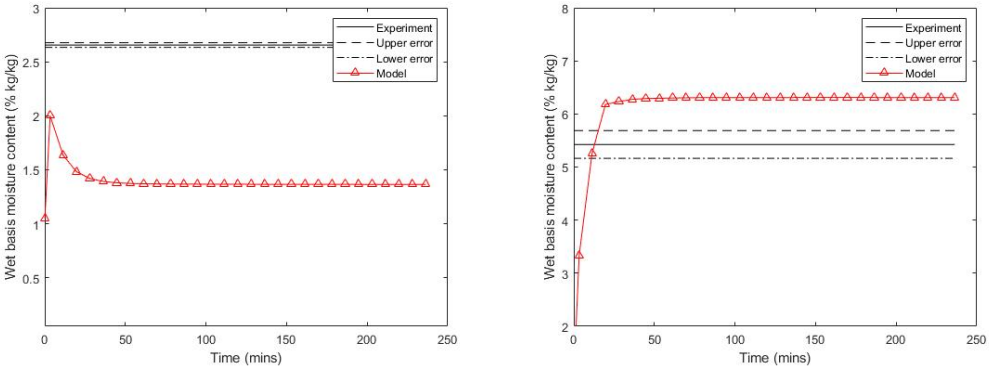

(g) (h)

Figure 7.6: A comparison of the granule moisture content between the experiment and model where subfigures (a)-(h) are experiments 1-8 where the upper and lower error boundaries are shown for each individual figure.

Chapter 8

Conclusion & Future Work

8.1 Major Conclusions

Through this thesis, a two compartment coupled 1-D population balance model for a continuous pilot scale fluidised bed granulator is developed. The work integrates novel aspects such as the particle coating number (following the work of Kariuki et al. [2013]), in addition to well established methods proposed by Burgschweiger et al. [1999] to simulate both particle growth and drying. These integrated methods has led to the formulation of a novel, validated, particle wetting model and agglomeration model that is useable within a population balance equation.

The model extends the current granulation mechanisms by including spray drying as part of the framework for granule growth. By compartmentalising the spray and the bed, a two compartment model is developed which can predict the extent of spray drying, bulk bed drying and particle growth. The particle growth model is driven by a coupled 1-D framework which considers internal granule co-ordinates of the solid composition, liquid content, gas content and the solid content within the solvent phase. This population balance framework allows for a novel, physically representative, wetting and agglomeration model to be proposed and implemented. The wetting model is validated against lab scale data and the agglomeration model captures key dynamics which experimental studies have suggested, yet current models have not regularly to demonstrated. By combining the novel population balance framework with a two-compartment structure and drying, this offers a new model formulation which captures more dynamics and granulation mechanisms than the current works of the literature.

A core achievement of the model demonstrates that the particle growth, the drying and the particle properties are sensitive to all changes of the key process control parameters, in particular, the mass spray rate, the inlet air temperature and inlet

air flow rate. This is demonstrated through sensitivity studies and model validation against experimental data from a continuous pilot scale fluidised bed granulator. The experiments not only vary the spray rate, inlet air temperature and inlet air flow rate individually, but also, a varied combination of these parameters. There is good agreement between the measured outputs and the model despite limitations with regards to over-damped dynamics. This is very impressive given the breadth of the experiments which are performed on a pilot scale unit.

The fundamental focus of this thesis is to develop a suitable modelling framework which physically represents the granulation mechanisms and the fluidised bed process. The model showed strengths and a few weaknesses. For example, the model struggled to show rapid growth and collapsing of the particle bed as a result of a large spray flux. This issue is attributed to the numerical framework of a 1-D coupled population balance model and the over-tuned nature of the wetting model which would see preferential growth of the larger particles. This leads to a bi-modal distribution which suggests that the liquid content is swept along the particle grid, which accelerates the growth of larger particles.

A simple robust methodology was used to describe the bed hydrodynamics. This provides good results for drying but poor results for predicting the product flow rate. There is room to improve how the model treats particle flow out of the granulator

8.2 Future Work

While this thesis focuses on developing a computationally cheap population balance framework, by employing a fully distributed 2-D framework which considers the particle size and liquid content as key internal co-ordinates will help improve the treatment of granule growth and drying. With an appropriate wetting function, the bias for large particles can be subverted towards a bias of the particle flow-state (such as whether the particle is likely to move into the spray zone or not). This could lead to more growth of not only large particles but also the smaller particles, a property which a 1-D coupled framework struggles to encompass.

The product discharge model could be improved by using an alternative method. Instead of using a simple discharge model, this could be expanded into using hybrid methods such as DEM and/or CFD, or preferentially, a continuous method such as an analogous CSTR discharge approach. By introducing one of these methods, the segregation of particles and the prediction of the particle residence times can be enhanced, though at a much greater computational cost.

Appendix A

Simplified Analytical Model for Batch Growth and Drying

This appendix is added as a point of interest which follows from the work of Chapter 3. The analytical model provided here is not novel in its formulation, but rather, an extension of the work found in Heinrich and Mörl [1999], Salman et al. [2006] and Mörl et al. [2007] through the use of the particle coating number, ϕ_p.

A.1 Introduction

Analytical solutions are valuable in providing immediate heuristic analysis of the fundamental mechanistic behaviours for a majority of rate processes and phenomena. Often, the criticisms of analytical solutions is the need to make many sweeping assumptions to develop a solution. This results in overly simplified models which do not respect the reality of the process. However, due to the almost non-existent computational costs, stability and sensitivity of the functional parameters can be identified immediately without arduous computational effort. This provides an easy method for apriori analysis for process design and optimisation.

A.2 Particle Growth Model

Initial assumptions are made about the system:

- The particle bed is exposed to a two-fluid spray which has some solids mass fraction of x_{spray} over some residence time t
- The bed is well mixed such that the liquid to solid ratio for particles of all size classes is fixed.

- The solid density is constant.
- The drying gas flows through the bed in a plug-flow like manner, where there is no radial mixing or re-circulation.

To define the initial particle space, it is assumed that the particle distribution is a vector along the length co-ordinate of some total number of particles, N_p, that exists as a Gaussian distribution of some mean value and standard deviation with a total length of N gridpoints. This is formally expressed as Equation A.1:

$$f(d_p|\mu,\sigma) = \frac{N_p}{\sigma\sqrt{2\pi}} \exp \frac{-(d_p-\mu)^2}{2\sigma^2} \tag{A.1}$$

Where N_p is the total number of particles within the granulator, σ is the standard deviation and μ is the mean particle size. It is assumed that the total number of particles of each size class does not change with time, therefore, the total at $t = 0$ is constant.

For a real solution of the growth equation to exist, a simplification must be made around Equation 3.11 as x_{LS}, the liquid-to-solid ratio, cannot have dependency on the particle diameter. For a well mixed bed, the liquid-to-solid ratio is defined as Equation A.2:

$$x_{LS} = \frac{\int_0^t \dot{M}_{spray} dt}{M_{bed}} \tag{A.2}$$

Where $\dot{M}_{spray}$ is the spray rate of the two-phase liquid added to the system, M_{bed} is the mass of the particle batch within the bed.

Equation 3.10 can be simplified into the following form as Equation A.3 by converting the integral into an equivalent summation:

$$\frac{dd_p}{dt} = \frac{2\sigma_p}{\sum_{p=1}^{p=N} n_p \sigma_p A_p \rho_p} \dot{M}_{spray}(1 - x_{spray}) \tag{A.3}$$

where σ_p is the surface coating of the particle, n_p is the number of particles within a size class, A_p is the particle surface area, ρ_p is the particle density, $\dot{M}_{spray}$ is the mass flow rate of the spray and x_{spray} is the solids fraction of the spray inlet.

Both sides of the equation can be integrated respectively with the appropriate limits as shown in Equation A.4:

$$\int_{d_{p0}}^{d_p} dd_p = \int_0^t \frac{2\sigma_p}{\sum_{p=1}^{p=N} n_p \sigma_p A_p \rho_p} \dot{M}_{spray}(1 - x_{spray}) dt \tag{A.4}$$

which results in the explicit form:

$$d_p(t) = d_{p0} + \frac{2\sigma_p}{\sum_{p=1}^{p=N} n_p \sigma_p A_p \rho_p} \dot{M}_{spray}(1 - x_{spray})t \tag{A.5}$$

For a constant spray rate the liquid-to-solid ratio of the particle bed can be simply expressed $x_{LS} = \frac{\dot{M}_{spray}t}{M_{bed}}$. By substituting this expression into Equation A.5 the final form of the model is shown as Equation A.6:

$$d_p(x_{LS}) = d_{p0} + \frac{2\sigma_p}{\sum_{p=1}^{p=N} n_p \sigma_p A_p \rho_p}(1 - x_{spray}) M_{bed} x_{LS} \tag{A.6}$$

which further can be simplified as:

$$d_p(x_{LS}) = d_{p0} + G x_{LS} \tag{A.7}$$

Equation A.7 can be rewritten in matrix form as the initial particle size distribution is a distributed property, this follows as Equation A.8:

$$\begin{bmatrix} d_{p,1} \\ d_{p,2} \\ \vdots \\ d_{p,i} \\ \vdots \\ d_{p,N-1} \\ d_{p,N} \end{bmatrix} = \begin{bmatrix} d_{p0,1} \\ d_{p0,2} \\ \vdots \\ d_{p0,i} \\ \vdots \\ d_{p0,N-1} \\ d_{p0,N} \end{bmatrix} + \begin{bmatrix} G_1 \\ G_2 \\ \vdots \\ G_i \\ \vdots \\ G_{N-1} \\ G_N \end{bmatrix} x_{LS} \qquad i = 1, 2, \ldots \ N \tag{A.8}$$

or

$$\overrightarrow{d_p} = \overrightarrow{d_{p0}} + \overrightarrow{G} x_{LS} \tag{A.9}$$

This model shows the implication of the liquid-to-solid ratio as being the primary factor in controlling the growth of a particle within a steady-state bed. If it was assumed that all the particles within the particle bed were initially all the same size, σ_p would eliminate itself from both the numerator and denominator. This solution would therefore collapse to the same model which Mörl et al. [2007] has initially proposed.

A.3 Drying Model

To model the drying of the liquid from the surface of the particle an adapted approach from Heinrich and Mörl [1999] is used and simplified. Here, we replace the

defined "wetness" parameter as the fractional coating function, σ_p, and perform similar mathematical processes to form an analytical drying model.

From Heinrich and Mörl [1999] it is possible to define the rate of change of humidity against the bed height by Equation A.10 assuming no re-circulation of the gas phase:

$$\frac{dY}{dz} = \beta_{l\rightarrow g}\frac{\tilde{M}_a P_T}{RT}\frac{\bar{\sigma_p} A_{sp}}{\dot{M}_a}(Y^* - Y) \tag{A.10}$$

where $\beta_{l\rightarrow g}$ is the mass transfer coefficient of the solvent to the gas phase, $\tilde{M}_a$ is the molecular mass of the gas phase, P_T the total internal pressure of the fluidised bed, R the gas constant, T the temperature of the gas phase, $\bar{\sigma_p}$ the mean fractional coating of the particle bed, A_{sp} the specific solids surface area of the particle bed, $\dot{M}_a$ the specific mass flow rate of the gas phase, Y^* the equilibrium moisture content of the gas and Y the humidity of the gas.

Equation A.10 can be made non-dimensional by the appropriate substitution. Here, $\zeta = \frac{z}{L}$ is chosen resulting in Equation A.11:

$$\frac{dY}{d\zeta} = \beta_{l\rightarrow g}\frac{\tilde{M}_a P_T}{RT}\frac{\bar{\sigma_p} A_{sp} L}{\dot{M}_a}(Y^* - Y) \tag{A.11}$$

where L is the total length of the fluidised particle bed. By defining the number of transfer units as $\beta_{l\rightarrow g}\frac{\tilde{M}_a P_T}{RT}\frac{A_{sp}L}{\dot{M}_a} = NTU$, both sides can be integrated as shown by Equation A.12:

$$\int_{Y_0}^{Y}\frac{dY}{Y^* - Y}dY = \int_0^{\zeta} NTU\bar{\sigma_p}d\zeta \tag{A.12}$$

where the final result can be expressed by Equation A.13:

$$\frac{Y^* - Y(\zeta)}{Y^* - Y_0} = e^{-NTU\bar{\sigma_p}\zeta} \tag{A.13}$$

The gas temperature as a function of dimensional bed height can be calculated directly from Heinrich and Mörl [1999] by an enthalpy balance around the system. This is shown by Equation A.14 assuming steady-state:

$$T(\zeta) = \frac{h_{g,0} - Y(\zeta)\Delta H_{evap}}{C_{p,g} + Y(\zeta)C_{p,e}} \tag{A.14}$$

where the initial gas enthalpy, $h_{g,0}$, can be further defined as:

$$h_{g,0} = T_{g,0}(C_{p,g} + Y_0 C_{p,w}) \tag{A.15}$$

By substituting Equations A.13 and A.15 into Equation A.14 the final result for the function of gas temperature with dimensionless height is:

$$T(\zeta) = \frac{T_{g,0}\frac{(C_{p,g}+Y_0C_{p,w})}{Y^*-Y_0} - \Delta H_{evap}(1-e^{-NTU\bar{\sigma_p}\zeta})}{\frac{(C_{p,g}+Y_0C_{p,w})}{Y^*-Y_0} + C_{p,w}(1-e^{-NTU\bar{\sigma_p}\zeta})} \tag{A.16}$$

Given that $T_{g,0}$ is the initial gas temperature of the fluidisation air, $C_{p,g}$ is the specific heat capacity by mass of the gas, $C_{p,w}$ is the specific heat capacity of the solvent, ΔH_{evap} is the enthalpy of evaporation of the solvent and the other parameters are previously defined.

Finally, the average value of the gas humidity and temperature can be determined by taking the integral bounded by the dimensionless height over Equations A.13 and A.16. The explicit results are shown as Equations A.17a and A.17b:

$$\bar{Y} = Y^* - \frac{(Y^*-Y_0)}{NTU\bar{\sigma}_p}(1-e^{-NTU\bar{\sigma}_p}) \tag{A.17a}$$

$$\bar{T} = \frac{1}{NTU\bar{\sigma}_p}\Big(\frac{\Delta H_{evap}}{C_{p,w}} + \frac{C_2}{C_3}\Big)\ln\Big[\frac{C_{p,w}e^{-NTU\bar{\sigma}_p} - C_3}{C_{p,w}-C_3}\Big] + \frac{C_2}{C_3} \tag{A.17b}$$

where the constants are $C_1 = \frac{(C_{p,g}+Y_0C_{p,w})}{Y^*-Y_0}$, $C_2 = T_{g,0}C_1 - \Delta H_{evap}$ and $C_3 = C_1 - C_{p,w}$ as suggested in Salman et al. [2006] and Mörl et al. [2007].

A.4 Specific Mass Flowrate of Solvent

To determine the fraction of solvent evaporated a simple mass balance is conducted around the bed. Assuming steady-state and no backflow of gas, the mass balance can be written as Equation A.18:

$$\dot{m}_a(Y(\zeta=1) - Y_0) = \dot{M}_{spray}x_{spray} \tag{A.18}$$

where $\dot{m}_a$ is the mass flow rate of the air and the other parameters previously identified. By substituting Equation A.13 into EquationA.18 the specific mass flow rate of solvent can be determined and shown as Equation A.19:

$$\dot{M}_w = \frac{\dot{M}_{spray}x_{spray}}{\dot{m}_a(Y^*-Y_0)} = 1 - e^{-NTU\bar{\sigma}_p} \tag{A.19}$$

Table A.1: Table of parameters

Parameter Name	Symbol	Value
Liquid-to-Solid Ratio	x_{ls}	0.05-1 kg/kg
Granulator volume	V_{eq}	0.1 m^3
Number of size classes	N	50
Mean particle size	μ	350 μm
Standard deviation	σ	50 μm
Initial solid composition	x_s	1 kg/kg
Initial liquid composition	x_l	0 kg/kg
Density of solid phase	ρ_s	1300 kg/m^3
Density of liquid phase	ρ_l	1000 kg/m^3
Density of gas phase	ρ_g	1.2 kg/m^3
Droplet diameter	d_d	15-100 μm
Solid composition of the spray	x_{spray}	0.5 kg/kg
Contact angle	θ	30-60°
Specific heat capacity of the gas	$C_{p,g}$	1 kJ/kgK
Specific heat capacity of the solvent	$C_{p,w}$	2 kJ/kgK
Enthalpy of evaporation	ΔH_{evap}	2300 kJ/kg
Inlet gas humidity	Y_0	0.01 kg/kg
Saturation gas humidity	Y^*	0.0536 kg/kg
Inlet gas temperature	T_0	150 C
Number of transfer units	NTU	1-6 $(-)$

A.5 Model Parameters

Table A.1 provides the model parameters used to study the outputs of the analytical model.

A.6 Parametric Study

Figure A.1 shows how the mean particle size and the size distribution varies with the liquid-to-solid ratio of the fluidised bed. The mean particle size shows linear dependence with the liquid-to-solid ratio where there is some non-linearity with regards to the coating number. At larger droplet diameters, the growth rate at lower liquid-to-solid ratios is lower which agrees with Section 3.4 which showed similar results with respect to contact angle. The size distribution also shows linear behaviour such that $f(d_{p0}, 0)$ is a translation along the size co-ordinate for $f(d_{p0} - Gx_{LS}, x_{LS})$. As the liquid-to-solid ratio increases, the velocity from initial distribution is constant,

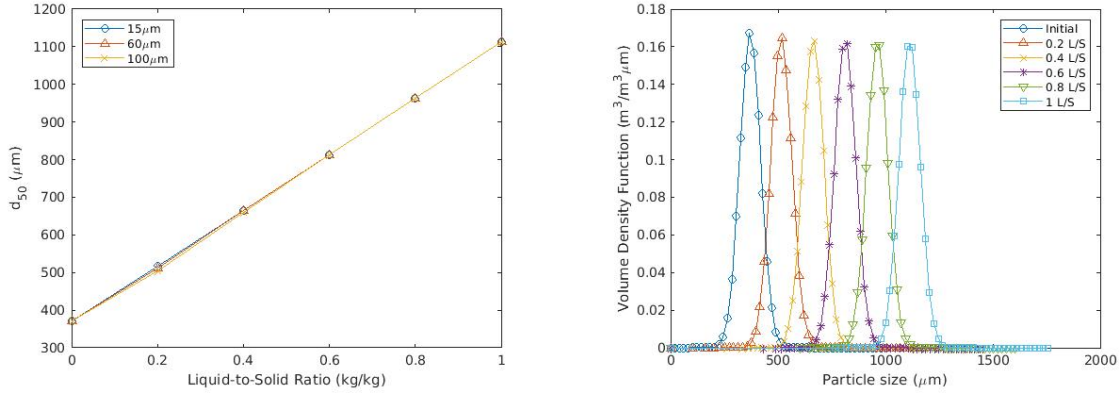

(a) (b)

Figure A.1: (a) the volume based mean granule size against liquid-to-solid ratio at multiple droplet diameters at and (b) the particle size distribution for varying liquid-to-solid ratios for droplet properties of $d_d = 15\mu m$ and $\theta = 30°$.

indicating that growth for all size classes is not size dependent. Linear growth is fundamentally true only under ideal conditions, particularly for large liquid-to-solid ratios. Realistically, agglomeration and breakage would be occurring simultaneously where non-linear growth can be observed. However, in certain cases for low liquid-to-solid ratios linear growth can be observed as found by Rieck et al. [2015].

Figure A.2 shows how the mean coating fraction varies with liquid-to-solid ratio at varying droplet diameters and contact angles. The most prominent difference is found on A.2a where for a $15\mu m$ droplet the necessary liquid-to-solid ratio is roughly 0.12, but, for a $100\mu m$ droplet it is a 5-fold increase. With an increase in droplet diameter, the number of droplets decreases greatly. As the coating number, ϕ_p, is derived on the basis of a Bernoulli trial; the lower the number count of droplets, the lower the N number of stochastic interactions. Hence, poorer surface coating.

Figure A.2 shows with an increase of contact angle the overall coating of the particle bed decreases. The surface spreading of the droplet decreases with an increase in the contact angle, so the area covered per droplet decreases as a result.

In a practical scenario, the droplet diameter should be minimised as much as reasonably possible if complete surface coating is desired. The contact angle is often a formulation dependent property, which from a process control point-of-view, cannot be controlled.

The key gas properties during drying are shown on Figure A.3 for varying droplet diameters. At the individual boundaries of $x_{LS} = 0$ and $\zeta = 0$ the gas temperature sits at the initial value indicating that the solution sits at the boundaries reasonably.

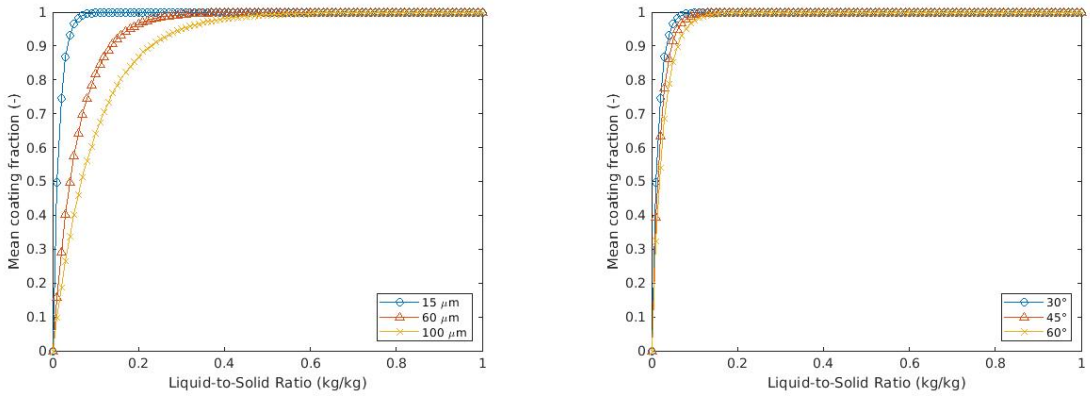

(a) (b)

Figure A.2: (a) the mean coating fraction of the particle bed for varying droplet sizes (b) for varying contact angles

This statement also stands true for the gas humidity.

With an increase in the droplet diameter the curvature of the surface plots along the liquid-to-solid ratio increases for both the gas temperature and humidity. This is because the surface coating of the particles reduce the effective surface area of drying, hence, the drying potential at lower to liquid-to-solid ratios decreases. This becomes more prominent at larger droplet diameters due to the overall lower coating values. Once a surface coating of 1 is attained, the drying is then dominated by the exponential behaviour across the bed height. This is quite beneficial, as it indicates that the most energetically stable value for drying is when the particle surface area is entirely covered by liquid. This maximises drying and therefore should considered as a design point for process design.

The mean gas temperature and humidity are shown on Figure A.4. With an increase in the number of transfer units, the greater the extent of drying. As a result, the gas temperature reaches an asymptote at a lower value, where in reverse, the humidity at a higher. At higher NTU's, the solution approaches some critical value which is limited by the mass balance of the system; as it is not possible to dry more than the available liquid within the system. This indicates a limit for the value of the NTU before the model becomes unrealistic. In a practical application, the number of transfer units is generally an unknown value as the mass transfer coefficient is specific to the product formulation and the drying medium among other equipment related properties.

The fraction of solvent evaporated is determined by the specific mass flow of solvent as shown on Figure A.5. As the liquid-to-solid ratio increases the specific

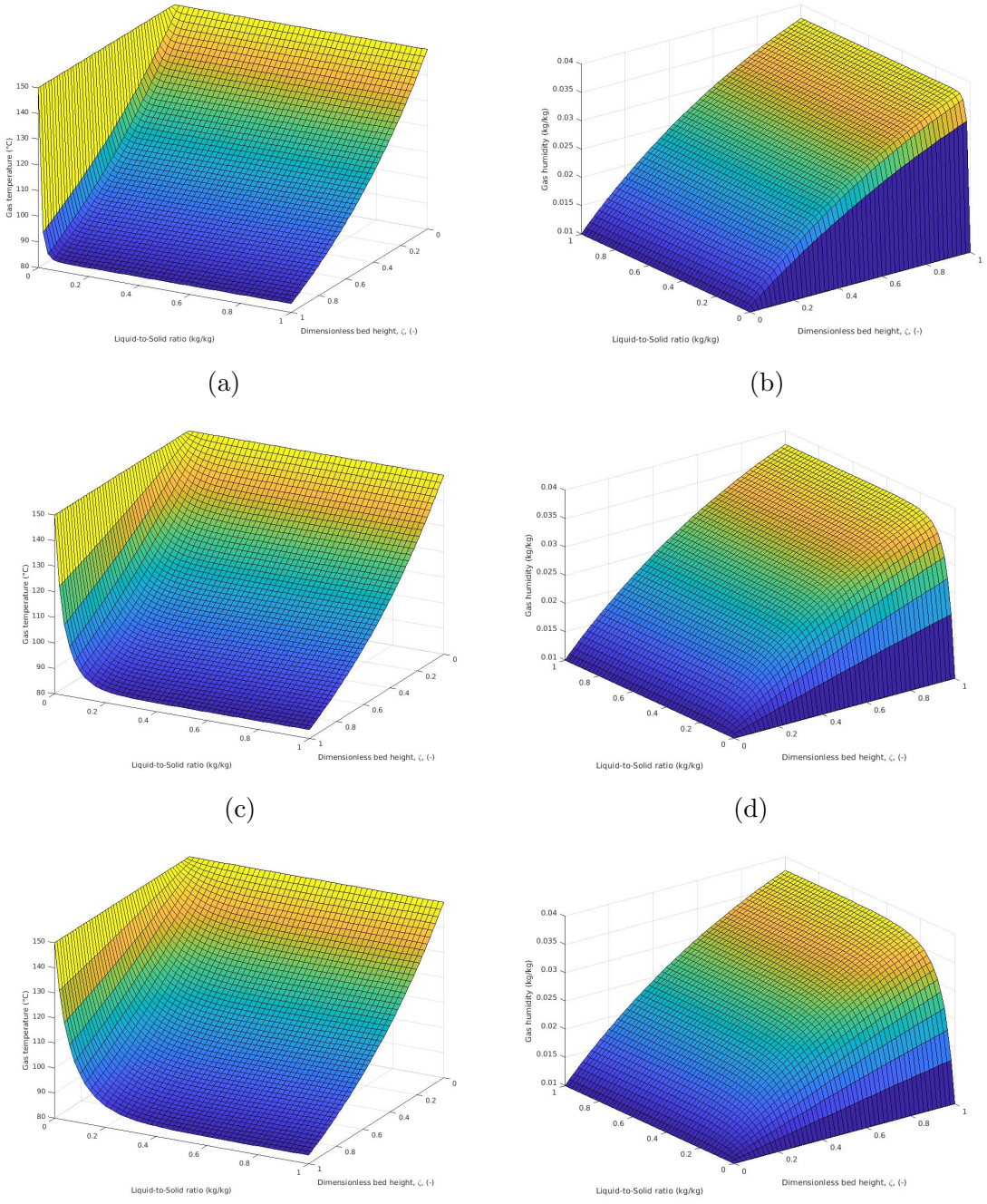

Figure A.3: (a)(c)(e) show the surface plot of the gas temperature against the dimensionless height, ζ, and liquid to solid ratio for varying droplet diameters where (a) $d_d = 15\mu m$, (c) $d_d = 60\mu m$, (e) $d_d = 100\mu m$ and (b)(d)(f) show the surface plot of the gas humidity against the dimensionless height, ζ, and liquid to solid ratio for varying droplet diameters where (b) $d_d = 15\mu m$, (d) $d_d = 60\mu m$, (f) $d_d = 100\mu m$. All simulations were performed at $NTU = 1$.

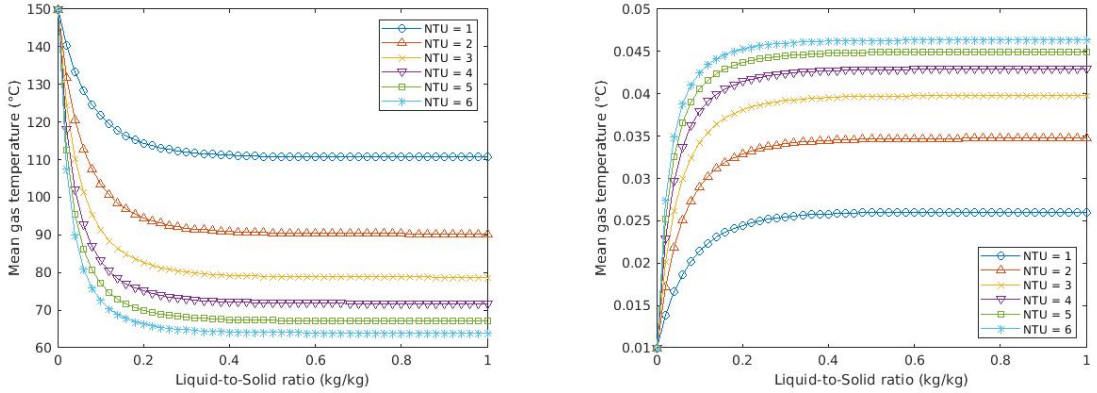

(a) (b)

Figure A.4: (a) the mean gas temperature of the bed against the liquid-to-solid ratio for varying number of transfer units (b) the mean humidity of the bed against the liquid-to-solid ratio for varying number of transfer units.

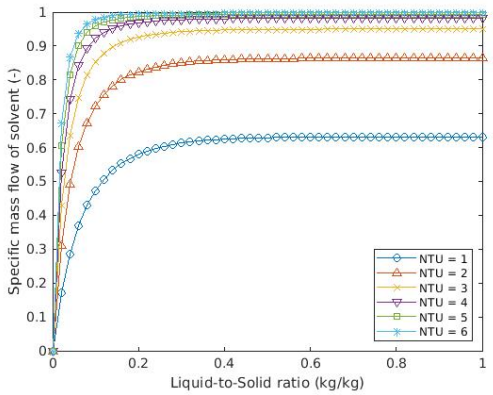

Figure A.5: The specific mass flow of the solvent against the liquid-to-solid ratio for varying transfer units.

mass flow approaches a constant. This is again due to the system approaching a surface coating of 1, where drying is the most energetically stable. With an increase in the NTU the specific mass flow approaches a value close to 1, where clearly, is unrealistic as this would imply that all the solvent is evaporated prior to the spray interacting with the particle bed.

A.7 Conclusions

By establishing a set of assumptions around the particle bed, the model was simplified to form a batch growth and drying model. With increasing x_{LS} growth was shown to increase linearly where the final distribution of the particle was a translation by

$f(d_{p0} - Gx_{LS})$. Similarly, to the numerical model the surface coating showed minimal effect on the particle growth. Drying was found to be strongly related to the surface coating of the particle, where the most energetically stable point was at a surface coating $\sigma_p = 1$. It is advised that when designing a fluid-bed process for simultaneous drying and growth, achieving a surface coating of 1 would be optimal. The number of transfer units, NTU, was found to also show a strong relationship with the drying. An NTU of greater than 4 showed unrealistic behaviour where the spray would dry before interacting with the bed. If process designers find that their experimental data is showing a value of 4 or greater then this would be indicative of errors in methodology or experimentation.

Appendix B

Calculating the Bubble Phase Properties of a Fluidised Bed

From Kunii and Levenspiel [1991] the minimum fluidisation velocity of the particle bed for a distribution is calculated by Equation B.1:

$$\frac{1.75}{\epsilon_{mf}^3 \phi_s}\left(\frac{d_{3,2} u_{mf} \rho_g}{\mu_g}\right)^2 + \frac{150(1-\epsilon_{mf})}{\epsilon_{mf}^3 \phi_s^2}\left(\frac{d_{3,2} u_{mf} \rho_g}{\mu_g}\right) = \frac{d_{3,2}^2 \rho_g (\rho_s - \rho_g) g}{\mu_g^2} \tag{B.1}$$

where u_{mf} is the minimum fluidisation velocity for particle, ϵ_{mf} is the minimum bed porosity, ϕ_s is the shape factor of the particle, $d_{3,2}$ is the sauter mean diameter of particle, ρ_g is the gas density, μ_g is the fluidisation gas viscosity, ρ_s is the particle density and g the gravitational constant.

The minimum fluidisation velocity allows for the calculation of the initial bubble diameter at the orifice. This is expressed as Equation B.2:

$$d_{b0} = \frac{2.78}{g}(u_0 - u_{mf}) \tag{B.2}$$

where u_o is the superficial gas velocity through the inlet and u_{mf} is the minimum fluidisation velocity of the bulk.

The superficial gas velocity this is calculated by Equation B.3:

$$u_0 = \frac{\dot{Q}_g}{A_{bed}} \tag{B.3}$$

where A_{bed} is the area of the distributor plate and $\dot{Q}_g$ is the volumetric flow rate of the fluidisation air.

The limiting bubble diameter can be estimated by Equation B.4:

$$d_{bm} = 0.65\left[A_{bed}(u_0 - u_{mf})\right]^{0.4} \tag{B.4}$$

If linear growth of the bubbles is assumed across the length of the bed, the average bubble diameter across the height of the bed can be estimated by Equation B.5:

$$\bar{d_b} = d_{bm} - \frac{(d_{bm} - d_{b0})d_{bed}}{3H_{bed}}\left\{\exp\left(\frac{-3H_{bed}}{d_{bed}}\right) - 1\right\} \tag{B.5}$$

where d_{bed} is the average diameter of the fluidised bed vessel and H_{bed} is the height of the particle bed. If it is then assumed that the bubble velocity is only the component of it's rise velocity, then the overall bubble velocity can be estimated by Equation B.6:

$$U_b = 0.711(g\bar{d_b})^{0.5} \tag{B.6}$$

Appendix C

Analytical Solution to the Agglomeration Number in Fluidised Beds

The agglomeration number provides a quantitative approach to determine whether agglomeration is the dominant mechanism within a granulation process. Formally, the agglomeration number takes the form of Equation C.1:

$$AN = \frac{1}{2N} \int_0^\infty \eta_{eff}(d_p, d'_p, t) St_{cond}(d_p, d'_p, t) dd_p \tag{C.1}$$

where a double integral is solved across the functions, η_{eff} and St_{cond} for the particle size of interest and any associated particles in which it may agglomerate with.

Practically, Equation C.1 only has value within computational simulations as solving the double integral for a dynamic bed is time-consuming and impractical; not of any value for apriori design of equipment. Analytical forms are cheap and quick, and provide a quick approach to attain insight. An analytical form of Equation C.1 can be derived, given that a few assumptions are made of the particle bed. These follow as:

1. The particle bed is mono-sized.
2. The bed is well-mixed.
3. All particles within the bed receive equal amounts of liquid from the spray.
4. The dominant growth mechanism leading to agglomeration is wetting only.
5. The number of particles before agglomeration does not change.

From these assumptions we can simplify Equation C.1 to a linear form as Equation C.2:

$$AN = \frac{1}{2}\eta_{eff}(d_p, t)St_{cond}(d_p, t) \tag{C.2}$$

where η_{eff} is the wetting probability factor and St_{cond} is the Stokes condition of the particle. Given that assumptions two and three hold, we can expand η_{eff} as a function of the surface wetting assuming wet-wet collisions only:

$$\eta_{eff} = 2f(1-f) + f^2 \tag{C.3}$$

which simplifies to

$$\eta_{eff} = 2f - f^2 \tag{C.4}$$

where f is the surface coating of the particles in the bed. We can expand f in terms of the particle coating number, which results in Equation C.5:

$$\eta_{eff} = 2(1 - e^{-\phi_p}) - \left(1 - e^{-\phi_p}\right)^2 \tag{C.5}$$

which simplifies to Equation C.6:

$$\eta_{eff} = 1 - e^{-2\phi_p} \tag{C.6}$$

where ϕ_p is the particle coating as shown by Equation C.7:

$$\phi_p(d_p, t) = \frac{6x_{LS}a_d}{\pi d_d^3 \rho_d A_{SA}} \tag{C.7}$$

where x_{LS} is the single particle liquid mass fraction -to-solid ratio, a_d is the droplet contact area, d_d is the droplet diameter from the spray, ρ_d is the droplet density and A_{SA} is the specific area of the particle.

We substitute Equation C.7 into Equation C.6 and collect terms where appropriate, we get Equation C.8:

$$\eta_{eff} = 1 - e^{-12C_1\frac{\dot{m}_{spray}}{M_{bed}}t} \tag{C.8}$$

where C_1 is:

$$C_1 = \frac{a_d}{\pi d_d^3 \rho_d A_{SA}} \tag{C.9}$$

Equation C.8 provides the complete expansion of η_{eff} which can be substituted into Equation C.2, but before doing so, we need to expand St_{cond} into an analytical form.

We take the definition of St_{cond} as Equation C.10:

$$St_{cond} = \begin{cases} 1 & St_v < St_{crit} \\ 0 & St_v < St_{crit} \end{cases} \tag{C.10}$$

where St_v is the viscous Stokes number of the particle and St_{crit} is the critical Stokes number which are given as Equations C.11 and C.12:

$$St_v = \frac{8\rho_p U_c d_p(t)}{9\mu_l} \tag{C.11}$$

and

$$St_{crit} = 2\ln\left(\frac{h}{h_0}\right) \tag{C.12}$$

We can convert Equation C.10 into a continuous form by taking a hyperbolic analogy for the case structure. This follows as Equation C.13:

$$St_{cond} = 0.5 - 0.5\tanh\left[A\left(St_{crit} - St_v\right)\right] \tag{C.13}$$

where A is some arbitrarily large number, for example, 1×10^6. Substituting Equations C.11 and C.12 into Equation C.13 we get the explicit form as Equation C.14:

$$St_{cond} = 0.5 - 0.5\tanh\left(A\left[2\ln\left(\frac{h}{h_0}\right) - \frac{8\rho_p U_c d_p(t)}{9\mu_l}\right]\right) \tag{C.14}$$

We can generalise h and $d_p(t)$, the liquid layer of the particle and particle diameter, by an analytical growth model. Given that assumption four holds true and we set the surface asperities height, h_0, to be 1% of the initial particle diameter, the height of liquid and particle diameter can be calculated by the analytical model found in Section 3 as Equations C.15 and C.16.

$$h = \frac{2\dot{m}_{spray}\left[(1 - x_w) + x_w\left(1 - e^{-NTU\times f}\right)\right]}{\rho_p n A_p} t \tag{C.15}$$

and

$$d_p(t) = d_{p,0} + \frac{2\dot{m}_{spray}\left[(1 - x_w) + x_w\left(1 - e^{-NTU\times f}\right)\right]}{\rho_p n A_p} t \tag{C.16}$$

where x_w is the liquid fraction of the spray, NTU is the number of transfer units which is equal to $NTU = \beta_{l\rightarrow g}\frac{\tilde{M}_a P_T}{RT}\frac{A_{sp}L}{\dot{M}_a}$ and n is the number of particles in the bed. Equations C.15 and C.16 can be simplified by substituting $n = \frac{M_{bed}}{\rho_p \frac{\pi}{6} d_p^3}$ and collecting terms where appropriate to form Equations C.17 and C.18:

$$h = \frac{8\dot{m}_{spray} d_{p,0} C_2}{3M_{bed}} t \tag{C.17}$$

and

$$d_p(t) = d_{p,0} + \frac{8\dot{m}_{spray} d_{p,0} C_2}{3M_{bed}} t \tag{C.18}$$

where C_2 is Equation C.19:

$$C_2 = \left[(1 - x_w) + x_w \left(1 - e^{-NTU \times f}\right)\right] \tag{C.19}$$

Substituting Equation C.17 and C.19 into Equation C.14 we can achieve the final analytical form of St_{cond} as Equation C.20:

$$St_{cond} = 0.5 - 0.5 \tanh \Bigg(A \left[2 \ln \left(\frac{0.08\dot{m}_{spray} d_{p,0} C_2}{3M_{bed}} t \right) - \left(\frac{8\rho_p U_c d_{p_0}}{9\mu_l} + \frac{192\rho_p U_c \mu_l \dot{m}_{spray} d_{p,0} C_2}{M_{bed}} \right) \right] \Bigg) \tag{C.20}$$

and finally, combining Equations C.20 and C.8 we find the overall form of the agglomeration number as Equation C.21:

$$AN = \frac{1 - e^{-12C_1 \frac{\dot{m}_{spray}}{M_{bed}} t}}{4} - \frac{1 - e^{-12C_1 \frac{\dot{m}_{spray}}{M_{bed}} t}}{4} \times \tanh \Bigg(A \left[2 \ln \left(\frac{0.08\dot{m}_{spray} d_{p,0} C_2}{3M_{bed}} t \right) - \left(\frac{8\rho_p U_c d_{p_0}}{9\mu_l} + \frac{192\rho_p U_c \mu_l \dot{m}_{spray} d_{p,0} C_2}{M_{bed}} t \right) \right] \Bigg) \tag{C.21}$$

Appendix D

Pilot Plant Raw Data

The pilot plant raw data is stored as excel files on a encrypted hard-drive. This hard-drive is managed by the Particle Technology Group at the University of Sheffield. If the reader wishes to have access of the raw data please contact Dr. Rachel Smith (rachel.smith@sheffield.ac.uk) and Prof. James Litster (james.litster@sheffield.ac.uk).

Bibliography

A. Adetayo and B. Ennis. Unifying approach to modeling granule coalescence mechanisms. *AIChE Journal*, 43(4):927–934, 1997.

A. Adetayo, J. Litster, S. E. Pratsinis, and B. Ennis. Population balance modelling of drum granulation of materials with wide size distribution. *Powder technology*, 82(1):37–49, 1995.

S. M. Ammar and C. W. Park. Validation of the gnielinski correlation for evaluation of heat transfer coefficient of enhanced tubes by non-linear regression model: An experimental study of absorption refrigeration system. *International Communications in Heat and Mass Transfer*, 118:104819, 2020.

R. d. B. Ashworth, J. Henriet, J. Lovett, A. Martijn, H. Povlsen, et al. Cipac handbook. 1970.

L. Austin and R. Klimpel. Modeling for scale-up of tumbling ball mills: Control'84. *JA Herbst (eds.)*, pages 167–184, 1984.

L. Austin, K. Shoji, V. Bhatia, V. Jindal, K. Savage, and R. Klimpel. Some results on the description of size reduction as a rate process in various mills. *Industrial & Engineering Chemistry Process Design and Development*, 15(1):187–196, 1976.

D. Barrasso. *Multi-scale modeling of wet granulation processes*. PhD thesis, Rutgers University-Graduate School-New Brunswick, 2015.

D. Barrasso and R. Ramachandran. A comparison of model order reduction techniques for a four-dimensional population balance model describing multi-component wet granulation processes. *Chemical engineering science*, 80:380–392, 2012.

S. Bellinghausen. *Modelling and scaling rules for high-shear wet granulation of pharmaceuticals*. PhD thesis, University of Sheffield, 2021.

S. Bellinghausen, E. Gavi, L. Jerke, P. K. Ghosh, A. D. Salman, and J. D. Litster. Nuclei size distribution modelling in wet granulation. *Chemical Engineering Science: X*, 4:100038, 2019.

D. Bertin, I. Cotabarren, J. Piña, and V. Bucalá. Population balance discretization for growth, attrition, aggregation, breakage and nucleation. *Computers & Chemical Engineering*, 84:132–150, 2016.

D. E. Bertin, I. M. Cotabarren, V. Bucalá, and J. Piña. Analysis of the product granulometry, temperature and mass flow of an industrial multichamber fluidized bed urea granulator. *Powder technology*, 206(1-2):122–131, 2011.

C. Biggs, P. Lant, and M. Hounslow. Modelling the effect of shear history on activated sludge flocculation. *Water science and technology*, 47(11):251–257, 2003.

R. Boerefijn and M. Hounslow. Studies of fluid bed granulation in an industrial r&d context. *Chemical Engineering Science*, 60(14):3879–3890, 2005.

M. Börner, M. Peglow, and E. Tsotsas. Derivation of parameters for a two compartment population balance model of wurster fluidised bed granulation. *Powder technology*, 238:122–131, 2013.

F. Boukouvala, A. Chaudhury, M. Sen, R. Zhou, L. Mioduszewski, M. G. Ierapetritou, and R. Ramachandran. Computer-aided flowsheet simulation of a pharmaceutical tablet manufacturing process incorporating wet granulation. *Journal of Pharmaceutical Innovation*, 8(1):11–27, 2013.

A. Braumann, M. J. Goodson, M. Kraft, and P. R. Mort. Modelling and validation of granulation with heterogeneous binder dispersion and chemical reaction. *Chemical Engineering Science*, 62(17):4717–4728, 2007.

A. Bück, C. Neugebauer, K. Meyer, S. Palis, E. Diez, A. Kienle, S. Heinrich, and E. Tsotsas. Influence of operation parameters on process stability in continuous fluidised bed layering with external product classification. *Powder technology*, 300: 37–45, 2016.

J. Burgschweiger, H. Groenewold, C. Hirschmann, and E. Tsotsas. From hygroscopic single particle to batch fluidized bed drying kinetics. *The Canadian Journal of Chemical Engineering*, 77(2):333–341, 1999.

I. Cameron, F. Wang, C. Immanuel, and F. Stepanek. Process systems modelling and applications in granulation: A review. *Chemical Engineering Science*, 60(14): 3723–3750, 2005.

A. Chaturbedi, C. K. Bandi, D. Reddy, P. Pandey, A. Narang, D. Bindra, L. Tao, J. Zhao, J. Li, M. Hussain, et al. Compartment based population balance model development of a high shear wet granulation process via dry and wet binder addition. *Chemical Engineering Research and Design*, 123:187–200, 2017.

A. Chaudhury and R. Ramachandran. Integrated population balance model development and validation of a granulation process. *Particulate Science and Technology*, 31(4):407–418, 2013.

A. Chaudhury, A. Niziolek, and R. Ramachandran. Multi-dimensional mechanistic modeling of fluid bed granulation processes: an integrated approach. *Advanced Powder Technology*, 24(1):113–131, 2013.

A. Chaudhury, H. Wu, M. Khan, and R. Ramachandran. A mechanistic population balance model for granulation processes: effect of process and formulation parameters. *Chemical Engineering Science*, 107:76–92, 2014.

A. Chaudhury, A. Tamrakar, M. Schongut, D. Smrcka, F. Stepanek, and R. Ramachandran. Multidimensional population balance model development and validation of a reactive detergent granulation process. *Industrial & Engineering Chemistry Research*, 54(3):842–857, 2015.

A. Clarke, T. Blake, K. Carruthers, and A. Woodward. Spreading and imbibition of liquid droplets on porous surfaces. *Langmuir*, 18(8):2980–2984, 2002.

I. M. Cotabarren, D. Bertín, M. Razuc, M. V. Ramírez-Rigo, and J. Piña. Modelling of the spray drying process for particle design. *Chemical Engineering Research and Design*, 132:1091–1104, 2018.

S. A. Cryer. Modeling agglomeration processes in fluid-bed granulation. *AIChE Journal*, 45(10):2069–2078, 1999.

A. Darelius, A. Rasmuson, I. N. Björn, and S. Folestad. High shear wet granulation modelling—a mechanistic approach using population balances. *Powder Technology*, 160(3):209–218, 2005.

N. Deen, M. V. S. Annaland, M. A. Van der Hoef, and J. Kuipers. Review of discrete particle modeling of fluidized beds. *Chemical engineering science*, 62(1-2):28–44, 2007.

K. Dewettinck and A. Huyghebaert. Fluidized bed coating in food technology. *Trends in Food Science & Technology*, 10(4-5):163–168, 1999.

E. Diez, K. Meyer, A. Bück, E. Tsotsas, and S. Heinrich. Influence of process conditions on the product properties in a continuous fluidized bed spray granulation process. *Chemical Engineering Research and Design*, 139:104–115, 2018.

A. Ding, M. Hounslow, and C. Biggs. Population balance modelling of activated sludge flocculation: Investigating the size dependence of aggregation, breakage and collision efficiency. *Chemical engineering science*, 61(1):63–74, 2006.

D. Djuric and P. Kleinebudde. Impact of screw elements on continuous granulation with a twin-screw extruder. *Journal of pharmaceutical sciences*, 97(11):4934–4942, 2008.

B. Ennis and J. Litster. Particle size enlargement. *Perry's Chemical Engineers' Handbook. 7th edition, McGraw-Hill, New York*, 20(20.89), 1997.

B. J. Ennis, G. Tardos, and R. Pfeffer. A microlevel-based characterization of granulation phenomena. *Powder Technology*, 65(1-3):257–272, 1991.

L. Fries, S. Antonyuk, S. Heinrich, D. Dopfer, and S. Palzer. Collision dynamics in fluidised bed granulators: A dem-cfd study. *Chemical Engineering Science*, 86: 108–123, 2013.

J. Z. Gao, A. Jain, R. Motheram, D. Gray, and M. Hussain. Fluid bed granulation of a poorly water soluble, low density, micronized drug: comparison with high shear granulation. *International journal of pharmaceutics*, 237(1-2):1–14, 2002.

V. Gnielinski. Heat transfer coefficients for turbulent flow in concentric annular ducts. *Heat transfer engineering*, 30(6):431–436, 2009.

M. Goldschmidt, R. Beetstra, and J. Kuipers. Hydrodynamic modelling of dense gas-fluidised beds: comparison of the kinetic theory of granular flow with 3d hard-sphere discrete particle simulations. *Chemical Engineering Science*, 57(11):2059–2075, 2002.

M. Goldschmidt, G. Weijers, R. Boerefijn, and J. Kuipers. Discrete element modelling of fluidised bed spray granulation. *Powder technology*, 138(1):39–45, 2003.

M. Goodson, M. Kraft, S. Forrest, and J. Bridgwater. A multi-dimensional population balance model for agglomeration. In *PARTEC 2004—International Congress for Particle Technology*, 2004.

H. Groenewold and E. Tsotsas. A new model for fluid bed drying. *Drying Technology*, 15(6-8):1687–1698, 1997.

K. P. Hapgood, J. D. Litster, and R. Smith. Nucleation regime map for liquid bound granules. *AIChE Journal*, 49(2):350–361, 2003.

K. P. Hapgood, J. D. Litster, E. T. White, P. R. Mort, and D. G. Jones. Dimensionless spray flux in wet granulation: Monte-carlo simulations and experimental validation. *Powder technology*, 141(1-2):20–30, 2004.

K. P. Hapgood, M. X. Tan, and D. W. Chow. A method to predict nuclei size distributions for use in models of wet granulation. *Advanced Powder Technology*, 20(4):293–297, 2009.

K. Hayashi and S. Watano. Novel population balance model for granule aggregation and breakage in fluidized bed granulation and drying. *Powder technology*, 342: 664–675, 2019.

S. Heinrich and L. Mörl. Fluidized bed spray granulation—a new model for the description of particle wetting and of temperature and concentration distribution. *Chemical Engineering and Processing: Process Intensification*, 38(4-6):635–663, 1999.

S. Heinrich, M. Peglow, M. Ihlow, M. Henneberg, and L. Mörl. Analysis of the start-up process in continuous fluidized bed spray granulation by population balance modelling. *Chemical Engineering Science*, 57(20):4369–4390, 2002.

M. Hemati, R. Cherif, K. Saleh, and V. Pont. Fluidized bed coating and granulation: influence of process-related variables and physicochemical properties on the growth kinetics. *Powder Technology*, 130(1-3):18–34, 2003.

M. Hounslow. The population balance as a tool for understanding particle rate processes. *KONA Powder and Particle Journal*, 16:179–193, 1998.

M. Hounslow, R. Ryall, and V. Marshall. A discretized population balance for nucleation, growth, and aggregation. *AIChE journal*, 34(11):1821–1832, 1988.

M. Hounslow, J. Pearson, and T. Instone. Tracer studies of high-shear granulation: Ii. population balance modeling. *AIChE Journal*, 47(9):1984–1999, 2001.

M. Hounslow, M. Oullion, and G. Reynolds. Kinetic models for granule nucleation by the immersion mechanism. *Powder technology*, 189(2):177–189, 2009.

M. Hussain, J. Kumar, M. Peglow, and E. Tsotsas. On two-compartment population balance modeling of spray fluidized bed agglomeration. *Computers & chemical engineering*, 61:185–202, 2014.

C. D. Immanuel and F. J. Doyle Iii. Computationally efficient solution of population balance models incorporating nucleation, growth and coagulation: application to emulsion polymerization. *Chemical Engineering Science*, 58(16):3681–3698, 2003.

H. Y. Ismail, S. Shirazian, M. Singh, D. Whitaker, A. B. Albadarin, and G. M. Walker. Compartmental approach for modelling twin-screw granulation using population balances. *International journal of pharmaceutics*, 576:118737, 2020a.

H. Y. Ismail, M. Singh, A. B. Albadarin, and G. M. Walker. Complete two dimensional population balance modelling of wet granulation in twin screw. *International Journal of Pharmaceutics*, 591:120018, 2020b.

S. M. Iveson. Limitations of one-dimensional population balance models of wet granulation processes. *Powder Technology*, 124(3):219–229, 2002.

S. M. Iveson, J. D. Litster, K. Hapgood, and B. J. Ennis. Nucleation, growth and breakage phenomena in agitated wet granulation processes: a review. *Powder technology*, 117(1-2):3–39, 2001.

P. Kapur and D. Fuerstenau. Coalescence model for granulation. *Industrial & Engineering Chemistry Process Design and Development*, 8(1):56–62, 1969.

W. I. Kariuki, B. Freireich, R. M. Smith, M. Rhodes, and K. P. Hapgood. Distribution nucleation: Quantifying liquid distribution on the particle surface using the dimensionless particle coating number. *Chemical engineering science*, 92:134–145, 2013.

G. Kaur, M. Singh, T. Matsoukas, J. Kumar, T. De Beer, and I. Nopens. Two-compartment modeling and dynamics of top-sprayed fluidized bed granulator. *Applied Mathematical Modelling*, 68:267–280, 2019.

H. G. Kristensen and T. Schaefer. Granulation: A review on pharmaceutical wet-granulation. *Drug development and industrial pharmacy*, 13(4-5):803–872, 1987.

J. Kumar, M. Peglow, G. Warnecke, S. Heinrich, and L. Mörl. Improved accuracy and convergence of discretized population balance for aggregation: The cell average technique. *Chemical Engineering Science*, 61(10):3327–3342, 2006.

J. Kumar, M. Peglow, G. Warnecke, and S. Heinrich. The cell average technique for solving multi-dimensional aggregation population balance equations. *Computers & Chemical Engineering*, 32(8):1810–1830, 2008.

S. Kumar and D. Ramkrishna. On the solution of population balance equations by discretization—iii. nucleation, growth and aggregation of particles. *Chemical Engineering Science*, 52(24):4659–4679, 1997.

D. Kunii and O. Levenspiel. *Fluidization engineering*. Butterworth-Heinemann, 1991.

K. F. Lee, M. Dosta, A. D. McGuire, S. Mosbach, W. Wagner, S. Heinrich, and M. Kraft. Development of a multi-compartment population balance model for high-shear wet granulation with discrete element method. *Computers & Chemical Engineering*, 99:171–184, 2017.

J. Li, B. Freireich, C. Wassgren, and J. D. Litster. A general compartment-based population balance model for particle coating and layered granulation. *AIChE Journal*, 58(5):1397–1408, 2012.

J. Litster. *Design and processing of particulate products*. Cambridge University Press, 2016.

J. D. Litster, K. Hapgood, J. N. Michaels, A. Sims, M. Roberts, S. Kameneni, and T. Hsu. Liquid distribution in wet granulation: dimensionless spray flux. *Powder Technology*, 114(1-3):32–39, 2001.

H. Liu and M. Li. Two-compartmental population balance modeling of a pulsed spray fluidized bed granulation based on computational fluid dynamics (cfd) analysis. *International Journal of Pharmaceutics*, 475(1-2):256–269, 2014.

H. Liu, S. C. Galbraith, S.-Y. Park, B. Cha, Z. Huang, R. F. Meyer, M. H. Flamm, T. O'Connor, S. Lee, and S. Yoon. Assessment of spatial heterogeneity in continuous twin screw wet granulation process using three-compartmental population balance model. *Pharmaceutical development and technology*, 24(1):105–117, 2019.

L. Liu and J. Litster. Population balance modelling of granulation with a physically based coalescence kernel. *Chemical Engineering Science*, 57(12):2183–2191, 2002.

L. Liu, J. Litster, S. Iveson, and B. Ennis. Coalescence of deformable granules in wet granulation processes. *AIChE Journal*, 46(3):529–539, 2000.

L. Liu, L. Zhou, D. Robinson, and J. Addai-Mensah. A nuclei size distribution model including nuclei breakage. *Chemical engineering science*, 86:19–24, 2013.

L. Madec, L. Falk, and E. Plasari. Modelling of the agglomeration in suspension process with multidimensional kernels. *Powder Technology*, 130(1-3):147–153, 2003.

B. Michael and E. A. Michael. Fluidised-bed granulation: a chronology. *Drug development and industrial pharmacy*, 17(11):1437–1463, 1991.

S. V. Moraga, M. P. Villa, D. E. Bertín, I. M. Cotabarren, J. Piña, M. Pedernera, and V. Bucalá. Fluidized-bed melt granulation: The effect of operating variables on process performance and granule properties. *Powder Technology*, 286:654–667, 2015.

L. Mörl, S. Heinrich, and M. Peglow. Fluidized bed spray granulation. In *Handbook of powder technology*, volume 11, pages 21–188. Elsevier, 2007.

S. V. Muddu, A. Tamrakar, P. Pandey, and R. Ramachandran. Model development and validation of fluid bed wet granulation with dry binder addition using a population balance model methodology. *Processes*, 6(9):154, 2018.

A. L. Mundozah, J. J. Cartwright, C. C. Tridon, M. J. Hounslow, and A. D. Salman. Hydrophobic/hydrophilic static powder beds: Competing horizontal spreading and vertical imbibition mechanisms of a single droplet. *Powder Technology*, 330:275–283, 2018.

A. L. Mundozah, C. C. Tridon, J. J. Cartwright, A. D. Salman, and M. J. Hounslow. Wetting of binary powder mixtures. *International journal of pharmaceutics*, 572: 118770, 2019.

A. Negiz, E. S. Lagergren, and A. Cinar. Mathematical models of cocurrent spray drying. *Industrial & engineering chemistry research*, 34(10):3289–3302, 1995.

C. Neugebauer, S. Palis, A. Bück, E. Tsotsas, S. Heinrich, and A. Kienle. A dynamic two-zone model of continuous fluidized bed layering granulation with internal product classification. *Particuology*, 31:8–14, 2017.

A. Nienow. Fluidised bed granulation and coating: applications to materials, agriculture and biotechnology. *Chemical Engineering Communications*, 139(1):233–253, 1995.

D. E. Oakley. Spray dryer modeling in theory and practice. *Drying Technology*, 22 (6):1371–1402, 2004.

M. Oh and C. C. Pantelides. A modelling and simulation language for combined lumped and distributed parameter systems. *Computers & Chemical Engineering*, 20(6-7):611–633, 1996.

M. Peglow, J. Kumar, S. Heinrich, G. Warnecke, E. Tsotsas, L. Mörl, and B. Wolf. A generic population balance model for simultaneous agglomeration and drying in fluidized beds. *Chemical Engineering Science*, 62(1-2):513–532, 2007.

M. W. A. Phillips. Agrochemical industry development, trends in r&d and the impact of regulation. *Pest management science*, 76(10):3348–3356, 2020.

K. Pitt, R. M. Smith, S. A. de Koster, J. D. Litster, and M. J. Hounslow. Kinetics of immersion nucleation driven by surface tension. *Powder Technology*, 335:62–69, 2018.

D. A. Pohlman. Multi-scale modeling of high-shear granulation. 2015.

J. M.-H. Poon, C. D. Immanuel, F. J. Doyle Iii, and J. D. Litster. A three-dimensional population balance model of granulation with a mechanistic representation of the nucleation and aggregation phenomena. *Chemical Engineering Science*, 63(5):1315–1329, 2008.

S. U. Pradhan, M. Sen, J. Li, J. D. Litster, and C. R. Wassgren. Granule breakage in twin screw granulation: Effect of material properties and screw element geometry. *Powder Technology*, 315:290–299, 2017.

A. V. Prakash, A. Chaudhury, D. Barrasso, and R. Ramachandran. Simulation of population balance model-based particulate processes via parallel and distributed computing. *Chemical Engineering Research and Design*, 91(7):1259–1271, 2013.

P. Rajniak, F. Stepanek, K. Dhanasekharan, R. Fan, C. Mancinelli, and R. Chern. A combined experimental and computational study of wet granulation in a wurster fluid bed granulator. *Powder Technology*, 189(2):190–201, 2009.

R. Ramachandran and P. I. Barton. Effective parameter estimation within a multi-dimensional population balance model framework. *Chemical Engineering Science*, 65(16):4884–4893, 2010.

R. Ramachandran, C. D. Immanuel, F. Stepanek, J. D. Litster, and F. J. Doyle III. A mechanistic model for breakage in population balances of granulation: Theoretical kernel development and experimental validation. *Chemical Engineering Research and Design*, 87(4):598–614, 2009.

D. Ramkrishna. *Population balances: Theory and applications to particulate systems in engineering*. Elsevier, 2000.

A. Rawle. Basic of principles of particle-size analysis. *Surface coatings international. Part A, Coatings journal*, 86(2):58–65, 2003.

J. Richardson and W. Zaki. Sedimentation and fluidisation: Part i. *Chemical Engineering Research and Design*, 75:S82–S100, 1997.

C. Rieck, T. Hoffmann, A. Bück, M. Peglow, and E. Tsotsas. Influence of drying conditions on layer porosity in fluidized bed spray granulation. *Powder Technology*, 272:120–131, 2015.

C. Rieck, A. Bück, and E. Tsotsas. Monte carlo modeling of fluidized bed coating and layering processes. *AIChE Journal*, 62(8):2670–2680, 2016.

C. Rieck, A. Bück, and E. Tsotsas. Estimation of the dominant size enlargement mechanism in spray fluidized bed processes. *AIChE Journal*, 66(5):e16920, 2020.

H. Rumpf. Grundlagen und methoden des granulierens. *Chemie Ingenieur Technik*, 30(3):144–158, 1958.

H. Rumpf. Physical aspects of comminution and new formulation of a law of comminution. *Powder Technology*, 7(3):145–159, 1973.

A. D. Salman, M. Hounslow, and J. P. Seville. *Granulation*. Elsevier, 2006.

K. V. Sastry. Similarity size distribution of agglomerates during their growth by coalescence in granulation or green pelletization. *International Journal of Mineral Processing*, 2(2):187–203, 1975.

R. Sayin. Mechanistic studies of twin screw granulation. 2016.

S. H. Schaafsma, N. W. Kossen, M. T. Mos, L. Blauw, and A. C. Hoffmann. Effects and control of humidity and particle mixing in fluid-bed granulation. *AIChE journal*, 45(6):1202–1210, 1999.

M. Sen and R. Ramachandran. A multi-dimensional population balance model approach to continuous powder mixing processes. *Advanced Powder Technology*, 24 (1):51–59, 2013.

R. N. Tamura and D. D. Boos. Minimum hellinger distance estimation for multivariate location and covariance. *Journal of the American Statistical Association*, 81(393): 223–229, 1986.

H. Tan, M. Goldschmidt, R. Boerefijn, M. Hounslow, A. Salman, and J. Kuipers. Building population balance for fluidised bed granulation: lessons from kinetic theory of granular flow. In *Proceedings of the World Congress on Particle Technology 4, 21–25 July 2002, Sydney, Australia.*, 2002.

H. Tan, M. Goldschmidt, R. Boerefijn, M. Hounslow, A. Salman, and J. Kuipers. Building population balance model for fluidized bed melt granulation: lessons from kinetic theory of granular flow. *Powder Technology*, 142(2-3):103–109, 2004a.

H. Tan, A. Salman, and M. Hounslow. Kinetics of fluidised bed melt granulation iii: tracer studies. *Chemical engineering science*, 60(14):3835–3845, 2005.

H. Tan, A. Salman, and M. Hounslow. Kinetics of fluidised bed melt granulation i: The effect of process variables. *Chemical Engineering Science*, 61(5):1585–1601, 2006.

H. S. Tan, A. Salman, and M. Hounslow. Kinetics of fluidised bed melt granulation: Iv. selecting the breakage model. *Powder technology*, 143:65–83, 2004b.

G. I. Tardos, M. I. Khan, and P. R. Mort. Critical parameters and limiting conditions in binder granulation of fine powders. *Powder Technology*, 94(3):245–258, 1997.

E. A. Truckenbrodt. *Fluidmechanik: Band 2: Elementare Strömungsvorgänge dichteveränderlicher Fluide sowie Potential-und Grenzschichtströmungen.* Springer-Verlag, 2008.

V. S. Vassiliadis, R. W. Sargent, and C. C. Pantelides. Solution of a class of multistage dynamic optimization problems. 1. problems without path constraints. *Industrial & Engineering Chemistry Research*, 33(9):2111–2122, 1994a.

V. S. Vassiliadis, R. W. Sargent, and C. C. Pantelides. Solution of a class of multistage dynamic optimization problems. 2. problems with path constraints. *Industrial & Engineering Chemistry Research*, 33(9):2123–2133, 1994b.

M. P. Villa, D. E. Bertín, I. M. Cotabarren, J. Piña, and V. Bucalá. Fluidized-bed melt granulation: Coating and agglomeration kinetics and growth regime prediction. *Powder Technology*, 300:61–72, 2016.

L. Vogel and W. Peukert. Determination of material properties relevant to grinding by practicable labscale milling tests. *International Journal of Mineral Processing*, 74:S329–S338, 2004.

A. Vreman, C. Van Lare, and M. Hounslow. A basic population balance model for fluid bed spray granulation. *Chemical Engineering Science*, 64(21):4389–4398, 2009.

J. B. Wade, J. E. Miesle, S. L. Avilés, and M. Sen. Exploring the wet granulation growth regime map–validating the boundary between nucleation and induction. *Chemical Engineering Research and Design*, 156:469–477, 2020.

L. G. Wang, S. U. Pradhan, C. Wassgren, D. Barrasso, D. Slade, and J. D. Litster. A breakage kernel for use in population balance modelling of twin screw granulation. *Powder Technology*, 363:525–540, 2020.

L. G. Wang, J. P. Morrissey, D. Barrasso, D. Slade, S. Clifford, G. Reynolds, J. Y. Ooi, and J. D. Litster. Model driven design for twin screw granulation using mechanistic-based population balance model. *International Journal of Pharmaceutics*, 607: 120939, 2021.

J. Werther. Bubble chains in large diameter gas fluidized beds. *International Journal of Multiphase Flow*, 3(4):367–381, 1977.

W. Wildeboer, J. Litster, and I. Cameron. Modelling nucleation in wet granulation. *Chemical Engineering Science*, 60(14):3751–3761, 2005.

H. Zhai, S. Li, G. Andrews, D. Jones, S. Bell, and G. Walker. Nucleation and growth in fluidised hot melt granulation. *Powder Technology*, 189(2):230–237, 2009.